

The Use of Cross-Flow Membrane Emulsification to Fabricate Large, Porous Polymeric Microparticles for Tissue Engineering Applications

Sanchita Sharmin Chowdhury

M. Pharm, M. Phil

Thesis Submitted to the University of Nottingham for the Degree of Doctor of Philosophy

November 2016

Abstract

A common approach in tissue engineering strategies is to deliver living cells together with supporting scaffolds to damaged or injured body parts and then induce cell proliferation and differentiation for the purpose of regenerating functional tissues. Porous polymeric microparticles (Por-MPs), as scaffolds have recently received extensive interest for their pores, facilitating exchange of nutrients throughout the scaffolds and, sizes (micrometre scale) and shapes (spherical), offering delivery of the cell-scaffold system via narrow bore needle with minimally invasive surgical intervention to repair irregularly shaped tissue defect. For fabrication of MPs, conventional emulsion-solvent evaporation (CE) methods are most commonly used; however the size distributions of the prepared MPs are broad, which could bring negative impacts on the efficiency of the scaffolds as cell-delivering vehicles. On the other hand, cross-flow membrane emulsification (X-ME) is a promising technique for preparation of uniform-sized MPs.

One of the aims of this study was to develop a robust protocol for preparing uniform-sized, large and porous poly (lactide-co-glycolide) (PLGA) MPs using the X-ME method. The method development process started with fabrication of solid polycaprolactone (PCL) MPs (Sol-MPs). Different process and formulation parameters, such as working pressure (P_w), membrane pore diameter (D_0), viscosity of disperse phase (η_{DP}) and emulsifier concentration ($Conc._{CP}$) were optimised for preparing Sol-MPs with mean diameter of approximately 100 μm. Span factor was used as a criteria of degree of monodispersity of the MPs; in

general the lower the span factor, the narrower the size distribution. The same emulsion conditions were taken into account for preparation of monodisperse porous PLGA MPs (Por-ME MPs) with mean dimeter of approximately 100 μm. The further aim of this study was to assess the performance of the novel porous MPs (Por-ME MPs) as scaffolds for delivery of stem cells in bone tissue regeneration. Immortalised human mesenchymal stem cells (ihMSCs) were seeded with Por-ME MPs and the attachment, viability, proliferation and osteogenic differentiation of the cells were assessed.

Under the optimal emulsification conditions, such as at certain P_w, D_0, η_{DP}, $Conc._{CP}$, Sol-MPs with mean diameter of 109 μm (± 20.75) and span factor of 0.52 (± 0.04) were prepared via the ME method. On the other hand, the mean diameter and span factor of Por-ME MPs prepared via X-ME were 114 μm (± 19) and 0.43 (± 0.02), respectively. The size distributions of the Por-ME MPs, prepared via X-ME were substantially narrower than those of the Por-CE MPs, prepared via conventional high shear homogenizer. The mean diameter and span factor of Por-CE MPs were 78 μm (± 25) and 0.70 (± 0.07), respectively. On the other hand, the novel porous MPs were biocompatible with ihMSCs in terms of viability, proliferation and osteogenic differentiation of the cells.

Via this study, a new platform for fabrication of porous PLGA MPs was introduction. The strategy used to prepare these MPs, could be applied for preparing MPs with other biodegradable polymers. The newly developed scaffold system (Por-ME MPs) has the potential to regenerate bone tissues; however, further research is necessary in order to establish the scaffold system as a reliable stem cell delivering vehicle.

Declaration

Name:	Sanchita Sharmin Chowdhury
Student identification number:	4158329
Registration period:	01st August 2012 to 31st July 2016 (Including thesis pending period)
Initial submission:	July 2016
***Viva voce* examination:**	September 2016
Final submission:	November 2016

Declaration: I hereby declare that this thesis and all the experimental results presented in it are my own, which were generated throughout the doctoral study period at this university. All main sources of help have been acknowledged.

Dedicated to my beloved husband-Kaafi Mahmud Sarker

Acknowledgement

First and foremost, all praise goes to Almighty Allah for His blessings which made me able to produce this thesis.

My heartfelt thanks and deep gratitude go to my honourable supervisors-Professor KM Shakesheff and Dr. Felicity RAJ Rose for their valuable guide throughout the study period.

I am also very much grateful to my bench supervisor Dr. Omar Qutachi and all other members of Tissue Engineering group, in particular, Dr. Glen Kirkham for cell culture training, and Dr. Lisa White and Dr. Helen Cox for training on microparticle fabrication. Not to mention that excellent companion of other fellow students (too numerous to mention) and their encouraging words, that helped me to get back in life from the frustrating moments in the research labs. Special thanks go to Yamina Boukari for proof reading of Chapter 2 to Chapter 5 of this thesis.

My sincere thanks go to Mrs. Teresa Marshall, Mrs. Christine Grainger-Boultby and Mr. Paul Cooling for their technical supports to use different laboratory equipment in the School of Pharmacy. I also would like to thank Mrs. Nicola Weston for helping me to get the images using ESEM instrument.

My profound thank to the authority of Islamic Development Bank (IDB) for their funding to support my PhD study in the University of Nottingham and also to the University of Nottingham for offering me their excellent research facilities.

The last but not the least, my thankfulness go to my husband and children (Nabiha and Samin), who sacrificed a lot but gave me a wonderful family life.

Table of Contents

Abstract i

Declaration iii

Acknowledgement v

Table of Contents vi

List of Figures x

List of Tables xxi

List of Abbreviations xxii

Chapter 1 General Introduction 1

1.1 Overview of Tissue Engineering and Regenerative Medicine 1

1.2 Stem Cells in Tissue Engineering 5

1.2.1 Background 5

1.2.2 Embryonic Stem Cells 8

1.2.3 Mesenchymal Stem Cells 9

1.2.4 Immortalized Human Mesenchymal Stem Cells 10

1.3 Osteogenic Differentiation of hMSCs 10

1.4 Scaffolds in Tissue Engineering 11

1.4.1 Introduction 11

1.4.2 Mass Transport Function and Pore Architectures of Scaffolds 14

1.4.3 Surface Topography of Scaffolds 15

1.5 Microparticles as Scaffolds 19

1.6 Material Selection for Microparticle Preparation 22

1.7 Porous Microparticles as Scaffolds in Tissue Engineering 25

1.8 Polymeric Microparticle Fabrication Methods 26

1.8.1 Conventional Emulsification 26

1.8.2 Membrane Emulsification 31

1.9 Aims and Objective of the Study 37

Chapter 2 Large, Porous Poly (Lactide-Co Glycolide) Microparticles as Injectable Cell Delivering Vehicles 41

2.1 Introduction 41

2.2 Materials and Methods 44

2.2.1 Equipment, Consumables and Materials 44
2.2.2 Fabrication of Large Solid PLGA Microparticles 44
2.2.3 Fabrication of Large, Porous PLGA MPs 47
2.2.4 Characterization of the Emulsion Droplets 49
2.2.5 Characterization of the Microparticles 49
2.2.6 Porosity Improvement by NaOH-EtOH Treatment 54
2.2.7 Characterization of Pore Size Distribution 54
2.2.8 Surface Wetting of Porous PLGA MPs by Ethanol Treatment 55
2.2.9 Culture and Maintenance of Immortalized Human Mesenchymal Stem Cells 56
2.2.10 Seeding Cells on Porous PLGA MPs 57
2.2.11 Assessment of Cell Adhesion, Proliferation and Viability on MPs 59
2.2.12 Statistical Analysis 63
2.3 Results and Discussion 64
2.3.1 Characteristics of Emulsion Droplets 65
2.3.2 Characteristics of MPs 68
2.3.3 Pore Size Distribution 75
2.3.4 Adhesion and Viability of Cells on MP (Cell Compatibility With Microparticles) 77
2.3.5 Influence of Static/Shaking Seeding and MP Density on Cell Viability 82
2.3.6 Live/Dead® Viability/Cytotoxicity Assay 85
2.4 Conclusions 87
Chapter 3 Cross-flow Membrane Emulsification to Fabricate Large and Uniform-sized Polycaprolactone Microparticles 89
3.1 Introduction 89
3.2 Experimental 92
3.2.1 Materials 92
3.2.2 Experimental Setup and Emulsification Procedure 93
3.2.3 Characterisation of the Emulsion Droplets 95
3.2.4 Characteristics of the Microparticles 95
3.2.5 Assessment of the Monodispersity of the Microparticles 95
3.2.6 Statistical Analysis 96

3.3 Results and Discussion 96
3.3.1 Fabrication of Large MPs Using Higher Molecular Weight PCL (PCL_{80kDa}) 96
3.4 Fabrication of Large MPs Using Lower Molecular Weight PCL (PCL_{45kDa}) 120
3.5 Relation Between Particle Size and Pore Size at Optimal Emulsification Conditions for PCL_{80kDa} and PCL_{45kDa} 127
3.6 Conclusions 129
Chapter 4 Fabrication of Large, Porous PLGA Microparticles Using Cross-Flow Membrane Emulsification 131
4.1 Introduction 131
4.2 Materials and Methods 134
4.2.1 Equipment, Consumables and Materials 134
4.2.2 Experimental Setup and Emulsification Procedure 135
4.2.3 Porosity Improvement by NaOH-EtOH Treatment 139
4.2.4 Characterization of Emulsion Droplets 139
4.2.5 Characterization of Microparticles 139
4.2.6 Characterization of Pore Size Distributions 140
4.3 Results and Discussion 140
4.3.1 Viscosity Study of Different Concentration of PLGA Solutions 141
4.3.2 Influence of New and Used Membranes on MP Size Distributions 144
4.3.3 Comparison of Emulsion Droplets Prepared Via CE and ME Methods 149
4.3.4 Effect of NaOH-EtOH Treatment on Porosity 151
4.3.5 Comparison of Characteristics of MPs Prepared Via X-ME and CE 153
4.3.6 Comparison of Pore Size Distribution of MPs Prepared Using CE and X-ME 158
4.1 Conclusions 162
Chapter 5 Assessment of the Novel Porous PLGA MPs Prepared via Cross-flow Membrane Emulsification for Cell Delivery Applications 164
5.1 Introduction 164
5.2 Materials and Method 166

5.2.1 Equipment, Consumables and Materials 166
5.2.2 Surface Wetting of the MPs by Tween 20 Treatment 166
5.2.3 Seeding Cells on Tween 80 Treated Porous MPs 166
5.2.4 Cell Fixation 167
5.2.5 Cell Viability, Proliferation and Cytotoxicity Assays 168
5.2.6 Osteogenic Differentiation of ihMSC on Por-ME MPs 172
5.2.7 Statistical Analysis 181
5.3 Results and Discussion 181
5.3.1 Effect of Densities of Por-ME MPs and ihMSCs On Cell Viability 181
5.3.2 Comparison of Cytocompatibility of Por-ME MPs with Cytx-CM MPs 184
5.3.3 Osteogenic Differentiation of ihMSCs on Por-ME MPs 192
5.4 Conclusions 210
Chapter 6 Summary and Future Work 212
6.1 Summary 212
6.2 Future Work 218
References 222
Appendices 239
Appendix I. Equipment, Consumables and Materials 239
Appendix II. Coating of nTC Plates with Pluronic F 127 247
Appendix III. Counting of Viable Cells using Trypan Blue 250
Appendix IV. Calibration curves developed for ihMSCs Viability Assays .251
Appendix V. Images of Supernatant Collected During Medium Removal for PrestoBlue® Cell Viability Assay 254
Appendix VI. Cleaning and Maintenance of SPG Membranes 257
Appendix VII. GPC Sample Injection Report for PCL and PLGA polymers 258
Appendix VIII. Optimisation of Calcein AM and EthD-1 Concentration for Live/Dead Imaging 261
Appendix IX. Preparation of 4 % w/v Paraformaldehyde (need to paraphrase) 262

List of Figures

Figure 1.1 The key elements in TE/RM: cells, scaffolds and signals. The figure is reproduced from reference [1] with a slight modification. 4

Figure 1.2 Patterns of stem cell division. **A – B)**Through symmetric division, one stem cell divides into either two daughter stem cells (renewal) or progenitor cells (towards differentiation), which later form fully differentiated cells. **C)** Aymmetric division gives rise to both stem cells and progenitor cells. Recent literature suggests that depending on the physiological state (diseased or healthy) of the tissues where the stem cells reside in, the cells undego both symmetric and asymmetric division. 7

Figure 1.3 Correlation between tissue functions and scaffold properties. Reproduced from reference [53] 13

Figure 1.4 hMSCs cultured on unpolished **(A-D)** and polished **(E-H)** surfaces of α-TCP-CDS scaffolds. The cell adhesion and proliferation were higher on the rough (polished) surfaces. The images were adapted from reference [61]. 16

Figure 1.5 Surface topography of non-porous PLGA/$PEI_{1.8k}$ **(A – B)** and porous PLGA/$PEI_{1.8k}$ **(C-D)** scaffolds. The images were adapted from reference [62]....18

Figure 1.6 Some of the MP-based tissue engineering strategies. **A)** cells are seeded on MPs and the cell-MP complexes are injected to the injured site for tissue regeneration; **B)** cells are seeded on bioactive molecule-loaded MPs and the cell-MP aggregates later implanted to the injured body part for tissue regeneration; **C)** blank MPs are injected to the injured site to fill the gaps formed due to trauma or disease and encourage the host cells to migrate to the MPs. 20

Figure 1.7 Chemical structures of PGA, PLA and their co-polymer (PLGA). 24

Figure 1.8 Schematic of a double emulsion method for preparation of drug-loaded or porous polymeric MPs. **A)** the compound (drug or pore forming agent) is homogenised with a polymer solution, which resulted in a primary (w/o) emulsion. **B)** the primary emulsion is then homogenised with a emulsion solution (aqueous), which resulted in a secondary (w/o/w) emulsion; evaporation of the solvent, washing out of the MPs and lyophilisation (drying) yield drug-loaded or porous MPs. The figure is reproduced from reference [92] with slight modificaiton.....28

Figure 1.9 Porous PLA MPs prepared via w/o/w double emulsion-solvent evaporation method. The MPs were prepared using smaller **(A1 – A3)** and larger **(B1 – B3)** amounts of the PLA solutions. As a pore forming agent, NH_4HCO_3 was used. The image were captured at low **(A1, A2, B1 and B2)** and high **(A3 and B3)** magnification. The images are reproduced from reference [87]. 30

Figure 1.10 A schematic of monodisperse MP fabrication via single- and multi-channel systems. A drop-by-drop emulsion formation is occurred in the case of the single channel system **(A)**, whereas, multiple emulsion droplets are formed at a time via the multi-channel system **(B)**.....33

Figure 1.11 Schematic of **A)** direct emulsification (X-ME) and **B)** Premix emulsification. In case of X-ME, CP flow is maintained cross-way to the flow of DP, whereas, no flow of CP is maintained in the case of the premix emulsification**.** 36

Figure 1.12 Schematic of the study flow diagram.....40

Figure 2.1 Schematic of the preparation of the solid PLGA MPs.....46

Figure 2.2 Schematic of the preparation of porous PLGA MPs. **A–B)** PLGA solution in DCM (oil phase) and PBS (water phase) are homogenized to prepare the w/o primary emulsion; **C)** 0.3 % w/v PVA solution is maintained stirring and the w/o primary emulsion is gradually added to the area surrounding the vortex created due to the stirring; **D)** w/o/w double emulsion is formed and maintained stirring at 300 rpm until DCM completely evaporated; **E)** the porous PLGA MPs are formed upon evaporation of DCM; **F)** an SEM image of the MPs harvested via centrifugation and freeze drying.....48

Figure 2.3 Shapes of size distribution curves **A)** Symmetric and **B-C)** asymmetric MP size distributions showing the degree of skewness. A symmetric distribution has no extreme value and the mean = mode = median. Positively (mean > mode) and negatively (mean < mode) skewed distribution indicate the presence of excessively large and small MPs, respectively, in the distributions. .52

Figure 2.4 Shapes of different size distributions in terms of kurtosis (g_2). A normal distribution is referred to as mesokurtic ($g_2 = 0$); a leptokurtic distribution (positive kurtosis) possesses a curve that is sharper than the normal curve ($g_2 > 0$); a platykurtic distribution (negative kurtosis) has a lower, broader peak than the normal curve ($g_2 < 0$).....53

Figure 2.5 Flow diagram of experimental design for cell viability and cytotoxicity assays.....62

Figure 2.6 Representative light microscopic images of **A)** single emulsion and **B)** double emulsion; scale bar = 100 µm; **C)** size distribution curves for the single and double emulsions as analysed using the data generated from Coulter LS 230. 67

Figure 2.7 Size distribution curves of the double emulsions and the respective MPs before and after the NaOH-ETOH treatment. 72

Figure 2.8 Representative SEM images of **A)** solid and **B)** porous MPs before NaOH-EtOH treatment; **C)** cross-section image of porous MPs before NaOH-EtOH treatment 73

Figure 2.9 Representative SEM images of the porous MPs after the NaOH-EtOH treatment showing their **A)** surface and **B)** internal porosity (cross-section images). 74

Figure 2.10 Pore size distributions. **A)** Before NaOH-EtOH treatment and **B)** after NaOH-EtOH treatment. Some representative pores (as observed in representative SEM images of the MPs; total pore count = 500; n = 3) were measured using the Image J image processing software and then analysed in Microsoft Excel to generate the histograms. 76

Figure 2.11 Representative microscopic images of ihMSCs-GFP with Por-CE MPs in nTC plates (images taken for the centre of the plates). Blank MPs (Por-CE MPs) under fluorescent light, in a 12-well nTC plate on day 1 post-seeding **(A)**; ihMSCs-GFP attached on a 12-well TC plate on day 1 post-seeding **(B)**; ihMSCs-GFP attached on the MPs on day 1 **(C-1 and C-2)**, day 3 **(D-1 and D-2)** and day 7 **(E-1 & E-2)** post-seeding. The single-headed arrows indicate the cell attachment on the bottom of the wells, the double-headed arrows indicate the size of the cell-MP aggregates. Scale bar = 100 µm 79

Figure 2.12 Representative microscopic images of ihMSCs-GFP with Por-CE MPs in nTC plates (images taken for the peripheries of the plates). ihMSCs-GFP attached on the MPs on day 1 **(A-1 and A-2)**, day 3 **(B-1 and B-2)** and day 7 **(C-**

1 & C-2) post-seeding. The arrows indicate the cell attachment on the bottom of the plates. Scale bar = 100 µm 80

Figure 2.13 Representative microscopic images of ihMSCs-GFP with Por-CE MPs, cultured in Pluronic F 127-coated nTC plates.ihMSCs-GFP attached on the MPs on day 1 **(A-1 and A-2)**, day 3 **(B-1 and B-2)** and day 7 **(C-1 & C-2)** post-seeding. Scale bar = 100 µm. 81

Figure 2.14 Influence of static and shaking seeding and the density of Por-CE MPs on the viability of ihMSC. ihMSCs were cultured with Por-CE MPs over a 5-days period, after seeding the cells via the static or shaking mode. Viabilities of the cells on day 1, 3 and 5 post-seeding were measured using the PrestoBlue® cell vibility assay kit. Values are presented as mean ± SD (n = 3; r = 3). Statistical significance between different groups are represented as: **p<0.01; ***p<0.001; ****p<0.0001; 'ns' denotes the non-significance of the difference, for which, p>0.05.....84

Figure 2.15 Representative fluorescence microscopic images of live (left-hand column, green fluorescent) and dead (middle column; a few red spot) cells on Por-CE MPs; optical light microscopic images of blank MPs (no cells; negative control). Scale bar = 100 µm.....86

Figure 3.1 Schematic of a typical X-ME process.....94

Figure 3.2 Mean particle diameter with corresponding span factor as a function of PVA concentration (0.1, 0.3, 1.0 % w/v in water). The MPs were prepared using 12.5 % w/v PCL_{80kDa} using membranes of pore diameters **A)** 20 µm and **B)** 50 µm. Values are represented as mean ± SD (n = 3; r = 3) 104

Figure 3.3 Emulsion droplets (left-hand column) and their corresponding MPs (right-hand column) prepared for 12.5 % w/v PCL_{80kDa} with 0.1 - **(A – B)** , 0.3 - **(C –D)** and 1.0 - **(E – F)** % w/v PVA, using SPG membranes with mode pore diameters of 20 µm. Scale bar = 100 µm. 105

Figure 3.4 Emulsion droplets (left-hand column) and their corresponding MPs (right-hand column)) prepared for 12.5 % w/v PCL_{80kDa} with 0.1 - **(A – B)** , 0.3 - **(C –D)** and 1.0 - **(E – F)** % w/v PVA, using SPG membranes with mode pore diameters of 50 µm. Scale bar = 100 µm. 106

Figure 3.5 Effect of viscosity of PCL solutions. 109

Figure 3.6 Effect of viscosities of different concentrations of PCL solutions. .110

Figure 3.7 Forces acting on a droplet under an X-ME setup (reproduced from reference [186] 111

Figure 3.8 Optical light microscopy images of emulsion droplets collected at different time points during the emulsification process. 116

Figure 3.9 Size distributions of emulsion droplets before DCM evaporation (DSD) and their corresponding MPs after DCM evaporation (PSD), under the optimum emulsification conditions. PSD = particle size distribution; DSD = droplet size distribution. 119

Figure 3.10 Effect of viscosities of DPs (for PCL_{45kDa}) on PSDs. 123

Figure 3.11 Representatative SEM images of MPs prepared using different concentrations of PCL_{45kDa} in DCM.....124

Figure 3.12 Volume mean diameters (D[4,3]) of MPs in relation to D_0 and polymer concentrations. The values are represented as mean ± SD (n = 3, r = 3). 128

Figure 4.1 Schematic of fabrication of porous PLGA MPs using X-ME process. **1-2)** w/o primary emulsion (PBS in PLGA solution) is formed using a high shear homogenizer; **3)** the w/o emulsion is passed through a 20 µm SPG membrane while a cross-flow of PVA-water (w) is maintained through the membrane; an w/o/w double emulsion is formed on the other side of the membrane and deposited in a beaker; **4)** the w/o/w emulsion is kept stirring until DCM is completely evaporated; **5)** The MPs are collected by centrifugation, washed three times with water and and then freeze dried. 138

Figure 4.2 A) Viscosities of a series of $PLGA_{27kDa}$ in DCM and PBS-$PLGA_{27kDa}$ emulsion. **B)** The viscosity of the 50% w/v $PLGA_{27kDa}$ with 25% v/v PBS emulsion is comparable with that of optimal PCL solution (37.5 % w/v PCL_{45kDa}. Values are represented as mean ± SD (n = 6; r = 3).....143

Figure 4.3 PCL (left-hand column) and porous PLGA (right-hand column) emulsion droplets prepared using new (the top images of both columns) and used membranes (the all other images). 146

Figure 4.4 PSD for the solid PCL MPs **(A)** and porous PLGA MPs **(B)** prepared using SPG membranes of pore diameter 20 µm. For both the solid and porous MPs, the first batches represent the size distribution curves obtained by using a new membrane. 147

Figure 4.5 SPG membrane geometry (reproduced from reference [189].....148

Figure 4.6 Optical light microscopic images of emulsion droplets prepared via **A)** CE and **B)** X-ME methods; scale bar = 100 µm. **C)** DSD for droplets prepared via the CE and X-ME methods; the skewness of the SD curves are shown as a perforated rectangle and circle for the droplets prepred via the CE and X-ME methods, respectively. 150

Figure 4.7 NaOH-EtOH treatment of Por-ME MPs to improve the porosity of the MPs. Untreated **(A-B)** and treated for 2min **(C-D)**, 4 min **(E-F)**, 6 min **(G-H)** and 10 min **(I-J)**. 152

Figure 4.8 Particle size distributions of Por-ME MPs and Por-CE MPs in terms of span factor before and after NaOH-EtOH treatment. 157

Figure 4.9 Surface and internal porosities of Por-ME MPs and Por-CE MPs before **(A, B, F and G)** and after **(C – E; H –J)** NaOH-EtOH treatment. 160

Figure 4.10 Pore size distribution of Por-CE MPs(left-hand column) and Por-ME MPs (right-hand column) before **(A, C)** and after **(B, D)** NaOH-EtOH treatment. 161

Figure 5.1 Flow diagram of experimental design for cell viability and cytotoxicity assays. 171

Figure 5.2 Schematic shows the experimental timeline for the osteogenic differentiation assays. 174

Figure 5.3 Effect of densities of Por-ME MPs and ihMSCs on viability of ihMSCs on day 1, 3 and 5 post-seeding. Values are presented as mean ± SD (n = 2; r = 3). Statistical significance between different groups are represented as: *p<0.05; ****p<0.0001; ‘ns’ denotes the non-significance of the difference, for which, p>0.05. 183

Figure 5.4 Viability of ihMSCs seeded with Por-ME MPs or Cytx-CM MPs on day 1, 3 and 5 post-seeding. The values are represented as mean ± SD (n = 2; r = 3).....186

Figure 5.5 Representative Live/Dead images of ihMSCs on Por-ME MPs (left-hand column) or Cytx-CM MPs (right-hand column) on day 3 post-seeding. The seeding density of the cells and MPs were 20×10^3 cells/well and 10 mg MPs/well, respectively. The live and dead cells are shown as bright green **(A and F)** and red **(B and G)** fluorescent, respectively. Scale bar = 100 µm.....188

Figure 5.6 CellMask Blue® staining of ihMSCs on Por-ME MPs or Cytx-CM MPs on day 3 post seeding. ihMSCs as bright blue fluorescent on Por-ME MPs **(A – D)** and on Cytx-CM MPs **(E – H)**; the red perforated circles **(B and F)** indicate a single MP with the cells on its surface; the red and white arrows indicate the morphologies of the cells in the denser and less dense fields, respectively; the yellow arrows indicate the position of cells between two MPs. Scale bar = 100 µm.....191

Figure 5.7 Alkaline phosphatase activities of ihMSCs cultured on Por-ME MPs or Cytx-CM MPs with osteogenic (OS) or non-osteogenic (Non-OS) medium for a period of 21-days. Values are presented as mean ± SD (n = 2; r = 3). Statistical significance between different groups are represented as: ****p<0.0001; 'ns' denotes the non-significance of the difference, for which, p>0.05. 195

Figure 5.8 Representative light photographs of ihMSCs with Por-ME MPs in OS or non-OD medium at day 21 post-seeding. On the day, the cultures were stained with alizarin red and von Kossa to identify calcium deposits, and with toluidine blue to identify the cells in the culture. The seeding densities for the cells and

MPs were 20 × 10^3 cells/well and 10mg Por-ME MPs/well of 24 well plates. Images were captured at magnification = 1×. 198

Figure 5.9 Representative ESEM images of ihMSCs on Por-ME MPs **(A)** and Cytx-CM MPs **(B**) that were cultured in an OS medium for 7 days. The cells are flattened on the surface of Por-ME MPs and forming a thin layer on the MPs and covering the pores; there is little evidence of individual cell boundary **(Ai)**. In contrast, the cells on Cytx-CM MPs are either elongated or circular shaped **(Bii)**; individual cells can be distinguished.....201

Figure 5.10 Representative ESEM images of ihMSCs on Por-ME MPs **(A)** and Cytx-CM MPs **(B)** in OS culture on day 14. The cells on Por-ME MPs were flattened and formed wide sheets which covering most of the surfaces of the MPs **(A)**; the cells also formed bridges between MPs as seen in the magnified image **(A)**. The cells on Cytx-CM MPs were elongated with a few cells of rounded shape **(B)**; most of the MPs were almost entirely covered by the cells **(B)**; the magnified image shows the bridges between adjacent Cytx-ME MPs **(B)**. Por-ME MPs **(C)** and Cytx-CM MPs **(D)** with no cells in OS medium on day 14; some of the Por-ME MPs deformed whereas the Cytx-CM remained intact on day 14 post-culture in OS medium.....202

Figure 5.11 Representative ESEM images of ihMSCs on Por-ME MPs **(A)** and Cytx-CM MPs **(B)** in OS culture on day 21.....203

Figure 5.12 Fluorescence calcification assay, using the fluorescent calcification assay kit, OsteoImage®. The cultures are in osteogenic media on day 21. All arrows indicate calcium deposition. Scale bar = 100 µm.....206

Figure 5.13 Fluorescence calcification assay using the commercially available kit OsteoImage®. Values are presented as mean ± SD (n = 2; r = 3). Statistical significance between different groups are represented as: ****p<0.0001; 'ns' denotes the non-significance of the difference, for which, p>0.05. 207

Figure 5.14 Immunocytochemical staining for human OCN, expressed by osteogenically differentiated ihMSCs on Por-ME MPs or Cytx-CM MPs at day 21 in OS-positive cultures. Representative images are shown. Scale bar = 100 µm. 209

List of Tables

Table 2.1 Particle Size Distribution 70

Table 3.1 Effect of Working Pressure and Membrane Pore Size.....101

Table 3.2 Optimal Conditions for Preparation of MPs with Diameters of Approximately 100 µm Using the Higher Molecular Weight PCL ($PCL_{80\ KDa}$).113

Table 3.3 Optimal Conditions for Preparation of '100 µm' MPs Using Lower Molecular Weight PCL (PCL_{45kDa}) 126

Table 4.1 Overview of Emulsification Conditions.....137

Table 4.2 Characteristics of the MPs prepared via X-ME and CE.....156

List of Abbreviations

ALP	Alkaline Phosphatase
AsAP	L-ascorbic acid 2-phosphate
BMPs	Bone Morphogenic Proteins
BMP-2	Bone Morphogenic Protein-2
BGP	Beta Glycerophosphate
CE	Conventional Emulsification
DMEM	Dulbecco's Modified Eagle Medium
DSD	Droplet size distribution
Dex	Dexamethasone
dH_2O	Double distilled water
EDTA	Ethylene Diamine Tetra Acetic Acid
ESEM	Environmental SEM
FBS	Fetal Bovine Serum
FDA	Food and Drug Administration
FGF	Fibroblast Growth Factor
g	Gram
g	Gravitational force
hMSC	Human Mesenchymal Stem Cell
hMSCs	Human Mesenchymal Stem Cells
ihMSCs	Immortalised Human Mesenchymal Stem Cells
hTERT	Human Telomerase Reverse Transcriptase
mL	Millilitre
µL	Microliter
µM	Micromolar
MP	Microparticle

MPs	Microparticles
ME	Membrane Emulsification
Mw	Weight Average Molecular Weight
Mn	Number Average Molecular Weight
o/w	Oil-in-Water
OD	Optical Density
PET	Polyethylene Terephthalate
Por-MPs	Porous Microparticles
Por-CE MPs	Porous Microparticles Prepared via Conventional Emulsification
Por-ME MPs	Porous Microparticles Prepared via Membrane Emulsification
PBS	Phosphate Buffer Saline
PLA	Poly Lactic Acid
PLGA	Poly (lactide-co-glycolide)
PVA	Polyvinyl Alcohol
pNPP	Para Nitro Phenyl Phosphate
pNP	Para Nitrophenol
RUNX2	Runt-related Transcription Factor 2
Sol-MPs	Solid Microparticles
Sol-CE MPs	Solid Microparticles Prepared via Conventional Method
w/o/w	Water-in-oil-in-water
X-ME	Cross-flow Membrane Emulsification

Chapter 1 General Introduction

1.1 Overview of Tissue Engineering and Regenerative Medicine

The term tissue engineering (TE) was first suggested by Professor Y. C. Fung (from the University of California, San Diego) at a National Science Foundation meeting in 1987 [1]. This led to the first meeting called 'tissue engineering' that was held in early 1988 at Lake Tahoe, California [2]. However, a proper definition of the term was given by Langer and Vacanti in 1993 [3] in the paper entitled 'tissue engineering'. They defined it as 'an interdisciplinary field that applies the principles of engineering and the life sciences toward the development of biological substitutes that restore, maintain, or improve tissue function.' It is important to note that nearly five years before TE was defined, in another paper [4], the same authors presented some examples of the proof of principle of tissue engineering. They demonstrated that some animal cells (hepatocytes, pancreatic islet cells and small intestinal cells) remained viable and proliferated in vitro in biodegradable artificial polymer scaffolds, and that after implantation of the cell-polymer scaffolds in the animals, some of the cell types (e.g., hepatocytes) exhibited viability and vascularisation.

On the other hand, the advancement of stem cell biology has led to a new field of research named regenerative medicine (RM), in early 21st century [5, 6]. Classically, 'regeneration' is used to describe 'the process in humans whereby lost specialised tissue is replaced by proliferation of undamaged specialised cells' [7]. Similarly, in classical terms, 'repair is the replacement of lost tissue by granulation tissue which matures to form scar tissue' [7]. There are many

definitions of RM; however, on the basis of a lengthy definition introduced by Greenwood et al. [8], Mason and Dunnill simplified the explanation of the term as follows : ‘ regenerative medicine replaces or regenerates human cells, tissues or organs, to restores or establish normal function’ [9]. Some refer to RM as a ‘code word’ for stem cell technology, while for others, RM is the broader and more generalized field, with TE representing only replacement, not repair and/or regeneration. Still, others use the terms TE and RM interchangeably. Whatever name is chosen, both TE and RM refer to a biological approach of replacing or restoring lost or missing body function by encouraging the body to return to normal.

There are three key elements in TE and RM: cells, scaffolds and signalling molecules (Figure 1.1). These elements are utilised together to produce appropriate regenerative medicines for human. The cells could be stem cells (unspecialised/non-tissue cells), progenitor cells or fully differentiated cells (tissue cells). Alternatively, a combination of cell types (differentiated and undifferentiated cells) could be used. The scaffolds could either be made of a synthetic biopolymer or be a natural extracellular matrix (ECM). Irrespective of the source of the scaffolds, they serve one or more of the following purposes: 1) offer a favourable surface for the cells to attach, proliferate and migrate; 2) retain and/or deliver bioactive molecules; 3) offer a porous environment for diffusion of nutrients and oxygen as well as removal of wastes and, 4) provide necessary mechanical rigidity or flexibility for the cells. The signalling molecules (e.g., bone morphogenetic protein [BMPs], vascular endothelial growth factor [VEGF] and transforming growth factor beta [TGF-β]) can stimulate cell adhesion,

proliferation and differentiation and, thus encourage endogenous repair of damaged body parts [10, 11]. However, it is well understood that they are secreted by the cells employed and a complete understanding about all the signals require for a particular tissue regeneration, is still far away from being realised [1].

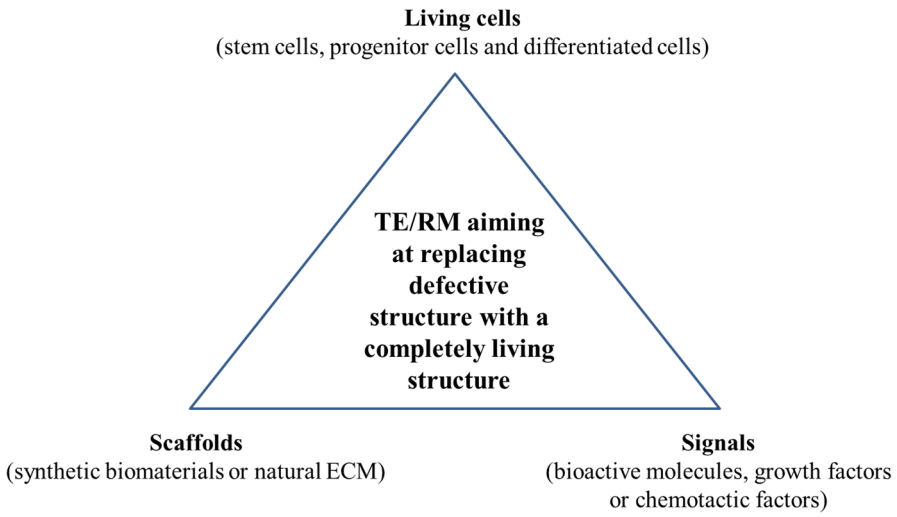


Figure 1.1 The key elements in TE/RM: cells, scaffolds and signals. The figure is reproduced from reference [1] with a slight modification.

1.2 Stem Cells in Tissue Engineering

1.2.1 Background

Stem cells are considered as one of the building blocks of the body, which play a major role in healing and regeneration of cells and tissues. They are unspecialised cells (not any tissue- or organ-specific cells) and possess self-renewal and clonogenic properties in normal state. Self-renewal is the capacity of extensive proliferation into daughter cells with the characteristic properties of the parent cells; a clonogenic cell has the potential to multiply into a colony of cells via proliferation [12]. On the other hand, they can differentiate into mature cells (tissue- or organ-specific cells) under certain physiological or experimental conditions. These unique properties of stem cells offer the promise of manipulating these cells for tissue regeneration.

For a long time, stem cell division was described as asymmetric [13], through which one stem cell divides to give rise to two daughter cells with different fates, i.e., one of them remains as a stem cell and the other enters in the process of forming fully differentiated cells. However, a recent study evidenced that stem cells exhibit both symmetric and asymmetric division, depending on the physiological state of the tissue (diseased or healthy), where the cells reside in [14]. Via asymmetric division stem cells renew (divide into daughter stem cells) as well as direct towards forming mature cells (differentiated cells or tissue-specific cells). Before forming the fully differentiated cells, stem cells undergo a process of several cell divisions and progressively become more mature and, eventually stop dividing. The cells which are in between the state of stem cells

and differentiated cells are defined as progenitor cells. A schematic of stem cell division patterns is shown in Figure 1.2.

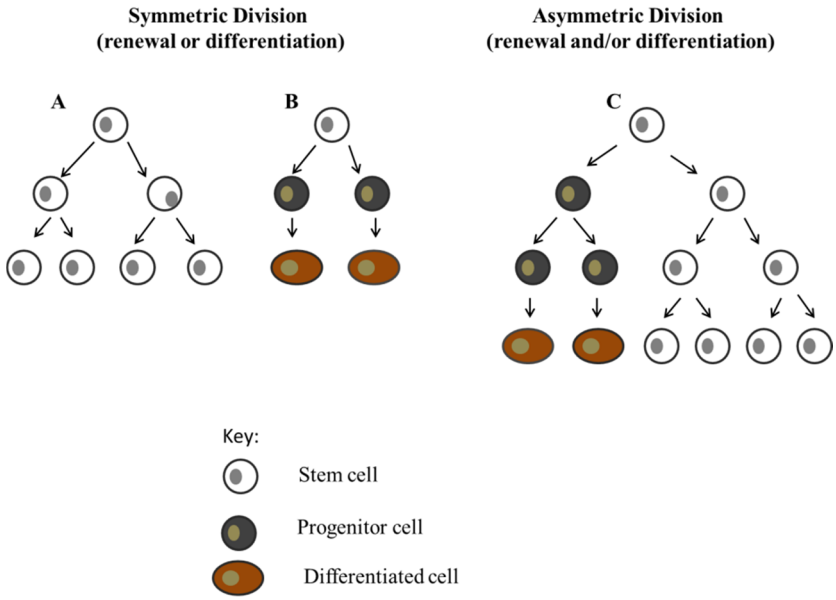


Figure 1.2 Patterns of stem cell division. **A – B)**Through symmetric division, one stem cell divides into either two daughter stem cells (renewal) or progenitor cells (towards differentiation), which later form fully differentiated cells. **C)** Aymmetric division gives rise to both stem cells and progenitor cells. Recent literature suggests that depending on the physiological state (diseased or healthy) of the tissues where the stem cells reside in, the cells undego both symmetric and asymmetric division.

In the process of tissue regeneration, stem cells not just differentiate into the tissue-specific cells; they serve as building blocks in the process by organising them into spatially appropriate models and by guiding them to specific physicochemical cues [13]. Hence, understanding the developmental biology of the tissue meant to repair as well as the origin of the stem cells are equally important for applying the cells in tissue engineering.

In human development, the first eight weeks is called embryonic period. During this period, most of the body parts appear. The subsequent period is termed as foetal period, when the tissues and organ become mature, and the body develops; although some developmental processes, such as lung development, continue postnatally. A particular cell fate is controlled by a number of signalling pathways (e.g., TGF-β/BMPs, FGF and Wnt/Wingless [Wg]) during the embryonic development. The signalling pathways become activate and interact spatiotemporally [13].

1.2.2 Embryonic Stem Cells

Embryonic stem cell (ESC) research has started to expand since 1981, after the first isolation of mouse ESCs (mESCs) from the inner cell mass (ICM) of mouse blastocyst (the structure formed in the early development of mammals) [15, 16]. Subsequently, in 1998, human ESCs (hESCs) were isolated from the ICM of human blastocysts. Due to these characteristic properties of ESCs, they have been a useful cell sources for tissue engineering. Over the last few years, ESCs mainly focused on understanding the culture conditions and media components that

require for the maintenance of self-renewal properties of the cells for a long time in the culture [17-20]. Some of the recent studies demonstrated the potential of ESCs in regeneration of bone [21], vascular [22], cardiac [23] and neuronal [24] tissues. However, in order to translate ESC-based therapy into clinic, a number of challenges yet to overcome, such as understanding the cues that direct the cell fate, improving the cost and feasibility of these cell-based therapy and ensuring their safety (i.e., eliminating the possibility of tumour formation).

1.2.3 Mesenchymal Stem Cells

Nearly half a century ago, Friedenstein and colleagues [25] identified a population of osteogenic progenitors in guinea-pig bone marrow with their potential to grow in vitro as fibroblast-like colony forming unit (CFU-F). They exhibited spindle-shaped morphology and showed their capacity to form bone-like tissues in vitro. Based on these studies, further research on these cells demonstrated that they are capable of multi-lineage differentiation towards bone, cartilage or fat tissues [26, 27], which eventually led to their re-naming as mesenchymal stem cells (MSCs). For cell therapies and TE, human MSCs (hMSCs), have been used for more than a decade. Bone marrow is the main source of hMSCs ; however, skin [28], blood [29], fetal blood [30], adipose tissue [31], liver [30], lungs [32], trabecular bone [33] and tooth pulp [34] have also been reported as the sources of hMSCs. The multi-lineage differentiation potential of these cells have been studied extensively [35, 36]. Moreover, these cells could give rise to other non-mesodermal cells, such as neuronal [37], hepatic cell [38] and cardiac cells [34].

1.2.4 Immortalized Human Mesenchymal Stem Cells

Unlike ESCs, primary human MSCs (hMSCs) quickly develop senescence, after a few passages, in vitro, which seriously affect the efficiency of these cells as a tissue engineering tool, when long term in vitro culture is necessary. In order to overcome this problem, some immortalised hMSCs (ihMSCs) cell lines were developed, which exhibit higher proliferative ability than primary MSCs, without affecting their multi-lineage differentiation potential [39-41].

HMPC 32F is one of the first immortalized cell lines, developed by Osyczka et al. [42] who transduced hMSCs with human papilloma virus type 16 E6/E7 genes. The HMPC 32F cells expressed mature osteogenic-, chondrogenic- and adipogenic-phenotypes in culture for up to 20 passages [42]. Okamoto and colleagues [39] attempted to immortalize hMSCs via retrovirus-mediated gene transfer. The retrovirus transfected cells expressed higher degree of human telomerase reverse transcriptase (hTERT) activity than primary MSCs; however, only a limited number of cells were immortalized via this approach. Their alternate approach successfully immortalised the cells without affecting the multi-lineage potential, in which case, the cells were treated with hTERT together with human papillomavirus E6 and E7 [39].

1.3 Osteogenic Differentiation of hMSCs

The classical method of hMSCs differentiation into osteogenic lineage involves a cocktail formulation of dexamethasone (Dex), L-ascorbic acid 2-phosphate (AsAP) and β-glycerophosphate (BGP) [34, 43-45]. For many years, the mechanisms and signalling of Dex-induced osteogenesis were unknown. This

changed when Hamidouche and colleagues [46] revealed the existence of the specific protein domain (FHL_2) that mediates the Dex-induced differentiation MSCs into osteoblasts via the activation of Wnt/β-catenin signalling-dependant Runx2 expression. AsAP induces collagen biosynthesis and cell proliferation [47], whereas, BGP enhances calcified matrix formation [47].

A number of key factors and signalling pathways are involved in the maturation process of hMSCs into osteoblasts. Runt-related transcription factor 2 (RUNX2) is one of the factors, the expression of which indicates the progression of osteogenesis [48, 49]. Hence, the RUNX2 gene expression is usually analysed during the early phase of osteogenesis. Alkaline phosphatase (ALP) is another early osteogenic marker, which is responsible for ECM mineralisation [50]. The main component of ECM is collagenous (collagen type I). On the other hand, a mature osteoblast expresses smaller but significant amount of non-collagenous bone proteins, such as, osteopontin (OPN), osteocalcin (OCN) and bone sialoprotein (BSP) [51]. The expression of OPN and OCN are analysed at the early and late stage of osteogenesis, respectively.

1.4 Scaffolds in Tissue Engineering

1.4.1 Introduction

Scaffolds are one of the key components in tissue engineering that play an important role to guide cell behaviour via offering appropriate physical support and providing suitable microenvironment for the cells in order to facilitate tissue regeneration [3]. Scaffolds can be seeded with cells (embryonic or adult stem cells, tissue cells, progenitor cells or combination of cells) to induce tissue

formation, in vitro and/or in vivo. Alternatively, they can be used as carriers of bioactive molecules (e.g., drugs and proteins) or spatio-temporal cues, and can be directly implanted in vivo in order to enhance the regeneration of functional tissues at the defective body parts. Biological functions are influenced by scaffold properties, at molecular, cellular and tissue levels, with temporal and spatial dimensions ranging from seconds to weeks and nanometre- to centimetre- scales, respectively [52]. Understanding the correlation between biological events and scaffold properties is important in designing scaffolds for TE applications.

Figure **1.3** shows a schematic of the correlation between scaffold properties and tissue formation. It is understood that ECM play a vital role in guiding cells for tissue formation. In one hand, in setting the design requirements of artificial scaffolds, the micro-environmental features of ECM are taken under consideration; i.e., the same topographical and micro-environmental features, which is offered by ECM, are tried to mimic while designing a scaffold; which further necessitate the choice of a proper scaffold fabrication method. On the other hand, scaffolds are designed to offer a cellular microenvironment with the provision of nutrients and oxygen transport, waste removal and, to promote cell proliferation and differentiation. In order to assess the performance of the scaffolds, some in vitro and in vivo studies are done.

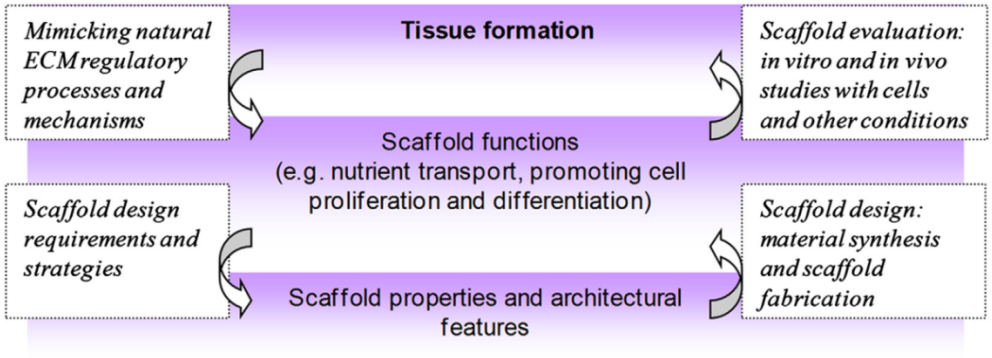


Figure 1.3 Correlation between tissue functions and scaffold properties. Reproduced from reference [53]

1.4.2 Mass Transport Function and Pore Architectures of Scaffolds

The mass transport function of a scaffold, is, what, affects the diffusion of nutrient and oxygen, and movement of cells in and out of the scaffold. All these functions (movement of fluid and cells) are also affected by the pore architecture of a scaffold, i.e., pore size, degree of porosity, interconnectivity or tortuosity of pores and surface area. At the beginning of cell culture on scaffolds, the chemical composition and pore architectures of the scaffold influence the mass transport. In the later stage, as the cell density is increased, the mass transport is influenced by the cellular microenvironment.

It has been demonstrated that in the case of the native tissues, most cells resided within 100 μm of a capillary; whereas, in engineered tissue constructs maintained in static culture, in vitro, the position of neo-tissue was within 100 – 200 μm of the scaffold periphery, possibly due the lack of fluid and nutrient flow in the scaffold interior [54-56]. It is important to note that these scaffolds were preformed and were of macro-sized 3D dimensions in millimetre scales. Due to the presence of macro-sized pores, cells can infiltrate into the scaffolds. However, oxygen supply in such macro-sized 3D scaffolds is limited within a maximum diameter of 200 μm, which limits the efficiency of these scaffolds for cell culture [57]. One solution to this problem is micro-vascularisation within the macro-constructs to facilitate oxygen diffusion. The other alternate is creation of micro-sized cellular constructs, which eventually would form macro-sized constructs. Building on the later strategy, many researchers have been interested in designing micro-sized scaffolds. These types of scaffolds are categorized as microparticles

(MPs) and they are generally spherical with a diameter of 100 – 400 μm [58]. Cells can be maintained within oxygen diffusion limits when they are cultured on these scaffolds/MPs.

Pore size of a scaffold influences the efficiency of the initial cell impregnation. For example, human placenta trophoblasts formed larger cellular aggregates, when the cells were seeded on fibrous poly (ethylene terephthalate) (PET) scaffolds with larger pore volumes between fibres [59]. Moreover, variations in the size of the cell aggregates also influenced the cell behaviour; the cell proliferative activities and differentiation were supressed in larger cell aggregates compared with the smaller ones [59, 60]

1.4.3 Surface Topography of Scaffolds

The surface topographical features of scaffolds, such as, grooves, steps and ridges play an important role in cytoskeletal assembly, cell adhesion and proliferation. In general, cell adhesion, proliferation and migration increase with increasing the surface roughness. For example, hMSCs adhesion and proliferation on the surface of the alpha-tri calcium phosphate (α-TCP) with di calcium silicate (DCS) scaffold (α-TCP-DCS) were surface roughness-sensitive [61]. As demonstrated in the paper, the cell viability and proliferation were higher with the rough surfaces in comparison with the smooth surface. As shown in Figure 1.4, the cell adhesion and proliferation are higher on the rough (unpolished) surfaces of α-TCP-DCS scaffolds.

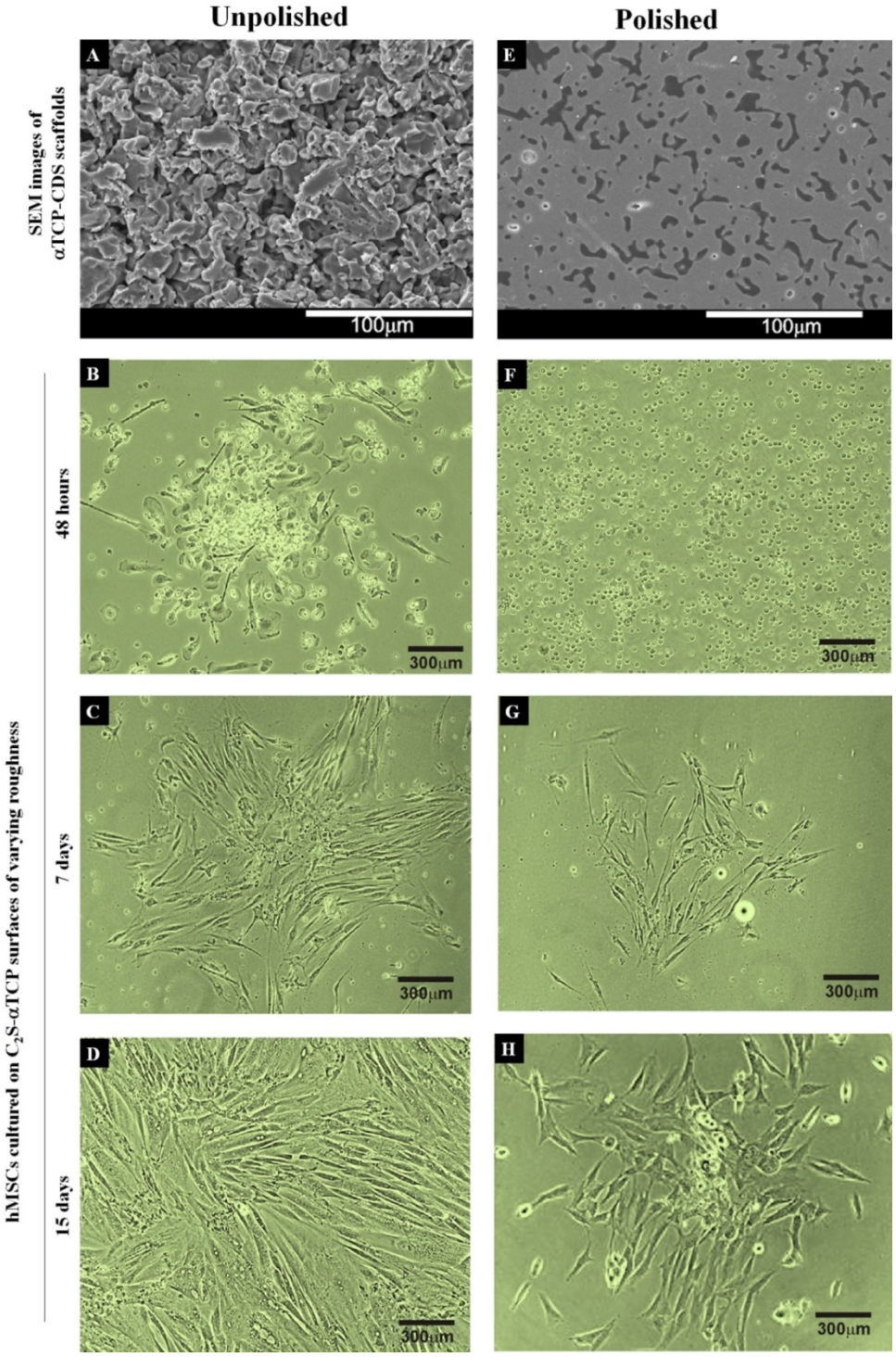


Figure 1.4 hMSCs cultured on unpolished **(A-D)** and polished **(E-H)** surfaces of α-TCP-CDS scaffolds. The cell adhesion and proliferation were higher on the rough (polished) surfaces. The images were adapted from reference [61].

On the other hand, scaffolds with porous or non-porous topography have an influence on cell behaviour. A considerable numbers of studies demonstrated that cells can grow and expand more efficiently on porous surface than on non-porous surfaces [62-65]. As an example, porous PLGA/$PEI_{1.8k}$ MPs (PPPMPs) exhibited better attachment of rat MSCs (rMSCs) than non-porous PLGA/$PEI_{1.8k}$ MPs (NPPMPs), when the cells were cultures in vitro with both porous and non-porous MPs [62]. The surface topographies of the MPs are shown in Figure 1.5.

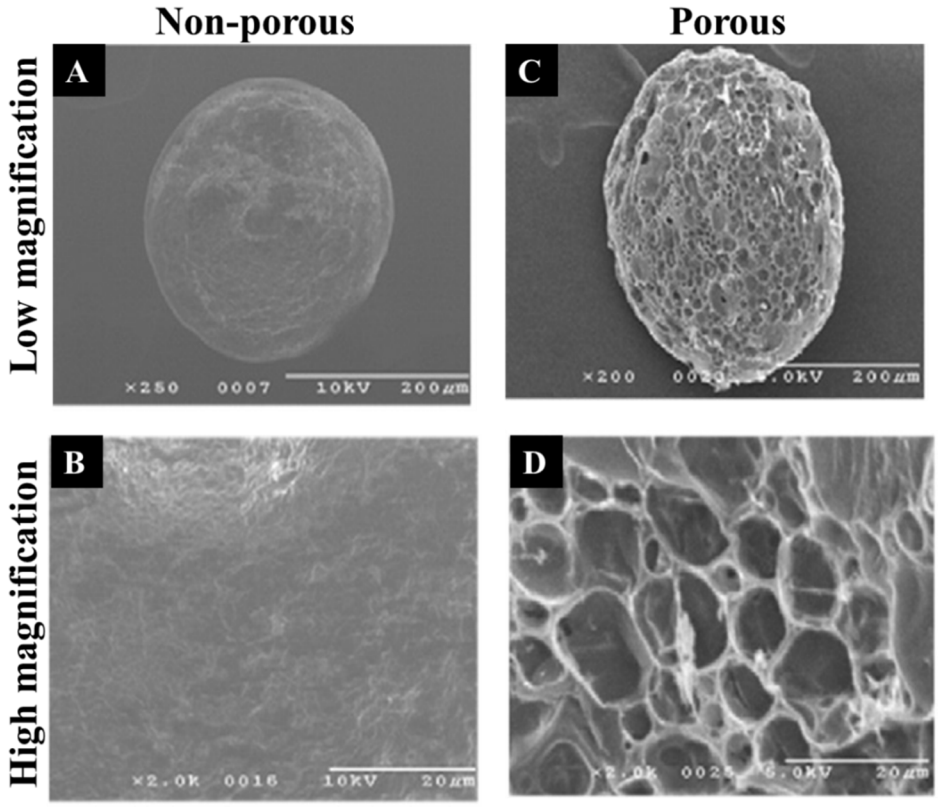


Figure 1.5 Surface topography of non-porous PLGA/$PEI_{1.8k}$ **(A – B)** and porous PLGA/$PEI_{1.8k}$ **(C-D)** scaffolds. The images were adapted from reference [62]

1.5 Microparticles as Scaffolds

MPs have recently received considerable interest as scaffolds in TE [66, 67]. The other scaffolds (macro-sized and preformed) possess specific dimensions of a millimetre or centimetre scale and for tissue engineering purposes, cells are impregnated with the macro-sized scaffolds; whereas, polymeric MPs are used as discrete micro-sized scaffold particles, i.e., cells are allowed to grow on individual MP. They can also be used as carriers of bioactive molecules [68] to facilitate tissue regeneration through the controlled release of the encapsulated molecules [69, 70]. For TE applications, cells can be seeded with blank or bioactive molecule-loaded MPs. Another MP-based TE strategy is to inject blank MPs (acellular MPs) to the injured site to fill the gap formed due to trauma or disease (e.g., tumour excision). Some of the MP-based tissue engineering strategies are schematically shown in Figure 1.6.

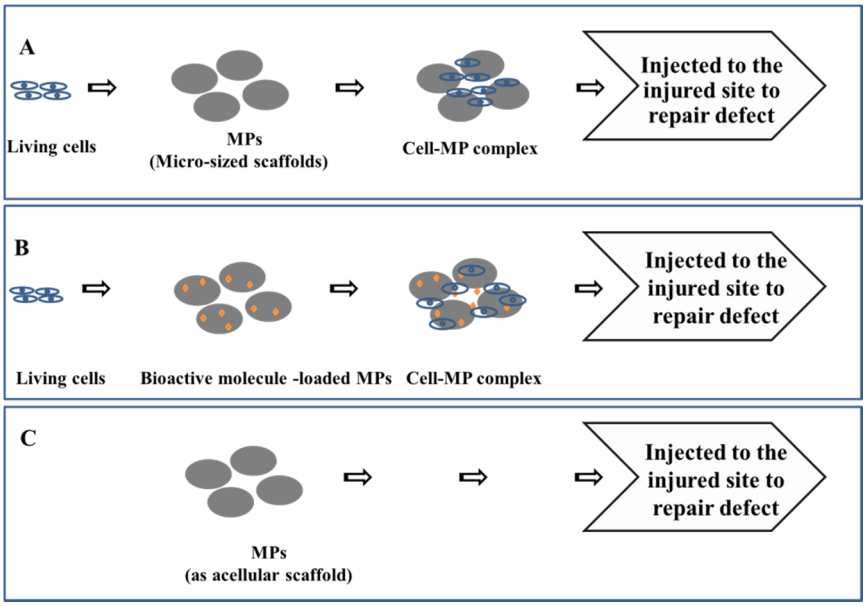


Figure 1.6 Some of the MP-based tissue engineering strategies. **A)** cells are seeded on MPs and the cell-MP complexes are injected to the injured site for tissue regeneration; **B)** cells are seeded on bioactive molecule-loaded MPs and the cell-MP aggregates later implanted to the injured body part for tissue regeneration; **C)** blank MPs are injected to the injured site to fill the gaps formed due to trauma or disease and encourage the host cells to migrate to the MPs.

As stated in section 1.2.1, scaffolds are one of the key components required for TE strategies. Scaffolds mainly provide the mechano-architectural support for the cells [5]. Moreover, they help to encourage the appropriate cell behaviour and signalling via cell-extracellular matrix (ECM) and cell-cell interactions [71]. Furthermore, scaffolds must provide a suitable microenvironment for the maintenance of the cellular phenotype and expression of the appropriate proteins, molecules and growth factors for the specific tissue function [5, 71]. Apart from these, scaffolds and their bi-product should be biodegradable so that ECM deposition and tissue formation by the host cells are facilitated over time. The rate of degradation of a scaffold is mainly governed by the chemical properties of the material that is used to prepare the scaffold. Moreover, the overall geometry and surface topography also affect the degradation pattern of a scaffold Therefore, the success of scaffold-based tissue regeneration primarily depends on the their macro- and micro-scale characteristics, including the surface topography (e.g., surface roughness, size, shape and porosity), hydrophobicity, hydrophilicity and surface charges [72].

1.6 Material Selection for Microparticle Preparation

The materials, that are used to prepare MPs for TE applications should meet several criteria. Firstly, they should be biocompatible, so that they can encourage cell viability, proliferation, migration and differentiation. Secondly, the materials as well as MPs (that are fabricated using the material) should possess appropriate mechanical properties for promoting cell survival and tissue regeneration. Thirdly, the materials and their bi-products should be non-toxic, non-inflammatory and non-immunogenic to the biological system. Apart from these, the physicochemical properties of the material should favour their easy manipulation and modification, so that diverse range of MPs with different size, shape and topography can be prepared as is required for a particular TE application.

Wide varieties of materials are available that can be used to prepare MPs. Depending on their chemical properties, all of the materials can be categorised as follows: 1) metals; 2) ceramics; 3) synthetic polymers; 4) natural polymers and 5) composite biomaterials (e.g., metal-synthetic polymer -, synthetic-natural polymer- and natural polymer-ceramic -composite).

Synthetic polymers are widely used in tissue engineering due to their easily controllable and modifiable physicochemical properties [73]. For the purpose of using in regenerative medicine applications, varieties of synthetic polymers are used, ranging from poly (anhydrides), poly (esters), poly (orthoesters) and poly (phosphazenes) [73]. Among these polymers, some of the poly (α-hydroxy esters) group, namely, poly (lactic acid) (PLA), poly (glycolic acid) (PGA) and their co-polymer (poly[lactide co-glycolide]) (PLGA) have been most frequently used in

the field of TE, as they are biocompatible and FDA (US Food and Drug Administration) approved [74]. See Figure 1.7 for the chemical structure of the polymers. It is well established that in the physiological environment, these polymers are gradually broken down into the respective water soluble monomer (s) and degraded via hydrolytic degradation, which eventually are removed from the body via normal metabolic pathways [75].

For more than a decade, PLGA have been used as scaffold in TE applications. In the beginning of this century, Yang and colleagues demonstrated that some of human osteoprogenitor cells exhibited good cell adhesion, proliferation and osteogenic differentiation when they were cultured on preformed peptide- and protein-coupled PLGA scaffolds [76]. Nearly at the same time, other researchers [77-79] have demonstrated that the viability, proliferation and osteogenic differentiation of human osteoblast cells were good when the cells were cultured with PLGA scaffolds of different surface properties, such as protein- or hydroxyapatite (HA)-coated. In two other recent studies, Bible et al.[80] and, Rahman and colleagues [81] demonstrated the potential of growth factor loaded PLGA scaffold for neuronal and bone tissue regeneration, respectively. 'Injectabone' is a novel PLGA-based scaffold system which can be used for the treatment of bone trauma by injecting the scaffold directly to in the affected bone [82]. Some other examples of PLGA MP-based scaffold systems that exhibited bone regenerative potential were reported by Kirby and associates [83], Ji and colleagues [84] and Fu et al. [85].

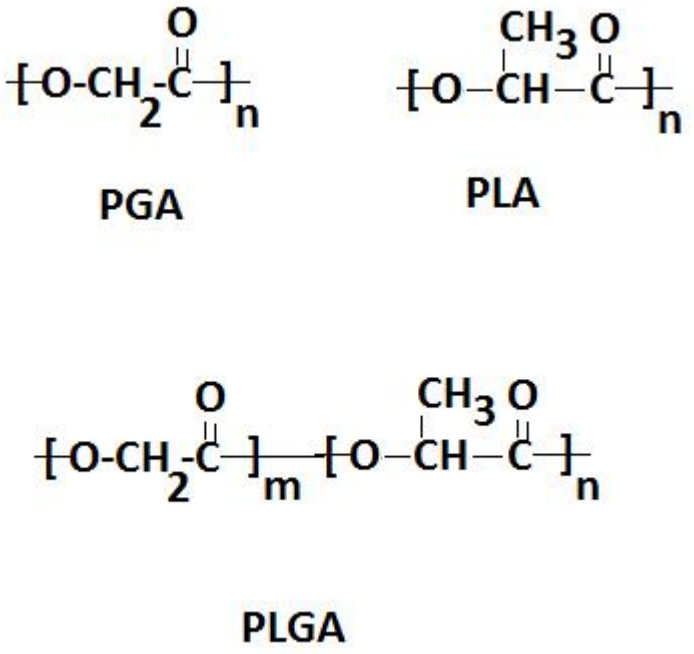


Figure 1.7 Chemical structures of PGA, PLA and their co-polymer (PLGA).

1.7 Porous Microparticles as Scaffolds in Tissue Engineering

Porous MPs (Por-MPs) have pores on their surface as well as in the core of the MPs and the pore are usually interconnected. A cross-linked polystyrene with macro-porous geometry was prepared in the 1950s using a novel polymerisation method [86]. However, the real progress on the use of Por-MPs, in biomedical field, started in the 1990s, when these MPs were identified as suitable candidates for drug delivery and TE applications [63]. For TE applications, Por-MPs are preferred over solid MPs (Sol-MPs) for a number of reasons. Firstly, cells can be cultured more efficiently on Por-MPs than on Sol-MPs, as evidenced from enhanced cell viability, proliferation and differentiation for the former type of MPs [62, 64]. Secondly, due to the presence of pores in Por-MPs, the diffusion of soluble factors (e.g., nutrients and cytokines) and oxygen, and removal of toxic wastes are facilitated. Thirdly, these MPs may not require further coating with cell-adhesion proteins or chemical modification for using as microcarriers of cells. Apart from these, it has been reported that by a simple wet-sintering method, Por-MPs can be made into highly porous macro-sized scaffold [70]. On the other hand, alike other MPs, these can be injected via narrow needle either alone or as a cell-MP complex. A considerable number of studies demonstrated that cellular adhesion, proliferation, migration and, matrix deposition largely are affected by the pore size, shape and pore-volume [64, 87-89].

1.8 Polymeric Microparticle Fabrication Methods

1.8.1 Conventional Emulsification

Although a number of methods have been used for the preparation of MPs, emulsion-solvent evaporation is the most widely used and conventional method for polymeric MPs preparation. The method was first introduced by Ogawa and colleagues [90], who prepared drug-loaded PLA and PLGA MPs on the basis of the principle that MPs can be harvested from the respective polymer droplets via evaporation of the organic solvent retaining the polymer into a larger volume of solvent with opposing solubility. A simple version of the method is termed as single emulsion, which is usually used to prepare pure polymeric MPs [91, 92] and in rare cases for preparing drug loaded-MPs [93, 94]. In the single emulsion method, a polymer is dissolved in an organic solvent and then emulsified with a larger volume of a solvent of opposing solubility containing an emulsion stabiliser. The emulsion is then kept stirring until the organic solvent is completely removed and the MPs hardened. Subsequently, the solidified MPs are harvested via centrifugation or filtration and lyophilisation. In some cases, the MPs are sieved for obtaining a desired size fraction from the original MPs.

On the other hand, for preparing drug-loaded polymeric MPs, double emulsion method is the most extensively used method [68, 74, 83, 95, 96]. Double emulsion is sometimes named as ‘emulsion-in-emulsion’, in which case the disperse phase of the final emulsion is itself an emulsion [96]. In order to prepare protein or drug loaded MPs, either a water-in-oil-in-water (w/o/w) or solid-in-oil-in-water (s/o/w) template of double emulsion is used. In the case of the s/o/s

emulsion, a drug or protein is homogenised in a polymer solution to form a primary emulsion, which is then homogenised in a solvent of opposing solubility to form a secondary emulsion. The emulsion is then kept stirring for evaporation of the organic solvent and hardening of the MPs. The harvesting process is the same as is used for harvesting of the pure MPs. Porous MPs are prepared via w/o/w double emulsion method. A schematic of the process of double emulsion is shown in Figure 1.8.

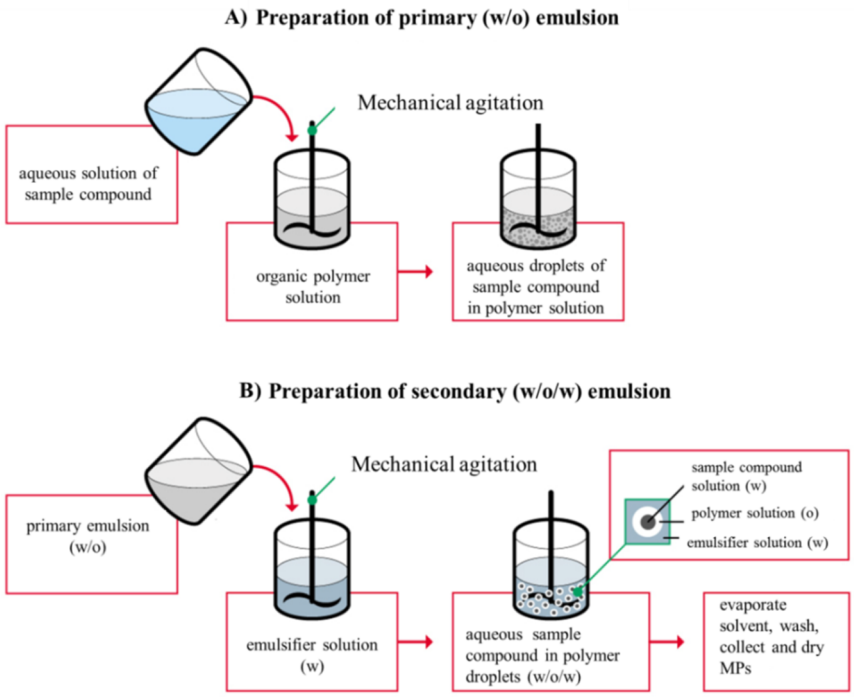


Figure 1.8 Schematic of a double emulsion method for preparation of drug-loaded or porous polymeric MPs. **A)** the compound (drug or pore forming agent) is homogenised with a polymer solution, which resulted in a primary (w/o) emulsion. **B)** the primary emulsion is then homogenised with a emulsion solution (aqueous), which resulted in a secondary (w/o/w) emulsion; evaporation of the solvent, washing out of the MPs and lyophilisation (drying) yield drug-loaded or porous MPs. The figure is reproduced from reference [92] with slight modificaiton.

The MPs that are prepared via these conventional emulsification methods are usually polydisperse. Therefore, to obtain a MP sample with a tighter size distribution from these polydisperse populations, the original MP population is fractioned using a sieve, which sometime results in up to 50% loss of the yield [69, 87].

For preparation of porous MPs, the w/o/w emulsion template is used. In this case, a pore forming agent, which is usually water soluble, is homogenised with a polymer solution to form a w/o primary emulsion. The primary emulsion is then homogenised with water containing an emulsion stabiliser, which results in w/o/w secondary emulsion. During the process of the organic solvent evaporation, the internal water droplets are released in the outer water phase and pores are generated in the solidified MPs. Several pore forming agents or porogens have been reported for the preparation of the porous polymeric MPs, namely, effervescent salts (e.g., ammonium bicarbonate [NH_4HCO_3]), inorganic salts (e.g., sodium chloride), linear polymers, hydrocarbon waxes, carbohydrates, gelatine and ice [97-99]. As an example, Shi and co-workers [87] used NH_4CO_3 as a porogen, to prepare porous PLA MPs with varying pore sizes. Varying the concentration of the polymer, the degree of porosity in the MPs varied (See Figure 1.9). The porosity of the original MPs was improved by a surface treatment using sodium hydroxide (NaOH) solution. The original MPs were polydisperse and they had to sieve the MPs, post fabrication, for achieving a sample with a diameter of 150–250 μm, for the cell culture study.

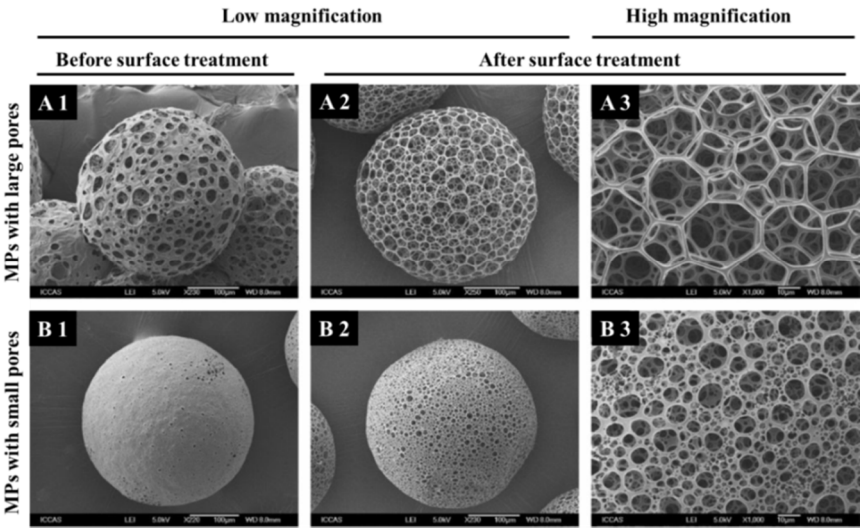


Figure 1.9 Porous PLA MPs prepared via w/o/w double emulsion-solvent evaporation method. The MPs were prepared using smaller **(A1 – A3)** and larger **(B1 – B3)** amounts of the PLA solutions. As a pore forming agent, NH_4HCO_3 was used. The image were captured at low **(A1, A2, B1 and B2)** and high **(A3 and B3)** magnification. The images are reproduced from reference [87].

1.8.2 Membrane Emulsification

1.8.2.i Introduction

Although conventional emulsification methods (single or double emulsion) are widely used for preparation of polymeric MPs, the resultant MPs are usually polydisperse and demand sieving, post fabrication for obtaining MPs with a desired diameter. On the other hand, there are some specialised methods that can be used for preparing monodisperse MPs. De La Vega and co-workers [100] have categorised all the specialised methods into two groups: 1) Monomer-based preparation method and 2) preformed polymer-based preparation method. In the monomer based preparation method, the starting material is a monomer, whereas, polymer is the starting material in the case of the preformed polymer-based preparation method. In the case of the monomer-based preparation method, as the MPs are prepared via a synthesis route, a further purification step is necessary in order to ensure an efficient use of the MPs for biomedical applications. Moreover, in a lab-based synthesis, usually a small amount of starting material is used in order to keep the production cost at a minimum level; which results in a small yield of the final product. On the other hand, the preformed polymer-based preparation method is further categorised as single- and multi-channel systems. In the case of the single-channel system, emulsion droplets are formed through a single channel or pore. Conversely, multiple emulsion droplets are formed at a time via multiple channels or pores. As such, the yield of the MPs produced using the multi-channel system is higher than that obtained using the single-channel system, due to the ‘drop-by-drop’ emulsion formation phenomenon of the later system [101]. A schematic of the single- and multi-channel system is shown in Figure 1.10. Both systems follow a common principle of passing a polymer

solution or disperse phase (DP) via microchannel(s) or pore(s) into a running continuous phase (CP) in order to form an emulsion with a controlled droplet size distribution.

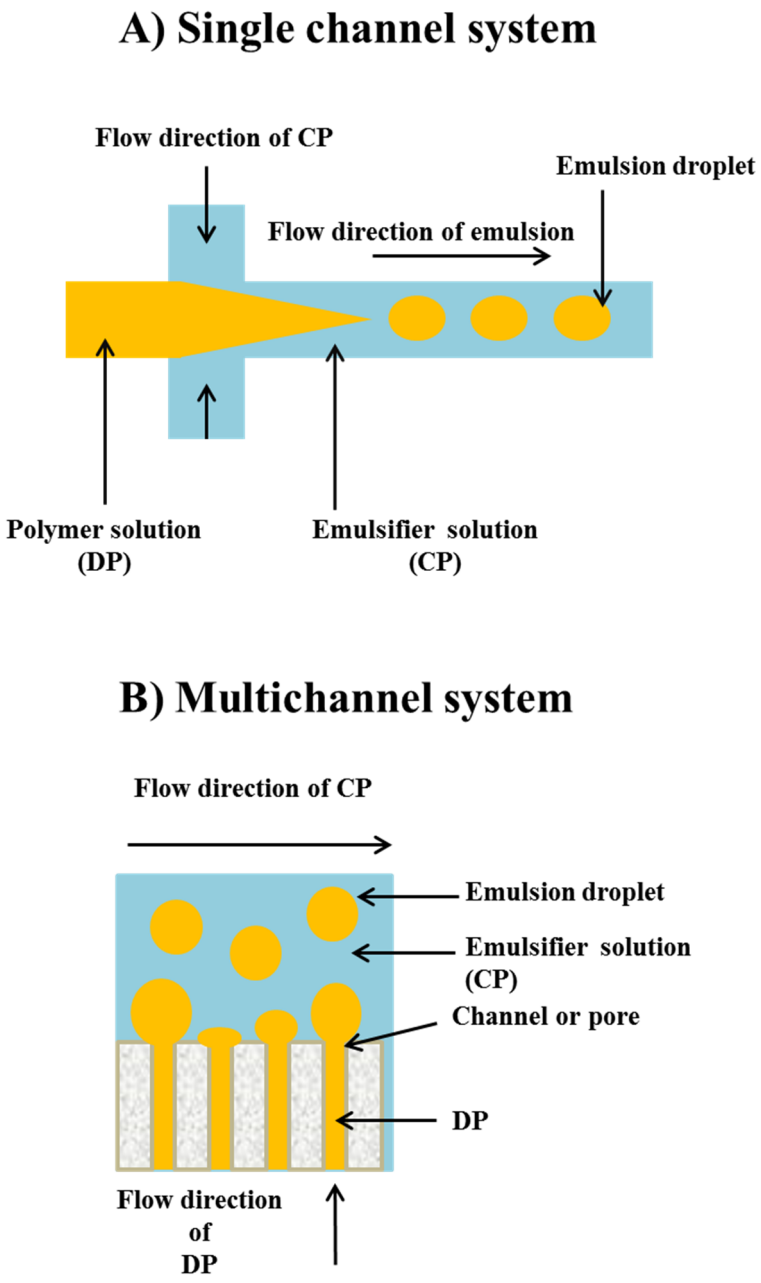


Figure 1.10 A schematic of monodisperse MP fabrication via single- and multi-channel systems. A drop-by-drop emulsion formation is occurred in the case of the single channel system **(A)**, whereas, multiple emulsion droplets are formed at a time via the multi-channel system **(B)**.

One of the most commonly used multichannel systems is membrane emulsification (ME). A single- or double-emulsion template is used in the case of the ME method. A controlled production of polymer droplets is occurred following the 'made-to-measure' principle. Depending on the experimental set up, the ME method is further categorised as: 1) direct emulsification (DE) and 2) premix emulsification (PE). A schematic X-ME and PE are shown in Figure 1.11 In case of DE, a polymer solution or primary emulsion is passed through a multi-porous membrane under a low pressure nitrogen gas and the emulsion droplets are detached into a running CP. Droplet detachment is facilitated by the shear caused by the running CP. Due to the flow direction of DP and CP in DE, this process is many occasions are named as cross-flow ME (X-ME). On the other hand, in case of PE, a pre-formed emulsion with irregular-shaped droplets is passed through a membrane under a high pressure of nitrogen gas. In this case, no cross-flow of CP is maintained. A schematic of DE and PE method is shown in Figure 1.11

Nakashima and co-workers [102] are the pioneers of the ME process, who used a X-ME set up for preparing simple oil droplets using a microporous glass membrane and they demonstrated the potential of this method for preparation of more complex emulsion (e.g., w/o/w or o/w/o emulsion)developed by Nakashima et al. [102]. Other than glass, metal, ceramic and polymers have also been used as the membrane materials [103]. However, one of glass type membrane, Shirasu Porous Glass (SPG) membrane has been most widely used. These membrane possesses the advantages of narrow pore size distributions, a wide range of available pore sizes (0.05 – 50 μm), and superior thermal stability [104]. Furthermore, SPG membranes have been used to prepare both single and double

emulsions [105, 106] which could be used for preparing both solid and porous MPs, following the o/w and w/o/w emulsion techniques respectively, using the same membrane.

1.8.2.ii Cross-flow Membrane Emulsification for Preparation of Large MPs

1.8.2.ii.a Introduction

As stated in section 1.8.2.i, there are two types of emulsification set up, one is X-ME and the other is PE. In PE set up, the formed emulsion droplets size could be equal to or smaller than the membrane pore size. This emulsification set up has been preferred for preparing MPs with a diameter of 20 μm or lower [107-112]. As such, this set up is not suitable for preparation of MPs with a diameter of above 50 μm. Moreover, in order to achieve an emulsion with a narrower size distribution, the same emulsion needs to pass repeatedly through the membrane [108, 113]. It is important to note that the MPs which serve as carrier of cells should to be at least larger than cells, so that cells can adhere and proliferate on top of the MPs. A considerable number of literature suggest MPs with a diameter of above 50 μm for purpose of using those as stem cell microcarriers [80, 87, 92]. In order to prepare MPs with a diameter of 50 μm or above, X-ME could be the method of choice. It has been reported that MPs with a diameter of three to ten times larger than a membrane pore size could be achieved using X-ME [114, 115]. As stated in section 1.8.2.i, the largest available membrane pore diameter is 50 μm, which could be used for preparation of MPs with a diameter of at least three times larger than the membrane pore diameter.

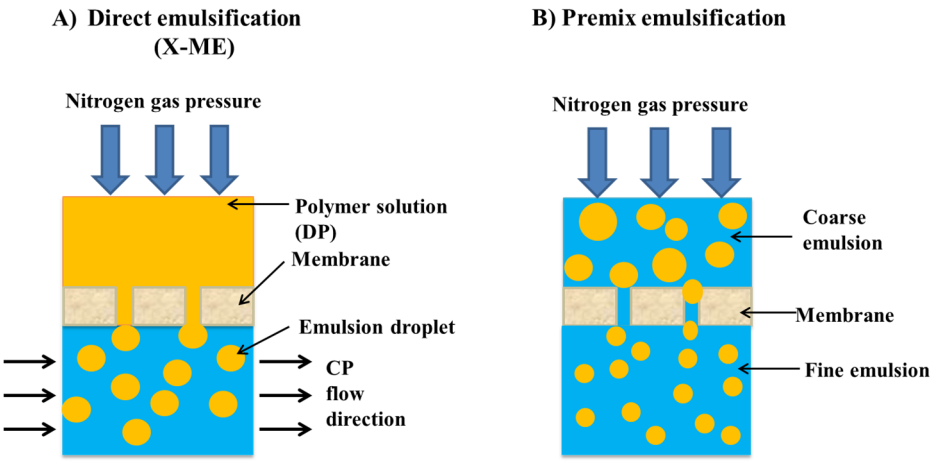


Figure 1.11 Schematic of **A)** direct emulsification (X-ME) and **B)** Premix emulsification. In case of X-ME, CP flow is maintained cross-way to the flow of DP, whereas, no flow of CP is maintained in the case of the premix emulsification**.**

1.8.2.ii.b Factors affect Size of MPs Prepared via X-ME

The size and size uniformity of emulsion droplets formed via X-ME are governed by a number of factors, such as membrane pore size (D_0) [102, 116], working pressure (P_w) [102, 116], DP concentration ($Conc._{DP}$), emulsifier concentration ($Conc._{CP}$) [117], flow rate of CP (V_{CP}), viscosity of DP (η_{DP}) [118, 119], viscosity of CP (η_{CP}) and DP/CP volumetric ratio ($\varphi_{DP/CP}$). Although each factors has its own effect on the size of the MPs, the effect of one factor is influenced by the other factors. For example, the larger the membrane pore diameter, the larger the emulsion droplets [120, 121]; however, using a membrane with a specific pore diameter, MPs with varing size and size uniformity could be prepared by altering the P_w [122]. Furthermore, using a certain P_w and a membrane with a specific D_0, MPs with different size and size uniformity could be prepared by changing $Conc._{CP}$. From the overall understanding about the factors related to X-ME, it is reasonable to asume that a co-ordication among different factors is necessary in order to investigate the optimal emulsificaiton conditions for prepering MPs with some particular properties. To be more specific, in order to obtain MPs with a certain size and size distribution using a specific polymer, optimisation of the emuslion conditions is necessary. As such, understanding the effect of each of the facotrs on the size and size distribution is pivotal.

1.9 Aims and Objective of the Study

As discussed in earlier sections, MPs are one of the types of scaffolds used as carriers of stem cells in TE applications. The cells are encouraged to grow on discrete MPs and the cell-MP complexes are injected to the targeted site via

minimally invasive surgical procedures. Conversely, the other scaffolds (macro-scaffolds), due to their large size, cannot be injected via narrow bore needles. Among the MPs of different surface properties, porous MPs (Por-MPs) are preferred over solid MPs (Sol-MPs) for several reasons. Firstly, diffusion of nutrients and oxygen in the environment, where cells reside in, are facilitated when the cell supporting materials are porous. Secondly, removal of waste products from Por-MPs becomes easier. Thirdly, the pores could facilitate tissue ingrowth and vascularisation. Moreover, the porous architecture makes the MPs lighter and as such, a less amount of by-product is generated from the degradation of the MPs. Furthermore, the degradation of Por-ME MPs could be faster than that of Sol-MPs. However, for preparation of MPs, the most commonly used method is conventional emulsification (CE). Though this method is simple and could be used to prepare MPs of a range sizes, the size distribution of the MPs are usually polydisperse; which could compromise the efficacy of the MPs as cell delivering vehicles. Use of MPs with an expected mean diameter and a narrower size distribution could increase the efficiency of the MPs. As described in earlier sections, X-ME can be a useful technique for preparation of MPs with expected sizes and narrower size distributions.

There are three distinct aim of this study. The first aim is to evaluate the efficiency of Por-MPs prepared via CE (Por-CE MPs) as microcarriers of hMSCs. The second aim is to investigate the feasibility of X-ME for preparation of large, porous polymeric MPs. The third aim is to evaluate the novel porous MPs prepared via X-ME (Por-ME MPs) for hMSC delivery applications. Several objectives are set under each aim. A schematic of the overall study aims and

objectives are shown in Figure 1.12 Schematic of the study flow diagram. As shown in the figure, the study began with the evaluation of the Por-CE MPs as carriers of MSCs. Suitable culture conditions, including the cell and MP densities were investigated. In the next phase of the study, an optimal method for preparation of monodisperse Sol-MPs, with a mean diameter of approximately 100µm, using X-ME (Sol-ME MPs) was developed. Subsequently a method for the preparation of porous Por-ME MPs was developed. In the last phase of the study, the novel porous MPs (Por-ME MPs) were evaluated for hMSCs delivery applications.

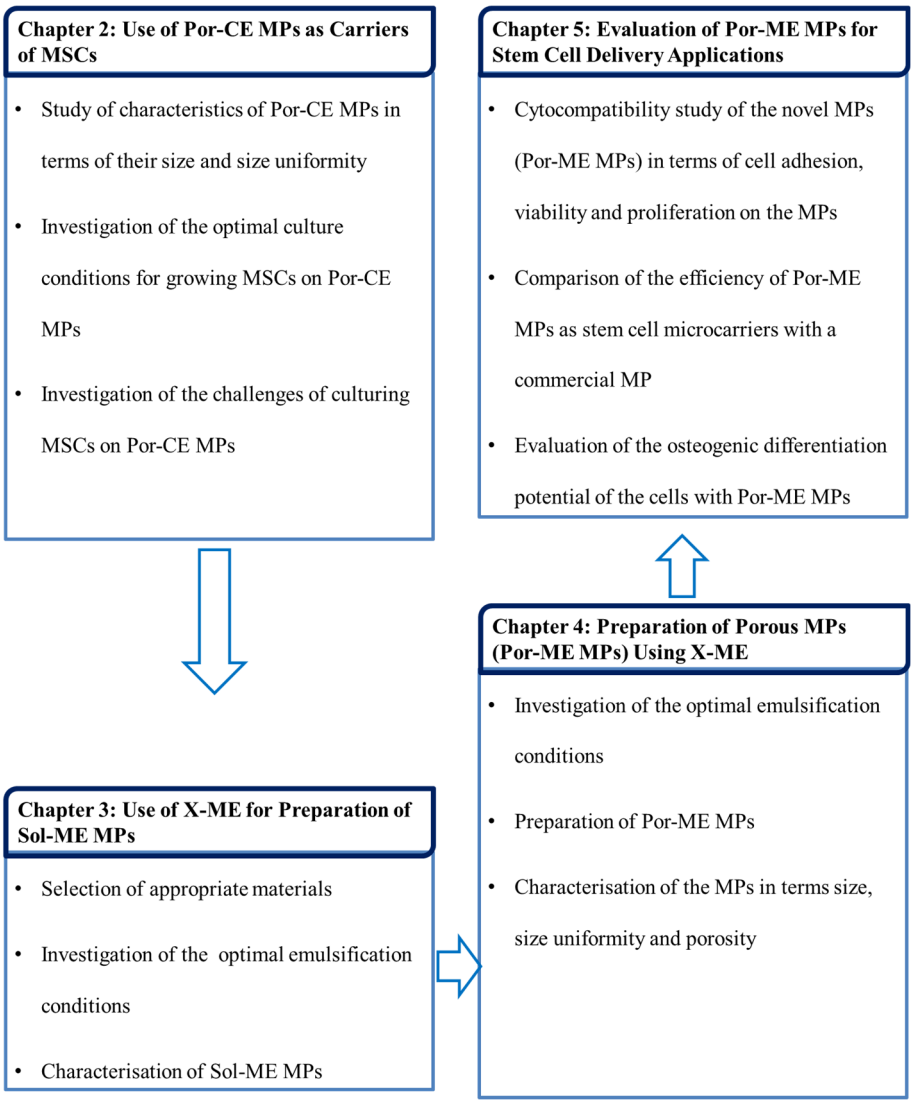


Figure 1.12 Schematic of the study flow diagram.

Chapter 2 Large, Porous Poly (Lactide-Co Glycolide) Microparticles as Injectable Cell Delivering Vehicles

2.1 Introduction

In tissue engineering, one of the strategies is to deliver living cells together with scaffolds to damaged or injured body parts and then induce cell proliferation and differentiation for the purpose of regenerating functional tissues [123], such as bone [124, 125], nerve [80] and skin [126]. Scaffolds, biological constructs or cell-delivery vehicles mainly serve as mechano-architechtural supports for the cells [5]. In addition, they help to encourage the appropriate cell behaviour and signalling via cell-extracellular matrix (ECM) and cell-cell interactions [71]. Furthermore, scaffolds must provide a suitable microenvironment for the maintenance of the cellular phenotype and expression of the appropriate proteins, molecules and growth factors for the specific tissue function [5, 71]. Therefore, the success of scaffold-based tissue regeneration primarily depends on the macro- and micro-scale characteristics of scaffolds, including the surface topography (e.g., surface roughness, size, shape and porosity), hydrophobicity, hydrophilicity and surface charges [72]. Porosity in a scaffold facilitates diffusion of nutrients and oxygen throughout the scaffold and helps removal of waste products from the scaffold-cell system [62]. Porous scaffolds are also expected to facilitate ingrowth of the host capillary and vascularization. Until now, extensive research has shown many effects of the aforementioned scaffold characteristics on cells [72, 127]; however, appropriately designed scaffolds for repairing irregularly shaped tissue defects with minimally invasive surgical intervention are still required [89]. In

this context, injectable scaffolds are of great interest over non-injectable scaffolds. Ideally, they should fill defects of varying sizes and shapes, irrespective of the patient-specific anatomical position. Additionally, to meet the criteria of minimal invasiveness and discomfort to the patient, they need to be delivered via a narrow bore needle [128].

Scaffolds have been prepared from either natural (gelatine [129], chitosan [130] , alginate [131] and collagen [126]) or synthetic (polycaprolactone[132], poly lactic acid [132] and poly-lactide-co-glycolide (PLGA) [80]) polymers. Both types of polymers possess characteristic differences in terms of their merits and demerits. For instance, the synthesis and molecular uniformity of the synthetic polymers can be better controlled, and there is little concern about their potential immunogenicity [133]. However, due to the absence of bioactive molecules or ligands and the lack of intrinsic porosity, these polymers, in many cases, require either surface treatment [80], an introduction of bioactive molecules [83], a composite formation with bioactive molecules [62] or the development of a manufacturing method in order to obtain a porous structure [133, 134] to increase the efficiency of the scaffolds. Based on the strategy of developing a scaffold with a porous structure for cell delivery, porous polymeric microparticles (Por-MPs) have started to attract interest in the field of tissue engineering.

The double emulsion-solvent evaporation method is commonly used for the preparation of Por-MPs [63]. In this method, a type of porogen or pore-forming agent is incorporated in the internal phase. During the MPs hardening process, the

porogen is leached out into the outer phase, leaving many hollow spaces in the MPs to make them porous. MPs-based injectable scaffolds (Inj-MPs), in many instances are fused together to form macro-sized 3D porous matrices, and cells are then seeded on the preformed matrices [70, 135]. However, these types of scaffolds are not suitable to fill irregular-shaped defects because of their pre-designed macro shapes. In contrast, cells seeded on individual micro scaffold particles are expected to adopt the precise shapes of different lesion cavities as they have the potential of delivering via narrow bore needles [69]. Designing such scaffolds is still challenging due to the rapid clumping of MPs after fabrication, inhomogeneous distribution of cells over individual MPs and inconsistent delivery of cell-particle systems via fine needles [92].

Researchers at the University of Nottingham have been working for over a decade on different types of injectable scaffolds, including Inj-MPs [136-138]. Porous PLGA MPs are one of the injectable systems recently developed by Qutachi et al. [70] at this university. The authors demonstrated the formation of a 3D porous scaffold using the MPs, which were then, seeded with mouse 3T3 fibroblast cells followed by assessment of cell attachment and viability.

The first major aim of the work presented in this thesis was to thoroughly investigate the characteristics of the porous PLGA MPs in terms of their size, size distribution, symmetry of distribution and porosity. Study of the degree of symmetry of distribution of a MP sample gives useful information about the fraction of smaller or larger MPs in the sample and helps in determining the

efficiency of the MPs for a particular application. In terms of sizes of MPs, most of the researchers have demonstrated the average diameter (± SD) and presented the size distribution curve. In this study, in order to investigate the degree of symmetry of the distribution, 'skewness' and 'kurtosis' (two statistical parameters) were incorporated, in addition to the mean (± SD), medium and mode values of the MPs.

A further aim of this study was to assess the feasibility of these MPs (Porous PLGA MPs) as injectable stem cell microcarriers. In order to do this, it was necessary to optimize the cell-seeding method and study the cell viability in different culture conditions to investigate the optimum culture condition. Moreover the cytocompatibility of these MPs was also assessed.

2.2 Materials and Methods

2.2.1 Equipment, Consumables and Materials

A detailed description of each of the materials used for the work described in this chapter is presented in Appendix I as Table AI-1, Table AI-2 and Table AI-3 for equipment, consumables and general chemicals/reagents, respectively.

2.2.2 Fabrication of Large Solid PLGA Microparticles

Solid PLGA MPs (Sol-MPs) were fabricated using the oil-in-water (o/w) single emulsion-solvent evaporation method. A schematic of the method is shown in Figure 2.1. A total mass of 1 g of PLGA was dissolved in 5 mL of dichloromethane (DCM; Fisher Scientific, Loughborough, UK). The polymer

solution was then emulsified with an aqueous solution of 0.3 % w/v poly (vinyl alcohol) (PVA; Sigma-Aldrich, Poole, UK) using a high-shear homogeniser (Silverson L5M, Silverson Machines Ltd., Chesham, UK) at 3000 rpm for 2 minutes. The resultant emulsion was then stirred magnetically (Variomag POLY 15, Thermo Scientific, UK) at 300 rpm for 4 hours to allow the complete evaporation of DCM and hardening of the MPs. The MPs were then allowed to settle for 30 minutes, the supernatant PVA solution was carefully removed and the rest of the MP-PVA suspension was transferred into a 50 mL centrifuge tube and centrifuged at 4500 rpm for 5 minutes. The MPs were then washed twice using dH_2O (double distilled water). After the final wash, the extra liquid was removed by centrifugation followed by decantation and the tube was then covered with a piece of laboratory blue tissue (Blue roll, Fisher Scientific UK Ltd.), snap frozen in liquid nitrogen and freeze dried (Freeze drier, Edward Modulyo D, IMA Edward, UK) for 48 hrs. The sample weights were measured after drying to obtain the percentage yield. They were then transferred into a 20 mL glass scintillation vial (VGA-050-300P; Fisher Scientific UK Ltd) and after closing the lid; the vial was placed in a sealable bag, sealed under vacuum using a vacuum packer (Orvid VM03, Scientific Laboratory Supplies Ltd.) and stored in a freezer (LabCold, Fisher Scientific UK Ltd.) until future use.

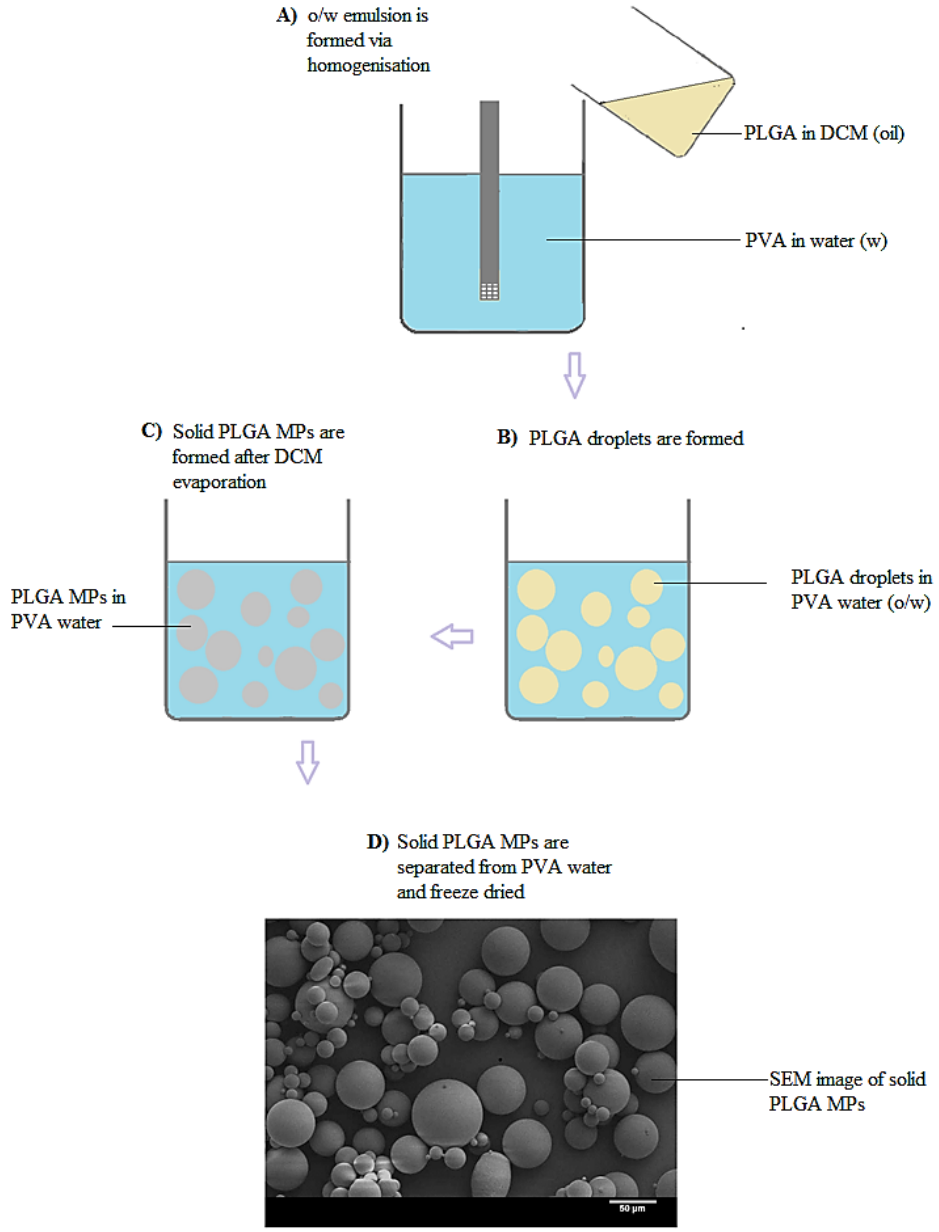


Figure 2.1 Schematic of the preparation of the solid PLGA MPs.
A) PLGA solution in DCM (o) is homogenized with 0.3 % w/v PVA (w) using a high shear homogenizer; **B)** PLGA droplets in PVA-water (o/w) emulsion is formed; **C)** subsequent stirring of the o/w emulsion at 300 rpm for 4 hours yields solid PLGA MPs; **D)** the MPs are then separated from water by centrifugation, washed three times with water and freeze dried to obtain solid PLGA MPs.

2.2.3 Fabrication of Large, Porous PLGA MPs

Porous PLGA MPs (Por-MPs) were fabricated using the water-in-oil-in-water (w/o/w) double emulsion-solvent evaporation method, as depicted in Figure 2.2. Briefly, 1 g of the PLGA mass was dissolved in 5 mL of DCM and then homogenised with 250 µL of phosphate buffer saline (PBS; Fisher Scientific UK Ltd) at 9000 rpm for 2 minutes using a high-shear homogeniser to form water-in-oil (w/o) primary emulsion. This primary emulsion was then homogenised with an aqueous solution of 0.3% w/v PVA at 3000 rpm for 2 minutes using the same homogeniser to form a w/o/w secondary emulsion. The w/o/w secondary emulsion was then stirred at 300 rpm on a magnetic stirrer for 4 hours to allow the evaporation of DCM and then the Por-MPs were harvested following the method as described in section 2.2.2 in the case of the Sol-MPs.

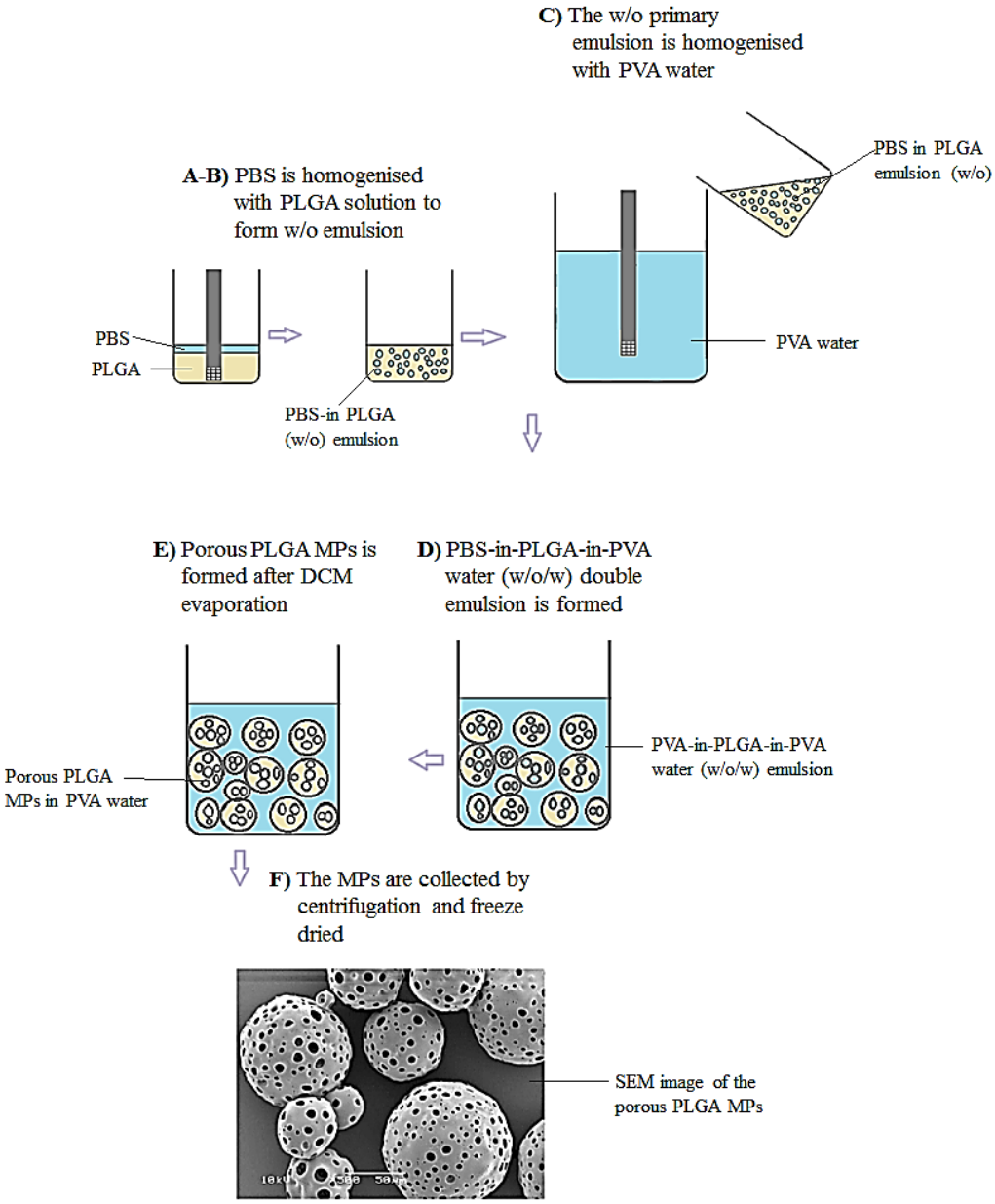


Figure 2.2 Schematic of the preparation of porous PLGA MPs. **A–B)** PLGA solution in DCM (oil phase) and PBS (water phase) are homogenized to prepare the w/o primary emulsion; **C)** 0.3 % w/v PVA solution is maintained stirring and the w/o primary emulsion is gradually added to the area surrounding the vortex created due to the stirring; **D)** w/o/w double emulsion is formed and maintained stirring at 300 rpm until DCM completely evaporated; **E)** the porous PLGA MPs are formed upon evaporation of DCM; **F)** an SEM image of the MPs harvested via centrifugation and freeze drying.

2.2.4 Characterization of the Emulsion Droplets

The emulsion droplets were imaged using an optical light microscope (Nikon Eclipse TS 100 inverted microscope, capture unit: Nikon DS-L3) and sized using a laser diffraction instrument (Coulter LS 230 instruments, Beckman-Coulter Co., Ltd., UK). A representative amount of the emulsion (o/w or w/o/w) was added in 0.3 % w/v PVA to a micro-volume sample cell after the background was normalized by using 0.3 % w/v PVA. Use of water instead of 0.3 % w/v PVA for the dilution and background normalization could destabilise the emulsion and affect the analysis; therefore, 0.3 % w/v PVA was used as it served as the emulsion stabiliser. The emulsion was gradually added to the cell until the obscuration indicated a value between 8 to 12 %. The obscuration or optical concentration is a measure of the percentage of light that is attenuated due to extinction (scattering and/or absorption) by the emulsion droplets or MPs [139]. Once the obscuration indicated a value between 8 to 12 %, a broadened beam of laser light was then passed through the MPs. The scattered light was then focussed by Fourier lenses onto a detector array and using an inversion algorithm, a particle size distribution was inferred from the collected diffracted light data using a garnet optical model [139]

2.2.5 Characterization of the Microparticles

The size distributions of the MPs (solid or porous) were determined using a laser diffraction analysis instrument (Coulter LS 230 instruments, Beckman-Coulter Co., Ltd., UK). The procedure was the same as that described in section 2.2.4, except water was used instead of 0.3 % w/v PVA for the background corrections

and dilution of suspension of MPs. The surface topography of the MPs was analysed using a scanning electron microscope (SEM) (JEOL JSM-6060LV, Jeol, UK). For the SEM imaging, the sample was first coated with a very thin layer of gold using a sputter coater (EM SCD005, Leica Microsystems [UK] Ltd. Milton Keynes, UK) to prevent charge build-up onto the sample, which otherwise may cause imaging artefacts. The coated sample was then bombarded by a focused beam of electrons, leading to the excitation of the atoms of the sample and the emission of various signals, including secondary electrons from the sample surface. The signal intensities of the emitted secondary electrons vary from one point of a sample surface to the other, and information about the surface topography of a sample, including the size, shape and texture, is revealed from the interpretation of the intensity values.

'Skewness' and 'kurtosis were analysed as part of characterization of the MPs. These are two different statistical parameters which indicate the shape of a size distribution. The skewness (g_1) and kurtosis (g_2) values for the different samples were directly obtained from the Coulter LS 230 instrument along with other data (such as mean, median, mode and standard deviation), which were generated by the in-built software.

A Gaussian or normal distribution is the standard against which g_1 and g_2 or peakedness of other non-ideal distributions was measured. The Gaussian curve is referred to as a symmetric distribution, which means, the mean, median and mode coincide (mean = median = mode) and the coefficient of the skewness equals zero ($g_1 = 0$; Figure 2.3 A) and the peakedness or kurtosis of a Gaussian curve is referred to as mesokurtic ($g_2 = 0$; Figure 2.4). On the other hand, an asymmetric distribution can be either positively- or negatively-skewed [140], as shown in

Figure 2.4 C (a long tail to the right of the distribution curve) and Figure 2.4 B (a long tail to the left of the distribution curve), respectively. The g_1 of the size distribution was analysed to see whether there were excessive smaller or larger MPs in a sample. A negatively or positively skewed curve is an indication of the presence of extremely small or large MPs, respectively, in the distributions [141].

On the other hand, if a distribution has a larger degree of kurtosis, g_2 than the normal curve, it is termed as leptokurtic ($g_2 > 0$); in such a distribution, most of the particle diameters are close to the mean diameter (Figure 2.4). The distribution that has a lower, broader peak than a normal curve is referred to as platykurtic ($g_2 < 0$); the particle sizes are more widespread in this type of distribution (Figure 2.4).

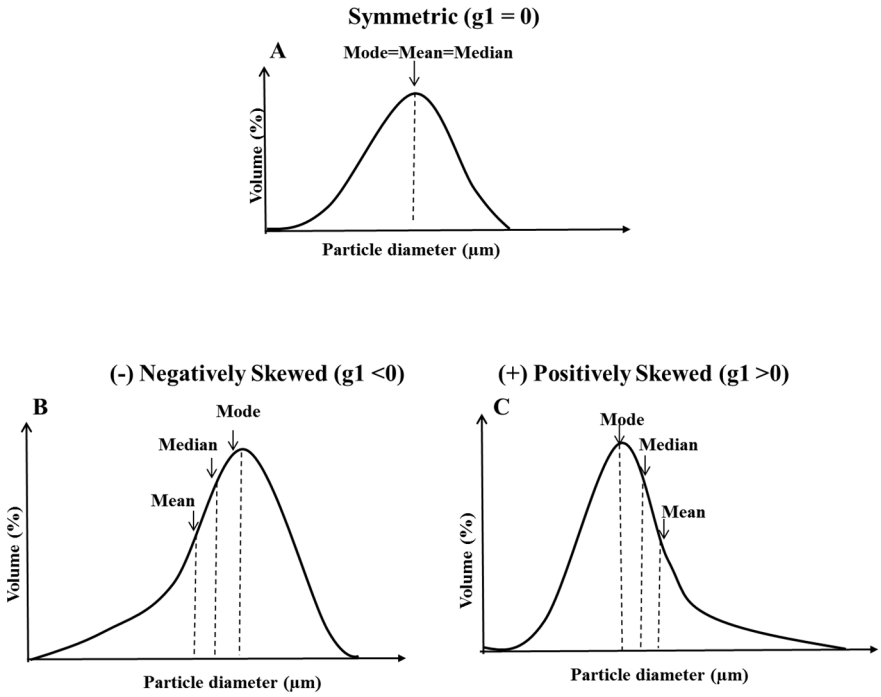


Figure 2.3 Shapes of size distribution curves **A)** Symmetric and **B-C)** asymmetric MP size distributions showing the degree of skewness. A symmetric distribution has no extreme value and the mean = mode = median. Positively (mean > mode) and negatively (mean < mode) skewed distribution indicate the presence of excessively large and small MPs, respectively, in the distributions.

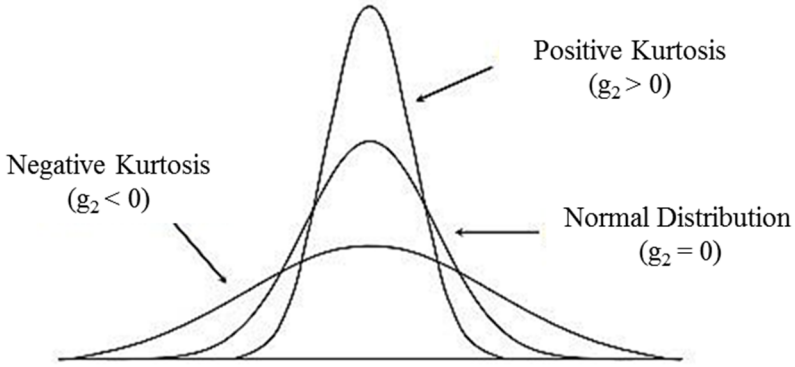


Figure 2.4 Shapes of different size distributions in terms of kurtosis (g_2). A normal distribution is referred to as mesokurtic ($g_2 = 0$); a leptokurtic distribution (positive kurtosis) possesses a curve that is sharper than the normal curve ($g_2 > 0$); a platykurtic distribution (negative kurtosis) has a lower, broader peak than the normal curve ($g_2 < 0$).

2.2.6 Porosity Improvement by NaOH-EtOH Treatment

The Por-MPs prepared using the w/o/w double emulsion-solvent evaporation method was further treated with a solution of 0.5 M sodium hydroxide (NaOH) and 96 %v/v ethanol (EtOH) at a 30:70 ratio (NaOH-EtOH), in order to improve the overall porosity of the MPs. The NaOH-EtOH mixture was chosen because alkali (such as NaOH) facilitates the exposure of the carboxyl and hydroxyl groups on the surface of polyesters, such as PLGA, via the hydrolytic degradation of the ester bonds [142, 143]. Additionally, EtOH, a water-miscible solvent, acts as a co-treating medium to enhance the EtOH-nucleophilic attack on the hydrophobic polymer surface. The whole process is very brief (for 30 seconds) in order to prevent the surface erosion of the MPs [144-146].

MPs (350-500 mg) were placed in a 50 mL centrifuge tube and placed on a vortex mixer set at 1400 rpm. NaOH-EtOH (10 mL) was quickly added to the MPs and the suspension was vortexed for two minutes. The treated MPs were immediately centrifuged at 1000 rpm for one minute, washed three times using ice-cold dH_2O, transferred to a 40 µm cell strainer, blotted using a blue paper roll (laboratory blue roll, CMC 790-01-1L, Fisher Scientific UK Ltd. UK) and then freeze dried for two hours.

2.2.7 Characterization of Pore Size Distribution

The images of the MPs captured under a SEM were further analysed using the Image J software (version IJ 1.46r). Each of the SEM images file was opened via the software and the pore sizes observed in all of the MPs in the image were

analysed. A total number of 500 pores were counted. In the software, the default unit for the length measurement was in 'pixel', which was changed to 'micron' unit. The scale bar presented in the original SEM image was considered for the measurement. Three replicate (technical repeat) images from each batch for three different batches of Por-MPs (n = 3) were considered in the measurement. The frequency distributions of the pore diameters were analysed using the frequency distribution analysis tool of Microsoft Excel 2010.

2.2.8 Surface Wetting of Porous PLGA MPs by Ethanol Treatment

The NaOH-EtOH treated Por-MPs are inherently hydrophobic and lighter-than-water. For this reason, when they are in contact with water and cell culture medium, they float on the surface of the liquids. Bible et al. [92] reported that the level of buoyancy (i.e., the degree of floating or sinking) of the MPs could affect the repeatability of cell delivery via needles. In this study, in order to improve the wettability and hydrophilicity of the MPs, the ethanol immersion method was applied. Different amounts of the NaOH-EtOH treated Por-MPs (5-, 10-, 15- and 20- mg; as required for the particular experiment) were weighed out into the appropriate numbers of glass scintillation vials. The vials were then brought to a sterile environment (hood, class II microbiological safety cabinet: Bio 2+) and the wetting process continued as follows: 2 mL of absolute ethanol was added to each of the MP samples and allowed to saturate for 5 minutes. Gradually, the MPs were washed with dH_2O and dried under the hood. Serum free DMEM (Dulbecco's Modified Eagle's Medium; Life Technologies; 2 mL) was added into each of the vials, which were then placed onto a roller mixer inside an incubator at 37^oC for 15 minutes. The vials were then taken out of the incubator and the

suspended MPs along with the media were transferred to the respective well plates (6-, 12- or 24- well plates, depending on the requirement of the experiment). The vials were washed with fresh medium (Complete DMEM; 1 mL) to transfer the rest of the MPs into the respective wells. Then the plates were incubated at 37^{o}C for 10 minutes to allow setting of the MPs on the bottom of the plates. The medium was replaced with fresh and warm complete DMEM prior to the addition of the cells.

2.2.9 Culture and Maintenance of Immortalized Human Mesenchymal Stem Cells

Primary hMSCs (bone marrow-derived, catalogue number SC-7500, TCS Cellworks, Buckingham, UK) were immortalized by Dr. James Dixon (University of Nottingham) according to the method described by Okamoto et al. [39]. Briefly, primary hMSCs were transfected with a combination of human telomerase reverse transcriptase (hTERT) and human papilloma virus type E6 and E7 oncogenes in order to activate telomerase and inactivate the Rb/p16 pathway. Eventually, the senescence which normally develops in primary hMSCs after a short period of culture was circumvented. Immortalised hMSCs (ihMSCs) were used for the cell viability and cytotoxicity assays. Acknowledgement goes to Dr. James Dixon for supplying the cells.

For the cell adhesion study, green fluorescent protein (GFP) labelled ihMSCs (ihMSCs-GFP) were used, which were genetically labelled, as described elsewhere [147], by the transduction of lentiviruses expressing GFP.

Acknowledgement is due to Dr. James Dixon for providing the ihMSCs-GFP cells.

The cells were cultured and expanded in a complete DMEM supplemented with 10% v/v foetal calf serum (FCS), 1% v/v antibiotic solution (consisting of 10,000 units/mL of penicillin and 100 mg/mL of streptomycin sulphate), 1% v/v L-glutamine (2 mM) and 1% v/v non-essential amino acids following the protocol developed in-house. The cultures were maintained at 37°C in 5% CO_2 in air on tissue culture treated flasks (TC flask; T75 or T175; for further detail of the flasks, please see Table AI-2 of Appendix I). At 80-90 % of confluency, the cells were passaged at 1/3rd of the density. The passaging or sub-culturing procedure for a T75 cm^2 flask was as follows: the medium was aspirated and the culture was rinsed with 5 mL of PBS and treated with 2 mL of trypsin/EDTA (0.5 g/L trypsin, 0.2 g/L EDTA) for no more than 5 minutes at 37°C. Once the cells had detached from the flask surface, 3 mL of the complete DMEM was added and the resultant suspension was centrifuged for 5 minutes at 180 × *g* (Centrifuge, Sigma, 2-16K, scientific laboratory supplies Ltd). The supernatant was then aspirated and the cell pellet re-suspended in a minimum amount (2–4 mL) of fresh culture medium, and the cells were counted using trypan blue (a diazo dye). The detailed procedure for the trypan blue counting is described in Appendix-III. The cell suspension was then either used for an experiment or re-suspended in the required amount of DMEM for sub-culturing in the respective numbers of T75 flasks.

2.2.10 Seeding Cells on Porous PLGA MPs

The cell seeding experiments were carried out in 12-well non-tissue culture treated (nTC) - or Pluronic F127-coated nTC-plates. The detailed procedure for the Pluronic F127-coating is described in Appendix-II. The number of plates

required for the experiments was calculated according to the experimental set up, considering the cells and MPs densities.

For cell culture experiment (cell adhesion, viability and cytotoxicity assays), the MPs used were NaOH-EtOH treated Por-MPs and before seeding, the MPs were treated with ethanol according to the procedure described in section 2.2.8. These MPs are denoted as Por-CE MPs.

For the cell adhesion experiment, 100×10^3 ihMSCs-GFP/well and 20 mg of Por-CE MPs/well were taken. For cell viability and live/dead assays non-GFP labelled ihMSCs were used with a density of 100×10^3 cells/well. The densities of Por-CE MPs were different for different experiments (5-, 10- and 15- mg /well for the viability study; 10 mg /well for the live/dead assay). The experimental flow diagram for the cell adhesion, viability and cytotoxicity assays are shown in Figure 2.5.

Por-CE MPs (20 mg) were transferred to the appropriate number of wells of the nTC- or Pluronic F127 coated-nTC-plates and immersed in the cell culture media following the method as described in section 2.2.8. A cell suspension of ihMSCs or ihMSCs-GFP was prepared following the method described in section 2.2.9 and counted following the procedure described in Appendix III. The suspension was then diluted with complete DMEM to result to a final concentration of 100×10^3 cells/100 µL. Cell culture medium (1 mL) was added to each of the wells, containing ethanol-treated Por-MPs and then 100 µL of the cell suspension was added to the wells. The plates were gently shaken back-to-forth and left to right, and then placed at 37 $^{\circ}$C in 5% v/v CO_2 for imaging or further analysis.

The above mentioned seeding procedure was also followed for the cell viability and live/dead assay, with the necessary adjustment of Por-CE MPs and ihMSCs densities.

2.2.11 Assessment of Cell Adhesion, Proliferation and Viability on MPs

2.2.11.i Assessment of Cell Adhesion

For the visualization of the adhesion and spatial distribution of the cells on the MPs, ihMSCs-GFP were seeded with Por-CE MPs following the method described in section 2.2.10 and fluorescent microscopic images were captured on day 1, 3 and 7 post seeding using a 'Nikon Eclipse TS 100' microscope. The light source of the microscope was a mercury lamp and the cells were excited using a blue excitation filter with a wavelength range 450 – 490 nm. The cell culture medium was replaced with fresh medium every two days during the experiment. The ihMSCs-GFP were also cultured on a tissue-culture plate (Nunc, 24 well, Fisher Scientific, UK, Ltd) without MPs which served as positive control.

2.2.11.ii Presto Blue® Cell Viability Assay

Cell viability and proliferation were assessed by measuring the number of metabolically active cells using a commercially available cell viability reagent, PrestoBlue® (Molecular Probe, Invitrogen, UK). PrestoBlue® is a resazurin-based and non-fluorescent blue-coloured solution that reduces to a highly fluorescent resorufin compound in the presence of a metabolising cell population. The conversion is proportional to the number of metabolically active or viable cells and, therefore, can be measured quantitatively. It is nontoxic to cells and therefore, it can be used repeatedly for the same sample at different time points.

The assay was performed following the manufacturer's protocol [148]. The reagent (10 ×) was diluted with the serum free DMEM before use. On the day of the assay, the medium was removed from the culture; 300 – 500 µL of the reagent was added to each of the wells and incubated at 37 ºC and protected from light for 40 minutes. An aliquot (100 µL) was taken from each of the wells and transferred to a black 96-well polystyrene plate for the fluorescent intensity measurement (excitation: 560 nm; emission: 590 nm) using a plate reader (Infinite^{TM} M200, Tecan, USA). To normalize the background fluorescence reading, the MPs with no cell (n = 3) were included in the culture as a negative control. The average background reading was subtracted from the sample measurements (n = 3). The number of cells per well was calculated using the straight line equation developed from a calibration curve of a series of known concentration of cells vs RFU (relative fluorescent unit). The calibration curve is referred to Figure AIV-1 in Appendix IV.

2.2.11.iii Static and Shaking Seeding

To investigate the proliferation of ihMSCs on NaOH-EtOH treated Por-MPs, ihMSCs were seeded on Por-CE MPs using static or shaking seeding method and then on day 1, 3 and 5 post-seeding, Presto Blue® cell viability assay (see section 2.2.11.ii for further details) was performed to measure the number of viable cells in the cultures. The seeding density was 100×10^3 cells with 5-, 10- or 20- mg of Por-CE MPs per well. The required number of MPs samples was calculated and treated with ethanol according to the procedure stated in section 2.2.8. An

appropriate amount of an ihMSC suspension, as required for the experiment, was prepared according to the method described in section 2.2.9.

The cells were seeded onto Por-CE MPs according to the method described in section 2.2.10 and the plates that were marked as 'static seeding' were kept in an incubator at 37 ºC in 5% v/v CO_2.The plates designated as 'shaking seeding' were kept at 37 ºC in 5% v/v CO_2 for the first 30 minutes and then placed on a 3D tumbling motion shaker (IKA® Rocker 3D digital, IKA, UK) at 5 rpm for another 6 hours. These plates were then placed at 37ºC in 5% v/v CO_2 until the Presto Blue® viability assay was performed on day 1, 3 and 5 post-seeding.

The experimental timeline for the cell adhesion, viability and cytotoxicity assays is shown in Figure 2.5.

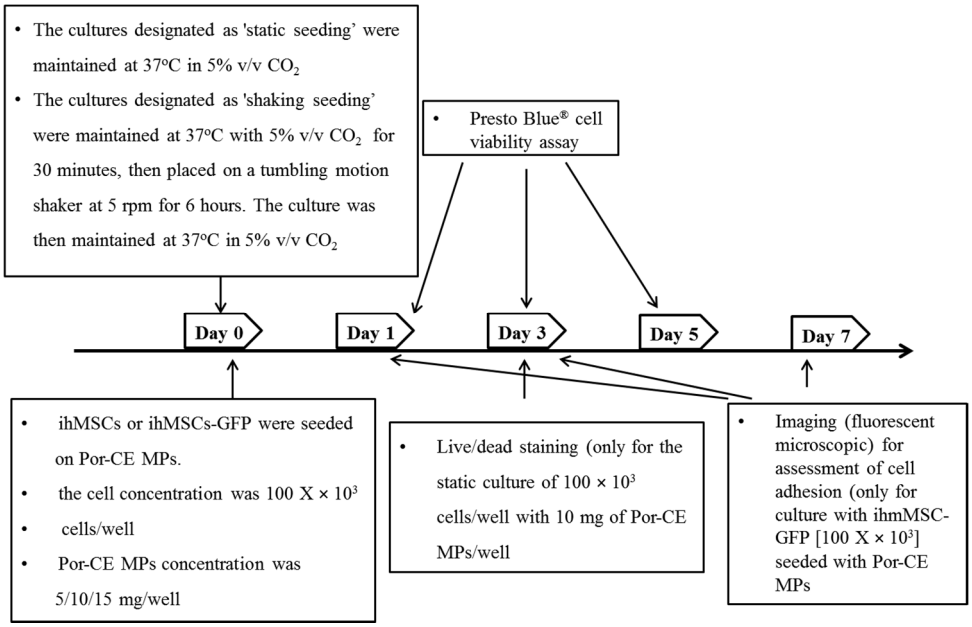


Figure 2.5 Flow diagram of experimental design for cell viability and cytotoxicity assays.

2.2.11.iv Live/Dead® Viability/Cytotoxicity Assay

A fluorescence-based method was used for the simultaneous determination of live and dead cells in a sample. A commercially available cell viability assay kit (Live/Dead Viability/Cytotoxicity Assay Kit, Invitrogen, UK) was used which contains two fluorescent probes; calcein AM (an acetomethoxy [AM] derivative of the fluorescent molecule calcein) and ethidium homodimer-1 (EthD-1). The non-fluorescent calcein AM is converted to green fluorescent calcein by intracellular esterases of live cells and EthD-1 enters cells with damaged membranes (dead cells) and undergoes a 40-fold enhancement of the fluorescence upon binding to nucleic acids, thereby, producing a bright red fluorescence in dead cells. The dye concentration was optimised following the manufacturer's protocol [149]. A dye concentration of 2.5 µM calcein AM and 5 µM EthD-1 in PBS was found to be optimal for the assay (see Appendix-IV). On the day of the assay, the medium was removed from each well and a solution of 2.5 µM/5 µM calcein AM/EthD-1 in PBS (200 µL per well, just enough to cover the sample) was added and incubated at 37 ºC for 15 minutes and directly viewed under a 'Nikon Eclipse TS 100' microscope using a blue (B-2A; wavelength: 450 – 490 nm) and green excitation filter (G-2B; wavelength: 510 – 560 nm) for the live and dead cells, respectively.

2.2.12 Statistical Analysis

The experimental data for different studies are expressed as mean ± standard deviation (SD) with at least three repeats (n = 3) and three technical replicates (r = 3) for each experiment.

The statistical significance among groups was analysed using the GraphPad Prism software (Version 6). The appropriate comparison test was carried out after performing normality tests for the data. Comparison between two experimental groups was carried out using an unpaired Student's t- test. Comparisons among more than two experimental groups with two or more than two variables were carried out using a one-way or two-way analysis of variance (ANOVA), respectively. To perform the pairwise comparisons between the experimental groups, the Tukey's post-hoc procedure was used after carrying out the ANOVA test. All the statistical tests were performed at the 5% significance level. Significance was denoted as follows: * $P \leq 0.05$, ** $P \leq 0.01$, *** $P \leq 0.001$ and **** $P \leq 0.0001$. The data are shown as mean ± SD.

2.3 Results and Discussion

Previous work related to microparticle (MP) fabrication at the University of Nottingham aided in choosing the conditions (polymer concentration, homogenizer speed, emulsifier concentration and DP/CP volumetric ratio) for preparation of porous PLGA MPs of a specific mean diameter, which were suitable for injectable cell delivery applications. As the starting point for the work presented in this thesis, porous PLGA MPs ranging from 50 – 100 µm were fabricated following the protocol developed by Qutachi et al. [70]. The MPs were then characterized in terms of their size and porosity, and to investigate the feasibility of the MPs as injectable microcarriers.

The w/o/w double emulsion-solvent evaporation method, as described in section 2.2.3, was used to fabricate the Por-CE MP. Solid PLGA MPs (Sol-CE MPs) was also prepared for comparison of their morphology with that of Por-CE MPs. The

o/w single emulsion-solvent evaporation method (see section 2.2.2) was used for the preparation of the Sol-MPs. The size and morphology of the emulsion droplets (before DCM evaporation) and the respective solidified MPs (after DCM evaporation) were characterized following the methods as described in section 2.2.4 and 2.2.5, respectively. The size and morphology of the emulsion droplet and the respective MPs were compared to investigate the effect of the MP hardening steps (solvent evaporation and stirring) on the size and shape of MPs. Some researchers have reported that a substantial level of shrinkage and deformation of the emulsion droplets occurred after the solvent evaporated and eventually the harvested MP topography, size and shape differed greatly from the respective emulsion droplets [150-152].

2.3.1 Characteristics of Emulsion Droplets

As depicted in Figure 2.6 A and Figure 2.6 B, both the single and the double emulsion droplets, prepared via o/w and w/o/w emulsion methods exhibited spherical morphology and the size distributions were polydisperse. The mean droplet diameter of the single and double emulsions were 54 μm (SD ± 25) and 72 μm (SD ± 26), respectively. The shapes of both of the curves are similar and the patterns indicate an asymmetry in the distributions as seen in Figure 2.6 C. In terms of the shape of the distributions, both are negatively skewed (a long tail to the left of the respective distribution), which means that most of the droplets (mode) were distributed to the right of the mean and the extremely small droplets are to the left of the size distributions curves [153]. On the other hand, in terms of kurtosis (the degree of peakedness), both size distributions were leptokurtic (g_2 >

0) with respect to a normal curve ($g_2 = 0$), which means most of the droplet sizes were close to the mean.

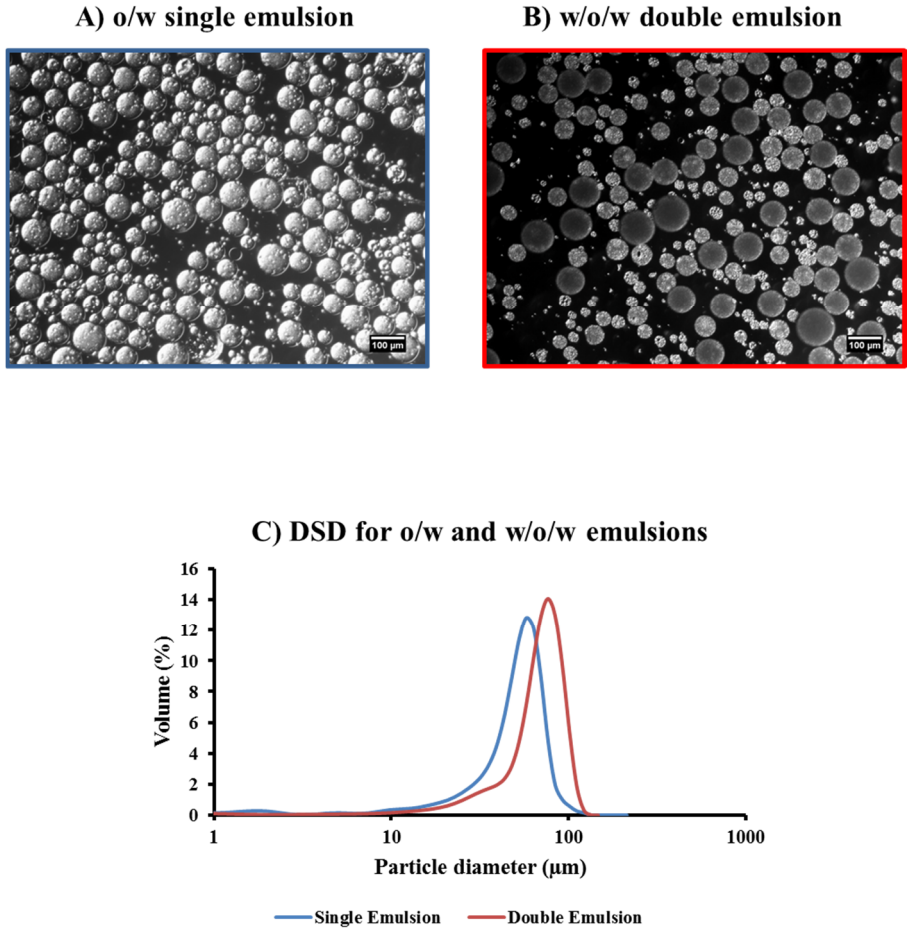


Figure 2.6 Representative light microscopic images of **A)** single emulsion and **B)** double emulsion; scale bar = 100 µm; **C)** size distribution curves for the single and double emulsions as analysed using the data generated from Coulter LS 230.

2.3.2 Characteristics of MPs

Table 2.1 shows the descriptive statistics for the solid and porous (before and after NaOH-EtOH treatment) PLGA MPs prepared by using the conventional emulsion-solvent evaporation method. All the data were directly obtained from a Coulter LS 230 instrument for the respective MP samples (see section 2.2.5 for detail methodology). The average size of the MPs was expressed as the volume mean diameter (D [4, 3]). As shown in the table, the mean diameter of the Por-CE MPs produced by the w/o/w emulsion-solvent evaporation method was 66 μm (SD ± 24). After treating the MPs with NaOH-EtOH solution, the mean size increased to 78 μm (SD ± 25). The NaOH-EtOH solution contained 70% v/v ethanol, which might have made the MP swell during the surface treatment [70]. The homogenization speed and polymer concentration are the two important factors that influence the MP size [154]. Although both the porous and solid MPs were prepared using the same concentration of PLGA (20% w/v) and homogenization speeds (3000 rpm), the mean diameter of the solid MPs was 13 μm less than that of the Por-CE MPs. This was not surprising because the polymer solution used to prepare the porous MPs contained 5% v/v PBS, as the pore-forming agent, which might have increased the mean droplet volume. Even after the diffusion of the internal PBS solution to the outer water phase during the freeze-drying step, some void spaces remained inside the MPs, which in turn might have caused the increase in the mean diameter. These results are in agreement with that observed by Wang and colleagues [155]. As they described, the size of the porous PLGA MPs were twice as large as the solid PLGA MPs prepared using a common homogenization speed and polymer concentration. They used ammonium bicarbonate (NH_4HCO_3) as a pore forming agent.

None of the size distributions could be considered as symmetrical because the related mean, median and mode values did not coincide and the distributions were skewed (for solid: $g_1 > 0$; for the porous before and after the treatment $g_1 < 0$ and $g_1 > 0$, respectively; see Table 2.1). On the other hand, the peakedness (g_2) of the size distribution before the treatment is comparable to a normal distribution ($g_2 = 0.06$). However, after the treatment, the degree of peakedness increased and the curve became sharper ($g_2 = 3.27$; see Table 2.1). As shown in Table 2.1, a certain volume fraction of the MPs for both the solid and porous MPs was below 10 μm. MPs with a size below 10 μm size (1.71 volume %) were also present in the NaOH-EtOH treated sample. A small fraction of the porous PLGA MPs was below 1 μm for both the treated and untreated MPs. On the other hand, the sizes of the solid MPs were all above 1 μm; however, a little less than two volume % of the distribution had a size of 10 μm.

Figure 2.7 represents the size distribution graphs of the emulsion droplets (before DCM evaporation) and their corresponding MPs (before and after NaOH-EtOH treatment). The shapes of the curves before and after the DCM evaporation are comparable, indicating that the solvent evaporation process had very little effect on the shapes of the curves. After the NaOH-EtOH treatment, the curve slightly shifted to the right, indicating a slight aggregation of the MPs (with little change in the mode diameter). The corresponding SEM images in Figure 2.9 also indicate the aggregation between the MPs, which might be due to the van der Waals attractions between the non-uniform-sized MPs [156].

Table 2.1 Particle Size Distribution

Descriptive Statistics	**Microparticles**		
	Solid	**Porous (before NaOH-EtOH treatment)**	**Porous (after NaOH-EtOH treatment)**
Mean diameter ($d_{4,3}$; µm ± SD)	53±19	66±24	78±25
Mode diameter (µm)	61	78	82
Median diameter(µm)	53	69	78
% CV	37	37	33
Volume % of MPs lower than 1 µm	0.00	1.06	0.88
Volume % of MPs lower than 10 µm	1.56	2.95	1.71
Volume % of MPs lower than 100µm	98.27	94.93	86.76
Skewness (g_1)	0.10	-0.62	0.15
Kurtosis (g_2)	0.44	0.06	3.27

The surface topography of the MPs was analysed under the scanning electron microscope (SEM), following the method described in section 2.2.5. The representative SEM images of the MPs prepared using the single- and double-emulsion-solvent evaporation methods are shown in

Figure **2.8**. As shown in the figure, the MP prepared using the single emulsion-solvent evaporation was mostly solid with a smooth texture and spherical appearance (

Figure **2.8**A). In contrast, the MPs prepared using the double emulsion-solvent evaporation method had a porous morphology, with a rough surface and spherical characteristics. The cross-section images of the MPs prepared using the single and double emulsion methods clearly indicate their non-porous and porous characteristics, respectively. On the other hand, when compared to the untreated MPs, the SEM images of the NaOH-EtOH treated MPs (Figure 2.9); indicate porosity both internally and on the surface. Both the size distribution patterns and the SEM images suggest a polydisperse distribution of the MPs, which is not surprising in the case of the MPs prepared using the emulsion-solvent evaporation method [155, 157]

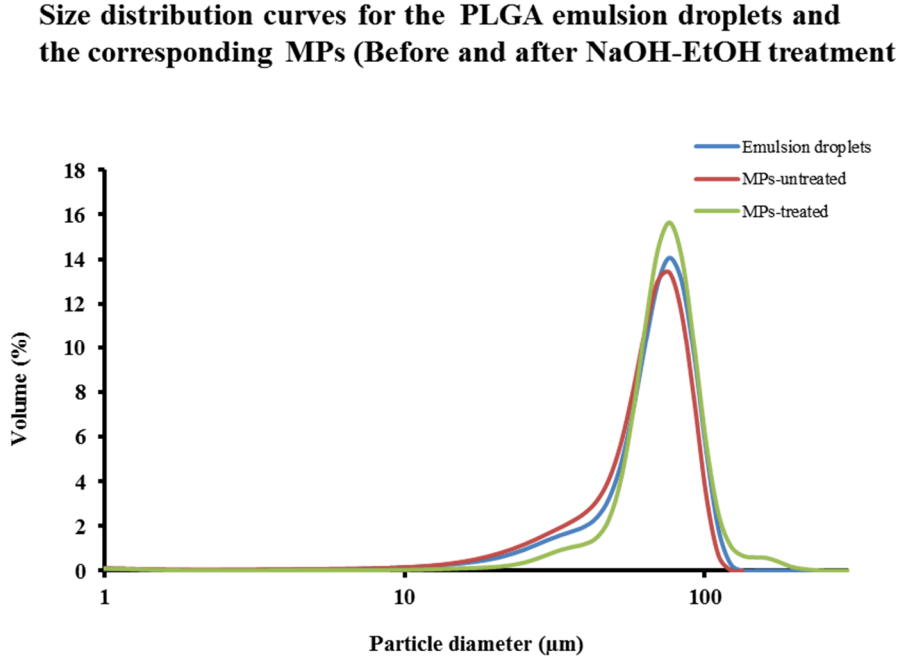


Figure 2.7 Size distribution curves of the double emulsions and the respective MPs before and after the NaOH-ETOH treatment.

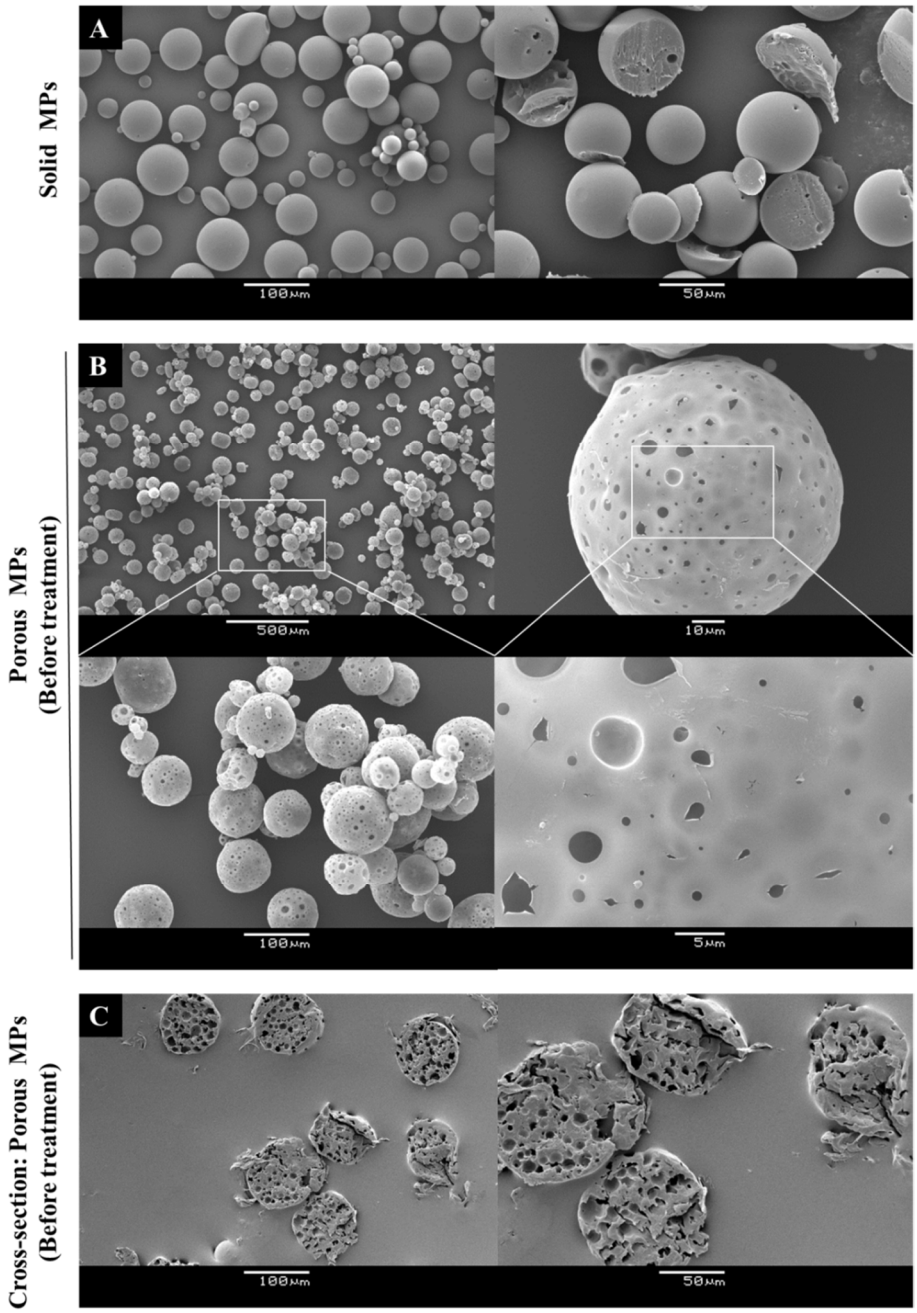


Figure 2.8 Representative SEM images of **A)** solid and **B)** porous MPs before NaOH-EtOH treatment; **C)** cross-section image of porous MPs before NaOH-EtOH treatment .

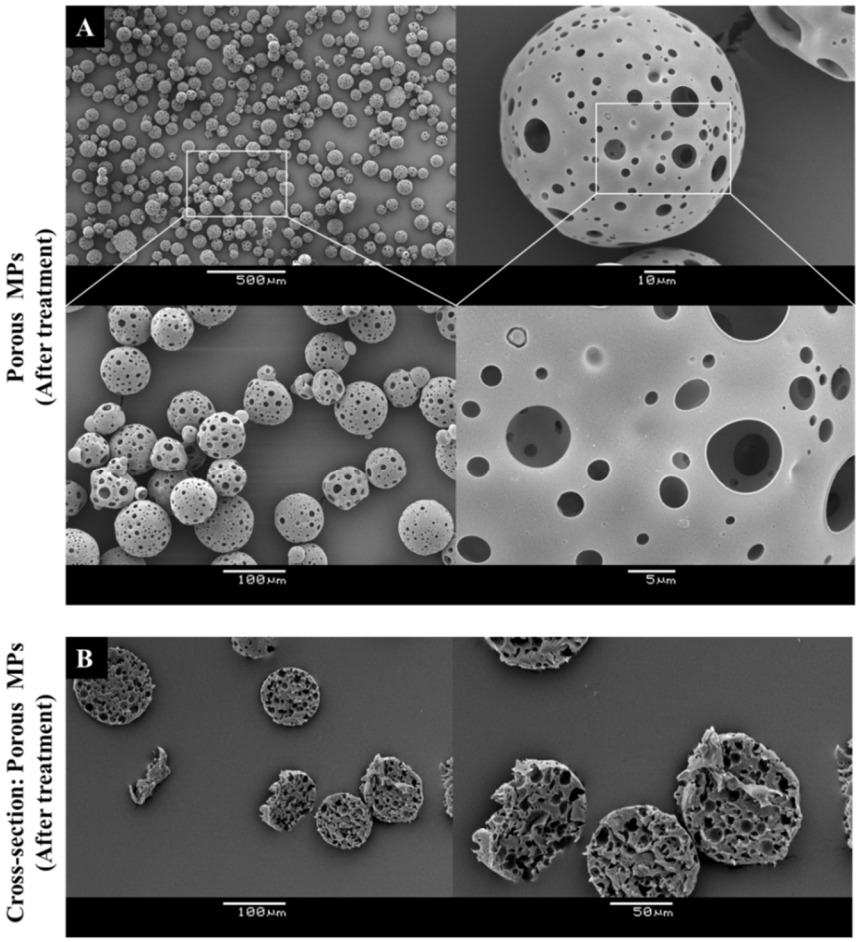


Figure 2.9 Representative SEM images of the porous MPs after the NaOH-EtOH treatment showing their **A)** surface and **B)** internal porosity (cross-section images).

2.3.3 Pore Size Distribution

Pore diameters of both the treated- and untreated MPs were measured using an image processing software (Image J, version: 1.48V) and then the data were further processed using Microsoft Excel 2010 to plot their frequency distribution graphs. The detailed method is described in section 2.2.7 section and the pore size distribution spans are shown in Figure 2.10. Only the surface pores were considered for the measurements. As observed, before the treatment, the pore diameter spanned from 0.4 to 10.8 µm and the most frequently observed pore diameter was between 2 to 2.5 µm, comprising 81 pores out of 500. After the treatment, pores of smaller sizes (0.4 up to 3 µm) decreased in numbers, whilst the number of larger sized pores slightly increased. Furthermore, there were some pores observed in the range of 9 – 10 µm and 11.0 – 14 µm, which were not observed in the untreated sample. The overall porosity of the MP increased after the treatment and the pore size distribution graphs are in agreement with the respective SEM images in

Figure **2.8** and Figure 2.9. It was also observed that the pore geometry on the surface differed from that of the internal pores, with a circular shape on the surface and an irregular shape internally. Similar observations were reported by Wang et al. [155], who used ammonium bicarbonate as a porogen to prepare porous PLGA MP with a size of 229 µm.

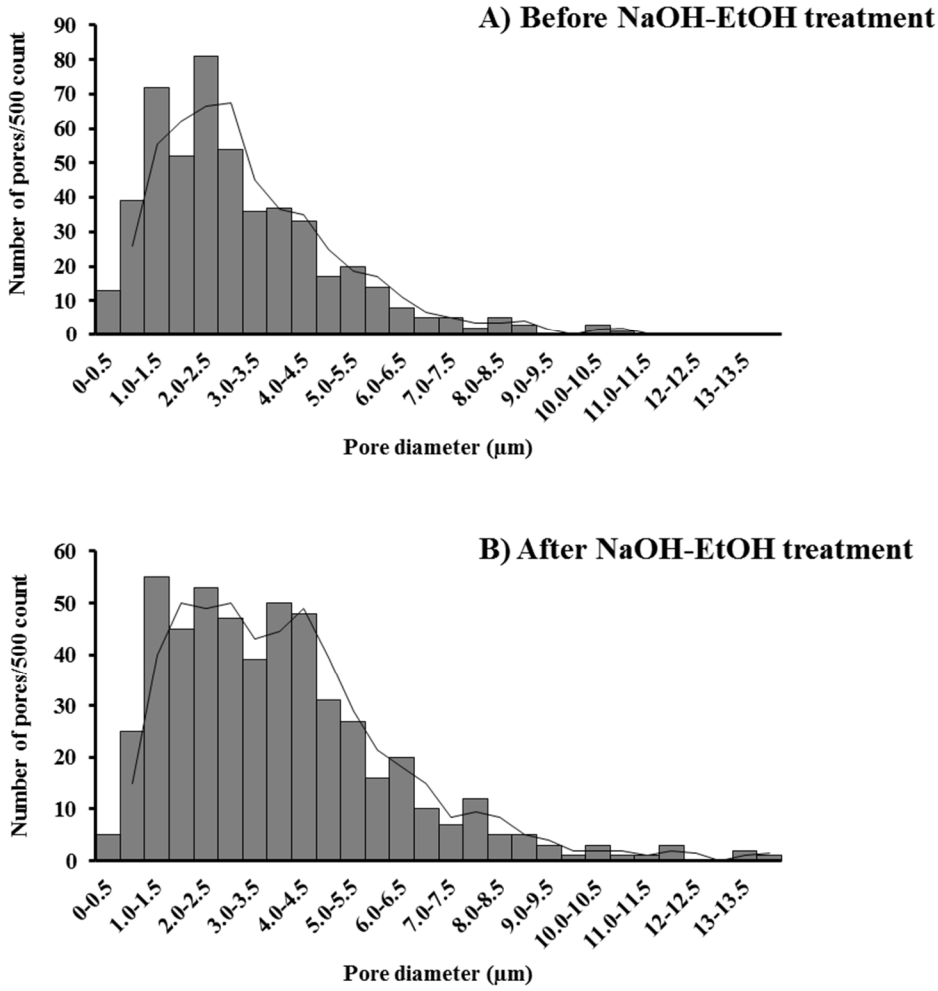


Figure 2.10 Pore size distributions. **A)** Before NaOH-EtOH treatment and **B)** after NaOH-EtOH treatment. Some representative pores (as observed in representative SEM images of the MPs; total pore count = 500; n = 3) were measured using the Image J image processing software and then analysed in Microsoft Excel to generate the histograms.

2.3.4 Adhesion and Viability of Cells on MP (Cell Compatibility With Microparticles)

Adhesion of cells on MPs is the first, necessary step involved in developing a MP-based tissue engineering (TE) strategy [133, 158]. Cell adhesion is also an indication of the biocompatibility of the material [158]. In this study, ihMSCs-GFP were seeded onto the Por-MPs (100×10^3 cells with 10 mg of MPs per well in nTC-12-well plates) and images were captured using an epifluorescence microscope at day 1, 3 and 7 post seeding. The seeding method is described in section 2.2.10 of this chapter. The study was repeated with five different batches of MPs and similar results were observed in terms of the cell attachment. The representative images for the central and peripheral area of the plates are shown in Figure 2.11 and Figure 2.12, respectively. The plates are slightly curved in the middle, which is why most of the MPs were concentrated in the centre of the plate, whereas the periphery of the plate surface contained relatively fewer MPs. For imaging, both the centre and the periphery of the plates were considered. The left-hand columns in Figure 2.11 (excluding the top left image) and Figure 2.12 represent optical light microscopic images of the cells onto the Por-MPs at day 1, 3 and d 7 post seeding. The right-hand columns of the respective images show the corresponding fluorescent microscopic images. Figure 2.11A and Figure 2.11B represent the MPs with no cells and ihMSCs-GFP with no MPs on tissue culture plates, respectively. As shown in Figure 2.11 C-2, the cells attached onto the outer surface of the MPs at day 1 post seeding (bright green). On the subsequent days, the brightness (Figure 2.11 D-2 and Figure 2.11 E-2) and size of the cell-MP aggregates increased. This observation is an indication of the cytocompatibility of the MPs and the suitability of the MPs surface for cell adhesion and sustained cell

expansion [64, 159]. However, a certain fraction of the cells were attached on the bottom of the plate (Figure 2.12). This could contribute to the measurement of cell viability or proliferation study. Therefore, for further cell culture experiments, Pluronic F127 (a cell repellent polymer)-coated nTC plates were used so that the cells preferentially attached to the MPs only. The detailed procedure of the coating is described in Appendix II. Figure 2.13 shows the representative microscopic images of ihMSC-seeded MPs that were cultured in Pluronic F127-coated nTC plates. As observed, coating of the plates with Pluronic F127 prevented the cell attachment to the plate surface, but did not affect the cell attachment to the MPs. These cell-MP aggregates on different days (day 1, 3, 5) in culture are comparable with those on the same days in nTC-treated plates (Figure 2.11), in terms of the cell adhesion pattern and size of the aggregates.

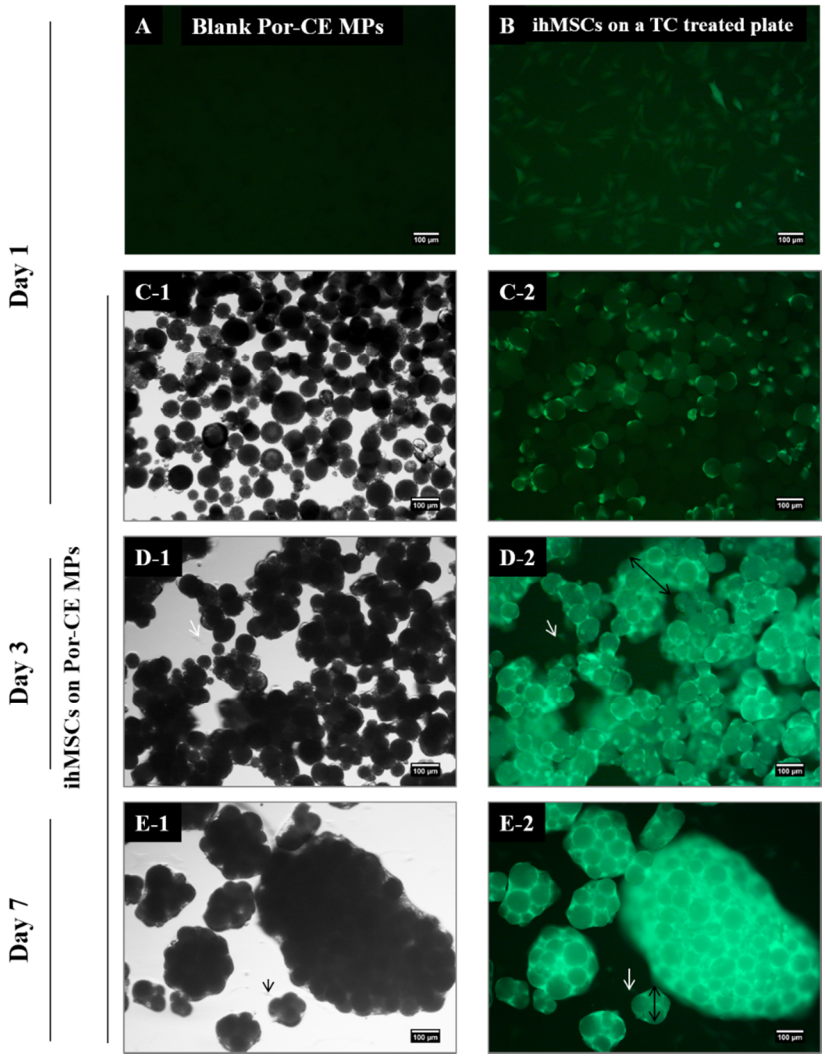


Figure 2.11 Representative microscopic images of ihMSCs-GFP with Por-CE MPs in nTC plates (images taken for the centre of the plates). Blank MPs (Por-CE MPs) under fluorescent light, in a 12-well nTC plate on day 1 post-seeding **(A)**; ihMSCs-GFP attached on a 12-well TC plate on day 1 post-seeding **(B)**; ihMSCs-GFP attached on the MPs on day 1 **(C-1 and C-2)**, day 3 **(D-1 and D-2)** and day 7 **(E-1 & E-2)** post-seeding. The single-headed arrows indicate the cell attachment on the bottom of the wells, the double-headed arrows indicate the size of the cell-MP aggregates. Scale bar = 100 µm

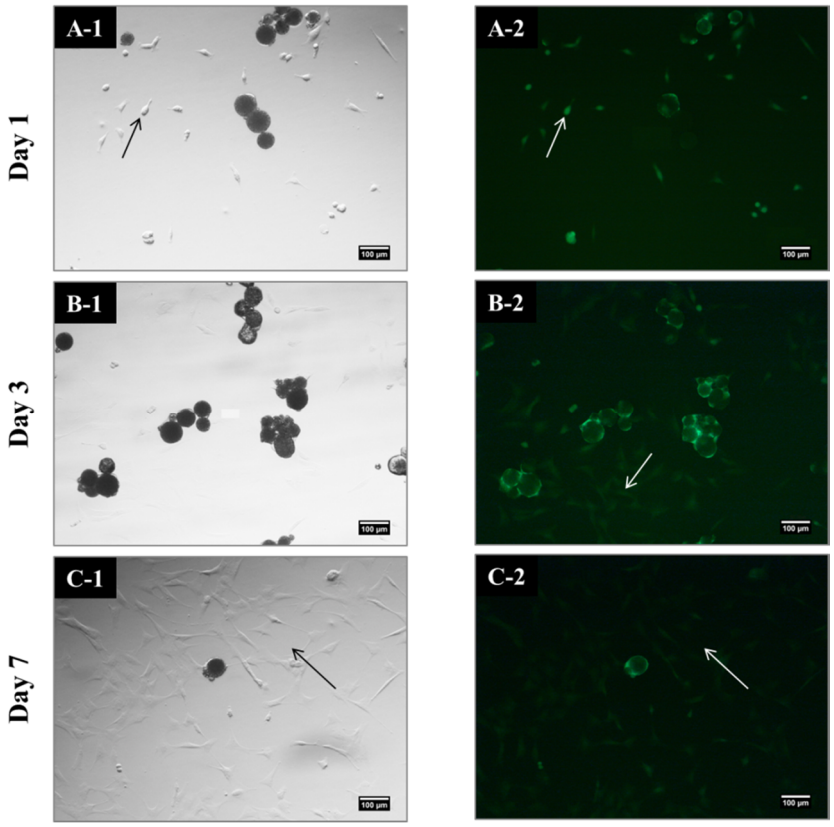


Figure 2.12 Representative microscopic images of ihMSCs-GFP with Por-CE MPs in nTC plates (images taken for the peripheries of the plates). ihMSCs-GFP attached on the MPs on day 1 **(A-1 and A-2)**, day 3 **(B-1 and B-2)** and day 7 **(C-1 & C-2)** post-seeding. The arrows indicate the cell attachment on the bottom of the plates. Scale bar = 100 µm

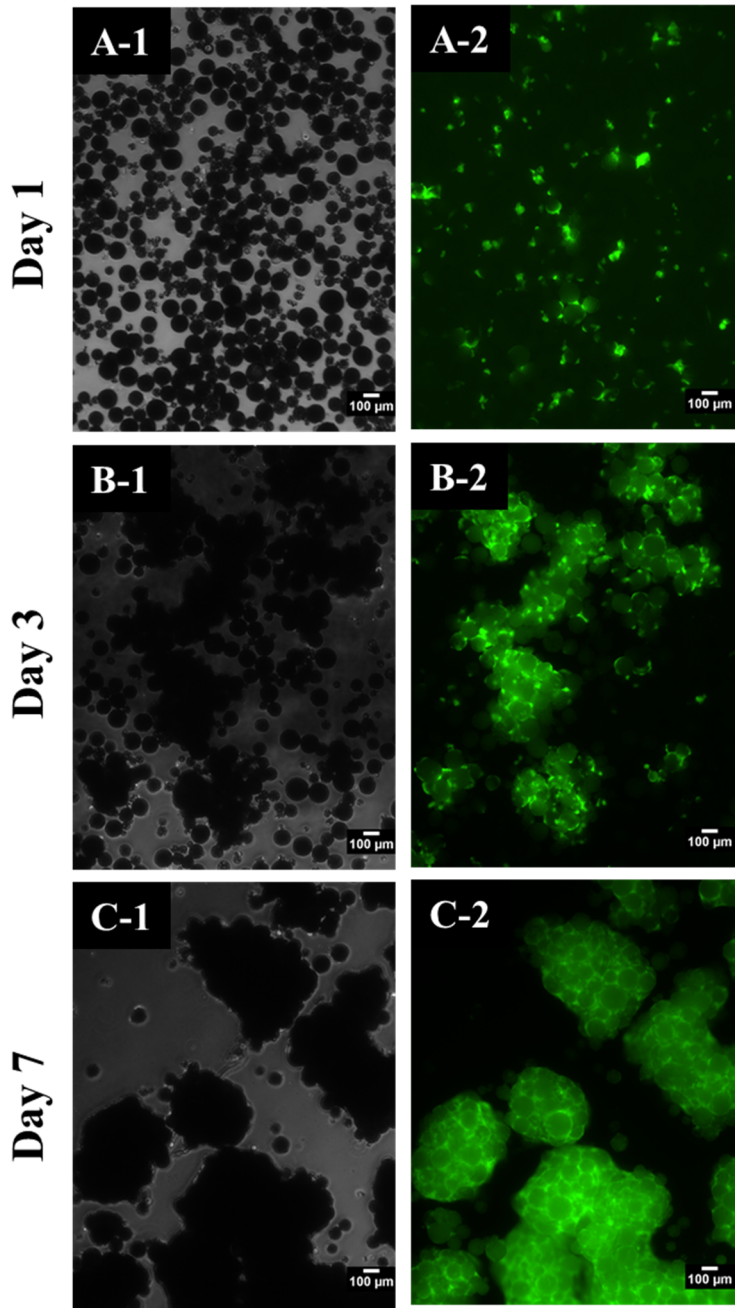


Figure 2.13 Representative microscopic images of ihMSCs-GFP with Por-CE MPs, cultured in Pluronic F 127-coated nTC plates.ihMSCs-GFP attached on the MPs on day 1 **(A-1 and A-2)**, day 3 **(B-1 and B-2)** and day 7 **(C-1 & C-2)** post-seeding. Scale bar = 100 µm.

2.3.5 Influence of Static/Shaking Seeding and MP Density on Cell Viability

For the purpose of promoting cell expansion on MPs or microcarriers, a variety of culture techniques have been utilised, including dynamic culture under shaking/agitation (e.g., spinner flasks, rotating wall vessels and perfusion system) [160]. Compared to static culture, the dynamic cultures stated above possibly provide more opportunities for cells to adhere to the surfaces of the microcarriers. Furthermore, they facilitate medium perfusion throughout the culture, leading to an improved nutrient supply in the cultures [161, 162]. In this study, immortalised hMSCs (ihMSCs) were seeded with NaOH-EtOH treated Por-MPs under static and dynamic conditions, according to the method described in section 2.2.11.iii; the cell viability on the MPs was assessed on day 1, 3 and 5 using Presto Blue® cell viability assay kit following the method described in section 2.2.11.ii. As shown in Figure 2.14, for all three MP concentrations (5, 10 and 20 mg/well) in both seeding conditions (static and shaking), the cell viability increased significantly from day 1 to 5. For example, the number of viable cells in static culture with 5 mg of MPs increased from 47×10^3 on day 1 to 102×10^3 on day 5 ($P < 0.01$). A similar trend was observed in the case of the shaking culture with 5 mg of MPs per well. On the other hand, for the cells cultured on 10 and 20 mg of MPs in a static culture, the number of viable cells on day 5 was approximately 3 to 4 times higher than that on day 1 (P value < 0.0001). For these densities of MPs, the shaking seeding demonstrated similar results. The overall viability results demonstrate that the shaking seeding was not advantageous over the static seeding, as evident from the insignificant differences in the cell numbers between the culture conditions at different time points ($p > 0.05$).

It was observed that the initial cell viabilities (viabilities at day 1) for all three MP densities were similar. However, over time, the cultures with 10 mg and 20 mg of MPs/well showed relatively higher numbers of viable cells than those with 5 mg of MPs/well. For example, with 20 mg of MPs in static culture, the number of viable cells on day 5 was 3.41 times higher than that on day 1 ($P \leq 0.0001$), whereas with 5 mg of MPs/well, the number of viable cells on day 5 was 2.32 times higher than those on day 1 ($P < 0.01$). It is not surprising that initially, there were less cells and less surface area was required for the cells to grow and remain viable. Over the time course of the experiment, the cells multiplied and required more space to survive. In the case of the results reported here, the surface area provided by 5 mg of MPs was possibly not sufficient [64, 159] for sustained cell proliferation over the time course that the culture was maintained. It is possible that 10- and 20-mg MPs might have facilitated cell viability and faster proliferation due to the higher surface area available to the proliferated cells. However, in order to be sure about the actual surface area for the respective amounts of MPs, further study is necessary.

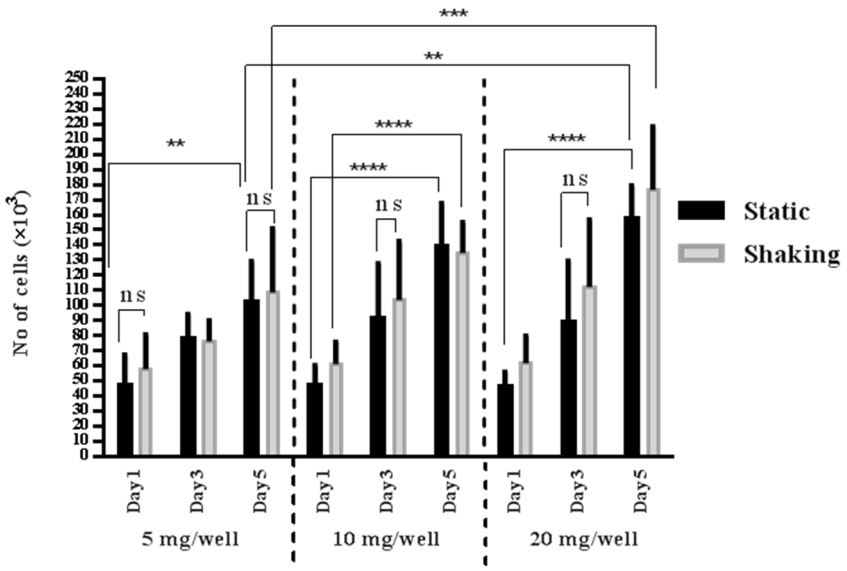


Figure 2.14 Influence of static and shaking seeding and the density of Por-CE MPs on the viability of ihMSC. ihMSCs were cultured with Por-CE MPs over a 5-days period, after seeding the cells via the static or shaking mode. Viabilities of the cells on day 1, 3 and 5 post-seeding were measured using the PrestoBlue® cell vibility assay kit. Values are presented as mean ± SD (n = 3; r = 3). Statistical significance between different groups are represented as: **p<0.01; ***p<0.001; ****p<0.0001; 'ns' denotes the non-significance of the difference, for which, p>0.05.

2.3.6 Live/Dead® Viability/Cytotoxicity Assay

For further qualitative assessment of the live and dead cells in the culture, a commercially available Live/Dead® stain was used to observe the live and dead cells simultaneously in a culture. The detailed method is described in section 2.2.11. The live cells fluoresce green and the dead cells fluoresce red, as shown in Figure 2.15 for 100×10^3 ihMSCs with 10 mg of the MPs /well. Initially (Figure 2.15; day 1), the live (green) ihMSCs covered most of the surface of the MPs. A few dead cells (red spots) are also observed on day 1. On subsequent days (day 3 and 5; Figure 2.15), a few dead cells were present; however, sustained cell viability was evident, as the cells spread out on more MPs and the size of the cell-MP constructs gradually increased. It is likely that as the number of cells increased, the frequency of cell-cell contact increased and to remain in close contact with each other, the cells formed aggregates with the substrate or MPs [163]. As the cells formed aggregates, it was difficult to identify the morphology of individual cells. Similar trends of cellular aggregate formation were observed for human and rat MSCs on porous PLGA (mean diameter: 290 μm) [62] and PCL (mean diameter: 422 μm) MPs [64]; although the porosity features were different than those observed in this study. The patterns of the cell- MP aggregates observed in this study is comparable with those presented above in Figure 2.11 of section 2.3.4 for the same concentration of ihMSCs-GFP with 10 mg of the MPs. The overall live/dead viability/cytotoxicity assay demonstrated the biocompatibility of Por-CE MPs with ihMSCs.

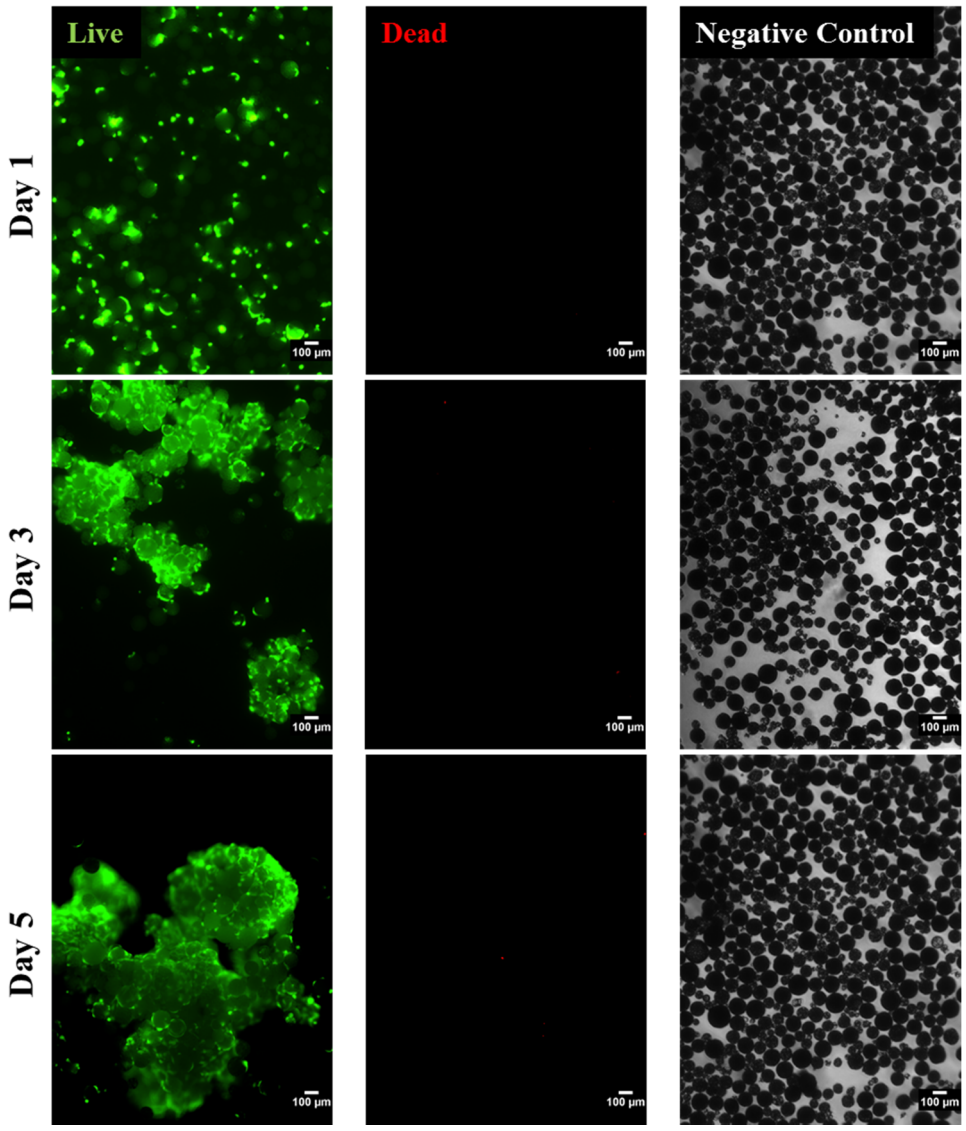


Figure 2.15 Representative fluorescence microscopic images of live (left-hand column, green fluorescent) and dead (middle column; a few red spot) cells on Por-CE MPs; optical light microscopic images of blank MPs (no cells; negative control). Scale bar = 100 µm.

2.4 Conclusions

In this chapter, PLGA MPs with closed and highly interconnected pores were prepared using the w/o/w double emulsion-solvent evaporation method and their porosity was improved by an EtOH-NaOH treatment. The MPs were characterised in terms of their size and pore size distribution. They were further assessed for ihMSCs adhesion, viability and proliferation on the discrete MPs.

To the best of our knowledge, in terms of MPs characterization, most of the literature reports the mean ± SD or median diameter using a laser diffraction instrument and a qualitative assessment of the MPs is done on the basis of the SEM images. In this chapter, in addition to the mean (± SD), median and mode values, two other important statistical parameters (skewness and kurtosis) were demonstrated that are rarely reported by others. The fractions of different sizes of the MPs within a distribution have also been reported in this study. This gave a clearer picture about the shapes of the MP size distributions. The pore size distribution results demonstrated that the MPs prepared using the w/o/w double emulsion-solvent evaporation method were highly porous and that the pores were interconnected. The pore and MP size distributions were wide and non-uniform.

The MPs were further studied for ihMSC adhesion, viability and cytocompatibility to evaluate their potential as injectable cell delivering vehicles. The cell viability study was carried out with varying amounts of MPs using both static and shaking modes. Repeated cellular assays (cell adhesion and viability) demonstrated that the size and topographic features of the MPs were favourable for sustainable cell growth within the culture period. The cytocompatibility of the

MPs was demonstrated by the presence of live cells and the expansion of live cells on the MPs. On the other hand, the degree of polydispersity of the MPs observed in this study is similar to that observed by others using the same technique. No attempt was made for the minimization of the broadness of the size distribution. Previously, researchers at the University of Nottingham applied sieving post fabrication to minimize the polydispersity of MPs in the size range of 50 – 100 μm. However, the final yield was compromised. It would be interesting to utilize alternative fabrication techniques with the aim of preparing MPs with narrower size distributions and this formed the aim of the next chapter of work.

Chapter 3 Cross-flow Membrane Emulsification to Fabricate Large and Uniform-sized Polycaprolactone Microparticles

3.1 Introduction

As described in Chapter 2, MPs used as injectable cell delivering vehicle should offer a favourable surface for a sufficient number of cells to attach and grow before the cell-microcarrier system is injected into a localized injured body part for repairing the damage. As such, the characteristics of the MPs including the size are very important for the efficient injectable capacity of the system.

MPs are expected to be substantially larger than the cells. MPs of an average diameter 50 to approximately 400 μm have been reported for delivery of stem cells via needles of varying diameters (18 to 22G) [62, 80, 130, 164]. The presence of very small MPs (i.e., smaller than the size of a cell) could result in unwanted effects. For example, MPs with diameters of 15 μm or less have been reported to be taken up by the cells through phagocytosis [165-167]; Secondly, MPs that are smaller than the size of a cell serve only as a linker between the cells and have been shown to form tight cell-MP aggregates with limited access to oxygen and nutrients at the core, which eventually led to a decrease in the viable cell yield [66]. Also, it has been reported that the cell attachment density varies according to the size of the MPs; larger particles allowed more cells to attach and grow per particle [69]. However, very large size MPs could block the needle and restrict the efficiency of the delivery vehicle [92]. Again, the repeatability of the ejection (delivery of a consistent number of particles at each injection) could be

affected by the size distribution of the MPs [92]. Therefore, the choice of a microcarrier with an appropriate size and a narrow size distribution is important.

Emulsification is the most widely used MPs fabrication method. Conventional emulsification techniques using a high shear homogeniser need a high energy input and usually result in MPs with broad size distributions [116, 168]. There are some specialized methods for the preparation of uniform-sized or monodisperse MPs. De La Vega et al. [100] classified all the methods into two groups, monomer-based- and preformed-polymer-based preparation methods. In the '-monomer-based-' preparation method, an additional polymerisation step is needed. Therefore, to remove impurities, further purification steps need to be considered [100]. The '-preformed-polymer-based-' preparation method is further classified into single- and multi-channel systems. Compared with the multichannel system, the yield of the MPs produced using the single-channel system is lower due to the 'drop-by-drop' emulsion formation that happens in the case of the later system [101]. One of the most commonly used multichannel systems is cross-flow membrane emulsification (X-ME) developed by Nakashima et al. [102]. Depending on the desired characteristics of the final emulsion, different types of membranes, such as - Shirasu Porous Glass (SPG), metal, ceramic and polymeric can be used [103]. Among these types of membranes, SPG possesses the advantages of narrow pore size distributions, a wide range of available pore sizes (0.05 – 50 μm), and superior thermal stability [104]. Furthermore, SPG membranes have been used to prepare both single and double emulsions [105, 106] which could be used for preparing both solid and porous

MPs following the o/w and w/o/w emulsion techniques respectively, using the same membrane.

In X-ME, either a disperse phase (DP) or a pre-emulsion is injected under low nitrogen gas pressure through a multichannel membrane into a continuous phase running crosswise to the flow direction of the DP [169]. Although X-ME exhibits several advantages over other emulsification techniques, there are limited publications on the preparation of larger-sized pure polymeric microparticles with high yields and narrow size distributions. Monosized poly (divinylbenzene) with a mean diameter of 12 – 36 μm were fabricated by Haoa et al. [170] using SPG membrane emulsification followed by suspension polymerization, which required an additional step in order to obtain the final products or MPs and the yield was low. Gasparini et al. [171] fabricated 50 – 100 μm PLGA MPs using a flat metallic membrane. However, the flow rate of the disperse phase was only 0.5 mL/min for a total volume of only 10 mL, which resulted in a low yield of the final product/particles. Furthermore, the microphotograph of the MPs suggested a lack of size uniformity. Using a similar membrane, solid PCL MPs with mean diameter of approximately 20 μm were prepared by Imbrogno and colleagues [150]. The preparation of pure polymeric MPs with diameters of approximately 100 μm and a high yield has not been reported previously.

The aim of this study was to prepare monosized PCL MPs with diameters of approximately 100 μm using the X-ME technique in a minimum amount of time and expected to achieve a workable yield. To achieve MPs with a tighter span of

distribution, several factors such as working pressure (P_w), disperse phase (DP) and continuous phase (CP) concentrations, DP and CP viscosities and CP flow rate were required to control. A further aim of this study was to investigate the optimum emulsification conditions that could be used as a template to prepare even more complex emulsions using a different polymer, such as PLGA.

3.2 Experimental

3.2.1 Materials

PCL of two different molecular weights (Number average molecular weight, Mn = 80 kDa and Mn = 45 kDa) were purchased from Aldrich Chemistry, UK. PVA (weight average molecular weight, Mw= 13,000-23,000; 87-89% hydrolysed) was purchased from Sigma-Aldrich and was used as an emulsifier. Analytical reagent grade DCM was purchased from Fisher Scientific, UK and was used to prepare the disperse phase (PCL solution).

The pipe types Shirasu Porous Glass (SPG) membranes of two different pore diameters (actual length: 125 mm; effective length: 105 mm; internal diameter: 10 mm; thickness: 1mm; pore diameter, D_0 = 20 μm and 50 μm) along with the membrane emulsification kit (High Speed Mini Kit-KH125) were purchased from SPG Technology Co., Ltd. (Japan). The SPG membranes are inherently hydrophilic [172]. To prepare an o/w emulsion, this should be the membrane of choice so that the oily disperse phase does not become wetted in contact with the membrane surface.

3.2.2 Experimental Setup and Emulsification Procedure

A schematic of the emulsification process is shown in Figure 3.1. The tubular membrane has several cylindrical pores. The DP (PCL solution in DCM) was allowed to permeate through the membrane pores under an appropriate nitrogen gas pressure while a cross-flow of the CP (aqueous PVA solution) was maintained using a low shear magnetic pump. Once the droplets formed at the end of the pore opening, they detached from the pore opening into the CP due to the shear force caused by the running CP. Two hydrophilic membranes of mean pore diameters 50 μm and 20 μm were used. Once the emulsification was finished, the emulsion was maintained stirring at 300 rpm on a multistage magnetic stirrer for 6 hours to allow evaporation of the DCM and hardening of the MPs. The MPs were then harvested following the method described in section 2.2.2 for harvesting of conventional solid PLGA MPs.

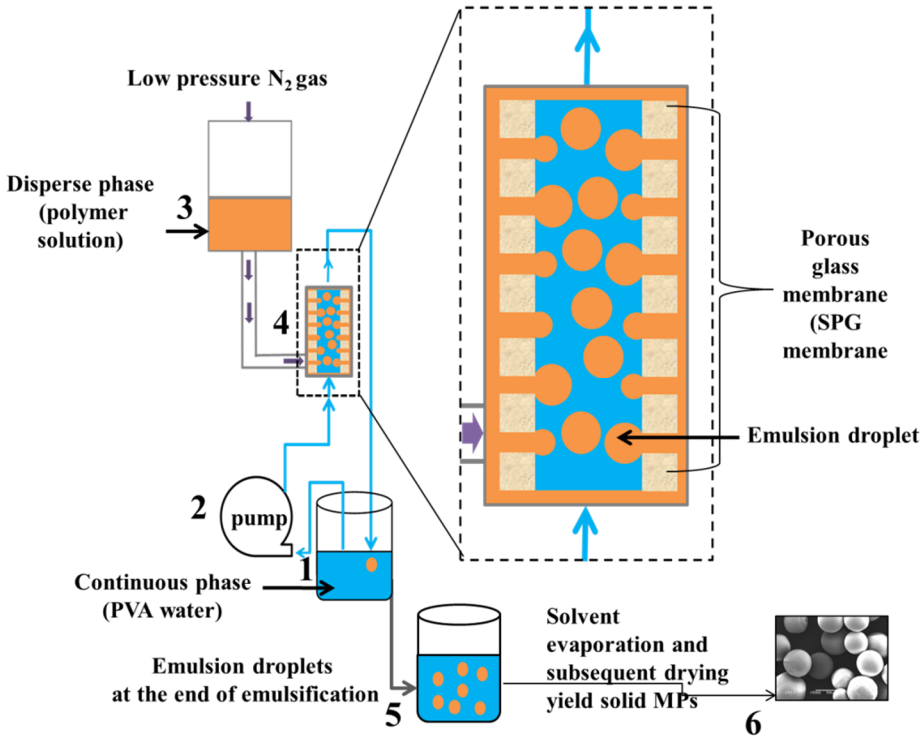


Figure 3.1 Schematic of a typical X-ME process.

1-2) Continuous phase (PVA in water) is circulating inside the membrane by a low shear magnetic pump; **3)** under a low nitrogen gas pressure, the disperse phase (polymer solution) is pushed through the membrane; **4)** emulsion droplets are formed at the pore opening inside the membrane and are detached due to the shear stress that was triggered by the flow of continuous phase; **5)** the detached droplets are deposited in a beaker; **6)** evaporation of the organic solvent and subsequent drying yield solid MPs.

Monodispersity of emulsion droplets could be influenced by several factors, such as D_0, Pw, CP flow velocity (V_{CP}), viscosity of DP(η_{DP}), viscosity of CP (η_{DP}), DP/CP volumetric ratio ($\varphi_{DP/CP}$), emulsifier type and emulsifier concentration ($Conc._{CP}$) [108, 116, 173]. Throughout the experiment, different P_w and $Conc._{CP}$ were used to achieve solid PCL MPs with mean diameter of approximately 100 μm and narrower size distribution using PCL solutions of different concentrations and viscosities. Viscosities of different polymer solutions were measured using a rheometer (Physica MCR 301, Anton Paar, UK) under a rotational mode.

The membrane was cleaned thoroughly before and after emulsification, and was maintained for further use. The membrane cleaning and maintenance process is referred to Appendix V.

3.2.3 Characterisation of the Emulsion Droplets

See section 2.2.4

3.2.4 Characteristics of the Microparticles

See section 2.2.5

3.2.5 Assessment of the Monodispersity of the Microparticles

Most of the literature referred to 'span factor' as an indicator of the degree of monodispersity of any particle size distribution [101, 171, 174], which is expressed by the following equation:

$$Span\ Factor = \frac{d_{90} - d_{10}}{d_{50}} \quad \text{---------- (i)}$$

where, d_{90}, d_{50} and d_{10} are the particle diameters at which 90, 50 and 10 volume % of the distribution fall below. Hence, the nearer the span factor towards '0', the narrower the size distribution. In general, if the span factor is less than one, the distribution is considered to be monosized [171].

The degree of symmetry in MPs size distribution was assessed by measuring skewness value. Further details are referred to section 2.2.5 of Chapter 2.

3.2.6 Statistical Analysis

See section 2.2.12 of Chapter 2.

3.3 Results and Discussion

3.3.1 Fabrication of Large MPs Using Higher Molecular Weight PCL (PCL_{80kDa})

3.3.1.i Effect of Working Pressure and Membrane Pore Size

For cross-flow membrane emulsification (X-ME), the P_w is one of the key factors that influence the emulsion droplet size, which eventually direct the shape of the solidified MPs. It has been reported that the P_w requires to set at a point that is slightly above the critical or capillary pressure (P_c) [102, 116]. P_c is the minimum pressure at which droplets first appear in the respective continuous phase. In this study, the Pc was determined experimentally for each membrane following the process stated by Nakashima et al. [121]; 9 KPa was the Pc for both membranes that were used. Nakashima et al. [102], the pioneers of the membrane

emulsification process, reported that monodisperse emulsions can be produced using SPG membranes within a certain pressure length (the length between the Pc and the upper limit of the P_w) and that the larger the pore size, the narrower the pressure length.

In this experiment, the term Pw was used to indicate the pressure used to push the disperse phase through the membrane. Some authors used the term transmembrane pressure (P_{tm}) instead of Pw to indicate the working pressure. In a most appropriate term, the P_{tm} is the difference between the pressure of the disperse phase (P_{DP}) and the mean pressure difference between the CP inlet ($P_{CP, in}$) and outlet point ($P_{CP, out}$). The following equation is used to express P_{tm}:

$$P_{tm} = P_{DP} - \left(\frac{P_{CP,in} - P_{CP,out}}{2}\right) \text{---------- (ii)}$$

Throughout the experiment, the CP flow velocity was kept constant; therefore, any change in the Pw value was presumed to be due to the variation in the P_{DP} only. Furthermore, measurement of the $P_{CP, in}$ and $P_{CP, out}$ was beyond the scope of the emulsification kit as there was no pressure gauge connected to the membrane module (see Figure 3.1). Additionally, MPs fabrication by modifying the instrumental set up was not the focus in this study. Therefore, in the context of this study, the Pw equates to the $P_{tm.}$

The membrane of the largest available pore diameter (50 µm) was used with an aim of producing larger size MPs (mean diameter of approximately 100 µm). A relatively smaller size membrane (20 µm) was used to study the effect of the membrane pore diameter on the sizes of MPs under the same emulsification

conditions. The optimum P_w, at which larger-sized MPs with a narrower span factor were obtained using both the 20 µm and 50 µm membranes, was 13 KPa; however, the expected size (mean diameter of approximately 100 µm) was achieved using the 50 µm membrane (see Table 3.1). This pressure was 1.44 times higher than the P_c and at a slightly higher Pw (20 KPa; Pw/Pc = 2.22), the size uniformity was compromised as evident from the higher span factors for both membranes. These results are comparable with those reported by Masato Kukizaki [116] and Liu et al. [175], who found that the size distribution broadened at a $P_{tm}/P_c > 1.13$ and >1.25, respectively, for 9.83 µm and 2.8 µm membranes, respectively. It is reasonable to assume that if the CP pressure ($P_{CP, in}$ and $P_{CP, out}$; see equation (ii)) were deduced from the DP pressure (Pw), the optimum P_{tm}/P_c value for this experimental set up was considerably less than the Pw/Pc value that was observed. In a recent paper, Zhao and colleagues [118] stated that only at an operating pressure of 0 KPa, uniform and larger-sized (mean diameter of 93 µm) agarose microspheres (microparticles) were prepared. The span factor they observed was 1.27 times as high as that observed in this experiment at the optimum pressure of 13 KPa. This pressure might have fallen in the 'size-stable-zone' [116, 176], at which the DP spontaneously transforms into spherical oil droplets in the running CP. On the other hand, the wider size distribution at a pressure of 20 KPa pressure might be because of entering of the pressure into the 'continuous outflow zone' [116, 176] . As noted in the literature, if the Pw falls in the range of the 'continuous outflow zone', the DP flows continuously out of the membrane into the CP. Although the average size of the MPs prepared with the 20 µm membrane was 1.8 times smaller than those prepared with the larger membrane, the size distribution span was similar (P >

0.05). For both membranes, the size distribution data also demonstrated that there was no MP with a diameter below 10 µm and only 38 volume % of the MP had a diameter below 100 µm when the 50 µm membrane was used. To the best of our knowledge, the sizes at the volume % level have not been reported before, for MPs prepared using the membrane emulsification technique, but it was of interest of this study to see if this process could exclude extremely small or large particles from the size distribution.

The % yield of the MPs was directly related to the P_w and D_0, i.e., both in the case of the lower P_w and smaller membrane, the MPs yield decreased. For examples, the % yield was lowest at a pressure of 10 KPa for both membranes and at the optimum pressure (13 KPa), the yield value was 1.42 times less for those prepared with the 20 µm membrane than those prepared with the 50 µm membrane (see Table 3.1 below). The lower % yield at the lower P_w or with the smaller membrane might be a consequence of Darcy's law [177], according to which the DP flux is lowered with the decreased pressure at a constant slope. It is not surprising that a lower DP flow rate (due to the lower Pw) will lengthen the emulsification time (t_{ME}). This study result supports the Darcy's law as seen in the Table 3.1; the wider size distribution might be a consequence of the longer t_{ME} [178, 179]. Three possible reasons, either alone or in combination, may have caused this effect. Firstly, the low DP flux allowed the oil droplets to stay longer at the pore opening until they grew large enough or experienced enough CP shear to detach into the running CP. During this time, the physical properties of the volatile DP might have changed, in terms of the droplet volume or shape, and formed a polydisperse emulsion. Secondly, the long-term exposure of the

membrane interior to the oil phase may have compromised the degree of hydrophilicity of the membrane, and the size distribution may have widened due to the wetting of the membrane with the oil phase [119]. Thirdly, due to a longer t_{ME}, the droplets that formed earlier might have coalesced with other droplets while they were moving through the CP circulation. Additionally, some droplets might have been damaged in the pump gear due to repeatedly passing through it [180], and eventually the emulsion droplets size may have become wider. In contrast, a completely different reason might be attributed to the higher span value at the highest pressure of 20 KPa. As stated earlier, the transition from the 'size-stable-zone' to the 'continuous-outflow-zone' should be avoided to prevent the 'jetting' of the disperse phase; the use of an overly high Pw, i.e., a pressure far away from the Pc increase the possibility of this transition [120]. A pressure of 20 KPa might have caused a shift in the droplet formation phenomenon from a 'dripping' to a 'jetting' regime and, therefore, may have affected the size uniformity.

Table 3.1 Effect of Working Pressure and Membrane Pore Size

Membrane Pore Size (Mean Pore Diameter)		**Working Pressure (KPa)**		
		10	**13**	**20**
20 µm	mean diameter (µm)) ± SD	42±11.07	60±12.59	75±18.68
	span factor ± SD	0.72±0.03	0.52±.02	0.64±0.02
	volume % of MPs lower than 1 µm	0.25	0.00	0.00
	volume % of MPs lower than 10 µm	0.59	0.02	0.10
	volume % of MPs lower than 100 µm	100	99.95	89.87
	% yield	20-22	39-42	40-42
	emulsification time (minute)	10	6	1.5
50 µm	particle diameter (µm)) ± SD	93±24.24	109±20.75	119±36.89
	span factor ± SD	0.64±0.04	0.51±0.04	0.72±0.06
	volume % of MPs lower than 1 µm	0.43	0.00	0.72
	volume % of MPs lower than 10 µm	1.03	0.00	1.69
	volume % of MPs lower than 100 µm	60.64	37.68	21.7
	% yield	51-52	55-60	56-60
	emulsification time (minute)	6	2.5	1

3.3.1.ii Effect of PVA Concentration

Both the emulsifier type and concentration play an important role in the size and size uniformity of the MPs prepared using membrane emulsification. PVA is the most widely used emulsifier in biomedical applications because of its low toxicity, good solubility in water and biocompatibility [181-183] compared with other emulsifiers such as sodium lauryl sulphate (SLS) and Tween 80. In this study, three different concentrations of PVA solutions, 0.1, 0.3 and 1.0 % (w/v) were used; however, only 0.3 % (w/v) PVA produced MPs of the expected size with a narrower span of the distribution when the 50 µm membranes was used (see Figure 3.2). MPs with a narrower span were also prepared with the 20 µm membrane and using 0.3wt% PVA concentration; however, the mean particle diameter was substantially smaller than '100'µm and it is reasonable to assume that the smaller-sized membrane would result in smaller MPs. This trend is comparable to those reported in the literature for SPG membranes [119, 184]. The representative SEM images, as shown in Figure 3.3 and Figure 3.4 are also in agreement with the data shown in Figure 3.2. Conversely, irrespective of the membrane pore size, the mean particle size decreased with the increase in the PVA concentration, as depicted in Figure 3.2. These results are in agreement with those reported for the X-ME setup [117, 185]. The possible explanation for these results is that at a higher concentration of PVA (1.0 % w/v), the oil/water interfacial tension ($\gamma_{o/w}$) force reduced quickly and the droplets detached from the pore opening more frequently. This allowed the droplets to grow to a minimum before detachment, no matter how large or small the membrane pore was [185]. Although the mean particle sizes for both membranes at 1.0 % w/v PVA were the smallest, the span values were nearly the same ($P > 0.05$). It is unknown why the

span factors for both the 0.3 % w/v and 1.0 % w/v PVA were similar. However, it is presumed that an emulsifier at an appropriate concentration prevents droplet aggregation by forming a thin layer that surrounds a newly formed droplet and, thus, helps to minimize the span value of the final emulsion. Once the o/w interface is saturated with the emulsifier film, a further increase in the emulsifier concentration has no effect on the droplet aggregation minimization. The droplets might have been saturated with a thin layer of the emulsifier when 0.3 % w/v PVA was used and any further increase in the concentration had no effect in terms of reducing the span value of the final emulsion.

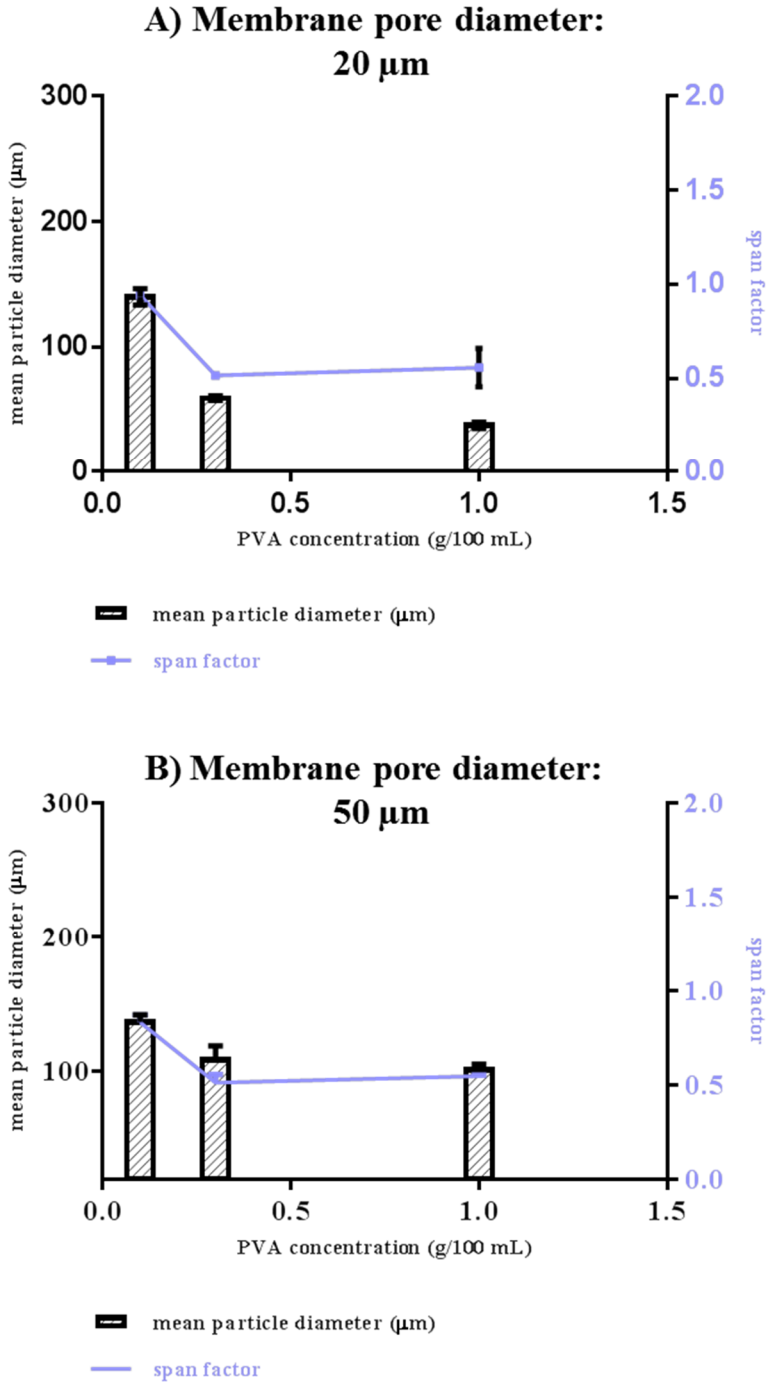


Figure 3.2 Mean particle diameter with corresponding span factor as a function of PVA concentration (0.1, 0.3, 1.0 % w/v in water). The MPs were prepared using 12.5 % w/v PCL_{80kDa} using membranes of pore diameters **A)** 20 µm and **B)** 50 µm. Values are represented as mean ± SD (n = 3; r = 3)

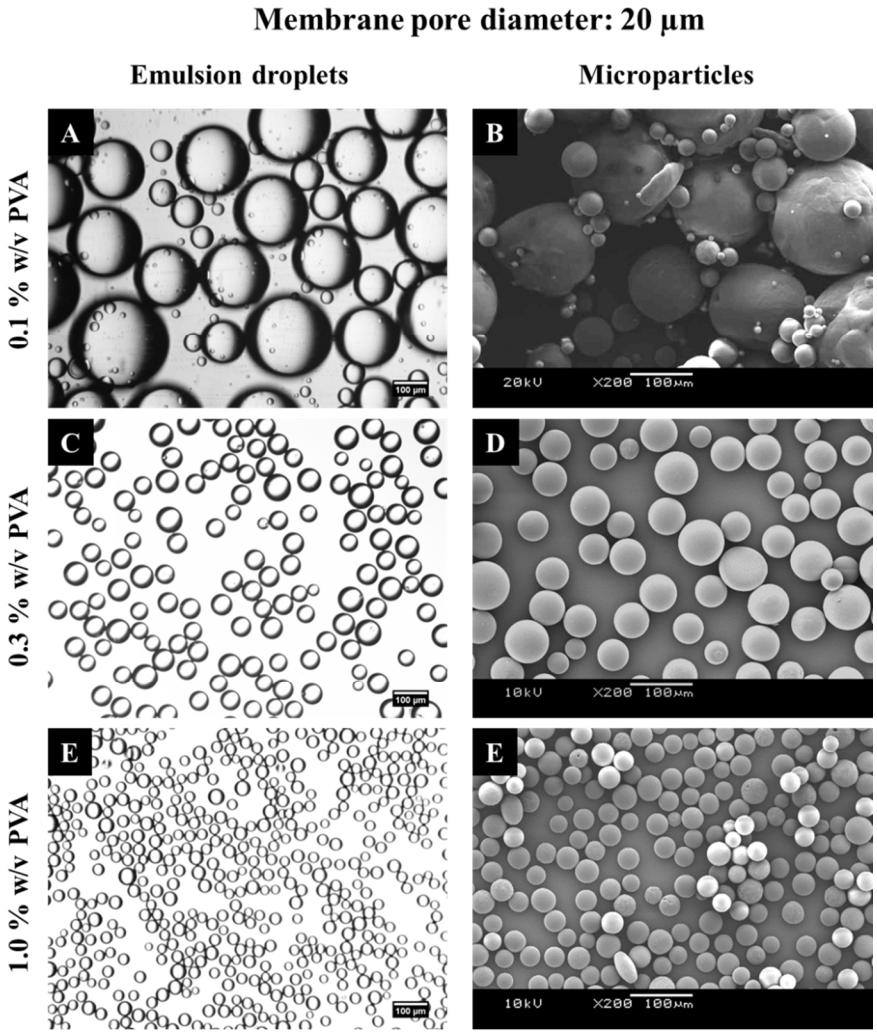


Figure 3.3 Emulsion droplets (left-hand column) and their corresponding MPs (right-hand column) prepared for 12.5 % w/v PCL_{80kDa} with 0.1 - **(A – B)** , 0.3 - **(C –D)** and 1.0 - **(E – F)** % w/v PVA, using SPG membranes with mode pore diameters of 20 µm. Scale bar = 100 µm.

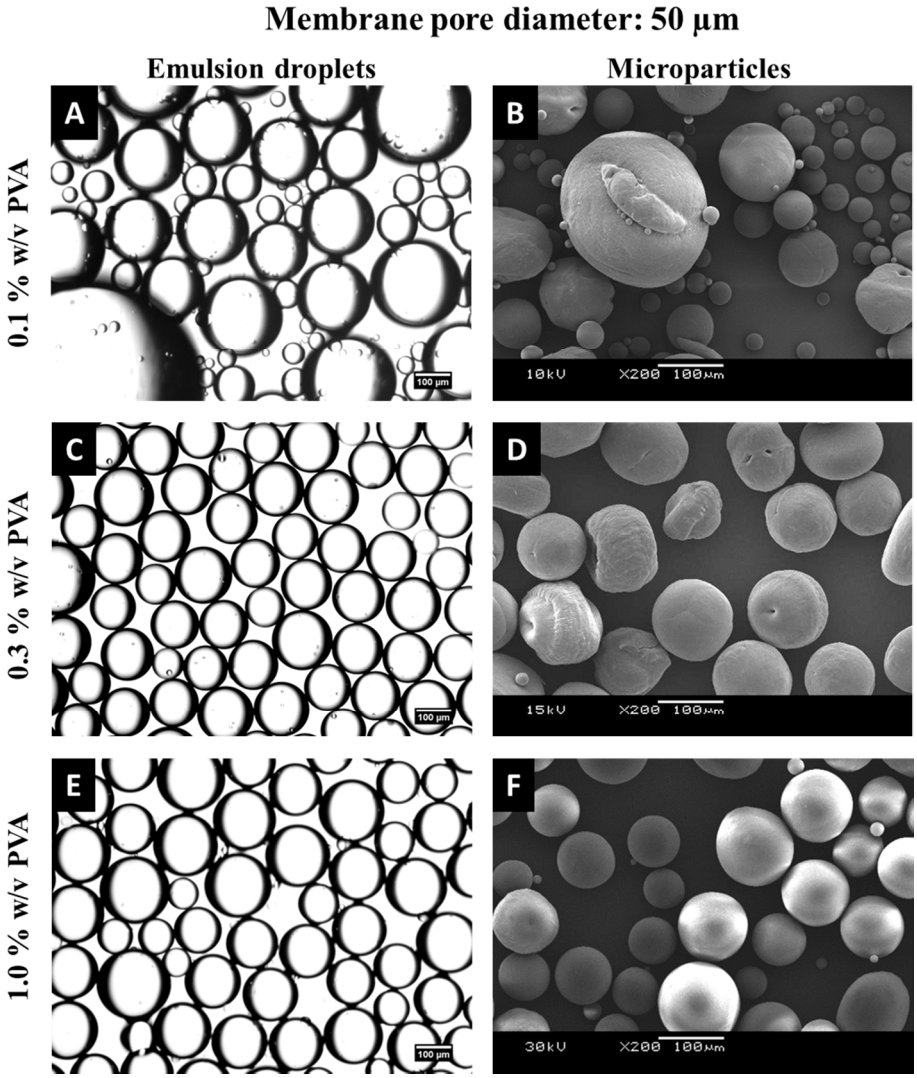


Figure 3.4 Emulsion droplets (left-hand column) and their corresponding MPs (right-hand column)) prepared for 12.5 % w/v PCL_{80kDa} with 0.1 - **(A – B)** , 0.3 - **(C –D)** and 1.0 - **(E – F)** % w/v PVA, using SPG membranes with mode pore diameters of 50 µm. Scale bar = 100 µm.

3.3.1.iii Effect of Viscosity of Polymer Solution

There have been several studies on the effect of the continuous phase viscosity [108, 117, 118, 185] or aqueous disperse phase viscosity [118, 119] on the uniformity of the emulsion droplets prepared using membrane emulsification. However, to the best of our knowledge, there are no previous studies on the effect of viscosity of the polymeric disperse phase on the droplet uniformity under the X-ME set-up. In this study, a series of PCL solutions in DCM were prepared and their viscosities were studied (see Figure 3.5A). Some of the solutions were used as DPs and the emulsification process was operated at a P_w of 13KPa and a $Conc._{CP}$ of 0.3 % w/v PVA using a membrane with D_0 of 50 µm. The DP of the 12.5 % w/v polymer concentration, which corresponds to η_{DP} = 1.33 Pa.s, produced relatively monodisperse emulsion droplets, as evidenced from the representative microscopic images in Figure 3.6 E. The resultant MPs were also relatively uniform, as seen in Figure 3.5 B and Figure 3.6 F. The other less concentrated or less viscous DPs produced emulsions with wide size distributions and their corresponding MPs were also polydisperse, as depicted in Figure 3.5 and Figure 3.6 A–D. In an equivalent study [186], a similar trend was observed for low viscosity divinylbenzene that produced emulsion droplets with a wider size distribution in relation to the highly viscous soybean oil. In the same report, the authors also demonstrated that emulsion droplets form spontaneously when there is a balance between the adhesion torques ($T_{adhesion}$) and detachment torques ($T_{detach;}$; [186]; Figure 3.7). Additionally, a more-uniform emulsion is formed when the droplet formation is spontaneous-transformation-based (STB) not shear (SHE) - induced [116, 187, 188]. As the operation-, membrane- and phase-parameters remained unchanged throughout the experiment, any imbalance

between $T_{adhesion}$ and T_{detach} was attributed to the phase parameters (viscosity and density). Considering the droplet detachment mechanisms, as stated in the aforementioned literature, the possible explanation for the effect of the viscosity on the particle size is as follows: for the low viscosity DPs (5 and 10 % w/v), the CP drag force might have dominated over the viscous force and the droplet detachment from the pore opening was SHE -induced, i.e., due to stronger CP shear, and eventually the monodispersity of the emulsion was spoiled. Conversely, for the highly viscous DP (12.5 % w/v PCL), its' flow through the membrane pores may have reduced due to the high inertia of the DP. This may have led to the droplets staying longer at the pore opening until $T_{adhesion} = T_{detach}$, and eventually forming spontaneously via the STB mechanism. Thus this phenomenon (STB mechanism) preserved the monodispersity of the final emulsion and the resultant MPs.

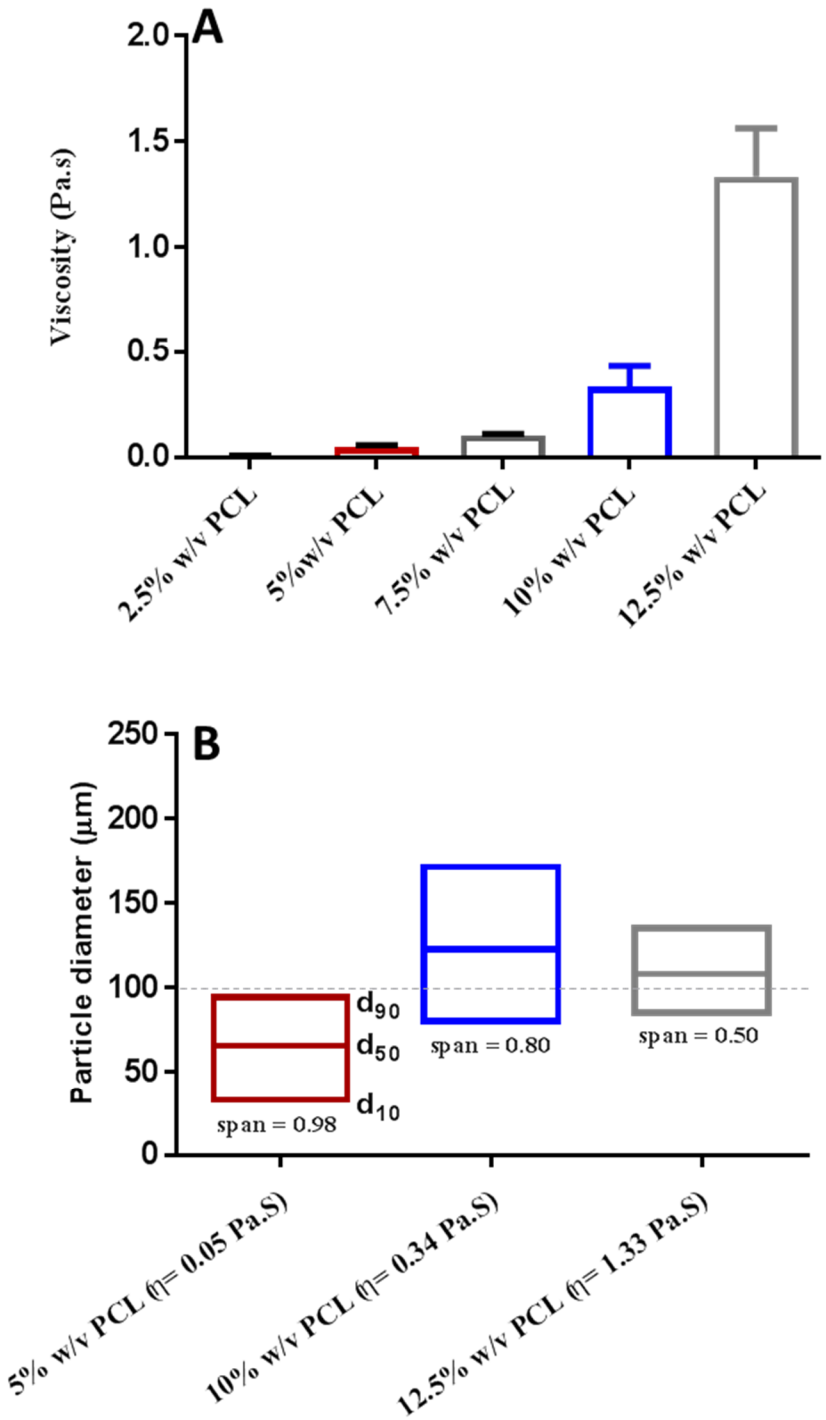


Figure 3.5 Effect of viscosity of PCL solutions.

Viscosities of a series of PCL80kDa solutions in DCM **(A)**; Size distributions of the MPs, in terms of particle diameter (MP diameter) and span factor for 5-, 10- and 12.5- % w/v PCL_{80kDa} in DCM **(B)**. Values are represented as mean ± SD (n = 3; r = 3).

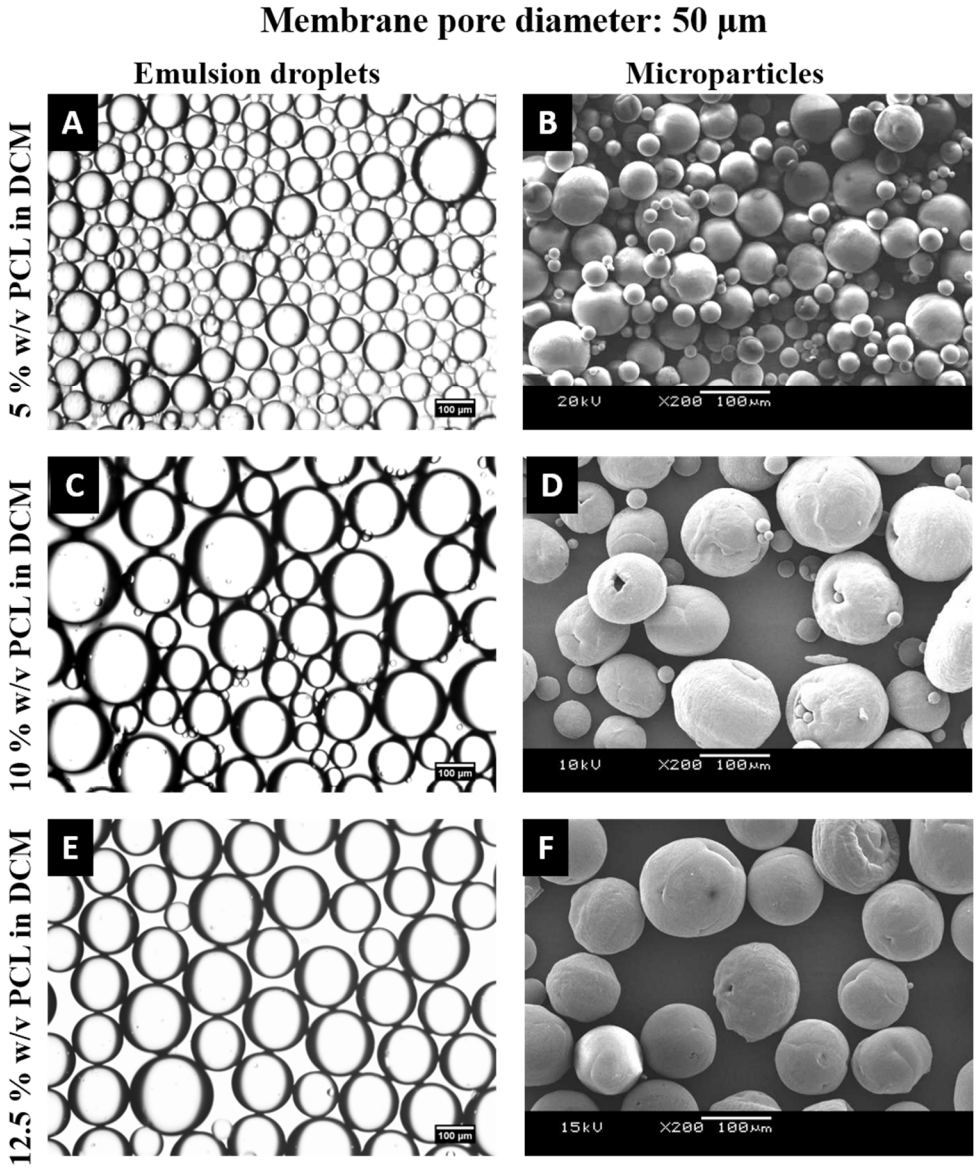


Figure 3.6 Effect of viscosities of different concentrations of PCL solutions.

The left-hand column shows the optical light microscopic images of the emulsion droplets prepared by **A)** 5-, **C)** 10- and **E)** 12.5-% w/v PCL in DCM. The right-hand column shows the SEM images of the corresponding MPs prepared by **B)** 5-, **D)** 10- and **F)** 12.5-% w/v PCL in DCM. Scale bar = 100 µm.

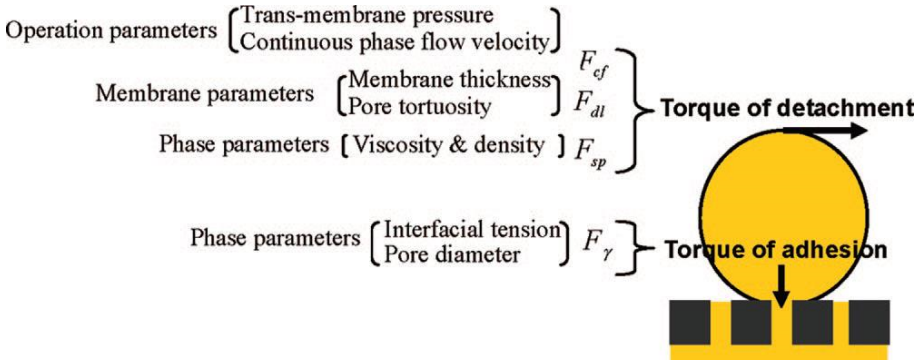


Figure 3.7 Forces acting on a droplet under an X-ME setup (reproduced from reference [186]

On the basis of the above-mentioned results, the optimum conditions for preparing PCL MPs with a mean diameter of approximately 100 μm using PCL_{80kDa} are presented in Table 3.2 below.

Table 3.2 Optimal Conditions for Preparation of MPs with Diameters of Approximately 100 μm Using the Higher Molecular Weight PCL ($PCL_{80\ KDa}$)

Emulsification Conditions	**Amount/Unit**
Disperse phase	
Concentration of disperse phase,$Conc._{DP}$	12.5 % w/v PCL in DCM
Viscosity of disperse phase, η_{DP}	1.33 Pa.s
Continuous phase	
Concentration of continuous phase, $Conc._{CP}$	0.3 % w/v
Volume flow rate of continuous phase, V_{CP}	1.55-1.63 l/min
SPG membrane pore size, D_0	50 μm
Volume ratio of oil to water phase, $\varphi_{DP/CP}$	1:26
Working pressure, P_w	13 KPa

3.3.1.iv Emulsion Droplet Characteristics during Emulsification

To assess the characteristics of the emulsion droplets, the emulsion samples were collected at different time points during the emulsification process and the droplets were viewed under the microscope. As shown in Figure 3.8, within a few seconds of the start of the emulsification process, droplets formed and detached into the running CP. As stated in the literature [102], the DP usually starts to permeate into the CP and forms droplets at the critical pressure, P_c [102]. Therefore, at a pressure of 13 KPa, which is a pressure 1.44 -times higher than the P_c, it is expected that the droplets would appear in the CP immediately after the start of the emulsification process. However, this does not tell the exact time point when the droplets first appeared in the CP. Real-time droplet formation was studied by others using SPG membranes [176, 189] or a micro-engineered membrane with uniform pores [190], where a flow of CP was maintained crossway to the DP flow, in a manner similar to this set-up, but without any recirculation of the CP. In the literature, the focus has been mainly on the droplet formation behaviour at different transmembrane pressures, or the DP flux under the same or different CP flow rates. In this experiment, the droplet characteristics were studied under the optimum emulsification conditions, with the same Pw, $Conc._{DP}$, $Conc._{CP}$, and $\varphi_{CP/DP}$. As stated in section 3.3.1.ii, the $\gamma_{o/w}$ force plays an important role in the droplet detachment. In general, the $\gamma_{o/w}$ reduces faster in the presence of a higher concentration of emulsifier, and sooner the $\gamma_{o/w}$ is reduced, the quicker the droplet detaches from the membrane pore opening into the running CP [185]. In the case of X-ME, the rate at which the $\gamma_{o/w}$ between a newly formed oil droplet and the surrounding water phase reduces would not be the same throughout the whole duration of the emulsification process. This is due to

the recirculation that causes a gradual increase in the droplet volume, but a depletion of the emulsifier concentration, in the system. In other words, initially the droplet formation rate would be faster because, a lot of 'free' emulsifier is available for the droplets that have just formed; however, the amount of 'free' emulsifier gradually decreases as the process progresses further. As a consequence, the droplets formed in the early stage of the emulsification process are expected to detach faster and would be relatively smaller in size than those formed in the later stage. The images of the droplets, as shown in Figure 3.8 are also in agreement with the aforementioned explanation. It was also observed that all the droplets captured at a particular time point were not of the same size and that this scenario was observed even at the start of the emulsification process. The structural properties of the SPG membrane may be responsible for this non-uniformity in droplet size. An SPG membrane contains tortuous, interconnected cylindrical pores and the degree of tortuosity varies at different parts of the membrane [191]. Due to this tortuosity, the pore length varies within the same membrane. Therefore, the droplets that passed through a shorter tortuous channel would grow and detach earlier than those that passed through a longer tortuous channel, which might cause a variation in the droplet size, even at a particular time point. Furthermore, as all the pores of a particular multichannel (multi-pore) membrane are not of the same size, the droplets formed from the membrane would not be the same size, irrespective of at which time point the droplets are collected.

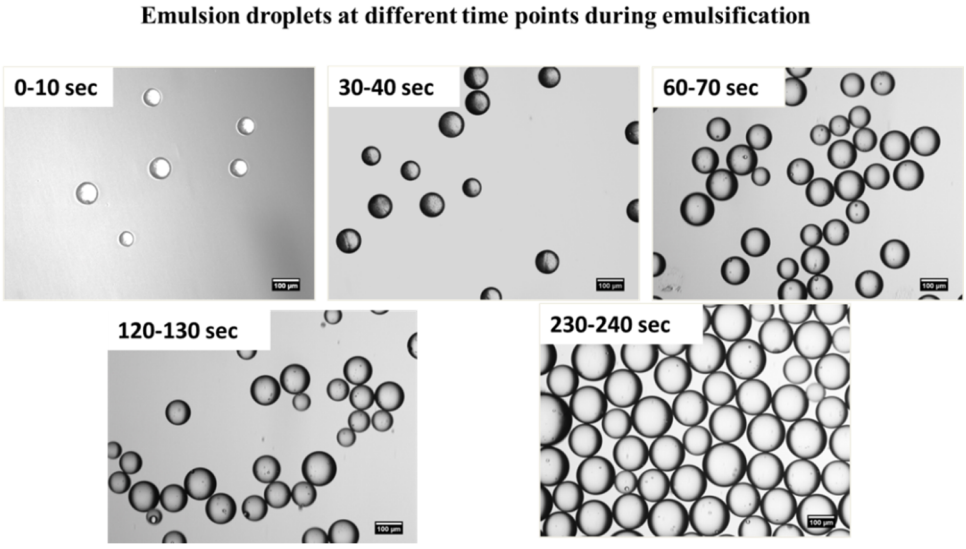


Figure 3.8 Optical light microscopy images of emulsion droplets collected at different time points during the emulsification process.

3.3.1.v Influence of MP Hardening Step

The effect of solvent evaporation and stirring on the particle shape, size and size distribution (SD) pattern was studied by analysing the size before and after the DCM evaporation step using a laser diffraction method. Figure 3.9 shows the droplet size distribution (DSD) and particle (MP) size distribution (PSD) before and after the DCM evaporation step. As seen in the figure, after the DCM evaporation, there is only a slight change in the SD graph, but the graph shape is the same as that before the DCM evaporation step. The change in the mean diameter due to DCM evaporation and stirring was statistically insignificant (P value = 0.63). These results are in contrast with those reported by Imbrogno and colleagues [150] who observed a 24% shrinkage of the emulsion droplets in relation to the solidified MPs prepared by using 8 – 30 % w/v PCL (Mw = 14 kDa) and a 10 µm circular-disc-type metallic membrane under a rotating-membrane emulsification set-up. Although the polymer concentration that was used in this study fell within the range that Imbrogno et al. used, the molecular weight used in this case was a lot higher than that reported in the literature. Due to this difference, there might have been a difference in the bulk density of the respective DPs. For a DP with a higher bulk density, which might be the case for the 12.5 % w/v PCL (Mn = 80 kDa), there will only be a small amount of shrinkage of the emulsion droplets after solidification. The graph pattern of the emulsion droplets and the respective MPs (Figure 3.9) is also an indication of the minimum shrinkage after the DCM evaporation. On the other hand, each of the frequency polygons in Figure 3.9 can be categorized as symmetrical distributions because there are no distinguishable long tails to the right or left of the distributions. The closeness among the mean, median and mode values for both

the emulsion droplets and MPs is also a sign of symmetry in the SD. The symmetric SDs, both for the emulsion droplets and MPs, mean that there were no extremely small or large droplets or MPs. It was also observed that the traceable (0.1 volume %) droplet or MP size was below 50 µm; however, all (100 volume %) the diameters were below 200 µm, which indicates the degree of narrowness in the SD. The degree of narrowness of the SD was measured quantitatively by measuring the span factor of the distribution, and is reported in the previous section. The span factor of the emulsion droplet size distribution was similar to that of the MPs size distribution (p value > 0.05). According to the aforementioned discussion, the solvent evaporation and stirring process had small effect on the MPs sizes and size distributions in terms of their monodispersity.

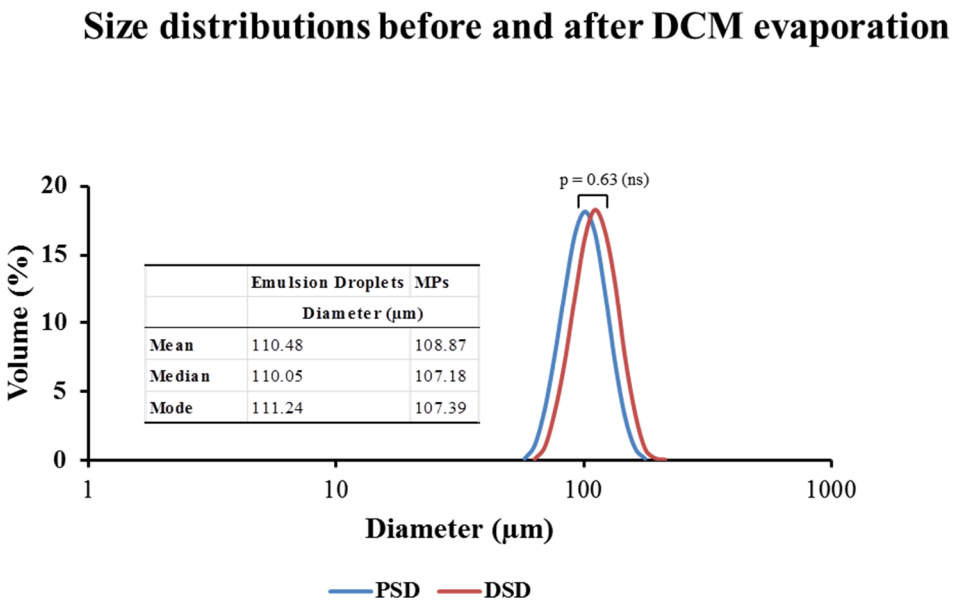


Figure 3.9 Size distributions of emulsion droplets before DCM evaporation (DSD) and their corresponding MPs after DCM evaporation (PSD), under the optimum emulsification conditions. PSD = particle size distribution; DSD = droplet size distribution.

3.4 Fabrication of Large MPs Using Lower Molecular Weight PCL (PCL_{45kDa})

In the previous section, it is demonstrated that $PCL_{80\ kDa}$ with DP of different viscosities resulted in MPs of different sizes and span factors under the same emulsification conditions (Pw, $Conc._{CP}$, $\varphi_{o/w}$ and V_{CP}), and that the MPs with an optimum size were prepared from a DP with a higher viscosity (viscosity, η_{DP} = 1.33 Pa.s). On the basis of this study, the interest was to investigate whether or not a lower molecular weight PCL (PCL_{45kDa}) with a viscosity close to that of the $PCL_{80\ kDa}$ could be used to make MPs with diameters of approximately '100 μm' and a narrower span factor. PCL_{45kDa} was chosen to prepare a series of PCL PCL_{45kDa} solutions in DCM, and then their viscosities were studied to investigate the DP with the optimum viscosity (closes to that of the PCL_{80kDa}). As discussed in the earlier sections, 13 KPa, 0.3 % w/v 12.5 % w/v, 1.33 Pa.s and 1:25 were the optimum working pressure, $Conc._{CP}$, $Conc._{DP}$, η_{DP} and $\varphi_{DP/CP}$, respectively. As shown in Figure 3.10 A, both 35 and 37.5 % w/v PCL_{45kDa} demonstrated viscosities close to that of the 12.5 % w/v PCL_{80kDa}, but the MPs prepared with these solutions (35 and 37.5 % w/v PCL_{45kDa}) had diameters that were above 150 μm and were highly polydisperse, which are represented as floating bars 'iii' and 'iv' in Figure 3.10 B. The respective SEM images in Figure 3.11 C and Figure 3.11 D also represent the polydispersity of the samples. The volumes of each of the DPs were kept the same as that of the PCL_{80kDa} (70 mL) and are marked as LV (large volume; Figure 3.10 B). There are several possible reasons that alone or in combination, might have caused the particle size distribution to be wide in the case of the samples prepared with 35 and 37.5 % w/v PCL_{45kDa}, even though both

samples had viscosity values close to that of the PCL_{80kDa}. The first reason is that because of the overall weight increment of the DPs (35 and 37.5 % w/v PCL_{45kDa} in DCM), the total droplet volume in the final emulsion was increased. Due to the recirculation in the system and the denser overall droplet volume, the droplets were in close contact with each other; therefore, eventually, the droplets may have experienced more shear stress, both between droplets and with the membrane surface. This might have caused the droplets to break off into smaller fractions. Secondly a longer emulsification time could have had a negative effect on the droplet uniformity; in the case of the PCL_{45kDa} solutions (35 and 37.5 % w/v), the emulsification time was longer when compared with that of the $PCL_{80\ kDa}$. Therefore, with a longer emulsification time the formed droplets would recirculate more repeatedly and would experience more shear stress, which would affect the droplet uniformity. Thirdly, a DP with a higher concentration result in droplets of a larger size [186], and in that case, two larger droplets from adjacent pores may coalesce and grow even bigger before they detach; this phenomenon would compromise the size uniformity of the droplets.

If the broader size distribution was due to the effect of the higher volume of the DPs, reducing the volume could narrow down the SD. It is important to note that when the volume of the DP was reduced, i.e., using a small volume (SV) of the DP, the width of the distribution was minimized; however, the mean particle size was still above 150 μm, for 50 μm membrane, as shown in Figure 3.10 B for the sample that corresponds to the floating bar 'v'. However, using a smaller membrane (20 μm), the same solutions with a SV of DP produced MPs of the expected size and with a narrower distribution. As shown in the floating bar 'vi'

and 'vii' of Figure 3.10 B for samples with 35 % w/v PCL_{45kDa}-SV and 37.5 % w/v PCL_{45kDa} -SV, respectively, both the samples produced MPs with diameter of approximately '100 µm' and their span factors were 0.46 and 0.54, respectively. The respective SEM images of the samples shown in Figure 3.11 F and Figure 3.11G also show that there were no extremely small or large MPs and that the SDs were relatively uniform. The use of a smaller size membrane might have increased the inertia of the DP inside the membrane pores and allowed the droplets to stay connected to the pore openings until $T_{adhesion} = T_{detach}$ [187, 188], after which they dropped off spontaneously in the running CP.

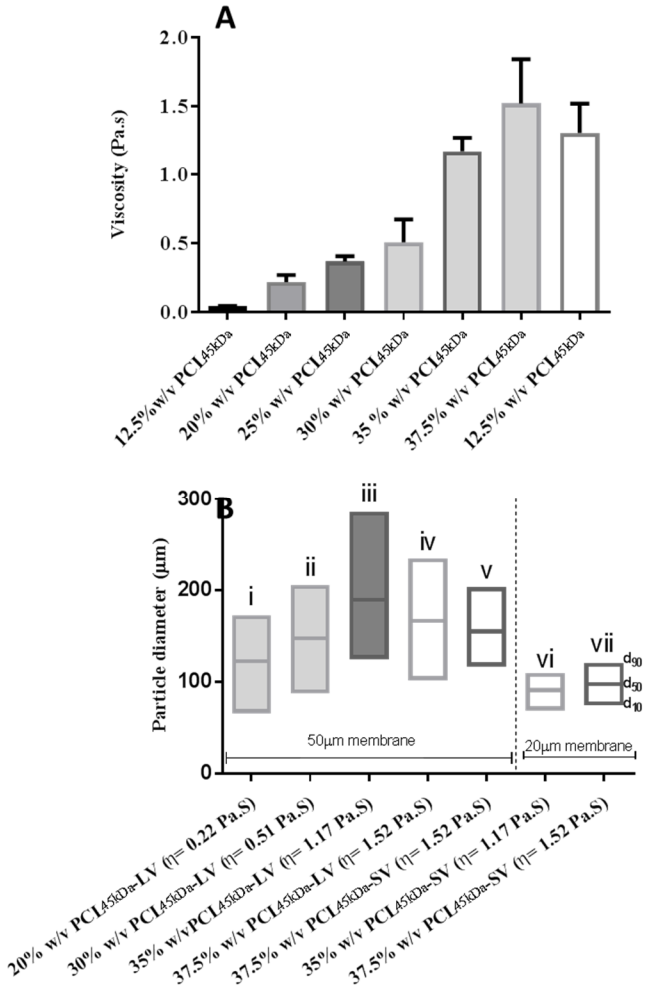


Figure 3.10 Effect of viscosities of DPs (for PCL_{45kDa}) on PSDs.
Viscosities of a series of PCL_{45kDa} in DCM **(A)**; as shown in the figure, 35- and 37.5- % w/v PCL_{45kDa} correspond to viscosities close to that of 12.5 % w/v $PCL_{80\ kDa}$ ($p>0.05$). PSDs for a series of PCL_{45kDa} in DCM **(Bi – Bv)**; different concentrations of large volume (LV) of PCL_{45kDa} (PCL_{45kDa}-LV) were used to prepare MPs using a membrane with pore diameter of 50 µm, which resulted in MPs with larger sizes and broader span of distributions **(Bi – Biv)**; The small volume (SV) PCL_{45kDa} (PCL_{45kDa}-SV) also resulted in larger-sized MPs with broader span factor **(Bv)**, although the viscosity of the DP was close to that of 12.5 % w/v $PCL_{80\ kDa}$. MPs with mean diameters of approximately 100 µm and narrower span factors were produced using 35 % w/v **(Bvi)** and 37.5 % w/v **(Bvii)** PCL_{45kDa}-SV via a membrane with pore diameter of 20 µm . Values are represented as mean ± SD (n = 3, r = 3).

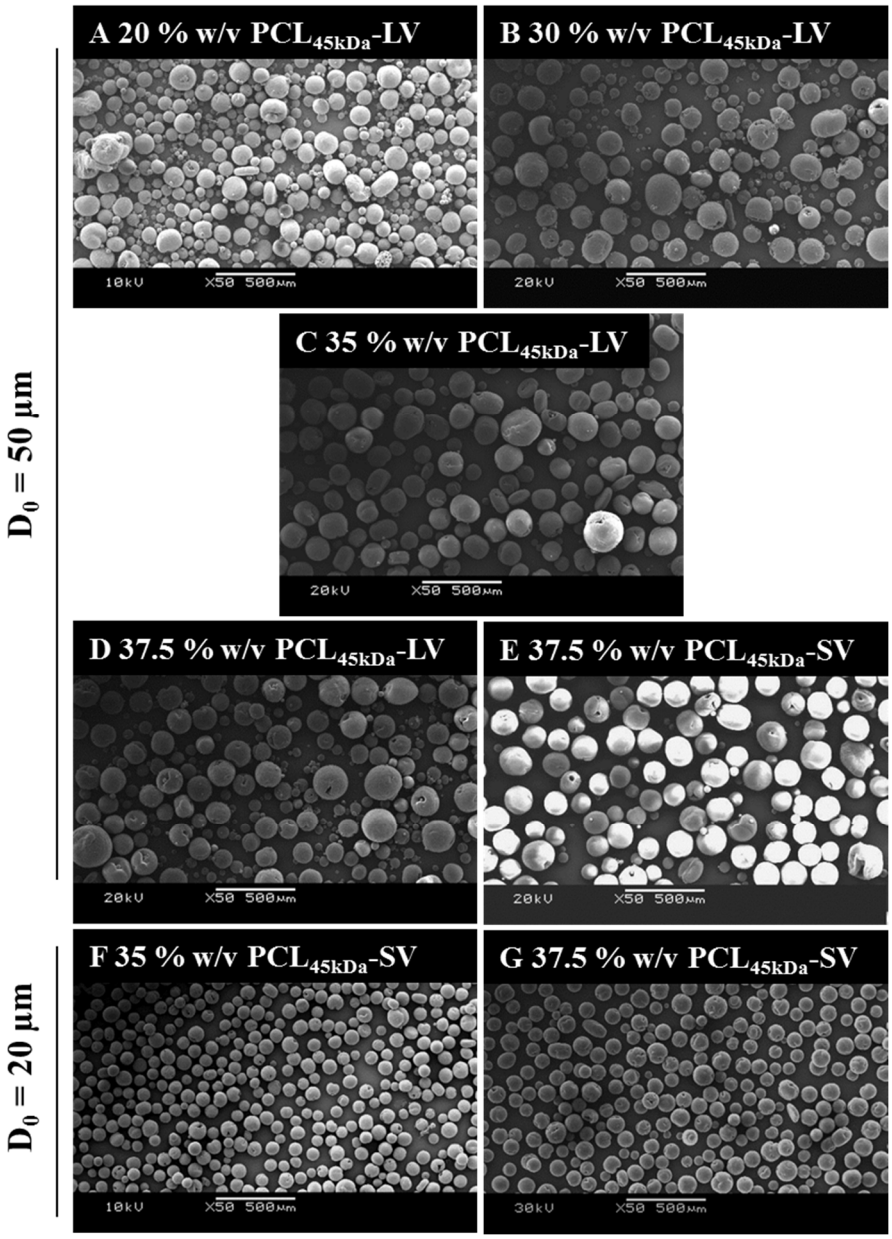


Figure 3.11 Representatative SEM images of MPs prepared using different concentrations of PCL_{45kDa} in DCM.

A – D) MPs prepared using PCL_{45kDa}-LV (20-, 30-, 35- and 37.5- % w/v PCL45kDa) via membraneS with pore diameters of 50 µm (D_0 = 50 µm); **E)** MPs prepared using PCL_{45kDa}-SV (37.5 % w/v PCL_{45kDa}) via a membrane with pore diameter of 50 µm (D_0 = 50 µm); MPs prepared using **F)** PCL_{45kDa}-SV (35 % w/v PCL_{45kDa}) and **G)** PCL_{45kDa}-SV (37.5 % w/v PCL_{45kDa}) via membranes with pore diameters of 20 µm (D_0 = 20 µm). Scale bar = 500 µm.

On the basis of the results described above, the optimum conditions for obtaining the large and uniform-sized PCL MPs using PCL_{45kDa} are shown in Table 3.3 below:

Table 3.3 Optimal Conditions for Preparation of '100 µm' MPs Using Lower Molecular Weight PCL (PCL_{45kDa})

Process parameter	**Amount/Unit**
Disperse phase	
Concentration of disperse phase, $Conc._{DP}$	37.5 wt% PCL in DCM
Viscosity of disperse phase, η_{DP}	1.57 Pa.s
Continuous phase	
Concentration of continuous phase, $Conc._{CP}$	0.3 wt%
Volume flow rate of continuous phase, V_{CP}	1.55-1.63 l/min
SPG membrane pore size, D_0	20 µm
Volume ratio of oil to water phase, $\varphi_{DP/CP}$	1:45
Working pressure, P_w	13 KPa

3.5 Relation Between Particle Size and Pore Size at Optimal Emulsification Conditions for PCL_{80kDa} and PCL_{45kDa}

There is a direct relationship between the particle size (D_p) and membrane pore diameter (D_0); in general, the larger the D_0, the greater the D_p [114, 119, 120]. The following equation shows the relationship between the D_0 and D_p:

$$D_0 = cD_P \text{-------- (iii)}$$

where, the value of c varies from 3 – 10 [114, 115]. As depicted in Figure 3.12 the D_p prepared using the 50 µm membrane was relatively larger than that of the MPs prepared using the 20 µm membrane. It was also shown that the final D_p was twice as large as the D_0 when a membrane with D_0 of 50 µm and the 12.5 % w/v PCL_{80kDa} were used. On the other hand, the MPs prepared using a membrane with D_0 of 20 µm, were almost five times larger than the D_0 for both the 35 % w/v and 37.5 % w/v $PCL_{45\ kDa}$. These findings are in agreement with the statement of Vladisavljevi´c et al. [189], who stated that in the case of direct membrane emulsification, the final emulsion droplet size could be more than two times or even greater than three times of the pore diameter.

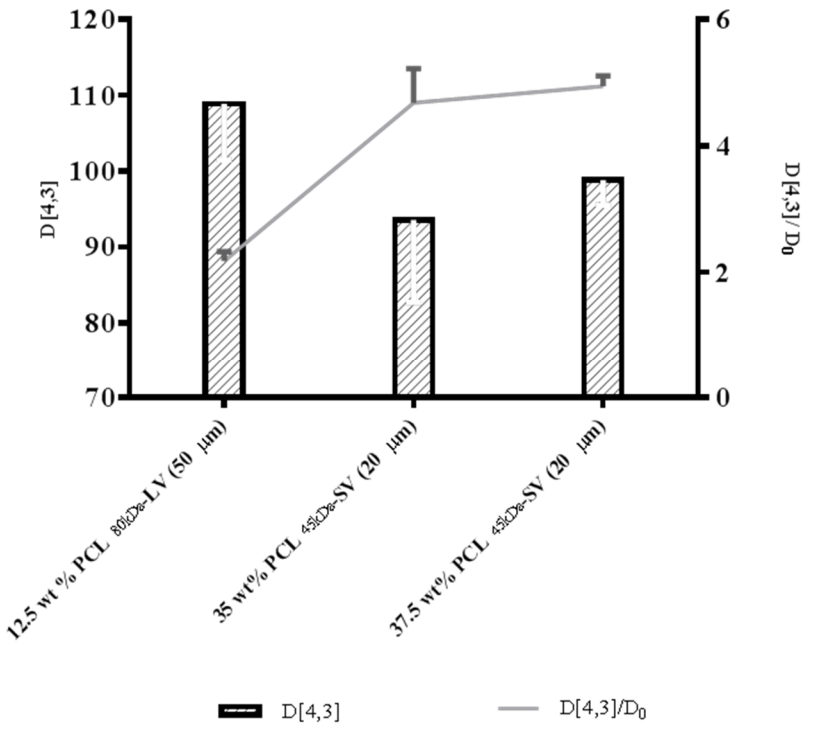


Figure 3.12 Volume mean diameters (D[4,3]) of MPs in relation to D_0 and polymer concentrations. The values are represented as mean ± SD (n = 3, r = 3).

3.6 Conclusions

The aim of the work presented in this chapter was to prepare uniform-sized PCL MPs with a mean diameter of approximately 100 μm and narrower size distribution, using the X-ME technique. PCL of number average molecular weights 80 and 45 kDa were used and, the MPs with optimal size and size uniformity were obtained by controlling different emulsion conditions, such D_0, Pw, $Conc._{CP}$, $Conc._{DP,}$ $\varphi_{DP/CP}$).

D_0 and P_w are the two most important factors that govern the size and size uniformity of MPs prepared using the X-ME technique. The two factors are interrelated; for example, the use of a smaller membrane requires the application of a higher pressure and vice versa. It is reasonable to assume that to prepare larger MPs, a higher D_0 would be required. Moreover, increasing the D_0 would decrease the capillary pressure of the membrane and would allow the continuous or turbulent flow of the DP, unless the DP reaches at a certain level of viscosity that is capable of resisting the turbulence of the flow. Uniform-sized emulsion droplets were achieved only when the flow of the DP was spontaneous and the P_w fell in the 'size-stable-zone', a P_w window at which the DP spontaneously transformed into spherical oil droplets. In this study, for both the 45 and 80 kDa PCL, MPs of an optimum size (approximately '100 μm' with narrower span of distributions) were prepared using the 20 and 50 μm membranes, respectively, with a P_w of 13 KPa only when the other parameters ($Conc._{DP}$, $Conc._{CP}$ and $\varphi_{DP/CP}$) were also set at the optimum levels.

The $Conc._{CP}$ or the emulsifier concentration (PVA -in -water) is the other factor that influenced the size of the MPs prepared using the X-ME technique in this study. Irrespective of the D_0, the D_p decreased by increasing the $Conc._{CP}$, possibly because of the faster reduction of the $\gamma_{o/w}$ with the more concentrated emulsifier that might have caused the quicker formation of the droplets. However, monodisperse MPs of expected size range were achieved only with 0.3 % v/v PVA using both the 20 and 50 μm membranes.

The viscosity study demonstrated that only those solutions of the 80 and 45 kDa PCL that had higher viscosities (for the 80 kDa with a η_{DP} = 1.33 Pa.s and for the 45 kDa with a η_{DP} = 1.17 to 1.52 Pa.s, P > 0.05) resulted in monodisperse MPs with a P_w of 13 KPa and a $Conc._{CP}$ of 0.3 % w/v PVA using a specific CP flow rate (V_{CP} = 1.55-1.63 l/min). However, a little adjustment of the $\varphi_{DP/CP}$ and the selection of the appropriate D_0 were required for preparing monodisperse solid MP_S with the lower molecular weight PCL (PCL_{45kDa}).

Taking into account the outcome of the work described in this chapter, the following chapter focuses on investigation of the optimum emulsification conditions for preparing porous PLGA MPs. It is expected that the PLGA solution that have viscosity close to that of the optimum 80 or 45 kDa PCL could be used as a DP for preparing the optimum size PLGA MPs under the same emulsification conditions (Pw, CP flow rate and concentration).

Chapter 4 Fabrication of Large, Porous PLGA Microparticles Using Cross-Flow Membrane Emulsification

4.1 Introduction

In the field of tissue engineering, PLGA in the form of spherical scaffold particles or MPs has attracted considerable interest for the support of cell attachment and viability, the delivery of bioactive molecules or growth factors, and bone regeneration in vivo [68, 81, 83, 192]. There are some practical advantages of using this polymer such as (i) it is biocompatible, which has been approved by the U.S. Food and Drug Administration (FDA) for clinical use; (ii) its biodegradation rate, which can be tailored according to its molecular weight and copolymer ratio and (iii) the surface properties of the products produced by the polymer, which can be modified to provide better interactions with the cells.

Emulsion-solvent evaporation is a traditional method for the preparation of polymeric MPs and is still extensively used [71, 193]. As described by Ogawa and co-workers [90], this method relies on the principle that an o/w emulsion is formed, where the organic solvent (oil phase) contains a polymer and later on, the evaporation of the solvent allows the hardening of the MPs. Consequently, the MPs are separated via centrifugation and lyophilised. The double emulsion-solvent evaporation method is a modified form of the emulsion-solvent evaporation method, where a bioactive molecule or compound is dissolved in the polymer solution to form more complex MPs. The principle of the double emulsion-solvent evaporation method can also be used to prepare porous

polymeric MPs, in which case a pore-forming agent is incorporated within the polymer solution, which is eventually released in the outer water phase, resulting in porous MPs.

Emulsion droplet formation is usually facilitated by some mechanical forces, such as high-shear homogenization, which requires high energy input. In which case, two or more immiscible liquids (e.g., o/w, w/o or w/o/w) are homogenized by vigorous stirring at a high shear [194, 195]. Due to the turbulence, caused by the shear, one phase is broken into droplets (discontinuous phase) and remains dispersed in the other (continuous phase). Although much effort has been made to improve the efficiency of this traditional 'cut-down-to size' emulsification approach, there are still some problems that may arise due to the use of the homogenizer [122, 174]. Firstly, the size distributions of the emulsion droplets and the resultant MPs are generally wide and they cannot be easily controlled even though the preferred mean droplet size can be obtained. Secondly, the efficiency of the energy used in the system gradually decreases as the size of the vessel increases i.e., the process can only be efficiently used for a small-scale MP fabrication. Thirdly, the batch-to-batch reproducibility on a single piece of equipment is often poor and the quality of the product may vary when prepared with equipment designed by one manufacturer or another, even in terms of the batch size.

Membrane emulsification (ME) is one of the alternatives to the traditional approaches, in which case the droplet formation relies on the 'made-to-measure'

principle in order to produce each droplet individually, at the final desired size. As in this method, the droplets formed individually, it is more efficient in terms of producing emulsions of desired sizes and with narrower size distributions when compared to the 'cut-down-to-size' approach. Moreover, this approach requires less energy input, and fewer thermal and mechanical stresses to the emulsion constituents; therefore, it is suitable for preparing emulsions of heat- and shear-sensitive products. Furthermore, this method is relatively versatile in terms of producing single emulsions with pure polymer solutions or producing even more complex multiple emulsions (e.g., bioactive molecule- or protein- containing emulsions).

As described in Chapter 3, we prepared solid PCL MPs with a mean diameter of approximately 100 µm and narrower span of distribution, using a specific ME set up, X-ME, with an SPG membrane, via controlling the different process and formulation parameters. Taking into account the same formulation and process parameters, this chapter describes the preparation of porous PLGA MPs with a mean diameter of approximately 100 µm, for the purpose of using the MPs as injectable stem cell delivery vehicles. To the best of our knowledge, there has been no previous report of the preparation of uniform-sized porous PLGA MPs using the X-ME technique. Qi and co-workers [196] prepared Exenatide-loaded PLGA MPs with a mean diameter of 22.69 µm using an SPG membrane with a premix ME set up; however, the size distribution of the MPs was not very tight, as evidenced from the span factor 0.678. Moreover, the disperse phase volume was only 8 mL with a minimum amount of the polymer (8 mg), indicating the low yield of the resultant MPs. In another recent study [109], they prepared relatively

smaller and spherical PLGA MPs with a mean diameter of 15.32 µm and of span factor 0.90 using the same disperse phase volume. On the other hand, twenty years ago, using the same technique, Shiga and colleagues [197] prepared highly uniform progesterone-loaded PLGA MPs, which were, smaller in size (mean diameter = 1.15 to 2.86 µm). Using a different technique, more than a decade earlier, Berkland and associates [198] prepared highly uniform PLGA MPs of a wide range of sizes (~5 to >500 µm) by varying the process parameters used to prepare the MPs. However, the droplet formation was on a 'drop-by-drop' basis, and to achieve the uniformity of the droplets, a very slow disperse phase flow rate (0.033 mL/min) was maintained. In addition, the overall batch size was small with a maximum amount of 1 g PLGA used for a batch. The work described in this chapter focuses on fabricating porous PLGA MPs with a mean diameter of approximately 100 µm and a span factor of 0.50 or lower under the same emulsification conditions as optimised in the previous chapter (see Chapter 3) in the case of PCL MPs.

4.2 Materials and Methods

4.2.1 Equipment, Consumables and Materials

A w/o/w double emulsion is the basis of the porous PLGA MPs described in this chapter. The primary (w/o) emulsion was prepared using a high shear homogenizer and the secondary (w/o/w) emulsion was prepared using a ME kit. The detailed specification of the equipment, other consumables and chemicals used in the work described in this chapter are described in Appendix I.

For the PCL polymers, the manufacturer provided the number-average molecular weight (Mn) data, whereas in the case of PLGA, the weight-average molecular weight (Mw) data was provided. In order to use the same unit of molecular weight for each of the polymers (PCL and PLGA), in the relevant discussions, a gel permeation chromatography (GPC) with differential refractometer detection set up was used. Chloroform was used as an eluent and the polymer solutions were calibrated against a polystyrene standard. For the viscosity study, a rheometer (Physica MCR 301, Anton Paar, UK) under rotational mode was used.

4.2.2 Experimental Setup and Emulsification Procedure

An overview of the emulsification process parameters and a schematic of the emulsification procedure are shown in Table 4.1 and Figure 4.1, respectively. The MPs were prepared following the principle of the w/o/w double emulsion-solvent evaporation technique. PBS was used as the internal water phase and served as a pore-forming agent at a concentration of 25 % v/v of the polymer solution (PLGA-in-DCM). As shown in Figure 4.1 (1–2), the primary emulsion (PBS-in-PLGA solution) was prepared using a high shear homogenizer at 9000 rpm for 2 minutes. The primary emulsion was then passed through a 20 µm SPG membrane fitted in the membrane emulsification kit, where PVA-water was running though the membrane before the emulsion added. Under a low-pressure (13 KPa) N_2 gas, the droplets of PBS-in-PLGA were formed at the membrane pore opening, detached into the running PVA-water and deposited in a beaker. The PBS-in-PLGA solution in PVA-water (w/o/w) emulsion was then kept stirring at 300 rpm on a magnetic stirrer for 6 hours. During this time, DCM evaporated and the

internal water phase (PBS-water) get trapped in the solidified MPs (Figure 4.1 (4)). The MPs dispersion was then kept at rest to allow the MPs to settle on the bottom of the beaker. After the decantation of the liquid, the MPs with a minimum amount of water were transferred in four different centrifuge tubes, keeping the volume approximately equal in each of the tubes. Then the dispersion was centrifuged, the MPs were washed three times in water, freeze dried. The freeze drying allowed the internal water phase to escape, as water vapour, from the MPs and hence the MPs became porous. The freeze-dried MPs are stored in freeze until further required.

Table 4.1 Overview of Emulsification Conditions

Composition of primary (w/o) emulsion	25 % v/v PBS in PLGA solution; PLGA solution: 50 % w/v PLGA in DCM
Composition of secondary (w/o/w) emulsion	PBS-in-PLGA solution in PVA-water
Internal water phase (pore forming agent)	PBS
Oil Phase (polymer solution)	PLGA in DCM
External water phase (emulsifier solution)	PVA-water
Preparation of primary emulsion	High shear homogenizer; speed: 9000 rpm; homogenization time: 2 minutes
Preparation of secondary emulsion	High speed mini kit (membrane emulsification kit); Membrane type: SPG; pore diameter: 20 µm; P_w (working pressure) : 13KPa; emulsification time: 5 minutes

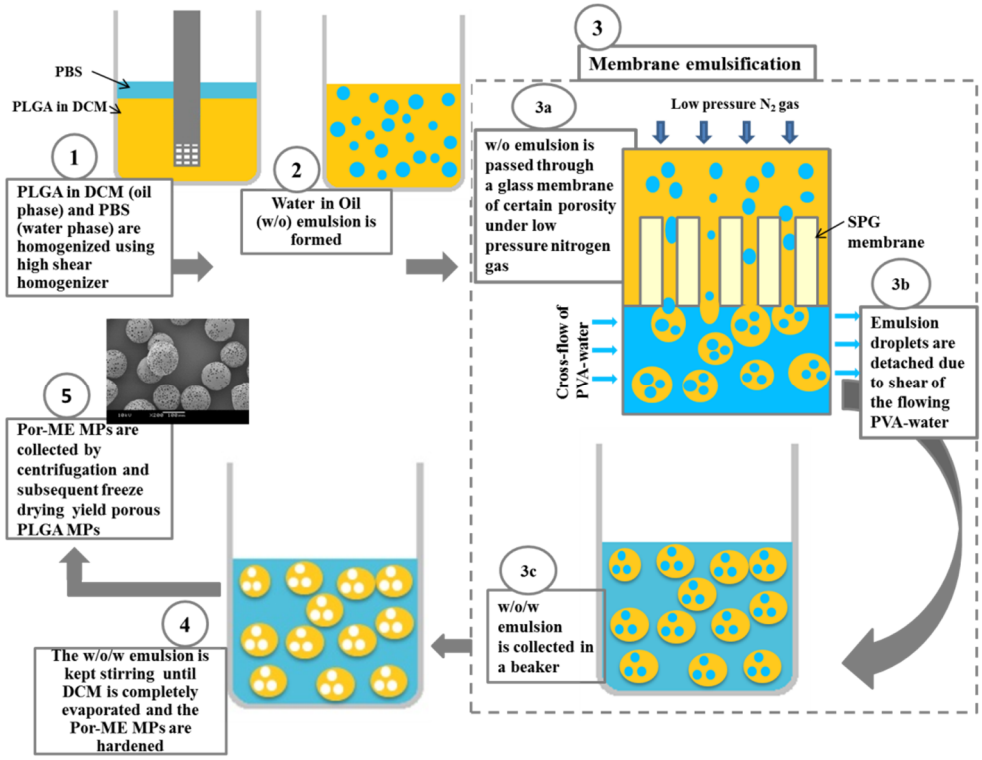


Figure 4.1 Schematic of fabrication of porous PLGA MPs using X-ME process. **1-2)** w/o primary emulsion (PBS in PLGA solution) is formed using a high shear homogenizer; **3)** the w/o emulsion is passed through a 20 µm SPG membrane while a cross-flow of PVA-water (w) is maintained through the membrane; an w/o/w double emulsion is formed on the other side of the membrane and deposited in a beaker; **4)** the w/o/w emulsion is kept stirring until DCM is completely evaporated; **5)** The MPs are collected by centrifugation, washed three times with water and and then freeze dried.

4.2.3 Porosity Improvement by NaOH-EtOH Treatment

In the case of porous MPs, prepared via conventional homogenization (CE), the work described in Chapter 2 suggests that a mild NaOH-EtOH treatment of the MPs post-fabrication could improve their surface and internal porosity. In the work described in this chapter, the same concentration of NaOH-EtOH was used to treat the MPs for different time periods. Briefly, 800–1000 mg of the MPs were placed into a 50 mL centrifuge tube and placed onto a vortex at 1400 rpm. A 20 mL aliquot of the NaOH-EtOH solution was quickly added to the MPs and vortexed for different time periods (2, 4, 6 and 10 minutes). The treated MPs were immediately centrifuged at 1000 rpm for 1 minute, washed three times using ice-cold dH_2O and transferred to a 40 µm cell strainer. As much water as possible was blotted using blue laboratory paper and then freeze-dried for two hours.

4.2.4 Characterization of Emulsion Droplets

See section 2.2.4 for the methodology.

The characteristics of the emulsion droplets prepared via X-ME were compared with that of the emulsion droplets prepared via CE.

4.2.5 Characterization of Microparticles

See section 2.2.5

The degree of monodispersity in a size distribution was assessed by measuring the span factor using the method described in section 3.2.5.

The characteristics of the MPs prepared via X-ME (Por-ME MPs) were compared with that of MPs prepared via CE (Por-CE MPs).

4.2.6 Characterization of Pore Size Distributions

See section 2.2.7

The characteristics of the Pore of the MPs prepared via X-ME were compared with that of the Pore of the MPs prepared via CE.

4.3 Results and Discussion

The study results, as reported in Chapter 3, suggests that the viscosity of the disperse phase that was used to prepare the emulsion droplets, using the ME method is an important factor. In the experiment, it is demonstrated that irrespective of the molecular weight of the polymer (PCL_{80kDa} and $PCL_{45\ kDa}$), the disperse phases that fell within a specific viscosity window produced MPs with a mean diameter of approximately 100 µm and narrow span factor, under a specific P_w. Building on this strategy, a series of PLGA solutions in DCM were prepared to study their viscosity and to investigate the solution that possessed a viscosity value close to that of PCL_{80kDa} or PCL_{45kDa}. In case of the solid PCL MPs, the disperse phase was a pure polymer solution of PCL in DCM. On the other hand,

to prepare porous PLGA MPs, a PBS-in-PLGA -solution was used as the disperse phase. Therefore, it was necessary to study the viscosity of the PBS-in-PLGA -solution to investigate the optimum PBS-PLGA dispersion for the emulsification.

4.3.1 Viscosity Study of Different Concentration of PLGA Solutions

The weight average molecular weight (Mw) data for PLGA was provided by the manufacturer. However, in previous chapters (Chapter 3 and Chapter 4), for the purpose of discussion related to PCL polymers, their number average molecular weight (Mn) values were considered. In order to maintain a consistency in the molecular weight information, all polymers (PCL and PLGA) were analysed using GPC and the number average molecular weight (Mn) data for all polymers were considered in the discussion (The GPC data are shown in Appendix VII).

As reported in Chapter 3, for the higher molecular weight PCL 80 kDa,), 12.5 % w/v of the polymer solution resulted in a viscosity value of 1.3 Pa.s. This was the optimum viscosity of the DP for preparing the MPs with a mean diameter of approximately 100 µm and a narrower size distribution (span factor = 0.51). As shown in Figure 4.2 A, the viscosity of polymer solutions gradually increased with the increasing polymer concentrations. However, the viscosity of the most concentrated solution (50 % w/v $PLGA_{27kDa}$) was still significantly less ($p<0.0001$) than that of the optimum PCL solution. Conversely, the w/o primary emulsions (PBS-in-PLGA -solutions) had relatively higher viscosities than the respective pure $PLGA_{27kDa}$. For example, the w/o emulsion that contained 25 % v/v PBS in 50 % w/v $PLGA_{27kDa}$ were significantly more viscous ($p<0.01$) than

the corresponding pure $PLGA_{27kDa}$ solution. The viscosity of the emulsion (η_{DP} = 1.09 Pa.s) was close to that of the optimum PCL solutions ($p>0.05$; 12.5 % w/v PCL_{80kDa}, and 35 and 37.5 % w/v PCL_{45kDa}). It is not surprising that when the concentration of a polymer increased, the viscosity of the respective polymer solution also increases. It is not certain why the viscosity of the PBS-PLGA emulsion was higher than the corresponding pure solution. However, as opposed to the pure $PLGA_{27kDa}$ solution, the presence of the PBS droplets in the emulsion possibly resulted in the increase of the emulsion resistance to flow, which eventually increased its viscosity.

Using 25 % v/v PBS in 50 % w/v PLGA as the DP and following the method described in section 3.2.2, porous PLGA MPs were prepared. The Pw, $Conc._{CP}$, $\varphi_{DP/CP}$ and V_{CP} were the same as those used for preparing the optimum 45 kDa PCL MPs, described in Chapter 3.

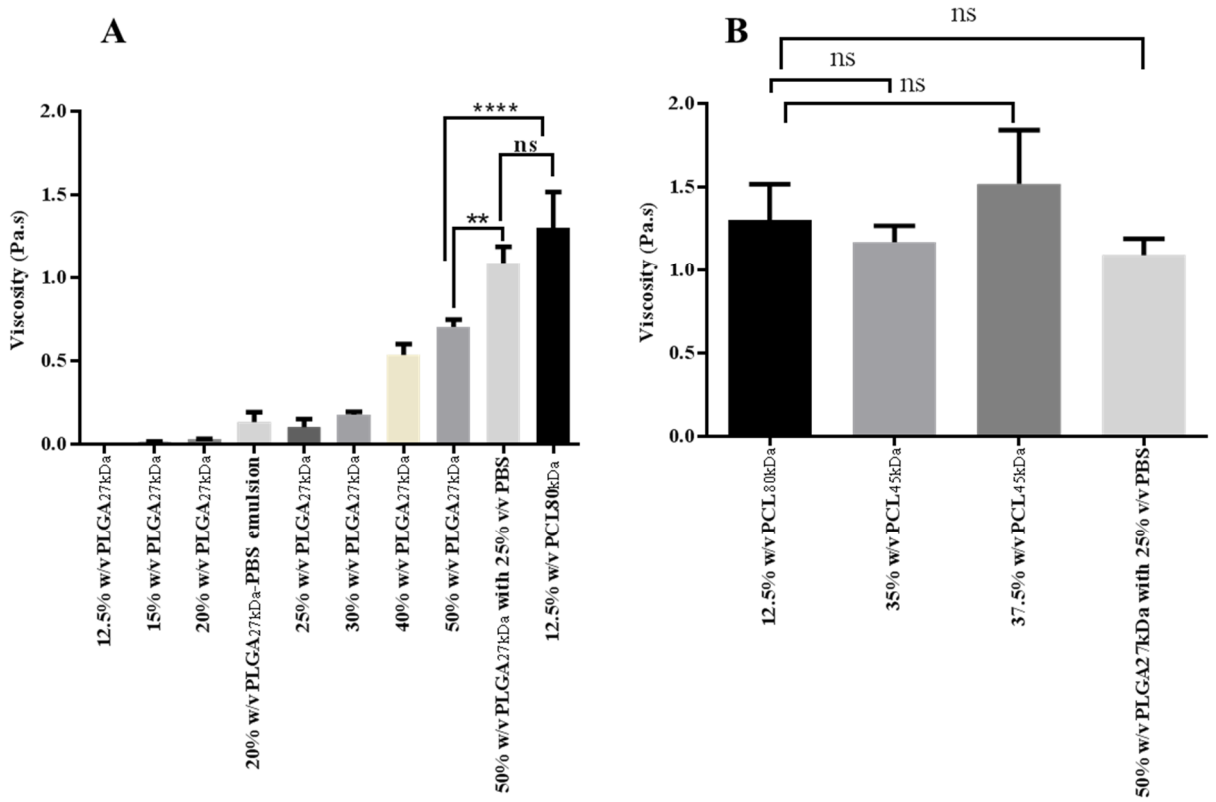


Figure 4.2 A) Viscosities of a series of $PLGA_{27kDa}$ in DCM and PBS-$PLGA_{27kDa}$ emulsion. **B)** The viscosity of the 50% w/v $PLGA_{27kDa}$ with 25% v/v PBS emulsion is comparable with that of optimal PCL solution (37.5 % w/v PCL_{45kDa}. Values are represented as mean ± SD (n = 6; r = 3).

4.3.2 Influence of New and Used Membranes on MP Size Distributions

A new membrane with a pore size of 20 µm was used to prepare all batches of the porous PLGA MPs. The corresponding emulsion droplets and MP size distributions are shown in Figure 4.3 (right-hand column) and Figure 4.4 B, respectively. Using another new membrane with a pore diameter of 20 µm, a series of solid PCL MPs of optimum size and size distribution were also prepared for comparison. The prepared PCL emulsion droplets (o/w emulsions) and the corresponding MPs size distributions are shown in Figure 4.3 (left-hand column) and Figure 4.4 A, respectively. As shown in Figure 4.3, for both polymers, the very first batches with the respective new membranes resulted in highly uniform emulsion droplets. The sizes of the corresponding MPs were uniform with a span factor 0.43 for both types of MPs and mean diameters of 30 and 63 µm for the solid and porous MPs, respectively. In contrast, the next batches produced using the respective membranes produced emulsion droplets of relatively larger sizes. These were less uniformly dispersed in comparison with those produced with the new membrane. The MP sizes and their span factors gradually increased as the membranes aged. For PCL MPs, the span factors of the first and the second batches were significantly different ($p<0.0001$). Although the span factors for the subsequent batches slightly increased, the values were similar to the second batch ($p>0.05$). A similar trend was observed for the porous PLGA MPs, as shown in Figure 4.4 B. There has been no previous report of the effect of new and used membranes on the MPs size and size distributions. The reason why the MPs size and size distributions of the first batch (produced using a new membrane) and the second batch (produced using the used membrane) were different is unknown.

However, once a membrane was used, it was necessary for it to be thoroughly cleaned by flushing DCM through the pores at a high pressure (80 KPa). It was then sonicated with DCM, 2M HCL or water for a total period of 2 hrs 5 minutes (see Appendix V for the detail description of the membrane cleaning process). The integrity of a fraction of the pores may have been compromised due to the long term sonication process, which might account for the size differences between MPs prepared using new and used membranes. Figure 4.5 (reproduced from Vladisavljevi´c et al. [189]) shows the geometry of an SPG membrane with a mean diameter of 15 µm, where the red perforated circles showing the thin junction between two adjacent pores. It is reasonable to assume that some of these thin boundaries between two adjacent pores of the membrane may have broken due to repeated sonication. However, further study of the characteristics of the membranes before and after the cleaning process is necessary to clarify information about the effect of the cleaning process on the membrane structural integrity and thereby the size and uniformity of the MPs.

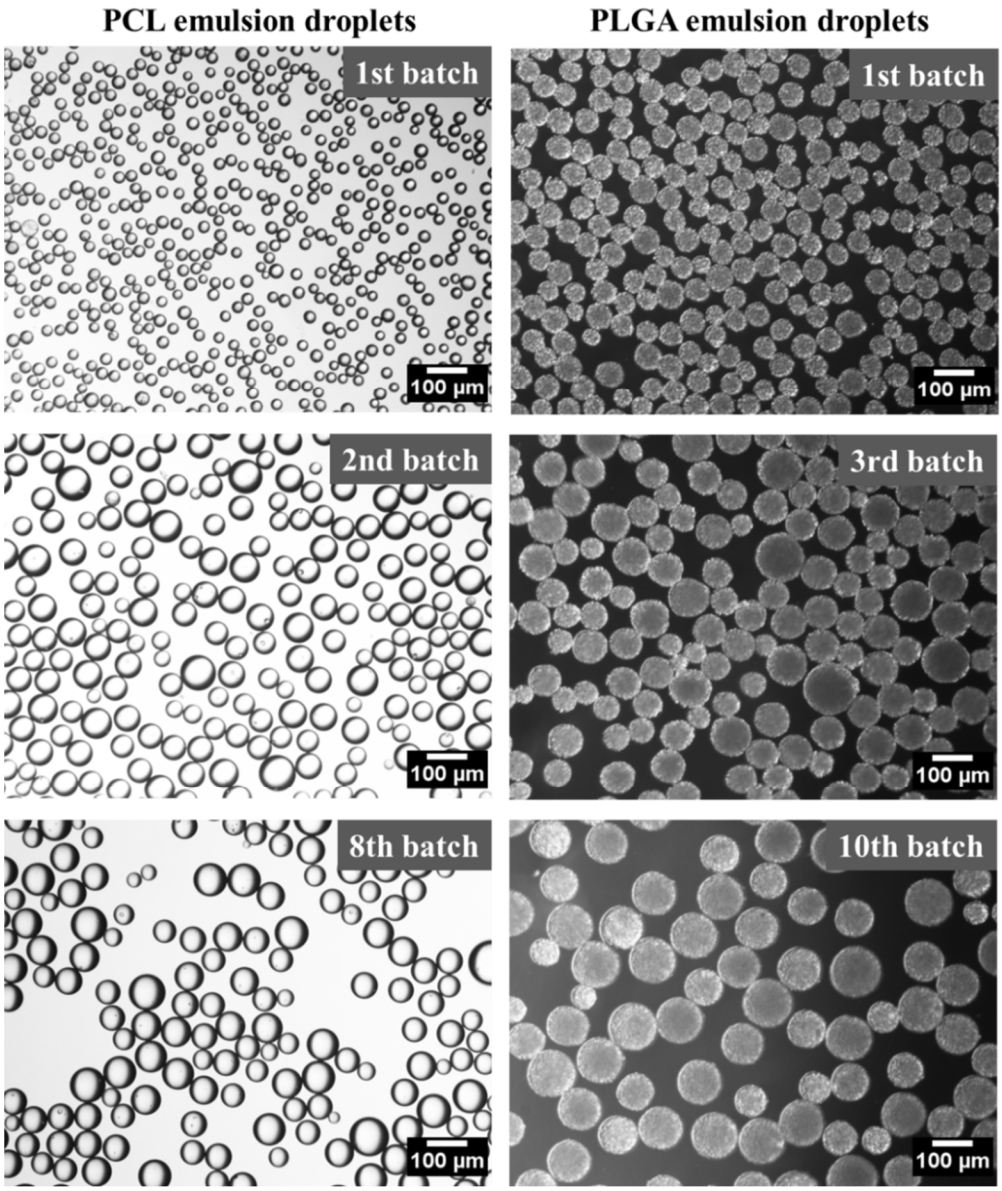


Figure 4.3 PCL (left-hand column) and porous PLGA (right-hand column) emulsion droplets prepared using new (the top images of both columns) and used membranes (the all other images).

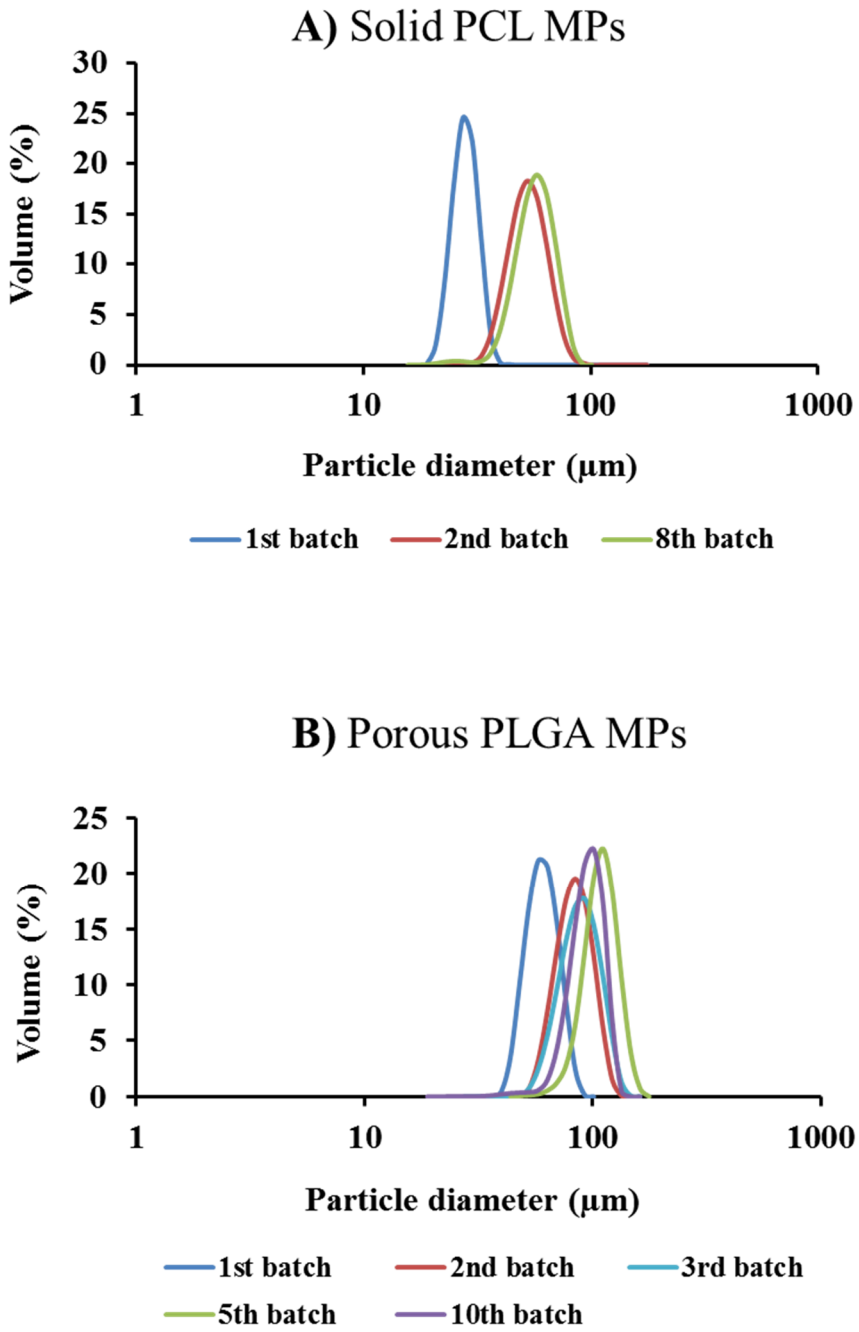


Figure 4.4 PSD for the solid PCL MPs **(A)** and porous PLGA MPs **(B)** prepared using SPG membranes of pore diameter 20 µm. For both the solid and porous MPs, the first batches represent the size distribution curves obtained by using a new membrane.

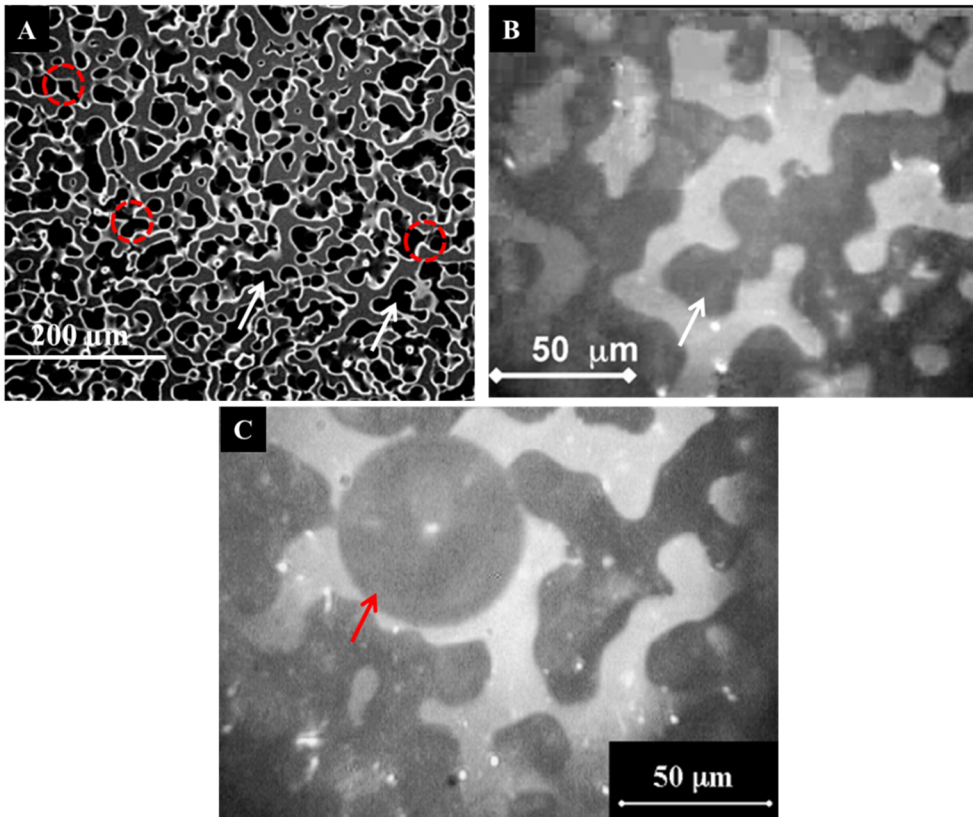


Figure 4.5 SPG membrane geometry (reproduced from reference [189]
A) SEM image of an SPG membrane with mean diameter of 15 µm, showing the tortuosity of the membrane; the white arrows indicate the pores; the red perforated circles showing the thin junctions between two adjacent pores. **B)** A magnified image of the membrane; the white arrow indicates a pore of the membrane. **C)** The surface of an SPG membrane during droplet formation. The red arrow indicates a droplet that is attached to a pore opening of the membrane.

4.3.3 Comparison of Emulsion Droplets Prepared Via CE and ME Methods

To study the efficiency of the X-ME technique, in terms of monodisperse droplet formation, the emulsion droplets produced via the technique (ME droplets) were compared with that produced via CE (CE droplets). As shown in Figure 4.6, ME droplets were relatively uniform with few extremely small or large emulsion droplets. The droplet size distribution (DSD) curves (see Figure 4.6 C) further indicate the narrower span of distribution for the ME droplets. In terms of skewness (see section 2.2.5 in Chapter 2 for further details), the DSD for the CE droplets were negatively skewed, as shown in Figure 4.6 Ci. The ME droplets were also slightly negatively skewed; however, with respect to CE droplets, the skewness of the ME droplets was substantially less. In the case of CE, a stronger mechanical force is applied to progressively break the dispersed fluid into smaller droplets until they fit within a required size range [174]. It is likely that during this process, the droplets that formed in the beginning of the process would repeatedly experience the force until the process ends, which results in the presence of some very small droplets in the system. Therefore the existence of the broad SD with a skewed SD curve in the CE droplets was not unexpected. In contrast, the ME droplets were more efficient prepared via ME process, as evidenced from the narrower DSD for the process.

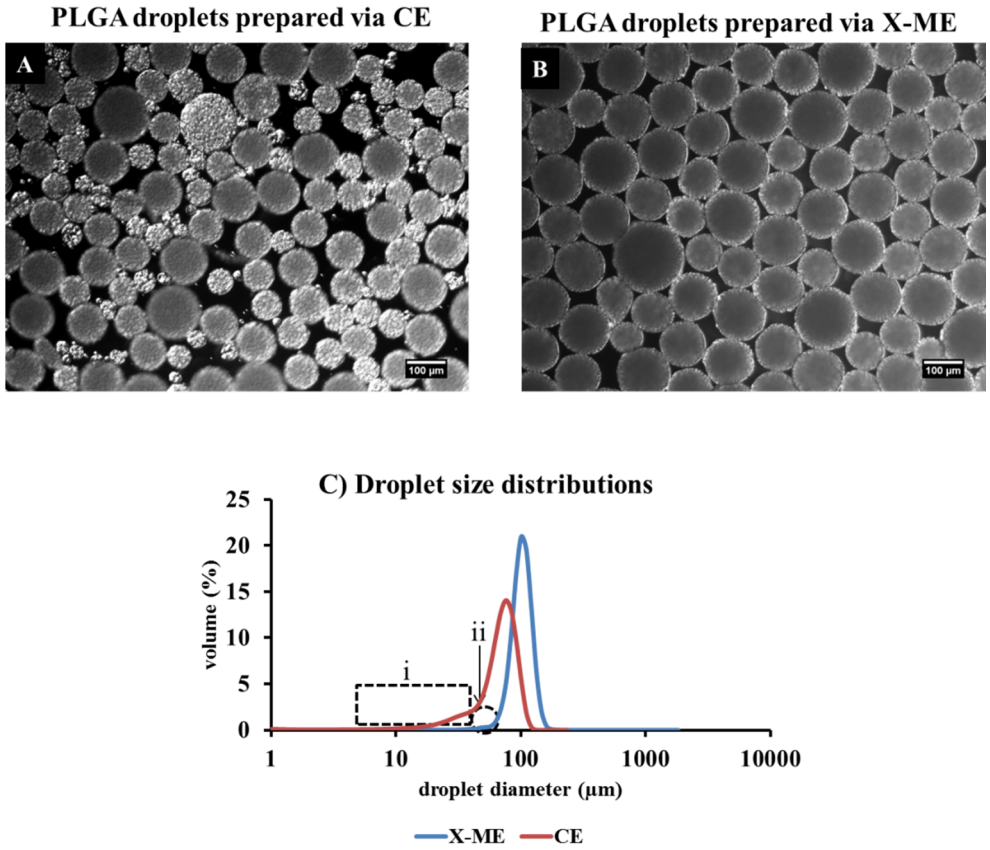


Figure 4.6 Optical light microscopic images of emulsion droplets prepared via **A)** CE and **B)** X-ME methods; scale bar = 100 µm. **C)** DSD for droplets prepared via the CE and X-ME methods; the skewness of the SD curves are shown as a perforated rectangle and circle for the droplets prepred via the CE and X-ME methods, respectively.

4.3.4 Effect of NaOH-EtOH Treatment on Porosity

As discussed in Chapter 2 (section 2.3.3), treatment of the porous MPs with mild NaOH-EtOH substantially improved the porosity of the conventional porous MPs (Por-CE MPs). The same concentration and ratio of NaOH and EtOH was used for treating the MPs prepared by ME (Por-ME MPs). However, the volume of the NaOH-EtOH and the treatment time were optimised for Por-ME MPs in order to obtain the most porous MPs without affecting their structural integrity. The method is described in section 4.2.3 and the results are shown in Figure 4.7. As shown in the figure, the porosity gradually increased upon increasing the NaOH-EtOH treatment time; however, after a certain time period (4 minutes), the integrity of the pores was compromised. A long-term treatment also caused MPs aggregation. These results are in agreement with those reported by Qutachi et al. [70], who used the same concertation of NaOH-EtOH solution to improve the porosity of Por-CE MPs and concluded that 2 minutes was the optimal time. In this study, a four-minute time period resulted in the optimal improvement in the porosity of the MPs. It is important to note that the polymer concentration used to prepare Por-ME MPs was 2.5 times higher than that used by Qutachi and co-workers to prepare the Por-CE MPs. The mechanical stability of the Por-ME MPs was possibly greater due to the higher concentration of the polymer. Therefore, in order for the NaOH-EtOH solution to break the Por-ME MPs structural integrity, a relatively longer time was required.

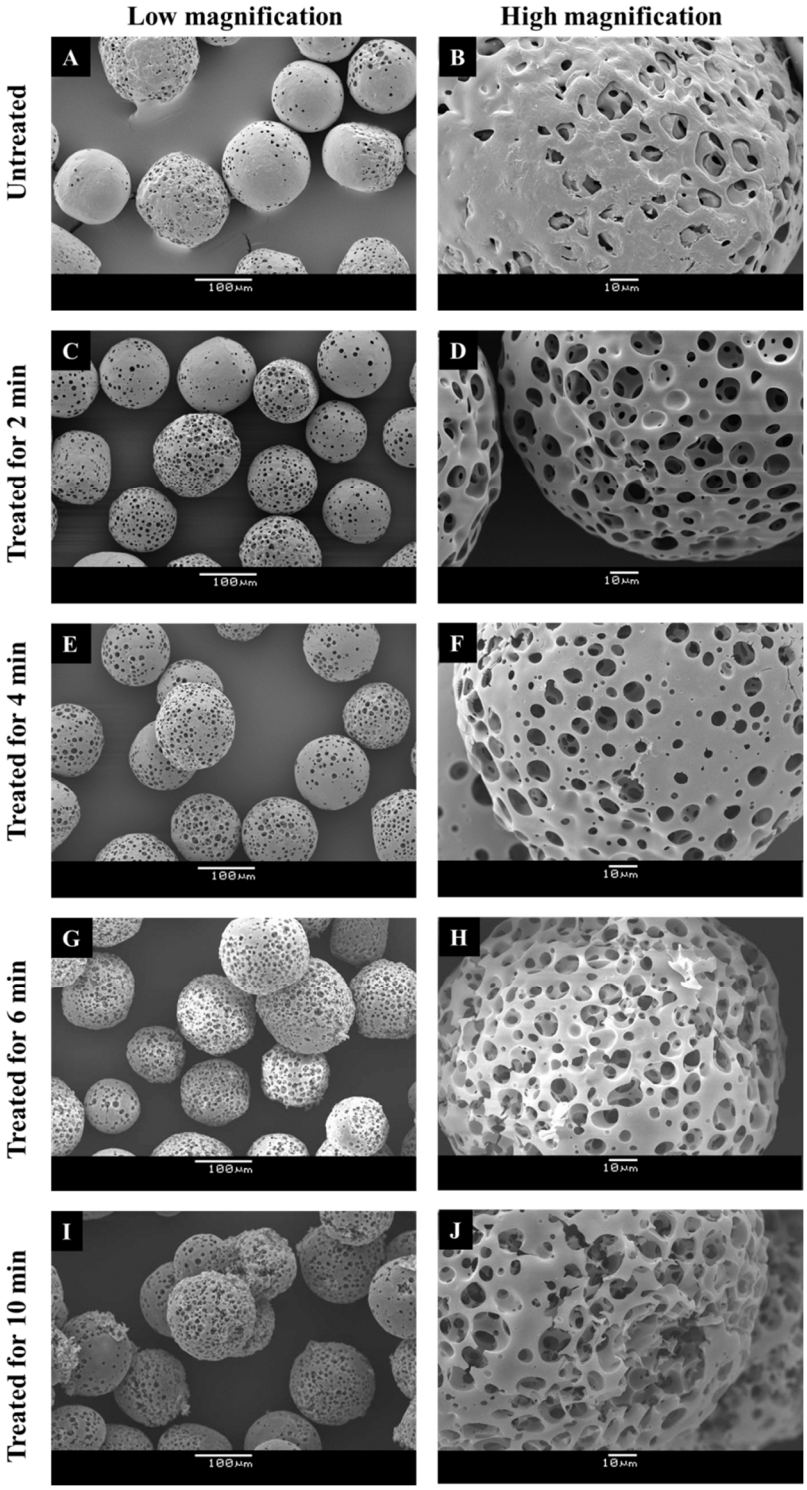


Figure 4.7 NaOH-EtOH treatment of Por-ME MPs to improve the porosity of the MPs. Untreated **(A-B)** and treated for 2min **(C-D)**, 4 min **(E-F)**, 6 min **(G-H)** and 10 min **(I-J)**.

4.3.5 Comparison of Characteristics of MPs Prepared Via X-ME and CE

The size and size distribution patterns of the MPs, prepared using the CE and ME methods were characterised following the method described in section 2.3.5 (Chapter 2) and the results are shown in Table 4.2 and Figure 4.8. As shown in the table, MPs with mean diameters of 114 and 66 µm were produced using the ME and CE methods, respectively. The mean diameter of the Por-CE MPs increased 1.18 times after the NaOH-EtOH treatment. It is important to note that the NaOH-EtOH solution contained 70 % v/v ethanol, which possibly enhanced the plasticity of the MPs and encouraged the MPs to swell [199]. Qutachi et al. [70] reported similar results, when they treated Por-CE MPs with the same concentration of NaOH-EtOH solution. In contrast, there was no noticeable change in Por-ME MPs, in terms of swelling, as a result of the treatment. As stated in section 4.3.4, the Por-ME MPs were more compact in comparison with the Por-CE MPs due to the presence of a higher amount of PLGA, which possibly strengthened their mechanical properties. As a consequence, the NaOH-EtOH treatment had little effect on the expansion of the polymer. Conversely, the frequency distribution of the Por-ME MPs was tighter and showed better repeatability than that of the Por-CE MPs, as evidenced from the substantially lower % CV value [200] for the Por-ME MPs shown in the table. Moreover, there was no traceable volume % of the MPs with a diameter of 10 µm or lower in the Por-ME MPs both before and after the treatment. Furthermore, the skewness (g_1) value of Por-ME MPs suggested that the PSD were symmetric ($g_1 = 0$) in comparison to that of Por-CE MPs. As described in Chapter 2, a size distribution is considered symmetrical when the shape is represented by a normal or Gaussian distribution. All the above

mentioned results indicate that the Por-ME MPs had a tighter PSD. On the other hand, both the treated and untreated Por-CE MPs showed skewed PSD curves, an indication of the asymmetry of the distributions. Moreover, 2.95 volume % of the Por-CE MPs was below 10 µm in diameter, among which 1.06 volume % had a diameter of 1µm or even lower. Although after the treatment the fraction of the smaller Por-CE MPs reduced to a certain degree, the levels of 1 and 10 µm size MPs were substantially higher than that observed in treated Por-ME MPs.

The degree of monodispersity in the respective MPs was assessed by determining the span factor using the method described in section 3.2.5 and the results are shown in Figure 4.8. The heights of the floating boxes in the figure indicate the degree of span factors, the higher the length of the box, the wider the distribution and higher the span factor. As shown in the figure, the span factors of both the NaOH-EtOH treated and untreated Por-ME MPs were substantially lower than that of the corresponding Por-CE MPs ($p<0.0001$). The NaOH-EtOH treatment had little effect on the span factor of the Por ME MPs, as evidenced from the similar span factors before and after the treatment. These results clearly indicate the efficiency of the ME method over the CE method in terms of producing MPs with a narrower span of distribution. In terms of monodispersity, some of the literature [116, 171] suggests that a distribution that possesses a span value of less than one could be considered monosized. In this study, although the span values for the Por-CE MPs (before and after the treatment) were less than one, the images of the respective emulsion droplets and MPs, as shown in Figure 4.6 A and Figure 4.9 A–D, respectively, do not represent monodisperse population. In contrast, the images of the Por-ME MPs shown in Figure 4.9 F–H clearly indicate

relatively monodisperse distribution when compared with Por-CE MPs. In terms of the span factor, there results are comparable to those reported by Imbrogno and colleagues [150] who prepared solid PCL MPs with a mean diameter of approximately 20 µm and a span factor of 0.51 using a disk-type metallic membrane for a small-scale batch size. In contrast, these results surpass those reported by Li and co-workers [201] who prepared agarose beads with a size of approximately 200 µm and a span factor of 0.76 using a rotating ME set up. Using a disk-type metallic membrane, Gasparini et al. produced PLGA MPs with median diameters within a size range of 40 – 140 µm [171]. However, the size distribution curves and the optical light microscopic images demonstrated relatively less uniform distributions when compared with the Por-ME MPs.

Table 4.2 Characteristics of the MPs prepared via X-ME and CE

Descriptive statistics	**X-ME**		**CE**	
	Before NaOH-EtOH treatment	**After NaOH-EtOH treatment**	**Before NaOH-EtOH treatment**	**After NaOH-EtOH treatment**
Mean ± SD	114 ± 19	114 ± 19	66 ± 24	78 ± 25
Mode	117	117	78	82
% CV	17	17	37	33
Volume % of MPs lower than 1 µm	0	0	1.06	0.88
Volume % of MPs lower than 10 µm	0	0	2.95	1.71
Volume % of MPs lower than 100 µm	24	24	94.92	86.76
Skewness	0.18	0.00	-0.62	0.15
Kurtosis	0.43	0.19	0.06	3.27

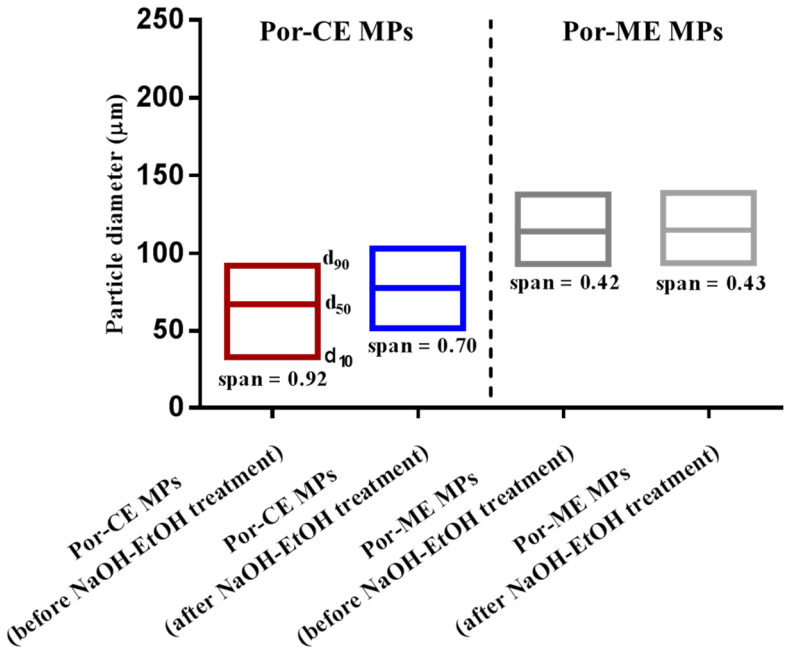


Figure 4.8 Particle size distributions of Por-ME MPs and Por-CE MPs in terms of span factor before and after NaOH-EtOH treatment.

4.3.6 Comparison of Pore Size Distribution of MPs Prepared Using CE and X-ME

The pore characteristics of the MPs were studied using SEM and the images were further processed using Image J and Microsoft Excel 2010, using the method described in section 2.2.7 and the results are shown in Figure 4.9 and Figure 4.10, respectively. The SEM images in Figure 4.9 clearly show an improvement in the porosity of the MPs after the NaOH-EtOH treatment, both when prepared with the CE and ME methods. The respective histograms in Figure 4.10 are also in agreement with the SEM images. As shown in the figure, in both the cases of the Por-ME and Por-CE MPs, the pore size distribution curves shifted to the right of the histograms and the number of smaller pores reduced. For the Por-CE MPs before the treatment, the pore size ranged from 0.4 to 10.8 µm; whereas after the treatment the pore distribution width increased, as demonstrated by a range of 0.41 – 13.89 µm size pores. Although the most frequently observed pores for both the treated and untreated MPs were within the same size range (2 – 2.5 µm), the frequency reduced from 81 to 53 after the treatment for the same number of pore counts (500 pores). On the other hand, for the Por-ME MPs, the pore sizes spanned from 0.21 to 18.87 µm before the treatment. After the treatment, the histogram shifted to the right of the distribution (minimum pore diameter = 0.61 µm; maximum pore diameter = 19.44 µm), which is an indication of the increase of overall pore size due to the treatment. The corresponding SEM images in Figure 4.9 are also in agreement with these results. It is not surprising that the pore size distribution curves for the Por-ME and Por-CE MPs are different from each other in terms of size. The polymer concentration as well as the volume of the

pore forming agent (PBS) were different for both methods. The PLGA concentration and PBS volume for the Por-ME MPs were 2.5 and 5 times higher, respectively. It is likely that the higher concertation of porogen would offer larger pore volume and size, which might explain the higher pore size distribution width for the Por-ME MPs.

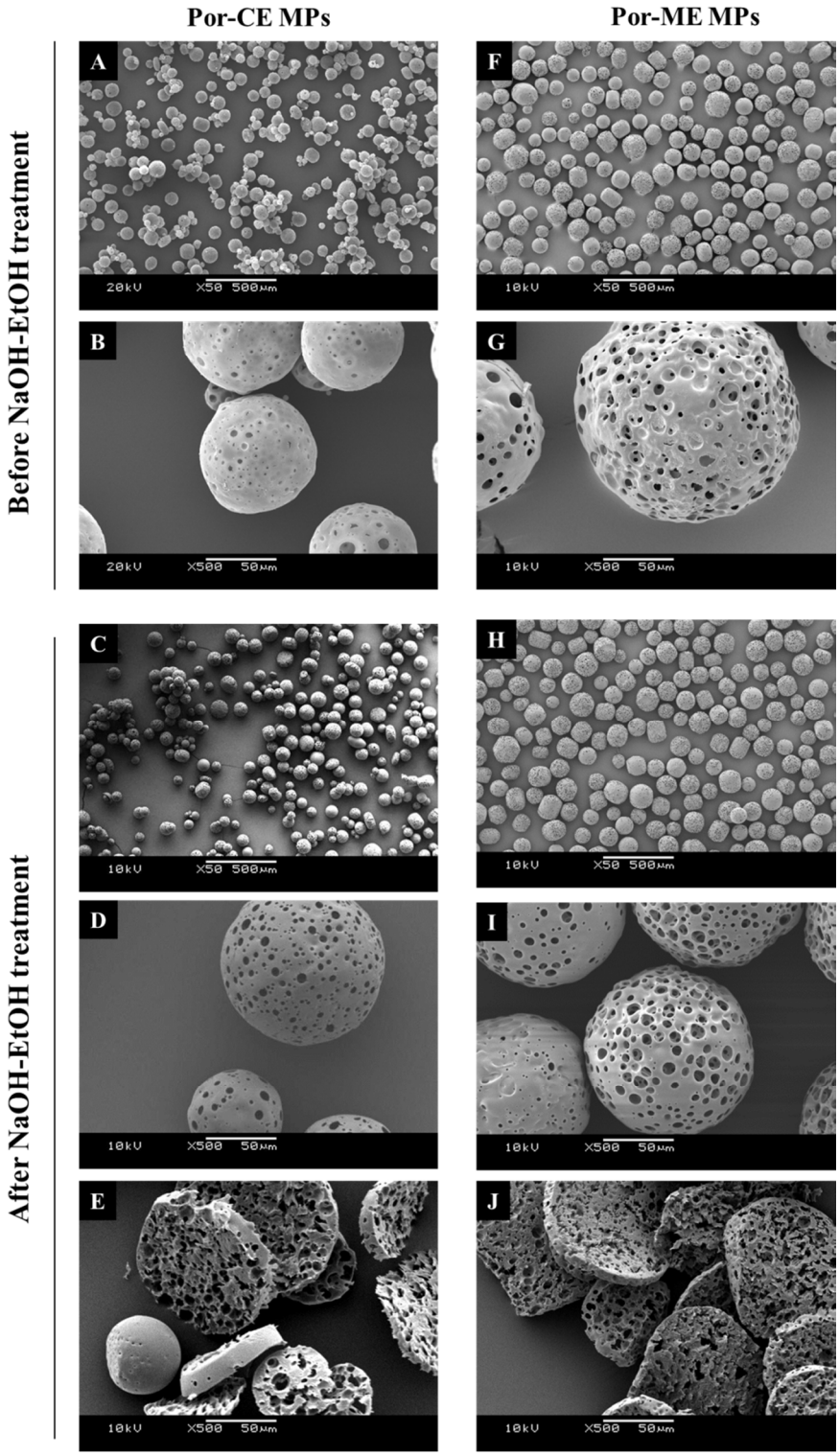


Figure 4.9 Surface and internal porosities of Por-ME MPs and Por-CE MPs before **(A, B, F and G)** and after **(C – E; H –J)** NaOH-EtOH treatment.

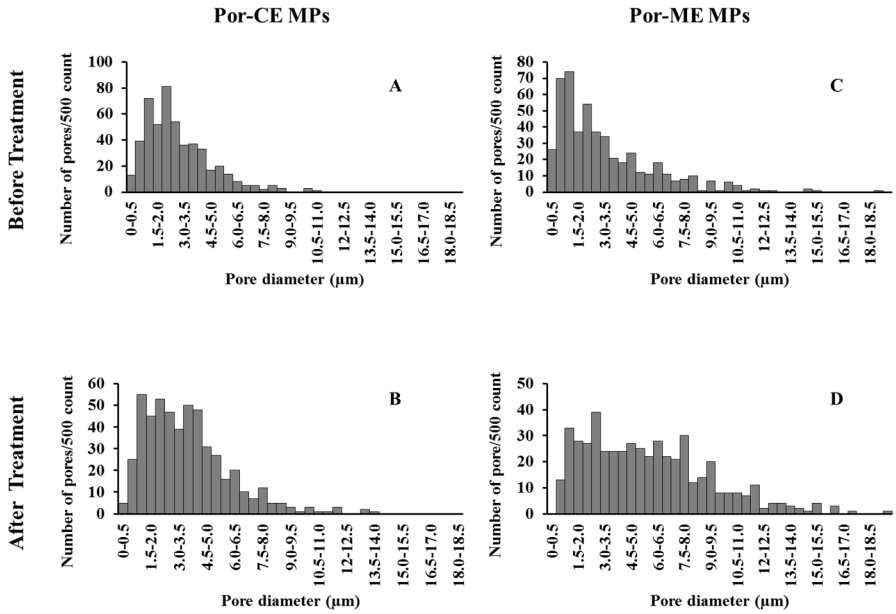


Figure 4.10 Pore size distribution of Por-CE MPs(left-hand column) and Por-ME MPs (right-hand column) before **(A, C)** and after **(B, D)** NaOH-EtOH treatment.

4.1 Conclusions

This chapter has focused on describing the fabrication of uniform-sized porous PLGA MPs with a mean diameter of approximately 100 µm, to act as carriers of hMSCs for injectable cell delivery applications in tissue engineering. To the best of our knowledge, there has been no previous report of the fabrication of monodisperse porous PLGA MPs with a mean of 100 µm using the X-ME technique. The emulsification conditions (P_w, $Conc._{CP}$, $\varphi_{DP/CP}$, V_{CP} and η_{DP}) used for preparing these MPs were very similar to those used for preparing the optimal monodisperse solid PCL MPs with a mean diameter of 100 µm using the 45 kDa polymer. A primary emulsion of PBS (25 % v/v) in PLGA solution (50 % w/v PLGA in DCM; $M_{w\ PLGA}$ = 50 kDa; $M_{n\ PLGA}$ = 27 kDa[1]), which had a viscosity value of 1.06 Pa.s, was found to be the optimum DP for producing the porous PLGA MPs of the expected size and uniformity. It is important to note that the viscosity of this DP was close to that of the optimum 80 and 45 kDa PCL polymer solutions ($Mn_{\ PCL}$ = 80 and 45 kDa). Porous PLGA MPs with a mean diameter of 114 µm (± 19) and a span factor of 0.43 were successfully prepared using the X-ME technique. The porosity of the MPs was improved by treating them with a mild NaOH-EtOH solution. In this study, the volumes of the solution and treatment time were optimised. The overall porosity (surface and internal) of the Por-ME MPs substantially improved after the treatment. However the numbers of the larger pores were higher in the Por-ME MPs when compared with the Por-CE MPs.

[1] The number average molecular weight (Mn) of PLGA was obtained via GPC analysis.

It was also demonstrated that a used SPG membrane was not as efficient as a new membrane in terms of producing monodisperse MPs. It was shown that a new membrane produced more uniform MPs in terms of their span factor. Moreover, the size of the MPs gradually increased as the membrane became old. However, further investigation of the pore characteristics of the new and used membranes would be useful to get a clear information about the changes in the pore characteristics, if any, due to the cleaning process.

To assess the efficiency of the X-ME technique in terms of producing uniform-sized MPs, the characteristics of the emulsion droplets and the resultant MPs were compared with those produced by the CE technique, reported in Chapter 2. The study results clearly indicate that the porous PLGA MPs produced using the X-ME technique were substantially uniform in comparison with that prepared using the CE technique, as evidenced from the significantly lower span factor for the Por-ME MPs produced using the X-ME technique (span factor for Por-ME MPs = 0.43; span factor for Por-CE MPs = 0.70; $p<0.0001$). In addition, the relatively lower % CV value for the SD of the treated Por-ME MPs also indicates a tighter and repeatable dispersion in comparison with that observed for the SD of the treated Por-CE MPs. Moreover, there was little evidence of the presence of extremely small MPs in the SD for the Por-ME MPs; whereas in the Por-CE MPs, a certain volume fraction of the MPs was lower than 10 or 1 µm. After the NaOH-EtOH treatment, the SDs of Por-ME and Por-CE MPs were positively skewed, which demonstrate that these MPs were less dispersed than those in a normal distribution. However, only the treated Por-ME MPs can be considered as symmetrical as they had a 'zero' skewness value ($g_1 = 0$) for the SD curves.

Chapter 5 Assessment of the Novel Porous PLGA MPs Prepared via Cross-flow Membrane Emulsification for Cell Delivery Applications

5.1 Introduction

Polymeric MPs are an attractive type of scaffolds in tissue engineering for cell delivery applications [83, 126, 193]. The characteristics of the MPs including size, shape and surface roughness largely affect the function of the cells populated on them [160]. As stated earlier in Chapter 3, MPs should be substantially larger than the cells that will eventually grow on the MPs. Moreover, for an efficient delivery of the cells via the MPs, the size distribution of the MPs should be as narrow as possible. The importance of a precise MP size distribution for cell delivery applications has been discussed in detail previously, in section 3.1 of Chapter 3. Apart from sizes, the topographical features need special consideration when designing MPs in order to improve the efficiency of the MPs as carriers of the cells. Compared to solid MPs, porous MPs have been reported as being more effective for hosting and carrying cells for tissue engineering applications [63, 70]

Researchers at the University of Nottingham have been using polymeric MPs, including PLGA for the delivery of drugs, proteins or cells for tissue engineering applications. MPs of a specific size range from 1 to 200 μm have been fabricated via a conventional emulsification method, high shear homogenisation. The sizes were mainly confirmed by the mean MP diameter (± SD). The researchers at the University of Nottingham demonstrated that PLGA MPs with mean diameter of

100 µm exhibited standard deviation of 24 – 30 [68, 83]. Friess and Schlapp [202], and Chun et al. [203] also reported PLGA MPs with high standard deviation, 89.38 (± 28.05) and 226 (± 100), respectively. In order to obtain MPs with a tighter size range distribution of 50 – 100 µm, some of the researchers at the University of Nottingham have sieved the MPs post fabrication, at the expense of the final yield [92]. However, if the polymers used to prepare the MPs are expensive (e.g., PLGA) or when the MPs are carrying expensive growth factors like BMP 2, sieving should be avoided.

The data presented in Chapter 4 demonstrated that novel porous PLGA MPs with a mean diameter of 114 µm (± 19) were fabricated via the X-ME emulsification method. The size distribution of the MPs was substantially narrower than that of MPs prepared via conventional homogenization, as reported in Chapter 2. Furthermore, the yield of the novel MPs was 3 to 4 times higher than that obtained via the homogenization method. On the other hand, the porosity features of the novel MPs were similar to those prepared via the conventional method.

The work presented in this chapter aimed to assess the efficiency of the novel MPs for stem cell delivery applications. In order to do that ihMSCs were seeded on the MPs in either proliferation or osteogenic differentiation medium and the cells viability, proliferation and osteogenic differentiation were assessed.

5.2 Materials and Method

5.2.1 Equipment, Consumables and Materials

A detailed description of each of the materials used for the work described in this chapter is presented in Appendix I as Table A-1, Table A-2 and Table A-3 for equipment, consumables and general chemicals/reagents, respectively.

5.2.2 Surface Wetting of the MPs by Tween 20 Treatment

Different amounts (5, 10 or 15 mg) of the porous PLGA MPs prepared using the X-ME methods (Por-ME MPs) were weighed out individually and transferred into 15 mL centrifuge tubes. Five millilitres of 0.05 % v/v Tween 20 was added to each of the centrifuge tubes, while vortexing at 1400 rpm. The lids were closed and then the tubes were left rolling on a roller mixer at 50 rpm for 30 minutes. During this time, the MPs sank down into the Tween 20 solution. The MPs dispersions were then centrifuged, the supernatants were removed by decantation and the wet MPs were washed three times with PBS. The MPs samples were then ready to use for cell culture.

5.2.3 Seeding Cells on Tween 80 Treated Porous MPs

Required numbers of Por-ME MPs samples were treated with Tween 20 solution according to the method described in section 5.2.2. Each of the samples was then transferred to the well of a 24-well Pluronic F 127-coated nTC plate (see Appendix II for the details of the Pluronic F 127 coating) under aseptic conditions. The samples were then soaked in AB/AM solution (2 % v/v; 1 mL of

the AB/AM solution/well) for 2 hours at 37º C. The AB/AM solution was then removed and the MPs were washed with PBS (3 × 5 minutes). Complete DMEM (1 mL) was added into each of the wells and incubated at 37º C for one hour. The medium was then replaced with 500 µL of fresh and warm DMEM. During this time, the required amount of the ihMSC cell suspension was prepared according to the procedure described in section 2.2.9; the cells were counted following the method described in Appendix III. The cell suspension was then diluted with complete DMEM in order reach a final concentration of 100×10^3 cells/100 µL. After adding 10, 20 or 30 µL of the cell suspension into each of the wells, the plates were incubated at 37º C with 5% v/v CO_2 until medium changed or analysis was required.

5.2.4 Cell Fixation

At the end of an experiment and before proceeding for further analysis or microscopy, cells or tissues are sometimes fixed in order to preserve the cellular morphology and ECM architecture. Fixation ceases any ongoing biochemical reaction and enhances the mechanical strength or stability of the treated samples. Paraformaldehyde (PFA), a polymerized form of formaldehyde is a commonly used fixative in histology. It cross-links with cellular proteins, primarily with the residues of the basic amino acid, lysine. However, being a relatively larger molecule than formaldehyde, it forms less cross-links than formaldehyde.

For some of the studies, as stated in section 5.2.5.iii and 5.2.6 in this chapter, ihMSC-bound MPs were fixed using 3.7 % w/v PFA solution. In brief, each of the

experimental samples were washed once with PBS and then incubated with the PFA solution at 4º C for 10 minutes. After the incubation period, PFA was removed, washed three times with water and the samples were preserved with PBS at 4º C until required for further staining or analysis.

5.2.5 Cell Viability, Proliferation and Cytotoxicity Assays

In order to assess the biocompatibility of the novel MPs (Por-ME MPs), the viability, proliferation and cytotoxicity of ihMSCs seeded on the MPs were studied. For the cytocompatibility assays, the MPs were pre-wetted in the cell culture medium, as described in section 5.2.2. Following this step, the cells were seeded on the pre-wet MPs as described in section 5.2.3.

5.2.5.i Presto Blue® Cell Viability Assay

As mentioned in section 2.2.12.2 of Chapter 2, there are several different cell viability assay methods, among which the Presto Blue® assays allows the culturing of the samples post- assay. Therefore, this assay offers the provision of monitoring the viability and proliferation level of live cells for the same sample over a certain period of time. For the work presented in this chapter, the Presto Blue® cell viability assay kit was used for measuring the viability of ihMSCs seeded onto Por-ME MPs. The experimental procedure was similar to that described in section 2.2.12.2, with the exception of altered seeding densities. The ihMSC seeding densities were 10×10^3, 20×10^3 or 30×10^3 cells with 5, 10 or 15 mg of MPs. Cytodex 3 MPs (Cytx-CM MPs) were also included in the experiment in order to compare their cell viability efficiency with Por-ME. The

Cytx-CM MPs consist of a thin layer of denatured collagen, chemically coupled to a matrix of cross-linked dextran. They have been used for the in vitro culture of mammalian cells, including hMSCs [58, 67, 204]. Moreover, their surface properties support the osteogenic differentiation of MSCs that grown on them [205]. For the cell viability experiment, as well as for different osteogenic differentiation assays, Cytx-CM MPs were prepared according to the manufacturer's protocol with a slight modification. In brief, the MPs were swollen and hydrated in Ca^{2+} and Mg^{2+} free PBS for 3 hours at room temperature (25^{o} C). The supernatant was decanted and the MPs were washed in fresh Ca^{2+} and Mg^{2+} free PBS for 3×5 minutes. The PBS was discarded and the MPs were sterilized using AB/AM solution (2 % v/v; 1 mL/10 mg MPs) following the method described in section 5.2.3.

5.2.5.ii Live/Dead® Viability/Cytotoxicity Staining

The Live/Dead® fluorescent stain was used to visualise the changes in ihMSCs viability in contact with Por-ME. For this study a concentration of 20×10^3 cells/10 mg Por-ME MPs was used. A parallel culture was maintained for the same concentration of ihMSCs with Cytx-CM MPs for comparison purposes. The detailed procedure was described earlier in section 2.2.11.iv.

5.2.5.iii HCS CellMask™ Blue Staining

HCS (high-content screening) CellMask™ Blue is a commercially available fluorescent staining kit that is used to label the entire cell (cytoplasm and the nucleus), in order to understand the cell morphologies in contact with substrates.

In this study, the staining kit was used in order to identify the cytoplasmic region and the position of the nucleus and, thereby, to understand the phenotypic characteristics of the cells when they were seeded on Por-ME MPs. The cells were also cultured on Cytx-CM MPs for comparison purposes. For this experiment, 20×10^3 cells (ihMSCs) were seeded with 10 mg of Por-CE MPs/well according to the procedure described in section 5.2.3. On the day of the assay, the cultures were removed from the incubator, fixed with 3.7 % PFA and stained with CellMask™ Blue according to the manufacturer's protocol [206].

The experimental design for PresoBlue® cell viability assay, live/dead viability and cytotoxicity assay and HCS cell mask blue is shown in Figure 5.1.

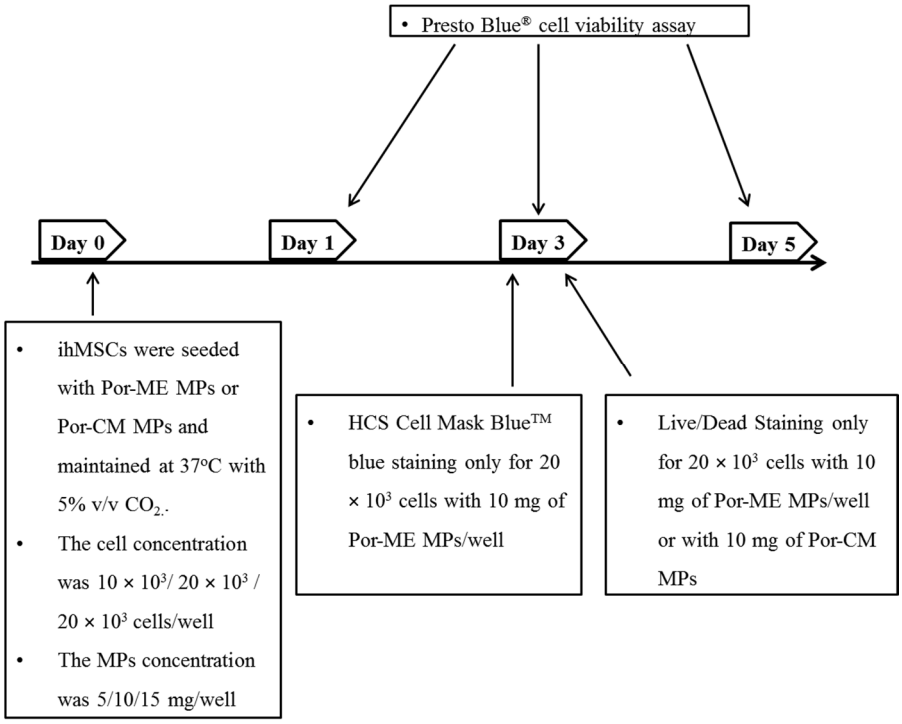


Figure 5.1 Flow diagram of experimental design for cell viability and cytotoxicity assays.

5.2.6 Osteogenic Differentiation of ihMSC on Por-ME MPs

For many osteogenic (OS) differentiation experiments, a cocktail formula of a glucocorticoid steroid (dexamethasone [Dex]), L-ascorbic acid 2-phosphate (AsAP) and β-glycerophosphate (BGP) have been frequently used [34, 43-45, 207]. For many years, the mechanisms and signalling of Dex-induced osteogenesis were unknown. This changed when Hamidouche and colleagues [46] revealed the existence of the specific protein domain (FHL_2) that mediates the Dex-induced differentiation of MSCs into osteoblasts via the activation of Wnt/β-catenin signalling-dependant Runx2 expression. AsAP induces collagen biosynthesis and cell proliferation [47], whereas, BGP enhances calcified matrix formation [47].

It is well established that multipotent hMSCs have the ability to differentiate down to the osteogenic lineage when they are stimulated with any appropriate osteogenic supplements. In this experiment, the focus was to investigate the osteogenic potential of the ihMSCs in the presence of the novel scaffolds (Por-ME MPs). The cells were seeded onto Por-ME MPs according to the method described in section 2.2.11. In total, 20×10^3 cells were seeded onto 10 mg of Por-ME MPs that were previously placed in the well of a 24-well Pluronic F 127-coated nTC plates. The medium was removed 24 hours post-seeding and replaced with the osteogenic medium (complete DMEM supplemented with AsAP [50 µg/mL], BGP [10 mM] and Dex [0.1 µM]. Every 3 – 4 days, the medium was replaced with the fresh osteogenic medium. On day 7, 14 and 21, the cultures were assessed for mineralization and their alkaline phosphatase activity. The cells were also seeded on Por-ME MPs in non-osteogenic (Non-OS) medium (complete DMEM) as a Non-OS control. As all the assays were end-point assays,

the appropriate number of experimental groups were designed so that the starting point for each of the experiments remained the same and, hence the results from different experiments could be compared efficiently. The experimental design is presented in Figure 5.2.

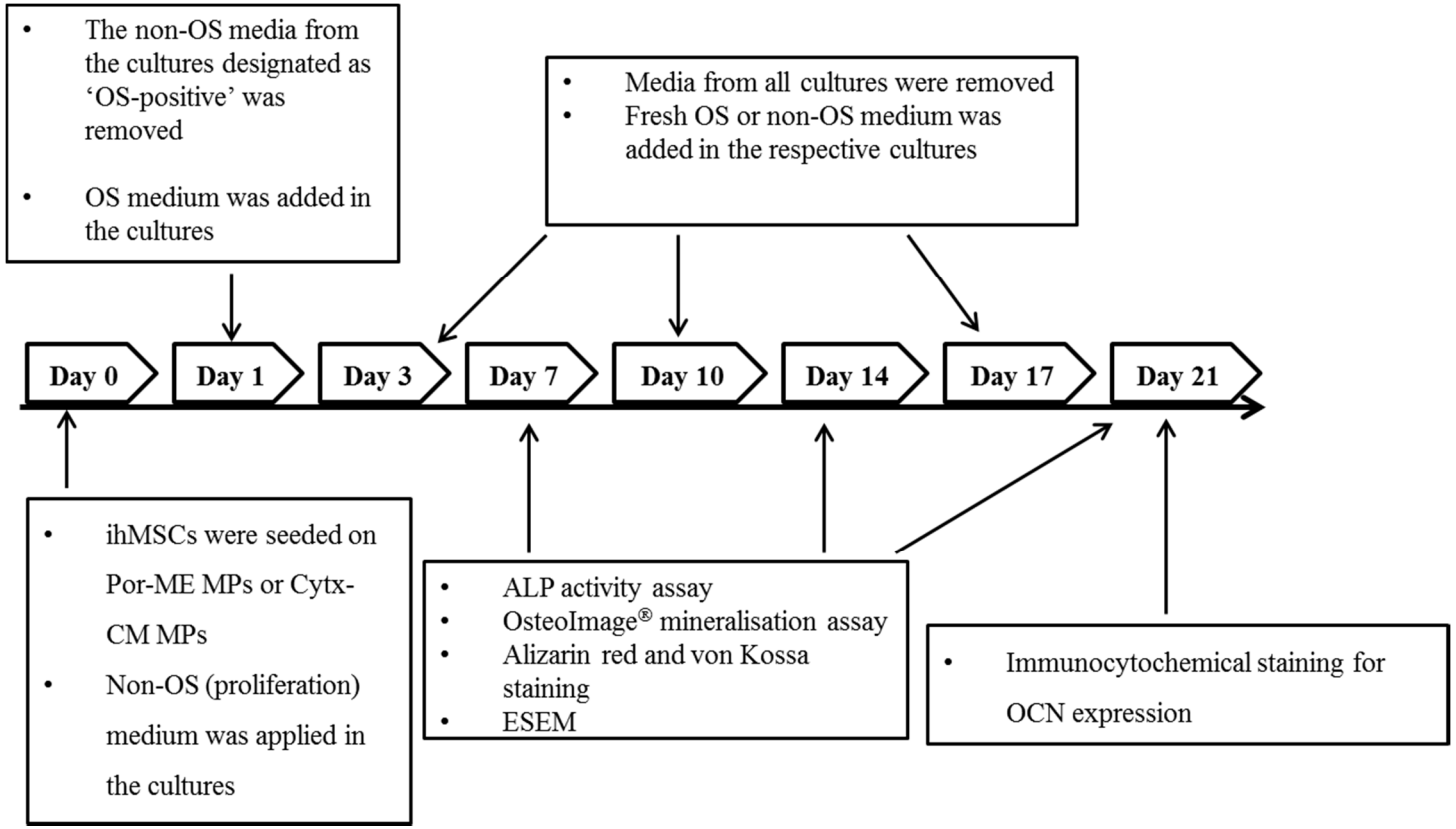


Figure 5.2 Schematic shows the experimental timeline for the osteogenic differentiation assays.

5.2.6.i Assessment of Alkaline Phosphatase Activity

Alkaline phosphatase (ALP) is an early osteogenic marker. Up regulation of ALP in an OS culture indicates that an osteoblastic phenotype is maintained in the culture. In OS culture conditions, the ALP activity of the ihMSCs on Por-ME MPs was measured at day 7, 14 and 21 using a commercially available ALP substrate kit (Colorimetric ALP assay kit, Abcam, UK). One of the kit components is para nitrophenyl phosphate (pNPP), which, in the presence of ALP, is reduced to para nitrophenol (pNP). Hence, the rate of pNP production is proportional to the ALP activity in the culture. The assay was carried out following the manufacturer's protocol [208]. In brief, on the day of the assay, the media was removed from the culture, which was then washed three times with PBS. The cell lysate was prepared by adding 500 µL of the ALP assay buffer into each of the wells and then by pipetting up and down 4 – 5 times. The cell lysate was then centrifuged to remove the insoluble materials (cell debris, MPs). From each of the cell lysate samples, 50 µL was added into a well of a 96-well plate with 30 µL of the assay buffer and 50 µL of the pNPP (5 mM). The plate was then incubated for 60 minutes at 25^{o} C, whilst being protected from light. After 60 minutes, 20 µl of the Stop Solution (3 N NaOH) was added into each of the wells, the plate was gently shaken and the optical densities (OD) of the samples were measured at 405 nm using a microplate reader. The background readings for the samples (without addition of pNPP) were subtracted from the sample readings. A standard curve was generated for a series of known concentrations of pNPP (µmol) that had reacted with a standard ALP enzyme. The sample readings were applied to the standard curve to get the amount of pNP generated by the samples'

ALP. The same method was applied to measure the ALP activity for Cytx-CM MP samples. Non-OS cultures were maintained as negative controls.

5.2.6.ii Biochemical Staining to Assess Mineral Deposition in Osteogenic Culture

Osteogenic differentiation is marked by the formation of mineralised nodules comprising inorganic hydroxyapatite (HA) [Ca_{10} $(PO_4)_6(OH)_2$] and organic components including type I collagen. Alizarin red and Von Kossa staining are two classical approaches that rely on a biochemical reaction between the components of the mineralized nodules and the stain components. Von Kossa is a 'precipitation reaction'-based assay, in which inorganic silver ions from silver nitrate react with phosphate, carbonate or other anionic groups of inorganic salts. Under light illumination, the silver salt degrades to metallic silver. A brown precipitate can be visualised in the sample when the unreacted silver salt further reacts with sodium thiosulphate. On the other hand, alizarin red (1 % w/v solution in water), forms a bright red/orange complex when it binds to the calcium portion of an inorganic mineral.

In order to assess the mineralization in the osteogenic culture, both the alizarin red and von Kossa staining assays were carried out following the protocol developed by Dr. Glen Kirkham, University of Nottingham. PFA-fixed cells-MPs complexes were washed three times with dH_2O and then treated with alizarin red S solution for 5 minutes. The stain was removed and the samples were washed repeatedly with water until no further unreacted stain leached out. The samples

were then imaged using standard light photography (Samsung S4 Zoom; Magnification = 1X). For Von Kossa staining, a silver nitrate solution (1 % v/v solution in distilled water) was added to the post-fixed samples and left under optical light for 60 minutes to allow the degradation of the silver salt into metallic silver. The cells-MPs complexes were then rinsed with several aliquots of dH_2O and further treated with sodium thiosulphate solution (5% w/v in distilled water) for 5 minutes to remove any unreduced silver. The samples were then washed three times and the OS positive cultures were expected to appear as a dark brown complex.

5.2.6.iii Toluidine Blue Staining

Toluidine blue (TB) or tolonium chloride is a basic thiazine metachromatic dye that has a high affinity for acidic nucleic acid components (sulphates, carboxylates and phosphate radicals) [209]. TB stains tissue on the basis of the principle of metachromasia, a process in which the cations of the staining reagent are stacked at the sites of high density of anionic groups in the tissue [210]. This phenomenon indicates that the dye intensity is directly proportional to the density of the nucleic acid components in the tissue. The TB staining process requires a minimal amount of time (less than a minute) and is very simple. In this study, 1 % w/v TB solution was added to the fixed samples and left for a minute for the reaction to complete. After this time, the samples were washed several times with water until all unreacted dye was removed which was evident from the appearance of a clear waste water.

5.2.6.iv Morphologies of the Cells on Por-ME MPs in Osteogenic Culture

In order the study the morphology of the ihMSCs on Por-ME in osteogenic culture, the cells-MPs complexes were imaged under an environmental scanning electron microscope (ESEM, Quanta 650, The Netherlands). Briefly, at day 7, 14 or 21 of the experiment, the medium was removed and the samples were washed three times with dH_2O. For the imaging, the cells along with the MPs were fixed as follows: an appropriate amount (500 µL/well; just enough to cover each sample) of 3 % v/v glutaraldehyde in PBS was added in each well. The plates were covered with the lid, sealed with parafilm and kept in the fridge ($2 – 8^{o}$ C). The following day, the glutaraldehyde solution was removed (in a fume hood) and washed with PBS for 3 × 5 minutes. The samples were further fixed in 1 % w/v osmium tetra oxide for 1 hour. The fixative was removed and the fixed samples were then washed with dH_2O for 3 × 5 minutes. These samples were maintained in wet conditions using dH_2O for ESEM imaging.

5.2.6.v Fluorescent Calcification Assay

The OsteoImage™ Mineralisation Assay is a relatively recent fluorescent-based calcification assay. The assay can be used for the qualitative and quantitative assessment of the mineral deposits in OS cultures. The staining reagent, which is tagged with a fluorescent compound, selectively binds to the hydroxyapatite portion of the mineralised nodules. In this study, the OsteoImage™ mineralization assay kit (Lonza, Walksville, MD, USA) was used to detect and quantify calcium deposition in the OS culture, following the manufacturer's protocol [211]. Immediately after performing the OsteoImage™ staining, the

same sample was counter stained with Hoechst 33258 (Sigma-Aldrich, UK), a fluorescent bisbenzimide dye. The dye binds to the A-T coupling in DNA and the fluorescent intensity amplified after the reaction is proportional to the amount of DNA present. The reagent was supplied at a concentration of 1 mg/mL, which was diluted to make a working concentration of 2 µg/ mL. This was added to the samples, incubated at 37 $^{\circ}$C for 10 minutes and directly imaged under a fluorescent microscope. Under a fluorescent light, the positively stained samples should exhibit green and blue fluorescent to indicate the presence of bone nodules and DNA, respectively. The same samples were analysed using a plate reader at an excitation/emission wavelength of 492/500 nm in order to quantify the mineral content. The relative fluorescent unit (RFU) would be proportional to the amount of bone nodules present in the culture.

5.2.6.vi Immunocytochemical Staining for Human Osteocalcin

In immunocytochemistry, an antigen or protein of interest in the cells of a tissue section is detected using the principle of 'antibodies binding specifically to antigens'. In most instances, to visualise the antigen, the antibody is labelled with a fluorophore, such as fluorescein or rhodamine. The antigen detection method can be categorized as- direct or indirect. In the direct method, the antibody (primary antibody) is labelled with a fluorophore, such as fluorescein or rhodamine, which eventually binds to the target antigen. On the other hand, in the indirect method, the fluorophore is bound to a secondary antibody, which targets the primary antibody that is already bound to the protein of interest. The direct method is simple and rapid; however, it is less sensitive than the indirect method.

For this experiment, an indirect method was used for the detection of a bone specific protein, osteocalcin (OCN) in the osteogenic cultures.

The cell-MP complexes were fixed according to the method described in section 5.2.4, washed with PBS (3 × 5 minutes) and then treated with 0.1 % v/v Triton X100 in PBS for 30 minutes to permeabilise the cell membranes. After removing the permeabilising reagent, the samples were washed out in PBS (3 × 5 minutes) and then soaked in goat serum (a blocking agent; 3 % v/v of the serum in 1% BSA in PBS) for 30 minutes, in order to prevent the non-specific binding of the secondary antibody with epitopes[2] and thereby to remove the background fluorescence from the image.[3] After removal of the blocking agent, the OCN antibody solution (anti-OCN primary antibody; rabbit polyclonal) was added to the sample and incubated overnight at 4^{o} C.[4] The following morning, the antibody was removed and the sample was washed with PBS (3 × 5 minutes). The secondary antibody (Alexa Fluor 488 bound goat anti-rabbit IgG; Invitrogen) was then added and the samples were incubated at room temperature for 2 hours.[5] The unreacted antibody was removed by washing in the samples with PBS (3 × 5 minutes). In order to locate the bone cells' positions in the culture, the same samples were counter stained with the Hoechst 33258 solution (2 µg/mL) for 15

[2] An epitope is the specific piece of an antigen to which antibodies bind non-specifically.

[3] The serum, which is used as blocking agent, is usually taken from the species that the secondary antibody was generated in. The secondary antibody (Alexa Fluor 488-bound goat anti-rabbit IgG; Invitrogen) used in this study was raised in goat.

[4] The primary antibody was supplied at a concentration of 500 µg/mL and was diluted to 200 times for the assay.

[5] The secondary antibody was supplied at a concentration of 2 mg/mL and a 1:200 dilution was used in the assay.

minutes at room temperature. The unreacted stain was removed by washing the samples with PBS (3 × 5 minutes) and then imaging them immediately under a fluorescent microscope.

5.2.7 Statistical Analysis

See section 2.2.13 in Chapter 2

5.3 Results and Discussion

5.3.1 Effect of Densities of Por-ME MPs and ihMSCs On Cell Viability

The effect of the Por-ME MP and ihMSC densities on the cells viability was assessed using the PrestoBlue® cell viability assay, following the method described in section 5.2.5.i. The results are shown in Figure 5.3 and are expressed as relative fluorescent unit (RFU) value, with respect to the cell seeding density and MP concentration at day 1, 3 and 5 in culture. The RFU values are proportional to the number of viable cells in the respective culture. As shown in the figure, for three different concentrations of Por-ME MPs with three different seeding densities, the change in cell the viability and proliferation over the time course of the experiment followed a similar pattern. To be more specific, for all different groups, the viability at day 1 was lowest and gradually, the number of cells in the culture increased. Variation in MP densities had little effect on the cell viability as evident from the insignificant difference ($p>0.05$) in viabilities for different MP concentrations at a particular time point. This result is in contrast to that reported in Chapter 2 for conventional MPs. It is important to note that the

seeding densities used in this phase of the study was 3.33 to 10 times less than that used in the work reported in Chapter 2. It is reasonable to assume that for fewer cells, less surface area would be required for the cells to attach and spread. As seen in the figure, for all three different MP concentrations, the RFU values were highest for the seeding density of 30×10^3 on day 5 and the values were comparable ($p>0.05$). At this time point, it is possible that the overall surface area that was provided by 5 mg of the MPs was sufficient for the cells to remain viable. If this was the case, then for the same seeding density (30×10^3 cells) with higher amounts of MPs (10 or 20 mg/well), the RFU values would not be expected to increase or decrease. In contrast, the cell viability was influenced by the seeding density; the cell viability and proliferation increased as the seeding density increased. For example, the RFU value on day 5 after seeding 20×10^3 ihMSCs with 10 mg of Por-ME MPs was 1.56 times higher than that at the same time point after seeding 10×10^3 ihMSCs with the same amount of the MPs. However, the difference was statistically insignificant ($p>0.05$). In contrast, using the same MP density, the viability after seeding 30×10^3 ihMSCs was significantly higher ($p<0.0001$) than that achieved with a seeding density of 20×10^3 cells at the same time point (day 5). The overall cell viability results suggest that the novel MPs, (Por-ME MPs) were biocompatible with ihMSCs, irrespective of the seeding densities used. The cells viability was largely influenced by the seeding density, but was unaffected by varying the mass of the MPs.

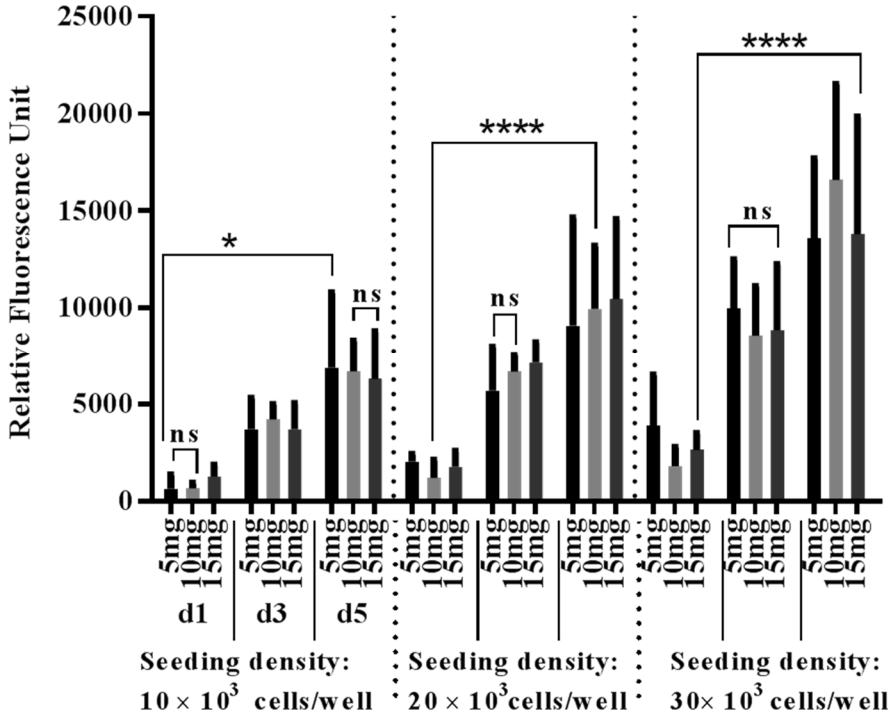


Figure 5.3 Effect of densities of Por-ME MPs and ihMSCs on viability of ihMSCs on day 1, 3 and 5 post-seeding. Values are presented as mean ± SD (n = 2; r = 3). Statistical significance between different groups are represented as: *p<0.05; ****p<0.0001; 'ns' denotes the non-significance of the difference, for which, p>0.05.

5.3.2 Comparison of Cytocompatibility of Por-ME MPs with Cytx-CM MPs

Initial studies, as described in section 5.3.1, demonstrated that irrespective of the MP concentrations, ihMSCs at three different seeding densities remained viable and proliferated on the MPs over the time course of the experiment. The MP concentrations had little effect on the ihMSCs' viability. In contrast, the number of viable cells gradually increased as a function of the seeding density. In order to compare the biocompatibility of Por-ME MPs with that of Cytx-CM MPs, 20×10^3 ihMSCs were seeded on 10 mg of Por-ME or Cytx-CM MPs, according to the method described in section 5.2.3. As shown in Figure 5.4, for both types of MPs, the number of viable cells gradually increased over time and the cell viability on the Por-ME MPs is comparable with that on the Cytx-CM MPs ($p>0.05$). On day 1, the number of viable cells reduced by 50% of the seeding densities for both types of MPs. In this regard, it is important to note that a certain fraction of the seeded cells did not adhere to the MPs and remained floating on the media (referred to Appendix V for the images of the supernatant). The cells were removed from the culture during the removal of the medium. Qutachi et al. [70] also reported a 50 % reduction in cell viability on day 3 with respect to seeding density (200×10^3 NIH-3T3 cells/scaffold) on a scaffold prepared from porous PLGA MPs. The cell viability of SaOs-2 (an osteoblast-like cell line) cells on Polullan (a natural biodegradable polymer) MPs with different surface properties at day 1 was between 29 – 30 % of the seeding density [212]. Goh and colleagues [213] reported that human fetal MSCs (hfMSCs) cultured on MPs of different surface properties (positively charged, collagen- or gelatine- coated) in a bioreactor system exhibited a lag phase for the first few days before they entered

the exponential phase. Although the growth kinetics of ihMSC on Por-ME were not studied, it is reasonable to assume that if the cells were in the lag phase at the early stage of the culture, which might be the case at day 1, they would expand less in numbers during this period. However, by the next three days, there were 7.5 fold expansions in cell numbers when compared with those on day 1. This is comparable with the numbers of hfMSCs observed after 10 days of culture with CultiSphere S (gelatine coated commercial MPs) with hfMSCs [213]. The trend in the cell viability over the time course of the experiment in the case of the Por-ME MPs is comparable with that observed for the Cytx-CM MPs ($p>0.05$).

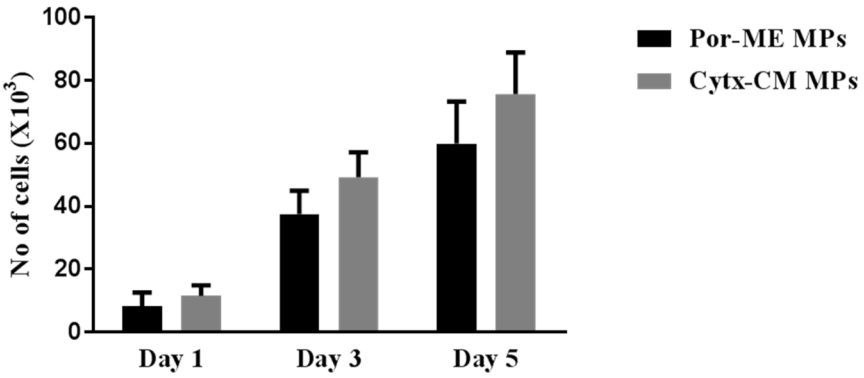


Figure 5.4 Viability of ihMSCs seeded with Por-ME MPs or Cytx-CM MPs on day 1, 3 and 5 post-seeding. The values are represented as mean ± SD (n = 2; r = 3).

On the other hand, the Live/Dead® viability/cytotoxicity study on day 3 revealed that most of the cells cultured with Por-ME were live (bright green fluorescence in Figure 5.5A with a few dead cells (red dots in Figure 5.5B; the white arrows indicate the position of the dead cells). Similar results were observed with the Cytx-CM MPs (Figure 5.5F and Figure 5.5G). However, a closer look at the images revealed that in the case of the Cytx-CM MPs, the cells spread out all over the surface of the MPs. In contrast, for the Por-ME MPs, the viable cells were only seen surrounding the periphery of the MPs. It is important to note that Cytx-CM MPs are collagen-coated dextran MPs, which are optically transparent (see the optical light microscopic images in Figure 5.5 H). Hence, it is reasonable to assume that irrespective of the spatial position of the cells on the Cytx-CM MPs, they could easily be visualised under the microscope. In contrast, as light did not pass through the Por-ME MPs (see the bright field images for both MPs in Figure 5.5 C), only the cells surrounding the MPs could be visualised under the fluorescent microscope. In general, the results of the Live/Dead® viability/cytotoxicity assay suggested that Por-ME MPs, prepared via the X-ME method were cytocompatible, in similarity with the commercial Cytx-CM MPs.

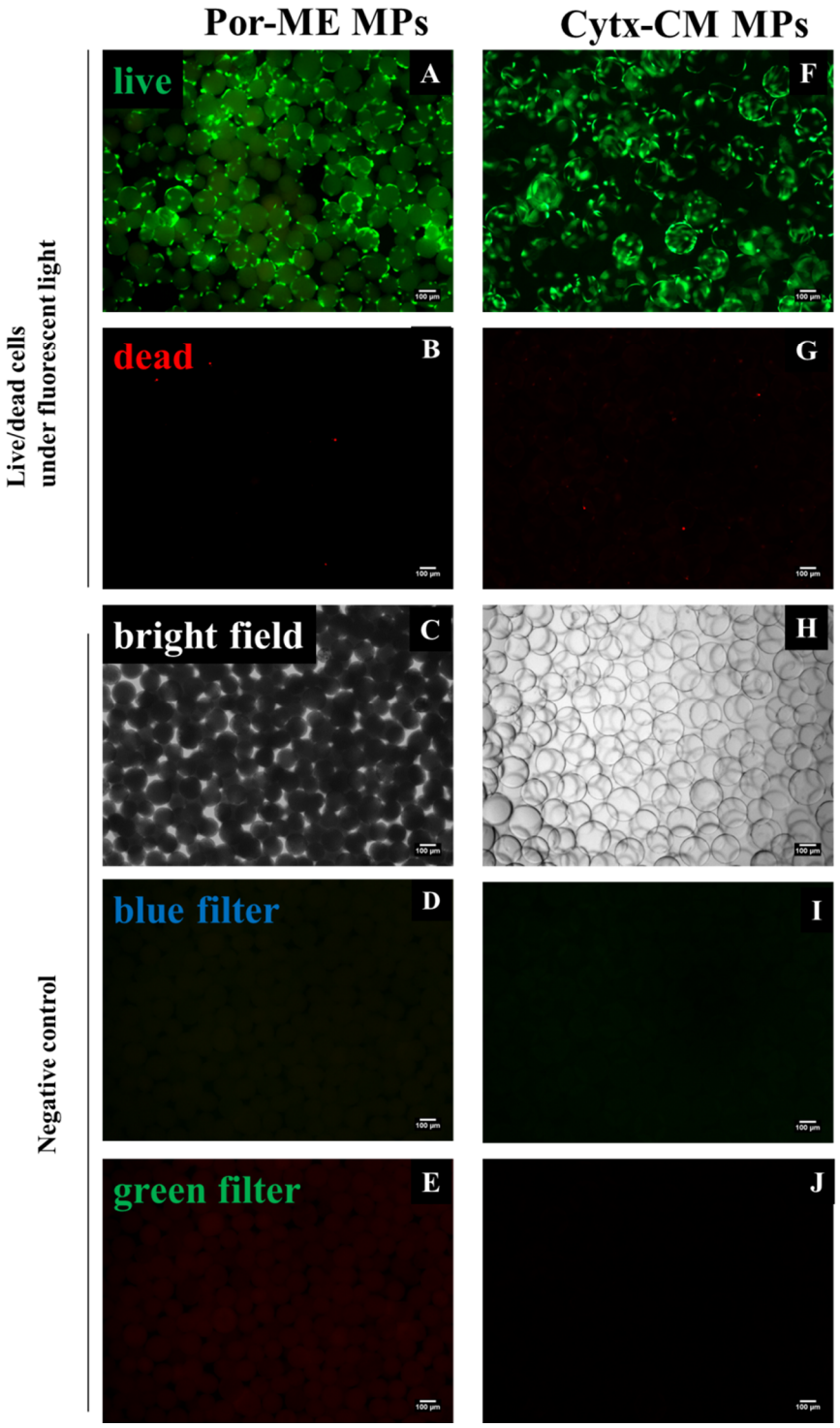


Figure 5.5 Representative Live/Dead images of ihMSCs on Por-ME MPs (left-hand column) or Cytx-CM MPs (right-hand column) on day 3 post-seeding. The seeding density of the cells and MPs were 20×10^3 cells/well and 10 mg MPs/well, respectively. The live and dead cells are shown as bright green **(A and F)** and red **(B and G)** fluorescent, respectively. Scale bar = 100 µm.

The cellular morphologies were not clearly visible with the Live/Dead® assay. Therefore, in order to understand the spatial arrangement of ihMSCs on Por-ME, the cell-MP complexes were stained with the HCS Cell Mask™ blue, following the method described in section 5.2.5.iii. The cells were also seeded on Cytx-CM MPs in order to compare their attachment and spreading with those on Por-ME MPs. The fluorescent microscopic images obtained after the staining are shown in Figure 5.6. The cytoplasmic regions and nuclei of the ihMSCs are clearly visible as light and dark blue areas, respectively. The cells appeared to adhere and spread on most the MPs, indicating the cytocompatibility of the scaffold; however, the shapes of the cells were heterogeneous. This is not surprising for stem cell population. Cells of heterogeneous morphologies were also observed on the Cytx-CM MPs and their spatial orientation differed from that on the Por-ME MPs. A closer look at one of the Por-ME MPs of interest (Figure 5.6B; red perforated circle), demonstrates that the MP contained relatively higher number of ihMSCs than the other MPs in the field, and almost all of the cells were flat and irregular (red arrow). On the other hand, a closer look at a Cytx-CM MP from a similar view point (Figure 5.6 F; red perforated circle) shows that the cells were fusiform or polygonal and relatively less spread out. The reasoning behind the difference in the shapes of ihMSCs grown on the Por-ME and Cytx-CM MPs is unknown. However, it is important to note that the surface properties of the Por-ME and Cytx-CM MPs are different. The Cytx-CM MPs are collagen-coated whereas the Por-ME MPs are uncoated but have a highly porous morphology. It is possible that due to the difference in their surface properties, the cells sensed the MPs differently and eventually they exhibited different spatial orientations on the MPs. On the other hand, the MPs with relatively less dense cells exhibited a completely

different cellular pattern, as indicated by white arrows in Figure 5.6 D, E and F. The cell membranes extended from two sides of the nuclei and can be defined as bipolar shapes.The migration of the cells from one MP to another was also visible from the images (Figure 5.6B and H indicated using yellow arrows), although the shapes of the cells were not clear. A possible explanation for this blurry cellular morphology at the MP-to-MP bridging point is that at this stage the cells were in the process of linking between two MPs, rather than spreading in a particular position; therefore, their cytoplasimic regions were not clearly seen. Another possible explanation is that some of the cytoplasimic regions of the cells at the linking points were out-of-focus or in a different focal plane, which might have caused an artefact in the actual morphologies.

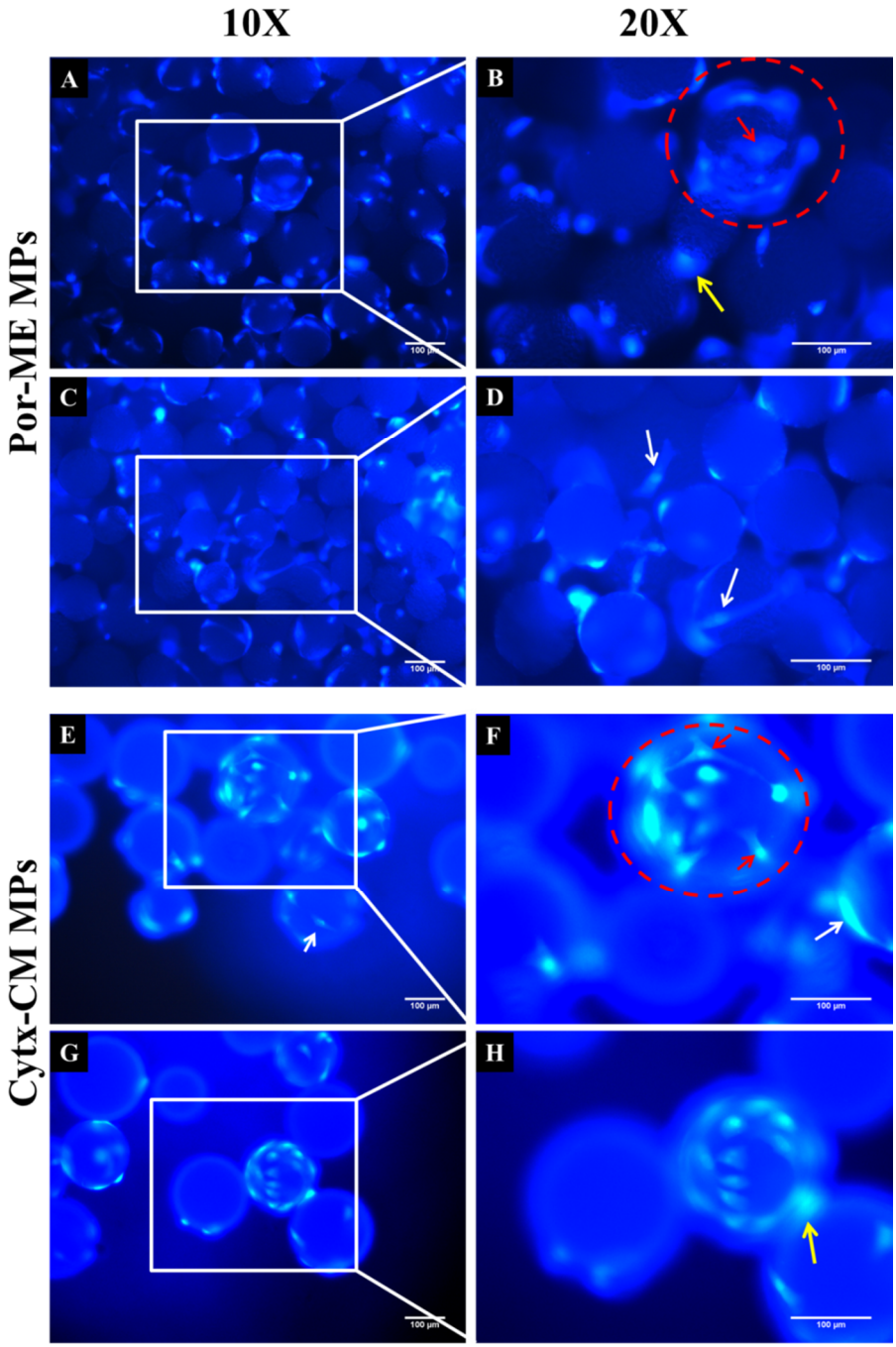


Figure 5.6 CellMask Blue® staining of ihMSCs on Por-ME MPs or Cytx-CM MPs on day 3 post seeding. ihMSCs as bright blue fluorescent on Por-ME MPs **(A – D)** and on Cytx-CM MPs **(E – H)**; the red perforated circles **(B and F)** indicate a single MP with the cells on its surface; the red and white arrows indicate the morphologies of the cells in the denser and less dense fields, respectively; the yellow arrows indicate the position of cells between two MPs. Scale bar = 100 µm.

5.3.3 Osteogenic Differentiation of ihMSCs on Por-ME MPs

MSCs are multipotent cells and can differentiate into chondrocytes, adipocytes and osteoblasts, in vitro, when they are subjected to an appropriate induction medium. Once osteoblasts arise from MSCs in vitro, they pass through the maturational stage. At the early stage of osteogenesis, the cells express a osteoblast related transcription factor, RUNX2 as well as the genes controlled by RUNX2, including ALP [214, 215]. However, in order to deposit calcium on the ECM for mineralized bone formation, the cells need to enter the late stage of osteogenesis [216, 217]. In order to facilitate the stepwise osteogenesis of the ihMSCs on the Por-ME MPs, they were cultured in standard osteogenic medium (a cocktail formula of Dex, AsAP and BGP, see section 5.2.6 for further details) or in proliferation medium (complete DMEM medium) for 21 days. To compare the efficiency of the Por-ME MPs in terms of supporting osteogenesis of ihMSCs, the cells were cultured on Cytx-CM MPs in either OS or Non-OS medium.

There are several different assays that are used for assessing the stepwise osteogenesis of MSCs, which include biochemical, fluorescent-based or immunocytochemical staining or quantification. However, in order to draw a reliable conclusion from the results, it is useful to perform multiple assays. In order assess the level of ALP in the OS culture an enzymatic colorimetric assay was performed. Moreover, calcium deposition was confirmed by a number of biochemical staining assays and a fluorescence-based calcification assay.

Furthermore, fluorescent immunostaining was carried out to confirm the presence of the late osteogenic marker, OCN.

5.3.3.i Assessment of Alkaline Phosphatase Activity

Intracellular ALP activity in the OS and control (Non-OS) medium for the Por-ME MP and Cytx-CM MP groups was assessed on day 7, 14 and 21 after the start of the experiment, following the method described in section 5.2.6.i using an ALP assay kit. The results are shown in Figure 5.7 as a function of the pNP concentration in the cultures. In principle, one of the kit components, pNPP reduces to pNP in the presence of ALP in an alkaline medium. Hence, the amount of pNP is directly proportional to the amount of ALP present in the culture. As shown in the figure, for both the Por-ME MP and Cytx-CM MP groups in OS media, the ihMSCs exhibited a gradual increase in their ALP activity over the culture period (21 days). At each time point, the level of ALP activity was greater in the OS cultures than in the control (Non-OS cultures). However, the difference was not significant until day 21, when the OS-positive cultures exhibited approximately 3 fold higher ALP activities than the OS-negative cultures ($p<0.0001$). The trend in the ALP activity changes over time is comparable to that observed by Chen et al. [218], who cultured hMSCs on CultiSphers S MPs (made of porcine gelatine) in standard osteogenic medium for 20 days; they observed a gradual increase in ALP activity throughout the course of the culture. It was reported that at the beginning of osteogenesis, there is an up regulation of ALP activity followed by a subsequent decrease as the cells lay down minerals and mature [51, 219]. However, the time point when the ALP activity is at its peak level largely depends on the experimental conditions and cell types. For example, the intracellular ALP activity of mouse MSCs cultured in standard osteogenic

medium was at its peak on day 3 and then declined by day 7 [220]. In the same study, the calcium content was highest on day 14; however, the ALP activity at this time point was not studied. Another study reported that both the ALP activity and mineral content were at their highest levels on day 10 when MC3T3-E1 cells (a mouse origin osteoblast cells) were cultured on BMP-2 loaded PLGA MPs [83]; the level then declined later in the experiment. In contrast, a recent study [221] reported that hMSCs cultured on polymeric scaffolds with pore gradients under OS conditions exhibited a raise in both their ALP activity and calcium content over time. Furthermore, both the enzyme and mineral content reached their peaks after day 28.

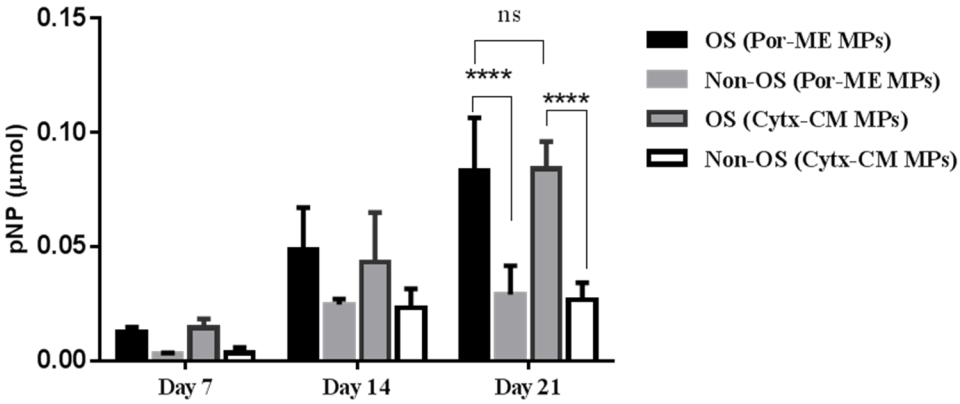


Figure 5.7 Alkaline phosphatase activities of ihMSCs cultured on Por-ME MPs or Cytx-CM MPs with osteogenic (OS) or non-osteogenic (Non-OS) medium for a period of 21-days. Values are presented as mean ± SD (n = 2; r = 3). Statistical significance between different groups are represented as: ****$p<0.0001$; 'ns' denotes the non-significance of the difference, for which, $p>0.05$.

5.3.3.ii Biochemical Staining

As stated earlier, a major process involved in bone formation is mineralisation, which occurs at the late stage of osteogenesis. HA is the major component of bone minerals; calcium and phosphate are the two important structural elements of HA. In order to confirm the presence of HA in an osteogenic culture, two biochemical reaction-based assays are often performed simultaneously. One of the assays uses the alizarin red staining reagent, the use of which confirms the presence of calcium in the sample. Another reagent, von Kossa contains silver nitrate, which exchanges its nitrate group with phosphate or other anions upon making contact with them. Later on, photochemical degradation of the silver phosphate releases metallic silver into the culture, which can be visualized as a brown nodule. The samples were also treated with Toluidine Blue (TB) in order to confirm the presence of cells in the culture, as TB reacts with acidic nucleic acid components. The detail methods for the biochemical and TB staining are described in section 5.2.6.ii and 5.2.6.iii, respectively. Some representative images of the biochemical staining at day 21 of the experiment are presented in Figure 5.8. As shown in the figure, treating the OS-positive culture with alizarin red transformed the colour of the cell-MP complexes from white to brick red, whereas, the control (non-OS culture) did not show any change in the colour after alizarin red treatment. These images suggest the presence of calcium in the OS-treated cultures. Moreover, upon reacting with the von Kossa reagent, the OS-positive cultures exhibited brown-coloured cell-MP complexes, an indication of the presence of a silver precipitate in the culture. These results indicate the presence of phosphate in the OS-positive culture. Similar results were observed on day 14; however, on day 7, the biochemical staining demonstrated negative

results (data not shown). The outcomes of the results of the alizarin red and von Kossa staining suggest that the bone mineralisation process started at a later stage in the OS-positive cultures. The colour intensity, as well as the morphology of the cell-MP complexes, observed for the Por-ME MP group after the alizarin red staining are comparable with those observed for the CultiSpher S MPs after the same treatment [218]. However, the intensity of the von Kossa staining was relatively brighter than that observed for MC3T3-E1 cell cultured on BMP-2 loaded PLGA MPs [83]. Further staining of the cells with TB confirmed the presence of cells in the culture. The images also show that the sizes of the cell-MP aggregates were different in the OS-positive and OS-negative cultures. To be more specific, all the OS-positive cultures exhibited relatively large aggregates. The reason why the OS-positive cell-MP complexes were larger is not certain. However, it has been reported that in the early stage of in vitro osteogenesis, a collagen type I matrix is expressed in the culture, onto which mineral is later deposited [222]. Hence, it is likely that when compared with the non-OS culture, the OS-positive culture would contain more collagenous matrix, and for MP-based cultures, more MPs would be trapped in the cell-MP complex. Eventually, the size of the cell-MP complexes in the OS-positive culture would be larger.

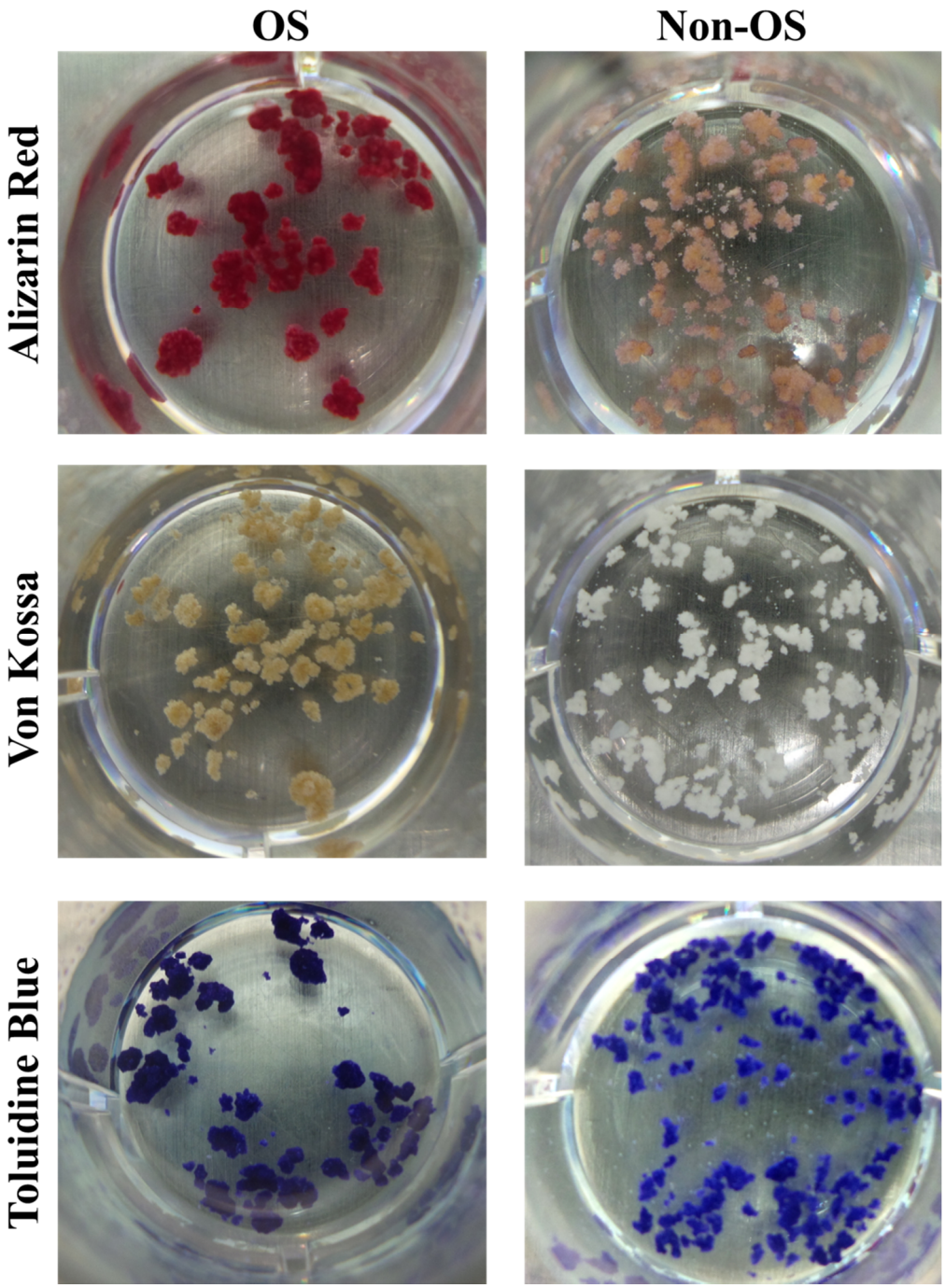


Figure 5.8 Representative light photographs of ihMSCs with Por-ME MPs in OS or non-OD medium at day 21 post-seeding. On the day, the cultures were stained with alizarin red and von Kossa to identify calcium deposits, and with toluidine blue to identify the cells in the culture. The seeding densities for the cells and MPs were 20×10^3 cells/well and 10mg Por-ME MPs/well of 24 well plates. Images were captured at magnification = 1×.

5.3.3.iii Morphology of the Cells on Por-ME in Osteogenic Culture

The ESEM images of the OS-positive cultures on day 7, 14 and 21 are shown in Figure 5.9, Figure 5.10 and Figure 5.11, respectively. As shown in Figure 5.9, on day 7, the cells cultured with the Por-ME MPs formed wide cell sheets that covered the surface of the MPs. The morphology of the cells was comparable to that observed using the HCS Cell Mask^{TM} Blue staining. The cells sheets also extended across the MPs. On the other hand, in the Cytx-CM MP group, the surfaces of most of the MPs were covered by the cells on day 7, and, the cellular orientations were distinctly different than that those on the Por-ME MPs. On the Cytx-CM MP surfaces, the cells spread as a monolayer. Most of the cells were fusiform with a few exhibiting a rounded shape; individual cells could be identified, which was less common in the case of the Por-ME MP group. The similar cellular morphologies were evident on day 14 (Figure 5.10), but indicated a denser cell population on the surface of both MPs. MP-MP bridging with the cells was even stronger at this time point. Some of the Por-ME MPs degraded at this time point, as evident from the presence of some deformed MPs in the negative control group. MP degradation was not evident in the Cytx-CM MP group at any time point. On the other hand, on day 21 (Figure 5.11), the cell sheets from the Por-ME MPs partially started to detach. It is well known that when anchorage-dependant cells become confluent, they often detach as cell sheets. As observed on day 7, some of the Por-ME surfaces were already saturated with the cells. It is not surprising that on further days in culture, more cells were stacked on the surface of the MPs and eventually to minimise the cell density, they detached from the surface as an intact cell sheet. In contrast, there was no sign of cell sheet detachment for the Cytx-CM MPs. It is important to note

that the surfaces of the Cytx-CM MPs were coated with denatured collagen and such a coating delays the detachment of cell sheets in a long term culture [223]. The Por-ME MPs surfaces had no such coating.

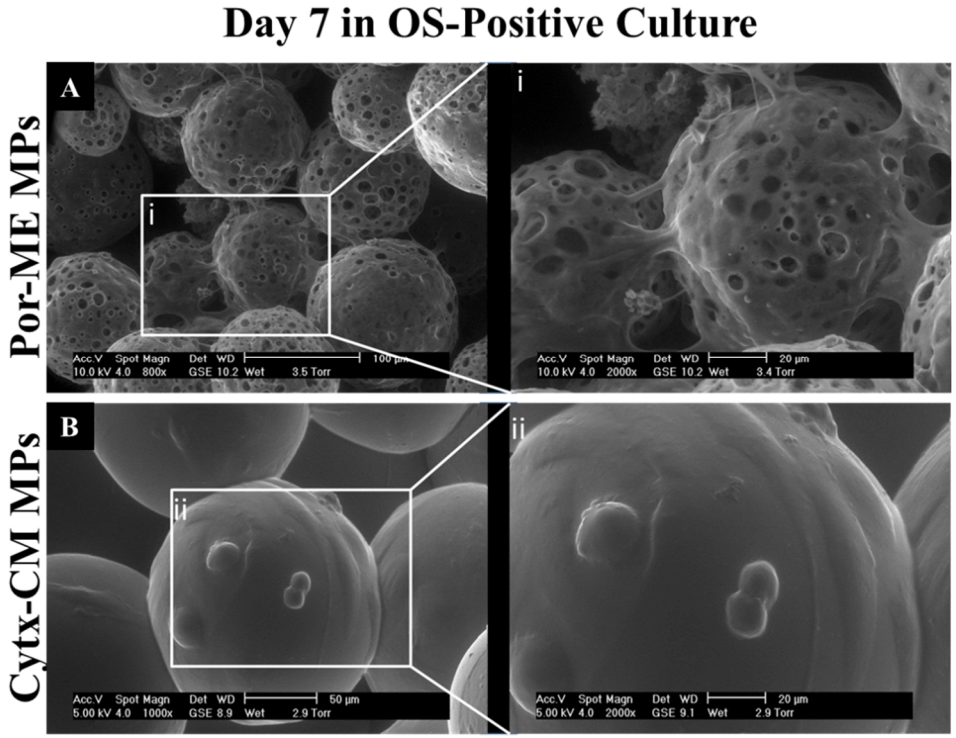


Figure 5.9 Representative ESEM images of ihMSCs on Por-ME MPs **(A)** and Cytx-CM MPs **(B**) that were cultured in an OS medium for 7 days. The cells are flattened on the surface of Por-ME MPs and forming a thin layer on the MPs and covering the pores; there is little evidence of individual cell boundary **(Ai)**. In contrast, the cells on Cytx-CM MPs are either elongated or circular shaped **(Bii)**; individual cells can be distinguished.

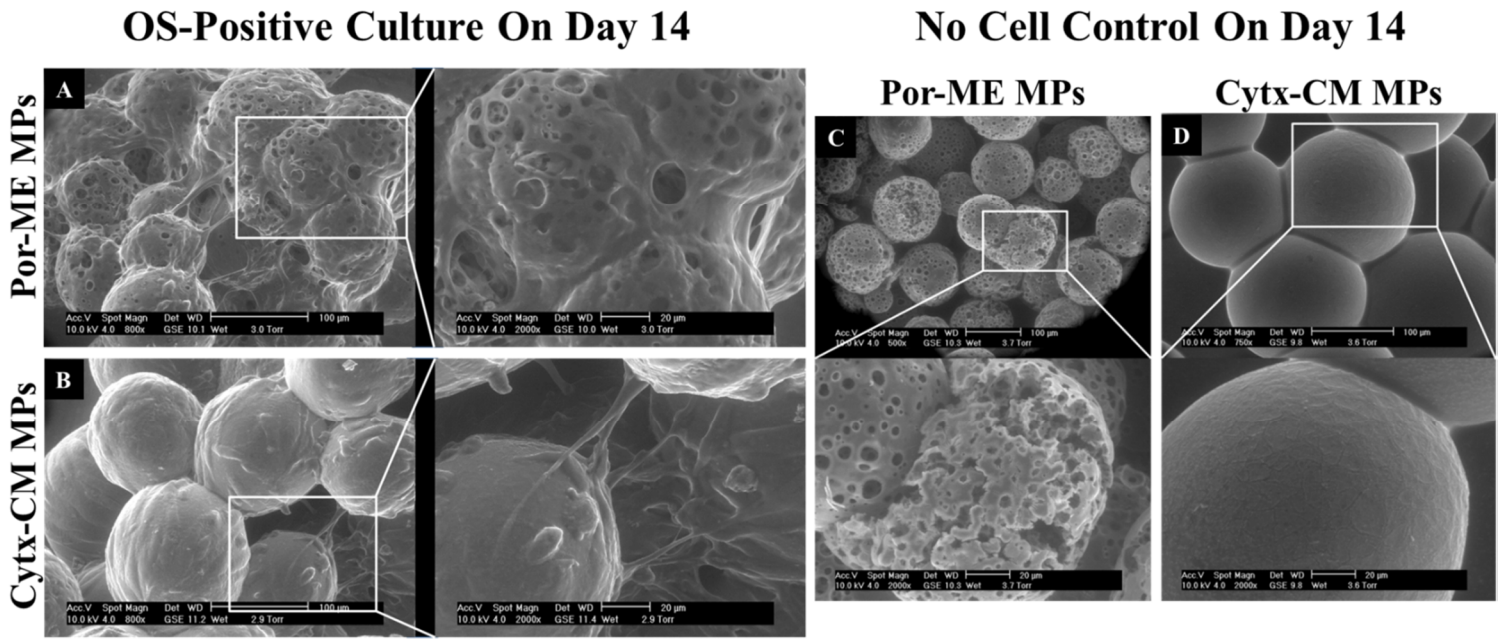


Figure 5.10 Representative ESEM images of ihMSCs on Por-ME MPs **(A)** and Cytx-CM MPs **(B)** in OS culture on day 14. The cells on Por-ME MPs were flattened and formed wide sheets which covering most of the surfaces of the MPs **(A)**; the cells also formed bridges between MPs as seen in the magnified image **(A)**. The cells on Cytx-CM MPs were elongated with a few cells of rounded shape **(B)**; most of the MPs were almost entirely covered by the cells **(B)**; the magnified image shows the bridges between adjacent Cytx-ME MPs **(B)**. Por-ME MPs **(C)** and Cytx-CM MPs **(D)** with no cells in OS medium on day 14; some of the Por-ME MPs deformed whereas the Cytx-CM remained intact on day 14 post-culture in OS medium.

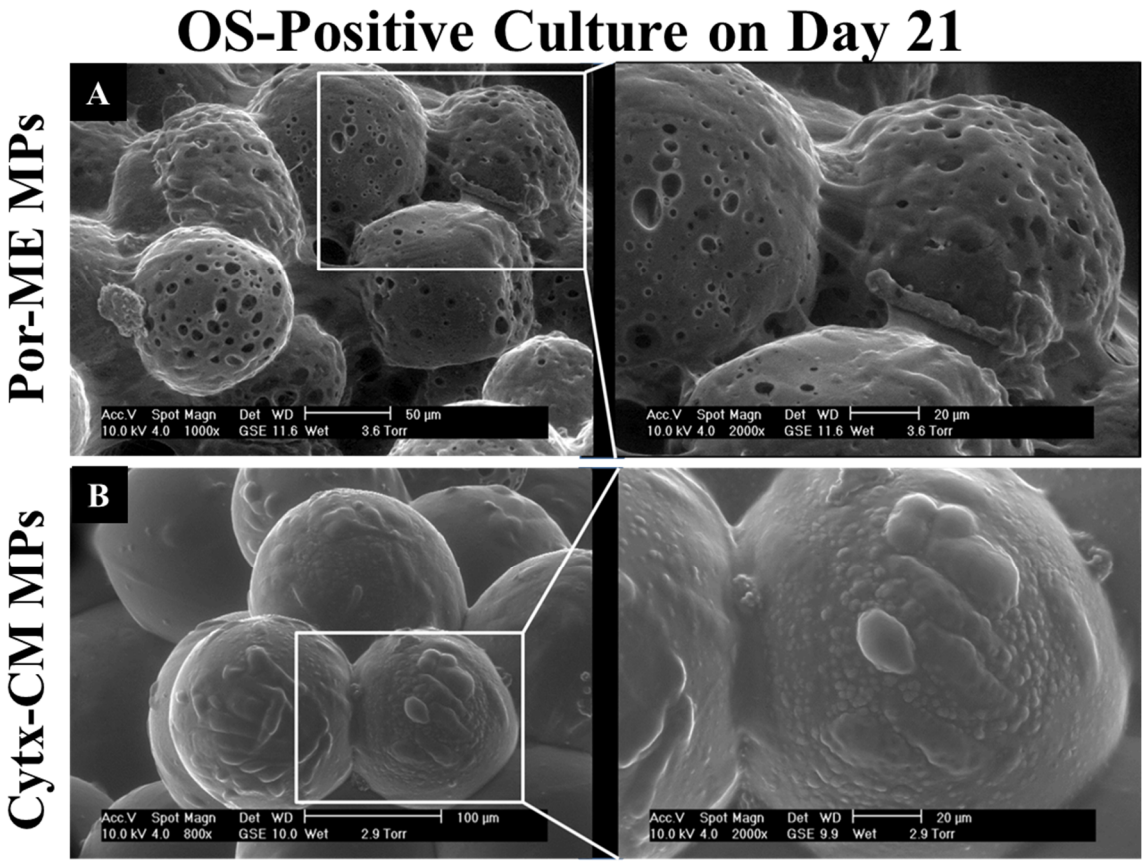


Figure 5.11 Representative ESEM images of ihMSCs on Por-ME MPs **(A)** and Cytx-CM MPs **(B)** in OS culture on day 21.

5.3.3.iv Fluorescent Calcification Assay

A fluorescent calcification assay was performed to confirm the presence of HA, the major component of bone nodules. The results are reported in section 5.3.3.ii were obtained by treating the samples with either alizarin red or von Kossa reagent, which indicted the presence of either calcium or phosphates, respectively. Thus, these results indirectly demonstrated the presence of bone nodules in the cultures. None of the tests are HA specific. In contrast, OsteoImage^{TM}, which is a fluorescence-based compound, directly binds to the HA portion of bone nodules and, thus, the nodules can be viewed under a fluorescent microscope. The degree of mineralisation can be quantified as a function of the RFU value, using a plate reader. In this study, the OsteoImage^{TM} mineralisation assay was carried out following the method described in section 5.2.6.v and the results are shown in Figure 5.12 and Figure 5.13. As shown in Figure 5.12, at day 21, the OS-positive culture stained green in reaction with the OsteoImage^{TM} reagent. A counter staining of the culture with Hoechst 33258 stained the cellular nuclei blue, which could be viewed under a fluorescent microscope. In contrast, the OS-negative cultures did not show any green fluorescence in reaction with the OsteoImage^{TM} reagent. The cultures were also treated on day 7 and day 14 with the OsteoImage^{TM} reagent and only on day 14, the OS-positive cultures stained positive (data not shown). Figure 5.13 demonstrates the fluorescence reading (RFU) for the osteogenic and non-osteogenic cultures. As shown in the figure, on day 7, there was no difference in RFU values for the OS and Non-OS cultures ($p>0.05$). However, on day 14 and 21, the RFU values of the OS cultures were significantly higher ($p<0.0001$; Figure 5.13) than that for the non-OS cultures. These results are in agreement with the imaging data shown in Figure 5.12 (for

day 7 and day 14, the images are not shown). These results are also in agreement with those reported by Zhu et al. [224], who showed that calcium deposition for human osteoblast cells, cultured on TGF-β1 coated PCL scaffolds continuously increased, from day 7, through- to-day 14 and, day 21.

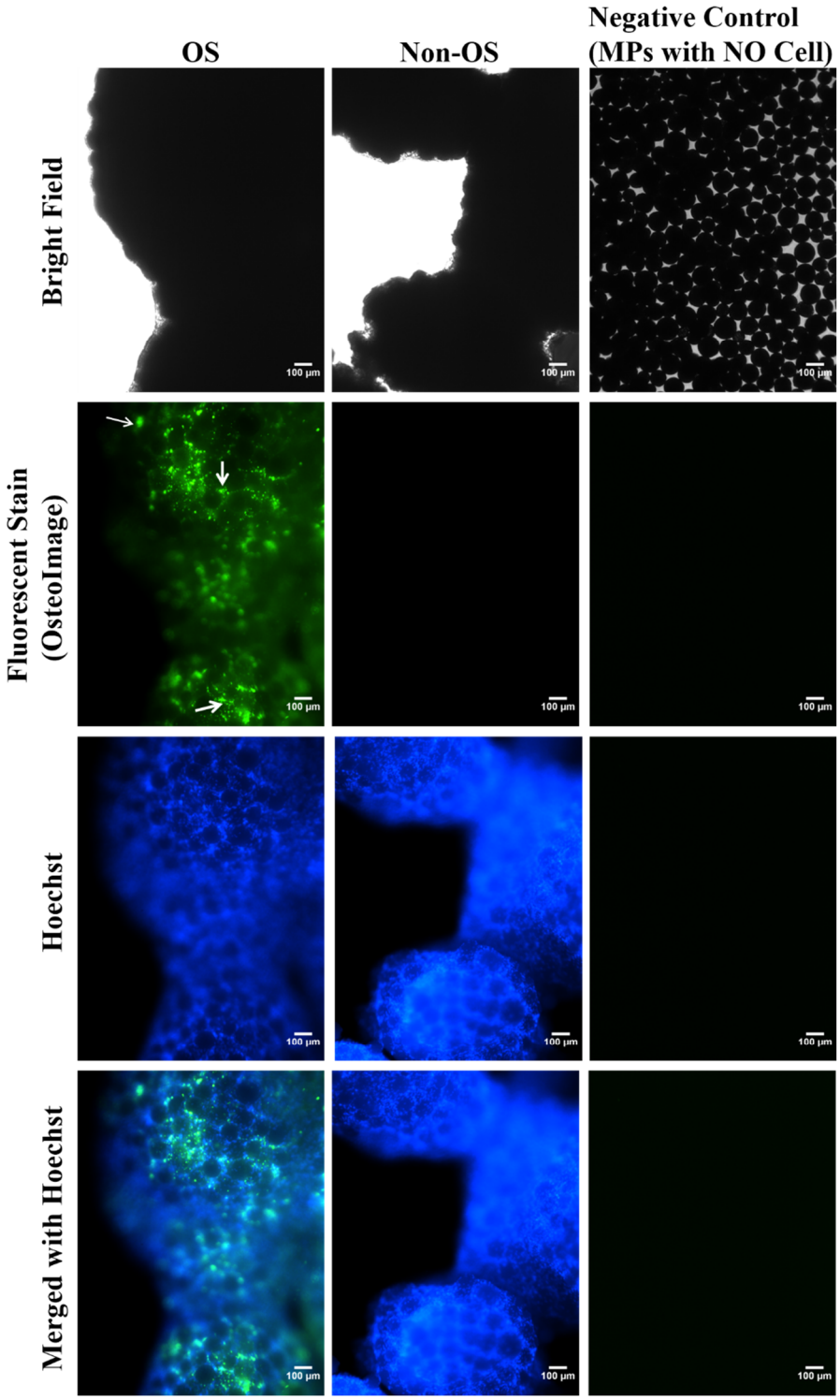


Figure 5.12 Fluorescence calcification assay, using the fluorescent calcification assay kit, OsteoImage®. The cultures are in osteogenic media on day 21. All arrows indicate calcium deposition. Scale bar = 100 µm.

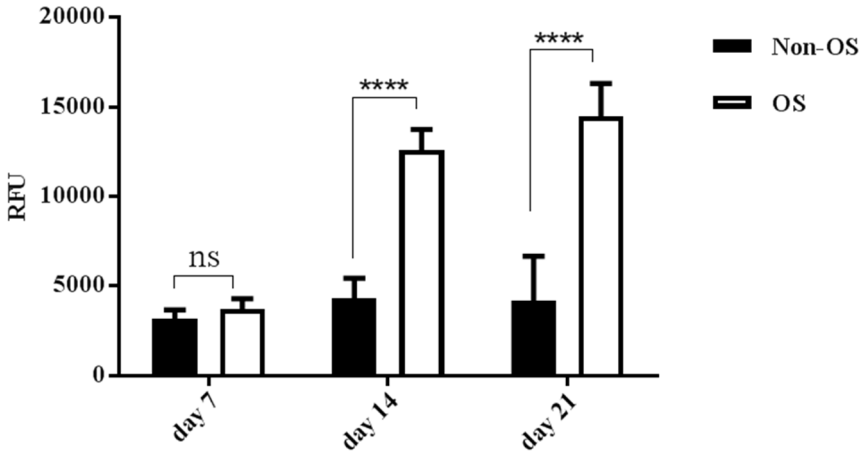


Figure 5.13 Fluorescence calcification assay using the commercially available kit OsteoImage®. Values are presented as mean ± SD (n = 2; r = 3). Statistical significance between different groups are represented as: ****p<0.0001; 'ns' denotes the non-significance of the difference, for which, p>0.05.

5.3.3.v Immunocytochemical Staining for Human Osteocalcin

Expression of OCN in an osteogenic culture indicates the presence of bone nodules in the culture. It is claimed that only the bone dentin and cementum of adults express this protein and it is solely secreted by osteoblast cells [225]; hence, it represents a good marker for osteogenic maturation. In this study, using the immunocytochemical staining tool, the expression of OCN in the OS-positive culture was confirmed. The method is described in section 5.2.6.vi and the results are shown in Figure 5.14. At day 21, OCN was present in both the OS-positive Por-ME MP and Cytx-CM MP groups. Although there was a distinct difference in the fluorescence intensities of the OS-positive and OS-negative cultures for the Cytx-CM MP group, these MPs exhibited an auto fluorescence property, which caused some artefacts in the imaging. Unlike in the case of the Por-ME MPs, discrete bone nodules were not observed for the Cytx-CM MP group; although the overall fluorescence intensity for the OS-positive culture was substantially higher than that of the OS-negative culture. On the other hand, the phase contrast microscopy images suggest that the OS-positive Por-ME MP group was more compacted than the corresponding OS-negative group. The morphological patterns of the cell-MP complexes in the Por-ME MP group are in consistent with those observed in the biochemical and fluorescent calcification assays, (described in section 5.3.3.ii and 5.3.3.iv, respectively.) In contrast, there was no noticeable difference between the Cytx-CM MP cultures in terms of the compactness of the cell-MP complexes. Counterstaining of the cultures with Hoechst 33258 suggested that both the undifferentiated and differentiated cells were highly spread on the surfaces of both types of MPs.

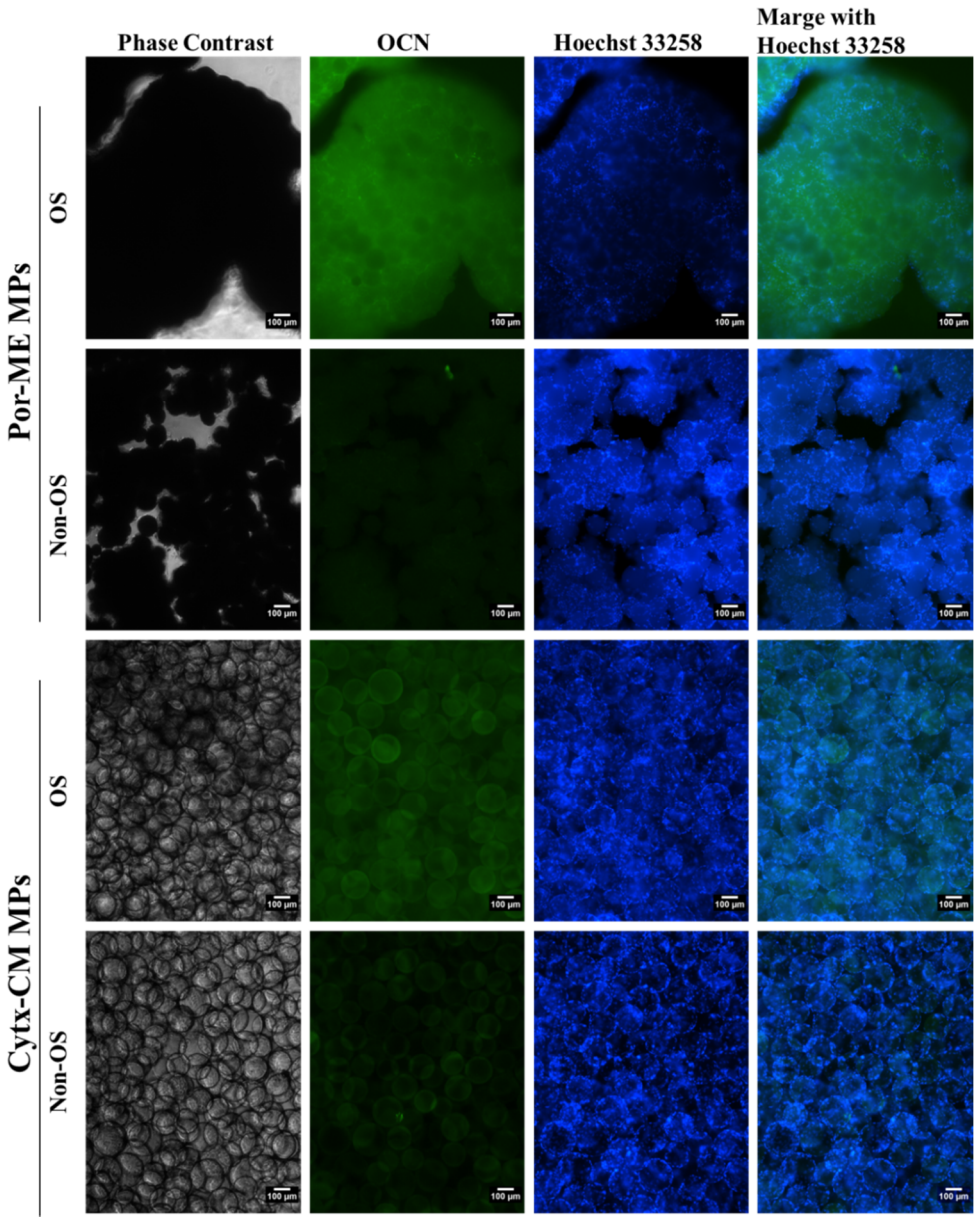


Figure 5.14 Immunocytochemical staining for human OCN, expressed by osteogenically differentiated ihMSCs on Por-ME MPs or Cytx-CM MPs at day 21 in OS-positive cultures. Representative images are shown. Scale bar = 100 µm.

5.4 Conclusions

The work presented in this chapter aimed to assess the efficiency of the novel porous PLGA MPs (Por-ME MPs) in terms hMSCs attachment, viability and osteogenic differentiation. The MPs were prepared using the X-ME method and the work related to the preparation is presented in Chapter 4. In this chapter, the efficiency of the MPs in terms of the viability, proliferation and osteogenic differentiation of ihMSCs cultured on the MPs are reported.

The cell viability study demonstrated that in contact with the novel MPs, ihMSCs remained viable and proliferated over the time course of the culture. The MPs supported cell adhesion and viability, with relatively low seeding densities when compared with other studies, where, for example, at least 10 to 100 times more cells were used for the cell viability experiment. MP densities in the culture did not affect the cell viability i.e., the numbers of viable cells on the minimum amount of MPs (5 mg/well) were comparable with those on the maximum amount of MPs (15 mg/well). The viability data for the novel MPs was comparable to that of the commercial MPs, Cytx-CM MPs. Further visualisation of live and dead cells on the MPs revealed that most of the cells on the MPs were viable, with a few dead cells. In this case, again, the performance of the novel MPs was comparable to that of the Cytx-CM MPs. However, for both the novel and commercial MPs, the distributions of the cells on the surface of the MPs were inconsistent.

The osteolineage potential of the ihMSCs in contact with the novel MPs was assessed using a number of assays, which included biochemical staining to detect

mineralisation, a fluorescent calcification assay, an ALP activity assay and immunocytochemical staining for the detection of the osteogenic marker, OCN. The outcomes of all of these assays were in agreement with each other and all indicated the positive osteogenesis of the cells when they were grown on the novel MPs under osteogenic condition.

The overall outcomes of the cell viability and osteogenic differentiation studies are encouraging in the context of the potential of the novel porous PLGA MPs for injectable stem cell delivery applications. The protocol for the preparation of the MPs is in place. In future, with the use of primary MSCs or other pre-osteogenic or osteogenic cell lines, the scaffolds biocompatibility could be assessed in terms of their viability and osteogenic differentiation potential.

Chapter 6 Summary and Future Work

6.1 Summary

The major aim of this study was to develop a new platform for fabrication of porous PLGA MPs of well-defined size with narrower size distribution using cross-flow membrane emulsification (X-ME) method, in order to use the MPs in tissue engineering (TE) applications. In the beginning of the study as described in Chapter 2, characteristics of porous PLGA MPs, prepared via a conventional method (Por-CE MPs) were studied and their efficiency as stem cell carrier were evaluated using ihMSCs, in terms of their cell adhesion, viability and cytotoxicity behaviours. In the subsequent two chapters (Chapter 3 and Chapter 4), the method development process for the novel MPs are described. In Chapter 5, the performance of the novel porous PLGA MP (Por-ME MPs) as carriers of ihMSCs, in terms of cell viability, adhesion and proliferation is demonstrated, using the seeding techniques developed for Por-CE MPs. Osteogenic differentiation potential of ihMSCs in contact with Por-ME MPs was also assessed and is described in Chapter 5.

In Chapter 2, PLGA MPs with highly interconnected pores (Por-CE MPs) were fabricated using a w/o/w double emulsion-solvent evaporation method, which was previously developed by the researchers at the University of Nottingham. In this phase of the study, the feasibility of Por-CE MPs as discrete scaffold particles for injectable stem cell delivery application was assessed. ihMSCs were the cells of choice so that there is sufficient supply of the cells for different experiments. In terms of characteristics of MPs, usually the mean ± SD with a size distribution

histogram is reported. For further morphological features, SEM images are analysed. In this chapter, for the purpose of characterization of the MPs, in addition to analysing the mean diameter, two other important statistical parameters (skewness and kurtosis) were considered, which rarely were reported by others. The size distribution curve was explained in terms of the degree of smallest size of MPs. The size distribution data suggested a polydisperse population, which is not surprising for MPs prepared by emulsion-solvent evaporation method. However, analysing the level of smallest and largest size MPs in a distribution could be useful when those MPs are the key components of a cellular microenvironment. The pore size distribution was also quantitatively measured. The size of the pores was large enough to facilitate diffusion of oxygen and nutrient, and the removal of metabolic wastes. However, the cells could not diffuse through the pores; they largely grown on the surface of the MPs. The MPs were further studied for ihMSCs adhesion, viability and cytocompatibility to evaluate the MPs as injectable cell delivery vehicles. From the cell adhesion experiment, it could be suggested that using a cell-repellent- coated plate guide the cells to preferentially adhere to the MPs. The cell viability was assessed for different amount of the MPs in a culture. The cells were seeded with the MPs using either static or dynamic (shaking) seeding mode and the viability assay demonstrated that there were no difference in number of cells for the static and shaking seeding modes. The cytocompatibility study demonstrated that the MPs (Por-CE MPs) size and topographic features were favourable for sustainable cell growth for the culture period (up to 5 days).

In Chapter 3, the method development processes for the preparation of solid PCL MPs with mean diameters of approximately 100 µm and narrower size distributions (lower span factor) using X-ME have been described. PCL of two different molecular weights (Mn = 80 and 45 kDa) were used in the experiment. In the beginning of the experiment, for the higher molecular weight PCL ($PCL80_{kDa}$), the emulsion conditions, such as working pressure (Pw), emulsifier concentration ($Conc._{CP}$) DP concentration ($Conc._{DP.}$), DP viscosity (η_{DP}) and DP/CP volumetric ratio ($\varphi_{DP/CP}$) were optimised to obtain monodisperse solid PCL MPs with expected size (mean diameter of approximately 100 µm). Solid PCL MPs of expected size (mean diameter = 109 µm) and size uniformity (span factor = 0.51) were prepared with a SPG membrane of pore diameter (D_0) 50 µm under a Pw of 13 KPa, $Conc._{DP}$ of 12.5% w/v, Conc.CP of 0.3 % w/v PVA solution, ηDP of 1.33 Pa.s and DP/CP volumetric ratio ($\varphi_{DP/CP}$) of 1:26. The same Pw and $Conc._{CP}$ (emulsifier concentration) were used for preparing the optimal size MPs with the lower molecular weight PCL (PCL_{45kDa}); however, the η_{DP} required to increase up to a level close to that of PCL_{80kDa} (ηDP for PCL_{80kDa} = 1.33 Pa.s; η_{DP} for PCL 45_{kDa} = 1.52; $p>0.05$) and a membrane with pore diameter of 20 µm were used. Effect of several factors-Pw, D_0, PVA concentration ($Conc._{CP}$) and the viscosity of polymer solution (η_{DP}) were investigated while optimising the emulsion conditions for MPs fabrication using PCL_{80kDa}. As observed, gradual increase in working pressure results in gradual increase of MPs size and polydispersity which is in agreement with literature followed X-ME technique [226] . As an emulsion stabiliser, 0.3wt% PVA was the optimum concentration. Below this concentration, both size and polydispersity increased, and above that only size decreased but no effect on MPs monodispersity. There

was a direct relation between Dp and D_0 which is in support of the literature followed the same experimental set up (X-ME). High DP viscosity was found as a pre-requisite to ensure particle size uniformity for larger size MPs. MPs with mean diameter of approximately 100 μm and narrower span of distributions were prepared using PCL_{80kDa} and PCL_{45kDa} under the same conditions of Pw, $Conc._{CP}$ with a little adjustment in $\varphi_{DP/CP}$ and changing of the D_0.

On the basis of the experimental finding, it is suggested that relatively monodisperse MPs with mean diameter of approximately 100 μm can be prepared using the X-ME emulsification technique, from a range of polymer solutions, under the same emulsification conditions, provided that the DP has a certain degree of higher viscosity that facilitate spontaneous droplet formation under the emulsification condition.

Chapter 4 concerned fabrication of porous PLGA MPs with a mean diameter of approximately 100 μm and span factor of approximately 0.50 using the X-ME method, in order to using these MPs for injectable stem cell delivery application. There are several factors that influence the size and size uniformity of MPs prepared by X-ME method, including P_w, $Conc._{DP}$, η_{DP}, $Conc._{CP,}$ $\varphi_{DP/CP}$ and V_{CP}. All these parameters were optimized for the preparation of uniform-sized solid PCL MPs with a mean diameter of approximately 100 μm, using PCL of two different molecular weights, as reported in Chapter 3. Those optimum conditions were taken into account while preparing the porous PLGA MPs. Investigation of the PLGA-PBS primary emulsion that possessed the viscosity (close to that of the optimum PCL solution) was the first experiment done in this chapter, in order to

use that as the DP for fabricating the porous PLGA MPs. Under the following emulsification conditions: P_w = 13 KPa, η_{DP} = 1.06 Pa.s, $Conc._{CP}$ = 0.3 % w/v, D_0 = 20 μm and V_{CP} = 1.55 – 1.63 l/min, uniform-sized (span factor = 0.43) porous PLGA MPs of mean diameter 114 μm was successfully prepared using a membrane emulsification apparatus under the X-ME set up. In this regard, it is important to note that the same emulsification conditions were used to obtain the optimum solid PCL MPs using the polymer of molecular weight = 45 kDa. Both the PLGA and PCL containing DP had similar level of viscosity. The overall study results as reported in Chapter 3 and Chapter 4 suggest that irrespective of types and molecular weights of polymers, uniform-sized, larger MPs with a mean diameter of approximately 100 μm could be obtained under a X-ME set up when the respective DP possesses a certain higher level of viscosity and some common emulsification conditions are maintained. On the other hand, while preparing the porous PLGA MPs, the author noticed that the performance of a new and used SPG membranes are not the same. The very first batch of the MPs prepared using a new membrane produced highly uniform MPs, both in the case of the preparation of porous and non-porous MPs. In contrast, the immediate next batch (the second batch for the membrane) showed significantly less uniform ($p<0.0001$) MPs in comparison to the very first batch. The sizes of MPs prepared by new membranes were also substantially smaller than those prepared by the used membranes. To the best of the knowledge of the author, there was no previous study focused on the performance of a new and used membrane. Apart from these experiments, to improve the porosity of the ME-MPs, these were treated with NaOH-ETOH solution for a brief time period. The experimental results demonstrated that the ethanolic NaOH (NaOH-EtOH) treatment had

substantially improved the porosity of the MPs. The method was the same as used to treat the conventional porous PLGA MPs. To assess the efficiency of the membrane emulsification method in producing monodisperse MPs, the MPs produced using this method was compared with those prepared using conventional emulsification (homogenization) in terms of their size, size uniformity and porosity. The study results clearly demonstrated that the MPs prepared using the ME method had narrower span factor, an indicator of the degree of monodispersity. Smaller the span factor, narrower the size distribution. In terms of porosity, the ME-MPs had larger pores with relatively wider pore size distribution.

The novel porous PLGA MPs, the preparation method of which was discussed in Chapter 4, were further assessed for their bone tissue engineering applications and the experimental outcomes are discussed in Chapter 5. The novel MPs supports ihMSCs attachment, viability and proliferation over a 5 days culture period. The degree of cell viability was influenced by the cell seeding densities; however, that was unaffected by changing the amount of MPs. The efficiency of the novel MPs in terms of cell viability and proliferation were comparable to commercially available MPs, Cytx-CM MPs. A further cellular morphology study using HCS Cell Mask^{TM} blue suggests that the cells spread more and remained more flattened on the surface of the novel porous MPs than on the surface of Cytx-CM MPs. Further cytotoxicity study results were in consistent with the results of the cell viability assay and confirm the cytocompatibility of the MPs. In this study, again, the performance of the novel MPs is comparable to the commercial MPs, Cytx-CM MPs. In order to assess whether or not ihMSCs retained their osteogenic

lineage potential in contact with the MPs, the cells were allowed to differentiate on the surface of the MPs, using a standard osteogenic medium and the level of osteogenesis was assessed via several quantitative and qualitative analysis. The presence of the early osteogenic marker, ALP was confirmed by an enzymatic colorimetric assay. The existence of calcium mineral in the osteogenic culture was confirmed via the following assays: 1) alizarin red s and von Kossa biochemical staining, and 2) fluorescent calcification assay using OsteoImage® bone mineral assay kit. The ESEM images of ihMSCs on the MPs in osteogenic culture further revealed that the cells on the novel MPs were relatively more flattened and spread. Moreover, the immunocytochemical staining for the osteogenic marker, osteocalcin confirmed the presence of the marker in the OS positive cultures. However, the immunocytochemical staining for the cells on OS positive Cytx-CM MPs groups was not very promising, as the OS negative cultures exhibited auto fluorescent property. In future, a more reliable assays need to perform to confirm the presence of osteocalcin or other osteogenic markers in the OS positive cultures with the novel porous MPs as well as Cytx-CM MPs.

6.2 Future Work

The work presented in this thesis demonstrates a platform for fabrication of a novel porous MPs or porous scaffold particles for cell delivery applications. The scaffold particles exhibit promise for their applications in bone tissue regeneration. However, in order to establish the scaffold system as a reliable and clinically relevant injectable cell delivery vehicle, yet many other in vitro experiments could be performed in near future. Firstly, the injectability of the

scaffold system has not been studied, which need to perform in order to investigate the optimal formulation and process parameters for delivery of stem cell via narrow bore needles. Secondly, large cell-MP aggregate formation was a problem identified in this study, which could negatively affect the injectability performance of the scaffold system. Some preliminary experiments were done for the minimisation of the aggregation; however, the outcome of the experiments was unsuccessful. In future, this could be another area of research as a part of improving the efficiency of the scaffold. Thirdly, although cell viability study was done and the results exhibited good cell viability, the method indirectly measured the number of cells in the respective culture, i.e., the number of viable cells were analysed on the basis of the amount of the metabolically active cells. A conclusive remark about the cell health cannot be done on the basis of a single experimental outcome [227]. One or two other studies, such as NucleoCounter, which are designed to directly count number of viable cells in a culture, could be performed and these results could be compared with those of the metabolic activity assay. Moreover, apoptosis levels of the cells were studied neither in the proliferative nor in the differentiation cultures; which need to study in future. Furthermore, there are scopes of further work to the confirmation of the reliability of the osteogenesis. A series of experiments-biochemical staining, fluorescence calcification assay and immunocytochemical staining confirm either the presence of bone mineral or an osteogenic marker gene, osteocalcin in the respective cultures of ihMSCs with the novel MPs. However, confirmation of the markers at genetic levels could give more confident on the results already obtained. In order to do that quantification of the osteogenic marker using the real-time quantitative polymerase chain reaction (RT-qPCR) analytical tool could be an option [228].

Other than osteocalcin, there are other osteogenic markers, which are expressed at different time points toward osteogenesis. For example, at the early level of osteogenesis, Runx2 is expressed, the expression of which could be studied using RT-qPCR. Another early marker is ALP; the level of expression of which already is studied at protein level and investigation of this protein at genetic level could be performed in future. Among other frequently detecting osteogenic markers, the osteopontin (OPN) is one example, which is expressed by both osteoblast and osteoclast cells [229]. In future, in addition OCN, OPN could be investigated at their gene expression level. Furthermore, for the osteogenic differentiation study, the presence of proliferative (at the state of stemness) or mature (differentiated) cells in the respective cultures were studied qualitatively using Hoechst 33258 kit. A quantitative study to measure the number of cells in the respective culture could strengthen the quality of the present data. Apart from these, it is important to note that only ihMSCs were used as a cell source throughout the study and it is obvious that these cells are not reliable for clinical translation. The experiments that already have been performed should be repeated with primary MSCs. Inclusion of some other cell sources, such as primary osteoblasts or co-culture of primary cells with MSCs, in future experimental design could be valuable.

Performing all the above mentioned experiments would be the continuation of the current study on the way to the development of a robust stem cell delivery model using a novel porous PLAG MPs. On the other hand, current study also opens some doors to some different research areas, where, this novel MPs could be used to understand cell fate using different experimental tools that are not explored in this study. A substantial number of researches have been performed in order to

investigate the influence of scaffold surface properties to cell fate [127]. The study focus of one such area could be related to understanding the influence of different surface chemical properties on cell fate. To be more specific, using the new platform of MP fabrication, monodisperse solid polymeric MPs could be prepared and then the chemical properties of their surfaces could be modified in terms of functional groups, surface charge and its density, and free surface energy. Characterisation of the surface properties these surface modified MPs could be an individual project. Moreover, understanding the effect of difference in surface chemistry of the scaffolds on cell fate could be another mini project. On the other hand, as another project, scaffolds with different surface topographies in terms of roughness, pore size, shape and interconnectivity could be developed. Detailed characterisation of the surface properties should be the first step towards defining the scaffolds appropriately. Subsequently, understanding the cell fate on the scaffolds could be performed.

A novel porous MP system for stem cell delivery is developed during the course of this study, which exhibits its potential for bone tissue engineering. To fulfil the requirement of an efficient scaffold system, the current study demand further experiments which have been discussed. It could be exciting to continue with the current work for defining the functions of the newly developed scaffold in tissue regeneration.

References

1. Nerem, R.M. and S.C. Schutte, *The Challenge of Immitating Nature*, in *Principles of Tissue Engineering*. 2014, Academic Press. p. 9-24.
2. *Tissue Engineering (UCLA Symposia on Molecular and Cellular Biology, New Series)*, ed. R. Skalak and C.F. Fox. 1989, N. Y.: Alan R Liss.
3. Langer, R. and J. Vacanti, *Tissue engineering.* Science, 1993. **260**(5110): p. 920-926.
4. Vacanti, J.P., et al., *Selective cell transplantation using bioabsorbable artificial polymers as matrices.* J Pediatr Surg, 1988. **23**(1 Pt 2): p. 3-9.
5. *Principles of Tissue Engineering*. Fourth ed, ed. R.L. Robert Lanza, Joseph Vacanti. 2014, Academic Press, London, UK Elsevier and Book Aid International.
6. Berthiaume, F., T.J. Maguire, and M.L. Yarmush, *Tissue engineering and regenerative medicine: history, progress, and challenges.* Annu Rev Chem Biomol Eng, 2011. **2**: p. 403-30.
7. Walter, J.B., et al., *Walter and Israel general Pathology*. 7th ed. Vol. . 1996, New York, USA: Churchill Livingstone. 154-196 ChurchillLivingstone, Newyork.
8. Greenwood, H.L., et al., *Regenerative medicine: new opportunities for developing countries.* International Journal of Biotechnology, 2006. **8**(1-2): p. 60-77.
9. Mason, C. and P. Dunnill, *A brief definition of regenerative medicine.* Regen Med, 2008. **3**(1): p. 1-5.
10. Nyberg, E., et al., *Growth factor-eluting technologies for bone tissue engineering.* Drug Delivery and Translational Research, 2016. **6**(2): p. 184-194.
11. Lee, K., E.A. Silva, and D.J. Mooney, *Growth factor delivery-based tissue engineering: general approaches and a review of recent developments.* Journal of the Royal Society Interface, 2011. **8**(55): p. 153-170.
12. Melton DA and C. C., *Stemness: definitions, criteria, and standards*, in *Essentials of stem cell biology*. 2009, Academic Press: San Diego, CA.
13. Samadikuchaksaraei, A., et al., *Stem Cells as Building Blocks*, in *Principles of Tissue Engineering*, R. Lanza, R. Langer, and J.P. Vacanti, Editors. 2014, Academic Press: London, UK. p. 41-55.
14. Inaba, M. and Yukiko M. Yamashita, *Asymmetric Stem Cell Division: Precision for Robustness.* Cell Stem Cell, 2012. **11**(4): p. 461-469.
15. Evans, M.J. and M.H. Kaufman, *Establishment in culture of pluripotential cells from mouse embryos.* Nature, 1981. **292**(5819): p. 154-156.
16. Martin, G.R., *Isolation of a pluripotent cell line from early mouse embryos cultured in medium conditioned by teratocarcinoma stem cells.* Proc Natl Acad Sci U S A, 1981. **78**(12): p. 7634-8.

17. Richards, M., et al., *Human feeders support prolonged undifferentiated growth of human inner cell masses and embryonic stem cells.* Nat Biotechnol, 2002. **20**(9): p. 933-6.

18. Amit, M., et al., *Human feeder layers for human embryonic stem cells.* Biol Reprod, 2003. **68**(6): p. 2150-6.

19. Richards, M., et al., *Comparative evaluation of various human feeders for prolonged undifferentiated growth of human embryonic stem cells.* Stem Cells, 2003. **21**(5): p. 546-56.

20. Hovatta, O., et al., *A culture system using human foreskin fibroblasts as feeder cells allows production of human embryonic stem cells.* Hum Reprod, 2003. **18**(7): p. 1404-9.

21. Marolt, D., et al., *Engineering bone tissue from human embryonic stem cells.* Proceedings of the National Academy of Sciences, 2012. **109**(22): p. 8705-8709.

22. Descamps, B. and C. Emanueli, *Vascular differentiation from embryonic stem cells: Novel technologies and therapeutic promises.* Vascular Pharmacology, 2012. **56**(5–6): p. 267-279.

23. Gálvez-Montón, C., et al., *Cardiac Tissue Engineering and the Bioartificial Heart.* Revista Española de Cardiología (English Edition), 2013. **66**(05): p. 391-399.

24. Chen, C.S., et al., *Human stem cell neuronal differentiation on silk-carbon nanotube composite.* Nanoscale Res Lett, 2012. **7**(1): p. 126.

25. Friedenstein, A.J., R.K. Chailakhjan, and K.S. Lalykina, *The Development of Fibroblast Colonies in Monolayer Cultures of Guinea-Pig Bone Marrow And Spleen Cells.* Cell Proliferation, 1970. **3**(4): p. 393-403.

26. Dennis, J.E. and A.I. Caplan, *Differentiation potential of conditionally immortalized mesenchymal progenitor cells from adult marrow of a H-2Kb-tsA58 transgenic mouse.* J Cell Physiol, 1996. **167**(3): p. 523-38.

27. Pittenger, M.F., et al., *Multilineage potential of adult human mesenchymal stem cells.* Science, 1999. **284**(5411): p. 143-7.

28. Chunmeng, S. and C. Tianmin, *Effects of plastic-adherent dermal multipotent cells on peripheral blood leukocytes and CFU-GM in rats.* Transplant Proc, 2004. **36**(5): p. 1578-81.

29. Zvaifler, N., et al., *Mesenchymal precursor cells in the blood of normal individuals.* Arthritis Res, 2000. **2**(6): p. 1-12.

30. Campagnoli, C., et al., *Identification of mesenchymal stem/progenitor cells in human first-trimester fetal blood, liver, and bone marrow.* Blood, 2001. **98**(8): p. 2396-402.

31. Zuk, P.A., et al., *Multilineage cells from human adipose tissue: implications for cell-based therapies.* Tissue Eng, 2001. **7**(2): p. 211-28.

32. in 't Anker, P.S., et al., *Mesenchymal stem cells in human second-trimester bone marrow, liver, lung, and spleen exhibit a similar immunophenotype*

but a heterogeneous multilineage differentiation potential. Haematologica, 2003. **88**(8): p. 845-52.

33. Sottile, V., et al., *Stem cell characteristics of human trabecular bone-derived cells.* Bone, 2002. **30**(5): p. 699-704.

34. Alhadlaq, A. and J.J. Mao, *Mesenchymal stem cells: isolation and therapeutics.* Stem Cells Dev, 2004. **13**(4): p. 436-48.

35. Pittenger, M.F.M., Alastair M.Beck, Stephen C. 1, Jaiswal, Rama K. Douglas, Robin, Mosca, Joseph D. Moorman, Mark A. Simonetti, Donald W. Craig Stewart, Marshak, Daniel R. , *Mulltilineage potential of adult human mesenchymal stem cells.* Science, 1999. **284**(5411): p. 143-147.

36. Yousefi, A.-M., et al., *Prospect of Stem Cells in Bone Tissue Engineering: A Review.* Stem Cells International, 2016. **2016**: p. 13.

37. Dezawa, M., et al., *Specific induction of neuronal cells from bone marrow stromal cells and application for autologous transplantation.* The Journal of Clinical Investigation, 2004. **113**(12): p. 1701-1710.

38. Luk, J.M., et al., *Hepatic potential of bone marrow stromal cells: development of in vitro co-culture and intra-portal transplantation models.* J Immunol Methods, 2005. **305**(1): p. 39-47.

39. Okamoto, T., et al., *Clonal heterogeneity in differentiation potential of immortalized human mesenchymal stem cells.* Biochemical and Biophysical Research Communications, 2002. **295**(2): p. 354-361.

40. Gong, M., et al., *Immortalized mesenchymal stem cells: an alternative to primary mesenchymal stem cells in neuronal differentiation and neuroregeneration associated studies.* J Biomed Sci, 2011. **18**: p. 87.

41. Stolzel, K., et al., *Immortalised human mesenchymal stem cells undergo chondrogenic differentiation in alginate and PGA/PLLA scaffolds.* Cell Tissue Bank, 2015. **16**(1): p. 159-70.

42. Osyczka, A.M., et al., *Multilineage differentiation of adult human bone marrow progenitor cells transduced with human papilloma virus type 16 E6/E7 genes.* Calcif Tissue Int, 2002. **71**(5): p. 447-58.

43. Alhadlaq, A. and J.J. Mao, *Tissue-engineered neogenesis of human-shaped mandibular condyle from rat mesenchymal stem cells.* J Dent Res, 2003. **82**(12): p. 951-6.

44. Alhadlaq, A. and J.J. Mao, *Tissue-engineered osteochondral constructs in the shape of an articular condyle.* J Bone Joint Surg Am, 2005. **87**(5): p. 936-44.

45. Marion, N.W., et al., *Borate glass supports the in vitro osteogenic differentiation of human mesenchymal stem cells.* Mechanics of Advanced Materials and Structures, 2005. **12**(3): p. 239-246.

46. Hamidouche, Z., et al., *FHL2 mediates dexamethasone-induced mesenchymal cell differentiation into osteoblasts by activating Wnt/beta-catenin signaling-dependent Runx2 expression.* Faseb j, 2008. **22**(11): p. 3813-22.

47. Jaiswal, N., et al., *Osteogenic differentiation of purified, culture-expanded human mesenchymal stem cells in vitro.* J Cell Biochem, 1997. **64**(2): p. 295-312.

48. Deng, Z.L., et al., *Regulation of osteogenic differentiation during skeletal development.* Front Biosci, 2008. **13**: p. 2001-21.

49. Ducy, P., T. Schinke, and G. Karsenty, *The osteoblast: a sophisticated fibroblast under central surveillance.* Science, 2000. **289**(5484): p. 1501-4.

50. Marom, R., et al., *Characterization of adhesion and differentiation markers of osteogenic marrow stromal cells.* J Cell Physiol, 2005. **202**(1): p. 41-8.

51. Aubin, J.E., *Regulation of Osteoblast Formation and Function.* Reviews in Endocrine and Metabolic Disorders, 2001. **2**(1): p. 81-94.

52. Griffith, L.G., *Emerging design principles in biomaterials and scaffolds for tissue engineering.* Ann N Y Acad Sci, 2002. **961**: p. 83-95.

53. Luo, Y., et al., *3D Scaffolds*, in *Principles of Tissue Engieering*, R. Lanza, R. Langer, and J. Vacanti, Editors. 2014, Academic Press: San Diego. p. 475-494.

54. Colton, C.K., *Implantable biohybrid artificial organs.* Cell Transplant, 1995. **4**(4): p. 415-36.

55. Freed, L.E., et al., *Chondrogenesis in a cell-polymer-bioreactor system.* Exp Cell Res, 1998. **240**(1): p. 58-65.

56. Ishaug, S.L., et al., *Bone formation by three-dimensional stromal osteoblast culture in biodegradable polymer scaffolds.* J Biomed Mater Res, 1997. **36**(1): p. 17-28.

57. Colton, C.K., *Oxygen supply to encapsulated therapeutic cells.* Adv Drug Deliv Rev, 2014. **67-68**: p. 93-110.

58. Leong, W. and D.-A. Wang, *Cell-laden Polymeric Microspheres for Biomedical Applications.* Trends in Biotechnology, 2015. **33**(11): p. 653-666.

59. Ma, T., et al., *Tissue engineering human placenta trophoblast cells in 3-D fibrous matrix: spatial effects on cell proliferation and function.* Biotechnol Prog, 1999. **15**(4): p. 715-24.

60. Ma, T., et al., *Effects of pore size in 3-D fibrous matrix on human trophoblast tissue development.* Biotechnol Bioeng, 2000. **70**(6): p. 606-18.

61. Mazón, P., et al., *Human mesenchymal stem cell viability, proliferation and differentiation potential in response to ceramic chemistry and surface roughness.* Ceramics International, 2015. **41**(5, Part A): p. 6631-6644.

62. Lee, Y.S., et al., *Development of porous PLGA/PEI1.8k biodegradable microspheres for the delivery of mesenchymal stem cells (MSCs).* Journal of Controlled Release, 2015. **205**: p. 128-133.

63. Cai, Y., et al., *Porous microsphere and its applications.* International Journal of Nanomedicine, 2013. **8**: p. 1111-1120.

64. Zhang, Q., et al., *Preparation of open porous polycaprolactone microspheres and their applications as effective cell carriers in hydrogel system.* Materials Science and Engineering: C, 2012. **32**(8): p. 2589-2595.

65. Hong, S.J., H.S. Yu, and H.W. Kim, *Tissue engineering polymeric microcarriers with macroporous morphology and bone-bioactive surface.* Macromol Biosci, 2009. **9**(7): p. 639-45.

66. Steve Oh, S.R., Allen Chen, *Microcarriers for Stem Cell Culture*, U.S. Patent, Editor. 2014, Agency for Science, Technology and Research, Connexis (SG). p. 1-134.

67. Frauenschuh, S., et al., *A microcarrier-based cultivation system for expansion of primary mesenchymal stem cells.* Biotechnol Prog, 2007. **23**(1): p. 187-93.

68. White, L.J., et al., *Accelerating protein release from microparticles for regenerative medicine applications.* Mater Sci Eng C Mater Biol Appl, 2013. **33**(5): p. 2578-83.

69. E. Bible, et al., *The support of neural stem cells transplanted into stroke-induced brain cavities by PLGA particles.* Biomaterials, 2009. **30**(16): p. 2985-94.

70. Qutachi, O., et al., *Injectable and porous PLGA microspheres that form highly porous scaffolds at body temperature.* Acta Biomater, 2014. **10**(12): p. 5090-8.

71. D. Y. S. Chau, K. Agashi, and K.M. Shakesheff, *Microparticles as tissue engineering scaffolds: manufacture, modification and manipulation.* Materials Science and Technology, 2008. **24**(9): p. 1031-1044.

72. Viswanathan, P., et al., *3D surface topology guides stem cell adhesion and differentiation.* Biomaterials, 2015. **52**: p. 140-147.

73. Ibim, S.M., et al., *Poly(anhydride-co-imides): in vivo biocompatibility in a rat model.* Biomaterials, 1998. **19**(10): p. 941-51.

74. Chau, D.Y.S., K. Agashi, and K.M. Shakesheff, *Microparticles as tissue engineering scaffolds: manufacture, modification and manipulation.* Materials Science and Technology, 2008. **24**(9): p. 1031-1044.

75. Sokolsky-Papkov, M., et al., *Polymer carriers for drug delivery in tissue engineering.* Advanced Drug Delivery Reviews, 2007. **59**(4-5): p. 187-206.

76. Yang, X.B., et al., *Human osteoprogenitor growth and differentiation on synthetic biodegradable structures after surface modification.* Bone, 2001. **29**(6): p. 523-531.

77. El-Amin, S.F., et al., *Human osteoblast cells: isolation, characterization, and growth on polymers for musculoskeletal tissue engineering.* J Biomed Mater Res A, 2006. **76**(3): p. 439-49.

78. Kim, S.S., et al., *Poly(lactide-co-glycolide)/hydroxyapatite composite scaffolds for bone tissue engineering.* Biomaterials, 2006. **27**(8): p. 1399-409.

79. Koegler, W.S. and L.G. Griffith, *Osteoblast response to PLGA tissue engineering scaffolds with PEO modified surface chemistries and demonstration of patterned cell response.* Biomaterials, 2004. **25**(14): p. 2819-30.

80. E. Bible, et al., *Neo-vascularization of the stroke cavity by implantation of human neural stem cells on VEGF-releasing PLGA microparticles.* Biomaterials, 2012. **33**(30): p. 7435-46.

81. Rahman, C.V., et al., *Controlled release of BMP-2 from a sintered polymer scaffold enhances bone repair in a mouse calvarial defect model.* Journal of Tissue Engineering and Regenerative Medicine, 2014. **8**(1): p. 59-66.

82. Hamilton, L., R. France, and K. Shakesheff, *Development of an injectable scaffold for application in regenerative medicine to deliver stem cells and growth factors.* Journal of Pharmacy and Pharmacology, 2006. **58**: p. A52-A53.

83. Kirby, G.T.S., et al., *PLGA-Based Microparticles for the Sustained Release of BMP-2.* Polymers, 2011. **3**(1): p. 571.

84. Ji, Y., et al., *BMP-2/PLGA delayed-release microspheres composite graft, selection of bone particulate diameters, and prevention of aseptic inflammation for bone tissue engineering.* Ann Biomed Eng, 2010. **38**(3): p. 632-9.

85. Fu, K., et al., *Prolonged osteogenesis from human mesenchymal stem cells implanted in immunodeficient mice by using coralline hydroxyapatite incorporating rhBMP2 microspheres.* Journal of Biomedical Materials Research Part A, 2010. **92A**(4): p. 1256-1264.

86. YN, C., et al., *Advances in porous polymer particles.* Polymer Materials Science and Engineering, 2008. **24**(8): p. 1-8.

87. Shi, X., et al., *Biodegradable polymeric microcarriers with controllable porous structure for tissue engineering.* Macromol Biosci, 2009. **9**(12): p. 1211-8.

88. Zeltinger, J., et al., *Effect of pore size and void fraction on cellular adhesion, proliferation, and matrix deposition.* Tissue Eng, 2001. **7**(5): p. 557-72.

89. Fang, J., et al., *Novel injectable porous poly([gamma]-benzyl-l-glutamate) microspheres for cartilage tissue engineering: preparation and evaluation.* Journal of Materials Chemistry B, 2015. **3**(6): p. 1020-1031.

90. Ogawa, Y., et al., *Controlled-release of leuprolide acetate from polylactic acid or copoly(lactic/glycolic) acid microcapsules: influence of molecular weight and copolymer ratio of polymer.* Chem Pharm Bull (Tokyo), 1988. **36**(4): p. 1502-7.

91. Rosca, I.D., F. Watari, and M. Uo, *Microparticle formation and its mechanism in single and double emulsion solvent evaporation.* Journal of Controlled Release, 2004. **99**(2): p. 271-280.

92. Bible, E., et al., *Attachment of stem cells to scaffold particles for intra-cerebral transplantation.* Nat Protoc, 2009. **4**(10): p. 1440-53.

93. Morita, T., et al., *Preparation of gelatin microparticles by co-lyophilization with poly(ethylene glycol): characterization and application to entrapment into biodegradable microspheres.* Int J Pharm, 2001. **219**(1-2): p. 127-37.

94. Jain, R.A., *The manufacturing techniques of various drug loaded biodegradable poly(lactide-co-glycolide) (PLGA) devices.* Biomaterials, 2000. **21**(23): p. 2475-90.

95. O. Qutachi, K. M. Shakesheff, and L.D. Buttery, *Delivery of definable number of drug or growth factor loaded poly(DL-lactic acid-co-glycolic acid) microparticles within human embryonic stem cell derived aggregates.* J Control Release, 2013. **168**(1): p. 18-27.

96. Garti, N., *Double emulsions — scope, limitations and new achievements.* Colloids and Surfaces A: Physicochemical and Engineering Aspects, 1997. **123–124**(0): p. 233-246.

97. Arnold, M.M., et al., *NanoCipro encapsulation in monodisperse large porous PLGA microparticles.* J Control Release, 2007. **121**(1-2): p. 100-9.

98. Li, J., et al., *A one-step method to fabricate PLLA scaffolds with deposition of bioactive hydroxyapatite and collagen using ice-based microporogens.* Acta Biomater, 2010. **6**(6): p. 2013-9.

99. Ma, Z., et al., *Paraffin spheres as porogen to fabricate poly(L-lactic acid) scaffolds with improved cytocompatibility for cartilage tissue engineering.* J Biomed Mater Res B Appl Biomater, 2003. **67**(1): p. 610-7.

100. J. C. De La Vega, et al., *Uniform polymer microspheres: monodispersity criteria, methods of formation and applications.* Nanomedicine (Lond), 2013. **8**(2): p. 265-85.

101. G. T. Vladisavljević, I. Kobayashi, and M. Nakajima, *Production of uniform droplets using membrane, microchannel and microfluidic emulsification devices.* Microfluidics and Nanofluidics, 2012. **13**(1): p. 151-178.

102. T. Nakashima, M. Shimizu, and M. Kukizaki. *Membrane emulsification by microporous glass*. in *2nd International Conference on Inorganic Membranes*. 1991. Montpellier, France.

103. C. Charcosset, I. Limayem, and H. Fessi, *The membrane emulsification process—a review.* Journal of Chemical Technology & Biotechnology, 2004. **79**(3): p. 209-218.

104. C. J. Cheng, et al., *Hydrophobic Modification and Regeneration of Shirasu Porous Glass Membranes on Membrane Emulsification Performance.* Chemical Engineering & Technology, 2008. **31**(3): p. 377-383.

105. W. Liu, X. L. Yang, and W. S. Ho, *Preparation of uniform-sized multiple emulsions and micro/nano particulates for drug delivery by membrane emulsification.* J Pharm Sci, 2011. **100**(1): p. 75-93.

106. V. T. Tran, J. P. Benoit, and M. C. Venier-Julienne, *Why and how to prepare biodegradable, monodispersed, polymeric microparticles in the field of pharmacy?* Int J Pharm, 2011. **407**(1-2): p. 1-11.

107. Qi, F., et al., *Preparation of uniform-sized exenatide-loaded PLGA microspheres as long-effective release system with high encapsulation efficiency and bio-stability.* Colloids Surf B Biointerfaces, 2013. **112**: p. 492-8.

108. G. T. Vladisavljevića, M. Shimizub, and T. Nakashima, *Production of multiple emulsions for drug delivery systems by repeated SPG membrane homogenization: Influence of mean pore size, interfacial tension and continuous phase viscosity.* Journal of Membrane Science, 2006. **284**(1-2): p. 373-383.

109. Fan, Q., et al., *Direct and controllable preparation of uniform PLGA particles with various shapes and surface morphologies.* Colloids and Surfaces A: Physicochemical and Engineering Aspects, 2016. **500**: p. 177-185.

110. Berendsen, R., et al., *Premix membrane emulsification to produce oil-in-water emulsions stabilized with various interfacial structures of whey protein and carboxymethyl cellulose.* Food Hydrocolloids, 2014. **38**: p. 1-10.

111. Nazir, A., K. Schroën, and R. Boom, *Premix emulsification: A review.* Journal of Membrane Science, 2010. **362**(1–2): p. 1-11.

112. Eisinaite, V., et al., *Preparation of stable food-grade double emulsions with a hybrid premix membrane emulsification system.* Food Chemistry, 2016. **206**: p. 59-66.

113. Sawalha, H., S. Sahin, and K. Schroën, *Preparation of polylactide microcapsules at a high throughput with a packed-bed premix emulsification system.* Journal of Applied Polymer Science, 2016. **133**(24): p. n/a-n/a.

114. Joscelyne, S.M. and G. Trägårdh, *Membrane emulsification — a literature review.* Journal of Membrane Science, 2000. **169**(1): p. 107-117.

115. Peng, S. and R.A. Williams, *Controlled Production of Emulsions Using a Crossflow Membrane.* Particle & Particle Systems Characterization, 1998. **15**(1): p. 21-25.

116. Kukizaki, M., *Shirasu porous glass (SPG) membrane emulsification in the absence of shear flow at the membrane surface: Influence of surfactant type and concentration, viscosities of dispersed and continuous phases, and transmembrane pressure.* Journal of Membrane Science, 2009. **327**: p. 234-243.

117. Hancocks, R.D., F. Spyropoulos, and I.T. Norton, *The effects of membrane composition and morphology on the rotating membrane emulsification*

technique for food grade emulsions. Journal of Membrane Science, 2016. **497**: p. 29-35.

118. Zhao, X., et al., *Preparation of uniform and large sized agarose microspheres by an improved membrane emulsification technique.* Powder Technology, 2014. **253**: p. 444-452.

119. Wang, L.-Y., G.-H. Ma, and Z.-G. Su, *Preparation of uniform sized chitosan microspheres by membrane emulsification technique and application as a carrier of protein drug.* Journal of Controlled Release, 2005. **106**(1–2): p. 62-75.

120. Christov, N.C., et al., *The Drop Size in Membrane Emulsification Determined from the Balance of Capillary and Hydrodynamic Forces†.* Langmuir, 2008. **24**(4): p. 1397-1410.

121. Tadao Nakashima, M.S., Masato Kukizaki, *Membrane emulsification operation manual*. 1991, Department of Chemistry Industrial Research Institute of Miyazaki Prefecture.

122. Williams, R.A., et al., *Controlled Production of Emulsions Using a Crossflow Membrane: Part II: Industrial Scale Manufacture.* Chemical Engineering Research and Design, 1998. **76**(8): p. 902-910.

123. Langer, R. and J.P. Vacanti, *Tissue engineering.* Science, 1993. **260**(5110): p. 920-6.

124. Bhat, A., et al., *Evaluation of cross-linked chitosan microparticles for bone regeneration.* J Tissue Eng Regen Med, 2010. **4**(7): p. 532-42.

125. Narayanan, G., et al., *Poly (lactic acid)-based biomaterials for orthopedic regenerative engineering.* Advanced Drug Delivery Reviews, 2016.

126. O'Brien, F.J., *Biomaterials & scaffolds for tissue engineering.* Materials Today, 2011. **14**(3): p. 88-95.

127. Idaszek, J., et al., *How important are scaffolds and their surface properties in regenerative medicine.* Applied Surface Science.

128. *Principles of Tissue Engineering*. Third ed, ed. R. Lanza, R. Langer, and J.P. Vacanti. 2011, Burlington, USA: Academic Press. 1344.

129. Lin, H., et al., *Cartilage tissue engineering application of injectable gelatin hydrogel with in situ visible-light-activated gelation capability in both air and aqueous solution.* Tissue Eng Part A, 2014. **20**(17-18): p. 2402-11.

130. Custodio, C.A., et al., *Cell selective chitosan microparticles as injectable cell carriers for tissue regeneration.* Biomaterials, 2015. **43**: p. 23-31.

131. Woo, E., H. Park, and K.Y. Lee, *Shear reversible cell/microsphere aggregate as an injectable for tissue regeneration.* Macromol Biosci, 2014. **14**(5): p. 740-8.

132. Asghari, F., et al., *Biodegradable and biocompatible polymers for tissue engineering application: a review.* Artif Cells Nanomed Biotechnol, 2016: p. 1-8.

133. Spector, M. and T.C. Lim, *Injectable biomaterials: a perspective on the next wave of injectable therapeutics.* Biomed Mater, 2016. **11**(1): p. 014110.

134. Anthony Atala, et al., *Principles of regenerative medicine*, ed. N.F. Keith H S Campbell, John D Gearhart, William A Haseltine, Peter Johnson, Robert Langer, Mychael Lysaght, Antonios G Mikos, David J Mooney, . 2008: Elsevier.

135. Wang, Y., et al., *Poly(lactide-co-glycolide)/titania composite microsphere-sintered scaffolds for bone tissue engineering applications.* J Biomed Mater Res B Appl Biomater, 2010. **93**(1): p. 84-92.

136. Salem, A.K., *An injectable degradable porous polymer scaffold for tissue engineering and drug delivery*, in *Pharmacy*. 2001, University of Nottingham. p. 246.

137. Unsworth, J.M., et al., *Seeding cells into needled felt scaffolds for tissue engineering applications.* J Biomed Mater Res A, 2003. **66**(2): p. 425-31.

138. Cox, H.C., *A biodegradable system for the tailored delivery of growth factors and its application to bone morphogenic protein-2 for bone repair*, in *Drug Delivery and Tissue Engineering*. 2013, University of Nottingham.

139. Webb, P.A. *A Primer on Particle Sizing by Static Laser Light Scattering* 2000.

140. Wheeler, D.J., *Advanced Topics in Statistical Process Control: The Power of Shewhart's Charts*. 2nd ed. 2004: SPC PRESS (Statistical Process Control).

141. Labuschagne, P.W., et al., *Preparation of rifampicin/poly(d,l-lactice) nanoparticles for sustained release by supercritical assisted atomization technique.* The Journal of Supercritical Fluids, 2014. **95**: p. 106-117.

142. Croll, T.I., et al., *Controllable Surface Modification of Poly(lactic-co-glycolic acid) (PLGA) by Hydrolysis or Aminolysis I: Physical, Chemical, and Theoretical Aspects.* Biomacromolecules, 2004. **5**(2): p. 463-473.

143. Yang, J., et al., *Enhancing the cell affinity of macroporous poly(L-lactide) cell scaffold by a convenient surface modification method.* Polymer International, 2003. **52**(12): p. 1892-1899.

144. Lee, J.Y., et al., *Enhanced bone formation by controlled growth factor delivery from chitosan-based biomaterials.* J Control Release, 2002. **78**(1-3): p. 187-97.

145. Nam, Y.S., et al., *Adhesion behaviours of hepatocytes cultured onto biodegradable polymer surface modified by alkali hydrolysis process.* J Biomater Sci Polym Ed, 1999. **10**(11): p. 1145-58.

146. Croll, T.I., et al., *Controllable surface modification of poly(lactic-co-glycolic acid) (PLGA) by hydrolysis or aminolysis I: physical, chemical, and theoretical aspects.* Biomacromolecules, 2004. **5**(2): p. 463-73.

147. Paik, I., et al., *Rapid micropatterning of cell lines and human pluripotent stem cells on elastomeric membranes.* Biotechnol Bioeng, 2012. **109**(10): p. 2630-41.

148. *PrestoBlue™ Cell Viability Reagent Documentation* [cited 2013 10th January]; Available from: https://tools.thermofisher.com/content/sfs/manuals/PrestoBlueFAQ.pdf.

149. *Live/Dead Viability/Cytotoxicity Kit *for mamalian cells** [cited 2012 20th May]; Available from: https://tools.thermofisher.com/content/sfs/manuals/mp03224.pdf.

150. Imbrogno, A., et al., *Preparation of uniform poly-caprolactone Microparticles by membrane emulsification/solvent diffusion process.* Journal of Membrane Science, 2014. **467**: p. 262-268.

151. Imbrogno, A., et al., *Polycaprolactone multicore-matrix particle for the simultaneous encapsulation of hydrophilic and hydrophobic compounds produced by membrane emulsification and solvent diffusion processes.* Colloids Surf B Biointerfaces, 2015. **135**: p. 116-25.

152. Sun, L., et al., *Preparation and characterization of porous biodegradable microspheres used for controlled protein delivery.* Colloids and Surfaces A: Physicochemical and Engineering Aspects, 2009. **345**(1–3): p. 173-181.

153. Kim, H.Y., *Statistical notes for clinical researchers: assessing normal distribution (2) using skewness and kurtosis.* Restor Dent Endod, 2013. **38**(1): p. 52-4.

154. Maia, J.L., M.H.A. Santana, and M.I. Ré, *The effect of some processing conditions on the characteristics of biodegradable microspheres obtained by an emulsion solvent evaporation process.* Brazilian Journal of Chemical Engineering, 2004. **21**: p. 01-12.

155. Wang, S.-y., et al., *Preparation of PLGA microspheres with different porous morphologies.* Chinese Journal of Polymer Science, 2015. **33**(1): p. 128-136.

156. Tadros, T.F., *Emulsion Formation, Stability, and Rheology,* in *Emulsion Formation and Stability*. 2013, Wiley-VCH Verlag GmbH & Co. KGaA. p. 1-75.

157. An, T., et al., *Sustained release of risperidone from biodegradable microspheres prepared by in-situ suspension-evaporation process.* International Journal of Pharmaceutics, 2016. **503**(1–2): p. 8-15.

158. Asti, A., et al., *Stem Cells Grown in Osteogenic Medium on PLGA, PLGA/HA, and Titanium Scaffolds for Surgical Applications.* Bioinorganic Chemistry and Applications, 2010. **2010**: p. 12.

159. Liu, X., X. Jin, and P.X. Ma, *Nanofibrous hollow microspheres self-assembled from star-shaped polymers as injectable cell carriers for knee repair.* Nat Mater, 2011. **10**(5): p. 398-406.

160. Park, J.H., et al., *Microcarriers designed for cell culture and tissue engineering of bone.* Tissue Eng Part B Rev, 2013. **19**(2): p. 172-90.

161. Yeatts, A.B. and J.P. Fisher, *Tubular perfusion system for the long-term dynamic culture of human mesenchymal stem cells.* Tissue Eng Part C Methods, 2011. **17**(3): p. 337-48.

162. Ma, J., et al., *Concise review: cell-based strategies in bone tissue engineering and regenerative medicine.* Stem Cells Transl Med, 2014. **3**(1): p. 98-107.

163. Hayashi, K. and Y. Tabata, *Preparation of stem cell aggregates with gelatin microspheres to enhance biological functions.* Acta Biomaterialia, 2011. **7**(7): p. 2797-2803.

164. Ferrari, C., et al., *Limiting cell aggregation during mesenchymal stem cell expansion on microcarriers.* Biotechnol Prog, 2012. **28**(3): p. 780-7.

165. Gottfried Lemperle, V.B.M., Vasumati Pestonjamasp, Richard L. Gallo, *Migration Studies and Histology of Injectable MIcrospheres of Different Sizes in MIce.* Plastic and Reconstructive Surgery, 2004. **113**(5): p. 1380-1390.

166. Tomazic-Jezic, V.J., K. Merritt, and T.H. Umbreit, *Significance of the type and the size of biomaterial particles on phagocytosis and tissue distribution.* J Biomed Mater Res, 2001. **55**(4): p. 523-9.

167. Morhenn, V.B., G. Lemperle, and R.L. Gallo, *Phagocytosis of Different Particulate Dermal Filler Substances by Human Macrophages and Skin Cells.* Dermatologic Surgery, 2002. **28**(6): p. 484-490.

168. D. Ibraheem, et al., *Effects of process parameters on the colloidal properties of polycaprolactone microparticles prepared by double emulsion like process.* Colloid and surfaces A: Physicochemical and Engineering Aspects, 2014. **445**: p. 79-91.

169. G. T. Vladisavljević, *Emulsification Using Microporous Membranes.* Mimitary Technical Courier, 2011. **LIX**(4): p. 62-78.

170. Dong-xia Haoa, et al., *Porogen effects in synthesis of uniform micrometer-sized poly(divinylbenzene) microspheres with high surface areas.* Journal of Colloid and Interface Science, 2008. **323**(1): p. 52-59.

171. G. Gasparini, et al., *Preparation and characterization of PLGA particles for subcutaneous controlled drug release by membrane emulsification.* Colloids Surf B Biointerfaces, 2008. **61**(2): p. 199-207.

172. M. Kukizakia and T. Wadab, *Effect of the membrane wettability on the size and size distribution of microbubbles formed from Shirasu-porous-glass (SPG) membranes.* Colloid and surfaces A: Physicochemical and Engineering Aspects, 2008. **317**(1-3): p. 146-154.

173. F. Ito, Y. Kanakubo, and Yoshihiko. Murakami, *Rapid preparation of monodisperse biodegradable polymer nanospheres using a membrane emulsification technique under low gas pressure.* Journal of Polymer Research, 2011. **18**(6): p. 2077-2085.

174. F. Spyropoulos, et al., *Advances in membrane emulsification. Part A: recent developments in processing aspects and microstructural design approaches.* J Sci Food Agric, 2014. **94**(4): p. 613-27.

175. Liu, R., et al., *Influence of process parameters on the size distribution of PLA microcapsules prepared by combining membrane emulsification technique and double emulsion-solvent evaporation method.* Colloids Surf B Biointerfaces, 2005. **45**(3-4): p. 144-53.

176. M. Yasunoa, et al., *Visualization and characterization of SPG membrane emulsification*

Journal of Membrane Science, 2002. **210**(1): p. 29-37.

177. Schröder, V., O. Behrend, and H. Schubert, *Effect of Dynamic Interfacial Tension on the Emulsification Process Using Microporous, Ceramic Membranes.* Journal of Colloid and Interface Science, 1998. **202**(2): p. 334-340.

178. Joseph, S. and H. Bunjes, *Evaluation of Shirasu Porous Glass (SPG) membrane emulsification for the preparation of colloidal lipid drug carrier dispersions.* European Journal of Pharmaceutics and Biopharmaceutics, 2014. **87**(1): p. 178-186.

179. Vladisavljevic, G.T. and R.A. Williams, *Recent developments in manufacturing emulsions and particulate products using membranes.* Adv Colloid Interface Sci, 2005. **113**(1): p. 1-20.

180. Aleksandra K. Pawlik and I.T. Norton, *Encapsulation stability of duplex emulsions prepared with SPG cross-flow membrane, SPG rotating membrane and rotor-stator techniques—A comparison.* Journal of Membrane Science, 2012. **415-416**: p. 459-468.

181. Lee, S.C., et al., *Quantitative analysis of polyvinyl alcohol on the surface of poly(d,l-lactide-co-glycolide) microparticles prepared by solvent evaporation method: effect of particle size and PVA concentration.* Journal of Controlled Release, 1999. **59**(2): p. 123-132.

182. Li, D., et al., *Preparation of uniform starch microcapsules by premix membraneemulsion for controlled release of avermectin.* Carbohydrate polymers, 2016. **136**: p. 341-349.

183. Liu, B.X., et al., *Fabrication of uniform sized polylactone microcapsules by premix membrane emulsification for ultrasound imaging.* Polymer Chemistry, 2014. **5**(5): p. 1693-1701.

184. Vladisavljevic, G.T. and H. Schubert, *Preparation and analysis of oil-in-water emulsions with a narrow droplet size distribution using Shirasu-porous-glass (SPG) membranes.* Desalination, 2002. **144**(1–3): p. 167-172.

185. Hancocks, R.D., F. Spyropoulos, and I.T. Norton, *Comparisons between membranes for use in cross flow membrane emulsification.* Journal of Food Engineering, 2013. **116**(2): p. 382-389.

186. Hao, D.-X., et al., *Controlling Factors on Droplets Uniformity in Membrane Emulsification: Experiment and Modeling Analysis.* Industrial & Engineering Chemistry Research, 2008. **47**(17): p. 6418-6425.

187. Kobayashi, I. and M. Nakajima, *Silicon Array of Elongated Through-Holes for Monodisperse Emulsion Droplets.* AiChE Journal, 2002. **48**(8): p. 1639-1644.

188. Kobayashi, I., S. Mukataka, and M. Nakajima, *Production of Monodisperse Oil-in-Water Emulsions Using a Large Silicon Straight-Through Microchannel Plate.* Industrial & Engineering Chemistry Research, 2005. **44**(15): p. 5852-5856.

189. Vladisavljević, G.T., et al., *Shirasu Porous Glass membrane emulsification: Characterisation of membrane structure by high-resolution X-ray microtomography and microscopic observation of droplet formation in real time.* Journal of Membrane Science, 2007. **302**(1–2): p. 243-253.

190. Abrahamse, A.J., et al., *Analysis of droplet formation and interactions during cross-flow membrane emulsification.* Journal of Membrane Science, 2002. **204**(1–2): p. 125-137.

191. Yasuno, M., et al., *Visualization and characterization of SPG membrane emulsification.* Journal of Membrane Science, 2002. **210**(1): p. 29-37.

192. Curran, J.M., et al., *The osteogenic response of mesenchymal stem cells to an injectable PLGA bone regeneration system.* Biomaterials, 2013. **34**(37): p. 9352-9364.

193. M. B. Oliveira and J.F. Mano, *Polymer-based microparticles in tissue engineering and regenerative medicine.* Biotechnol Prog, 2011. **27**(4): p. 897-912.

194. Stang, M., H. Schuchmann, and H. Schubert, *Emulsification in High-Pressure Homogenizers.* Engineering in Life Sciences, 2001. **1**(4): p. 151-157.

195. Dumay, E., et al., *Technological aspects and potential applications of (ultra) high-pressure homogenisation.* Trends in Food Science & Technology, 2013. **31**(1): p. 13-26.

196. Qi, F., et al., *Comparative studies on the influences of primary emulsion preparation on properties of uniform-sized exenatide-loaded PLGA microspheres.* Pharm Res, 2014. **31**(6): p. 1566-74.

197. Shiga, K., N. Muramatsu, and T. Kondo, *Preparation of poly(D,L-lactide) and copoly(lactide-glycolide) microspheres of uniform size.* J Pharm Pharmacol, 1996. **48**(9): p. 891-5.

198. Berkland, C., K. Kim, and D.W. Pack, *Fabrication of PLG microspheres with precisely controlled and monodisperse size distributions.* Journal of Controlled Release, 2001. **73**(1): p. 59-74.

199. Kranz, H., et al., *Physicomechanical properties of biodegradable poly(D,L-lactide) and poly(D,L-lactide-co-glycolide) films in the dry and wet states.* J Pharm Sci, 2000. **89**(12): p. 1558-66.

200. Walz, J.Y., *Effect of Polydispersity on the Depletion Interaction between Colloidal Particles.* Journal of Colloid and Interface Science, 1996. **178**(2): p. 505-513.

201. Li, X.-Q., et al., *Preparation of large-sized highly uniform agarose beads by novel rotating membrane emulsification.* Journal of Membrane Science, 2015. **476**: p. 30-39.

202. Friess, W. and M. Schlapp, *Release mechanisms from gentamicin loaded poly(lactic-co-glycolic acid) (PLGA) microparticles.* J Pharm Sci, 2002. **91**(3): p. 845-55.

203. Chun, K.W., et al., *Biodegradable PLGA microcarriers for injectable delivery of chondrocytes: effect of surface modification on cell attachment and function.* Biotechnol Prog, 2004. **20**(6): p. 1797-801.

204. Chen, A.K.-L., et al., *Increasing efficiency of human mesenchymal stromal cell culture by optimization of microcarrier concentration and design of medium feed.* Cytotherapy, 2015. **17**(2): p. 163-173.

205. Shekaran, A., et al., *Enhanced in vitro osteogenic differentiation of human fetal MSCs attached to 3D microcarriers versus harvested from 2D monolayers.* BMC Biotechnology, 2015. **15**(1): p. 1-13.

206. *HCS CellMask™ Stains*. Molecular Probes [cited 2015 5th June]; Available from: https://tools.thermofisher.com/content/sfs/manuals/mp32712.pdf.

207. Langenbach, F. and J. Handschel, *Effects of dexamethasone, ascorbic acid and beta-glycerophosphate on the osteogenic differentiation of stem cells in vitro.* Stem Cell Res Ther, 2013. **4**(5): p. 117.

208. *ab83369 Alkaline Phosphatase Assay Kit (Colorimetric) : Intructions for Use*. Abcam plc [cited 2015 4th July]; Available from: http://www.abcam.com/ps/products/83/ab83369/documents/ab83369%20Alkaline%20Phosphatase%20Assay%20Kit%20Colorimetric%20Protocol%20v2%20(website).pdf.

209. Epstein, J.B., C. Scully, and J. Spinelli, *Toluidine blue and Lugol's iodine application in the assessment of oral malignant disease and lesions at risk of malignancy.* J Oral Pathol Med, 1992. **21**(4): p. 160-3.

210. Sridharan, G. and A.A. Shankar, *Toluidine blue: A review of its chemistry and clinical utility.* J Oral Maxillofac Pathol, 2012. **16**(2): p. 251-5.

211. *OsteoImage Ineralization Assay: Instructions for Use*. Lonza Walkersville, Inc. [cited 2015 18th March]; Available from: http://www.lonzabio.jp/catalog/pdf/ri/I573.pdf.

212. Aydogdu, H., et al., *Pullulan microcarriers for bone tissue regeneration.* Materials Science and Engineering: C, 2016. **63**: p. 439-449.

213. Goh, T.K., et al., *Microcarrier culture for efficient expansion and osteogenic differentiation of human fetal mesenchymal stem cells.* Biores Open Access, 2013. **2**.

214. Malaval, L., et al., *Cellular expression of bone-related proteins during in vitro osteogenesis in rat bone marrow stromal cell cultures.* J Cell Physiol, 1994. **158**(3): p. 555-72.

215. Ducy, P., et al., *Osf2/Cbfa1: a transcriptional activator of osteoblast differentiation.* Cell, 1997. **89**(5): p. 747-54.

216. Nakashima, K., et al., *The novel zinc finger-containing transcription factor osterix is required for osteoblast differentiation and bone formation.* Cell, 2002. **108**(1): p. 17-29.

217. Nishio, Y., et al., *Runx2-mediated regulation of the zinc finger Osterix/Sp7 gene.* Gene, 2006. **372**: p. 62-70.

218. Chen, M., et al., *A modular approach to the engineering of a centimeter-sized bone tissue construct with human amniotic mesenchymal stem cells-laden microcarriers.* Biomaterials, 2011. **32**.

219. Thibault, R.A., et al., *Osteogenic differentiation of mesenchymal stem cells on pregenerated extracellular matrix scaffolds in the absence of osteogenic cell culture supplements.* Tissue Eng Part A, 2010. **16**(2): p. 431-40.

220. Birmingham, E., et al., *Osteogenic differentiation of mesenchymal stem cells is regulated by osteocyte and osteoblast cells in a simplified bone niche.* Eur Cell Mater, 2012. **23**: p. 13-27.

221. Di Luca, A., et al., *Gradients in pore size enhance the osteogenic differentiation of human mesenchymal stromal cells in three-dimensional scaffolds.* Scientific Reports, 2016. **6**: p. 22898.

222. Quarles, L.D., et al., *Distinct proliferative and differentiated stages of murine MC3T3-E1 cells in culture: an in vitro model of osteoblast development.* J Bone Miner Res, 1992. **7**(6): p. 683-92.

223. Konigsberg, I.R., *Skeletal myoblasts in culture*, in *Methods in Enzymology*. 1979, Academic Press. p. 511-527.

224. Zhu, B., S.R. Bailey, and C.M. Agrawal, *Calcification of primary human osteoblast cultures under flow conditions using polycaprolactone scaffolds for intravascular applications.* J Tissue Eng Regen Med, 2012. **6**(9): p. 687-95.

225. Manolagas, S.C., *Birth and death of bone cells: basic regulatory mechanisms and implications for the pathogenesis and treatment of osteoporosis.* Endocr Rev, 2000. **21**(2): p. 115-37.

226. Choi, Y.K., et al., *Enhanced solubility and oral bioavailability of itraconazole by combining membrane emulsification and spray drying technique.* Int J Pharm, 2012. **434**(1-2): p. 264-71.

227. Quent, V.M., et al., *Discrepancies between metabolic activity and DNA content as tool to assess cell proliferation in cancer research.* J Cell Mol Med, 2010. **14**(4): p. 1003-13.

228. Granéli, C., et al., *Novel markers of osteogenic and adipogenic differentiation of human bone marrow stromal cells identified using a quantitative proteomics approach.* Stem Cell Research, 2014. **12**(1): p. 153-165.

229. Yamate, T., et al., *Osteopontin expression by osteoclast and osteoblast progenitors in the murine bone marrow: demonstration of its requirement for osteoclastogenesis and its increase after ovariectomy.* Endocrinology, 1997. **138**(7): p. 3047-55.

230. Lin, Y. and P. Alexandridis, *Temperature-Dependent Adsorption of Pluronic F127 Block Copolymers onto Carbon Black Particles Dispersed in Aqueous Media.* The Journal of Physical Chemistry B, 2002. **106**(42): p. 10834-10844.

Appendices

Appendix I. Equipment, Consumables and Materials

Table AI-1 List of Equipment

Equipment	Manufacturer/ Model No	Supplier	Use
Centrifuge	MSE Mistral 1000	Scientific Laboratory Supplies Ltd.	General
Centrifuge	Sigma 2-16K	Scientific Laboratory Supplies Ltd.	Cell culture
Environmental SEM	Quanta 650	-	-
Freeze Dryer	Edwards Modulyo D	IMA Edwards, UK	MP drying
Fluorescence microscope	Leica-DMIRB	Leica microsystems, Austria	Imaging
Membrane Emulsification Equipment	High Speed Mini Kit KH-125	SPG Co. Ltd. Miyazaki-City, Japan	Membrane Emulsification
Oven	Binder	Scientific Laboratory Supplies Ltd	General
Optical light microscope	Nikon Eclipse TS 100	Leica Microsystems, Austria	Imaging
Plate Reader	Tecan Infinite M200	Tecan UK Ltd, UK	Flurescence Intensity Reading
Particle Sizer	Coulter LS 230	Beckman Coulter, UK	MP sizing

Table AI-1 List of Equipment (continued)

Equipment	Manufacturer/ Model No	Supplier	Use
Refrigerator	LabCold	Fisher Scientific UK Ltd	Storage
Rheometer	Physical MCR 301	Anton Paar, UK	Viscosity study
Shaker	IKA® 3D digital	IKA, UK	Dynamic cell culture
Scanning Electron Microscope	JSM 6060LV	Leica Microsystems, Austria	Imaging
Sputter Coater	Leica Microsystems EM SCD 005	Leica Microsystems, Austria	Gold coating of MPs for SEM imaging
Time Lapse Microscope	Leica, DMIRB	Leica Microsystems, Austria	Imaging
Vacuum packer	Orvid VM03	Scientific Laboratory Supplies Ltd.	General
Vortex Mixer	Stuart Scientific SA8	Scientific Laboratory Supplies Ltd.	General

Table AI-2 List of General Consumables

Consumables	Specification/ Catalogue No	Supplier	Use
Beakers	20-500ml	Fisher Scientific UK Ltd.	General
Bijou bottles (7ml)	CON 7524	Laboratory Supplies Ltd.	General
Centrifuge tubes (15/50ml)	15ml 188261 50ml 227270	Greiner Bio One	MPs harvesting/surface wettability study
Glass Scintillation Vial	VGA-050-300P	Fisher Scientific UK Ltd.	Collection of emulsion droplets/Polymer solution preparation
Glass Pipettes (5ml)	12314388	Fisher Scientific UK Ltd.	General
Filter Unit (0.2µm)	FIL6570	Laboratory Supplies Ltd	Filtration of PVA solution
Laboratory Blue Roll	CMC 790-011L	Fisher Scientific UK Ltd.	General/MPs Preparation
Parafilm	SEL0400030P	Fisher Scientific UK Ltd.	General

Table AI-2 List of General Consumables (continued)

Consumables	Specification/ Catalogue No	Supplier	Use
Pipette filler	FB69000	Fisher Scientific UK Ltd.	General
Pipette tips (all sizes)	FR1200/1250/1015	Alpha Laboratories	General
Pipettes (20-200, 100-1000)	S1122-18301/8810C	Starlab (UK) Ltd	General
Plastic pipettes (5, 10ml)	TVK-671-040Q/050N	Fisher Scientific UK Ltd.	General
PTFE screw cap jar	FB58832/FB58833	Fisher Scientific UK Ltd.	General
Sealable bags	BAG 10/18/20/26/28	Laboratory Supplies Ltd.	General
Tissue Culture Flasks	Nunc178905/178883	Fisher Scientific UK Ltd.	Cell culture
Tissue Culture Plates	Nunc 96/24/6 well	Fisher Scientific UK Ltd.	Cell culture/assay

Table AI-3 List of General Chemicals/Reagents

Chemicals/Reagent	Specification/ Catalogue Number	Manufacturer / Supplier	Use
Acetone	A/0560/17	Fisher Scientific UK Ltd.	General
Antibiotic antimycotic solution	A5955-100ml	Sigma-Aldrich, UK	MPs sterilization
Alkaline Phosphatase Assay Kit	Ab83369	Abcam, UK	ALP assay
Alexa Fluor(TM) 488 Goat Anti-Rabbit IgG (H+L) Invitrogen	A11008	Invitrogen/ Fisher Scientific UK Ltd	Immunohistochemical staining for Human Osteocalcin
Alexa Fluor(TM) 546 Goat Anti-Rat IgG (H+L) Invitrogen	A11081	Invitrogen/ Fisher Scientific UK Ltd	Osteogenic Mineralization Assay
Cytodex 3	17048501	GE Healthcare /Scientific Laboratory Supplies Ltd.	Cell viability and Bone mineralization assay
Dichloromethane	D/1856/17	Fisher Scientific UK Ltd.	MPs fabrication and Membrane cleaning
Distilled water	In-house supply		General
DMEM	VX42430025	Sigma-Aldrich, UK	Cell Culture
Dexamethasone	D9184	Sigma-Aldrich, UK	Osteogenic Mineralization Assay

Table AI-3 List of General Chemicals/Reagents (continued)

Chemicals/Reagent	Specification/ Catalogue Number	Manufacturer / Supplier	Use
Donkey Serum	D9663	Sigma-Aldrich, UK	
Ethanol	E/0650DF/17	Fisher Scientific UK Ltd.	General
Goat Serum	G9023	Sigma-Aldrich, UK	Immunohistochemical staining for Human Osteocalcin
HCS CellMask™ Blue stain	H32720 (mfg part no) 10555854	Molecular Probe by life technologies/ThermoFisher Scientific UK	Staining cells
Hoechst 33258 solution, 1 mg/mL in H_2O	94403	Sigma-Aldrich, UK	Nuclear staining
Industrial methylated spirit	M/4400/17	Fisher Scientific UK Ltd.	General cleaning
L-Glutamin	G7513	Sigma-Aldrich, UK	Cell culture
Liquid nitrogen	Cryospeed	BOC Industrial Gases	Span freezing of MPs
L-Ascorbic acid 2-phosphate sesquimagnesium salt hydrate, =95%	A8960 (mfg part no.)	Sigma-Aldrich, UK	Osteogenic Mineralization Assay

Table AI-3 List of General Chemicals/Reagents (Continued)

Chemicals/Reagent	Specification/ Catalogue Number	Manufacturer/ Supplier	Use
LIVE/DEAD® Viability/Cytotoxicity Kit for mammalian cells Invitrogen	L3224	Invitrogen/ Fisher Scientific UK Ltd	live/dead imaging
Mouse Osteopontin (OPN) Affinity Purified Polyclonal Ab	AF808	R&D Systems/ &D Systems Europe Ltd	Immunohistochemical staining for Human Osteocalcin
OsteoImage® Mineralization Assay Kit	PA-1503	Lonza Verviers s.p.r.l. Switzerland	Bone mineral assay
Penicillin/ streptomycin	Invitrogen VX15070063	Fisher Scientific UK Ltd.	Cell culture
Paraformaldehyde	158127	Sigma-Aldrich, UK	Tissue sample fixing
Phosphate buffer saline	BPE9739-1	Fisher Scientific UK Ltd.	MP sterilization/cell culture
Presto Blue Cell Viability Reagent	A13262	Invitrogen/Fisher Scientific UK Ltd	Cell viability assay
8515 Poly (DL lactide-co-glycolide) with acid group	8515 DLG-4CA LP-717	Evonik Industries, Birmingham, AI, USA	MP preparation

Table AI-3 List of General Chemicals/Reagents (Continued)

Chemicals/Reagent	Specification/ Catalogue Number	Manufacturer/ Supplier	Use
Poly (vinyl alcohol (87-89% hydrolysed)	363170	Sigma-Aldrich, UK	MP preparation
Poly(vinyl alcohol), M_w 13,000-23,000, 87-89% hydrolysed	363170	Sigma-Aldrich, UK	MP preparation
Polycaprolactone, M_n 70,000-90,000 by GPC	440744	440744	MP treatment
Silver nitrate	S-6506	Sigma-Aldrich, UK	Von-Kossa reagent preparation for bone mineralization assay
Sodium thiosulphate	13481	Sigma-Aldrich, UK	Von-Kossa reagent preparation for bone mineralization assay
Silver nitrate solution, 2.5 % (w/v) $AgNO_3$ in H_2O	85193	Sigma-Aldrich, UK	

Appendix II. Coating of nTC Plates with Pluronic F 127

Pluronic F 127 is a block copolymer of poly(ethylene oxide)-poly(propylene oxide)-poly(ethylene oxide) (PEO-PPO-PEO) and known to adsorb onto hydrophobic surface such as on polystyrene surface in either a brush or coil like conformation depending on the degree of hydrophobicity of the surface [230]. Its hydrophobic PPO moiety is attached to the surface and the hydrophilic PEO domains face upward in a way as shown schematically in Figure AII-1. This configuration renders the surface highly hydrophilic and is unfavourable for cell adhesion. Standard tissue culture plates or non-treated tissue culture plates are of hydrophobic polystyrene material and are expected to form a cell repelling surface if coated with Pluronic F127. The number of 12-well nTC plates required for the cell adhesion experiment was calculated and the required amount of 1.0 % (w/v) aqueous solution of Pluronic F127 was prepared by dissolving the polymer in dH_2O. The solution was sterilized using 0.2µm membrane filter and an amount just enough to cover the bottom of the plate was aseptically poured on each well of the plates. The plates were then incubated overnight at 37^0C. On the next day, the solution was aspirated and air dried inside a class II microbiological safety cabinet. The plates were successfully coated and shown cell repelling property as shown in Figure AII-2.

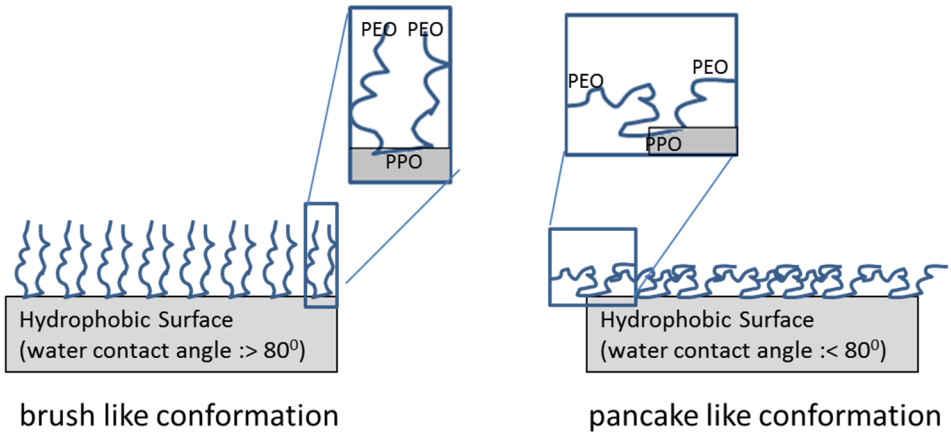


Figure AII-1: Schematic showing the conformations of Pluronic F127 on surfaces of different degree of hydrophilicity.

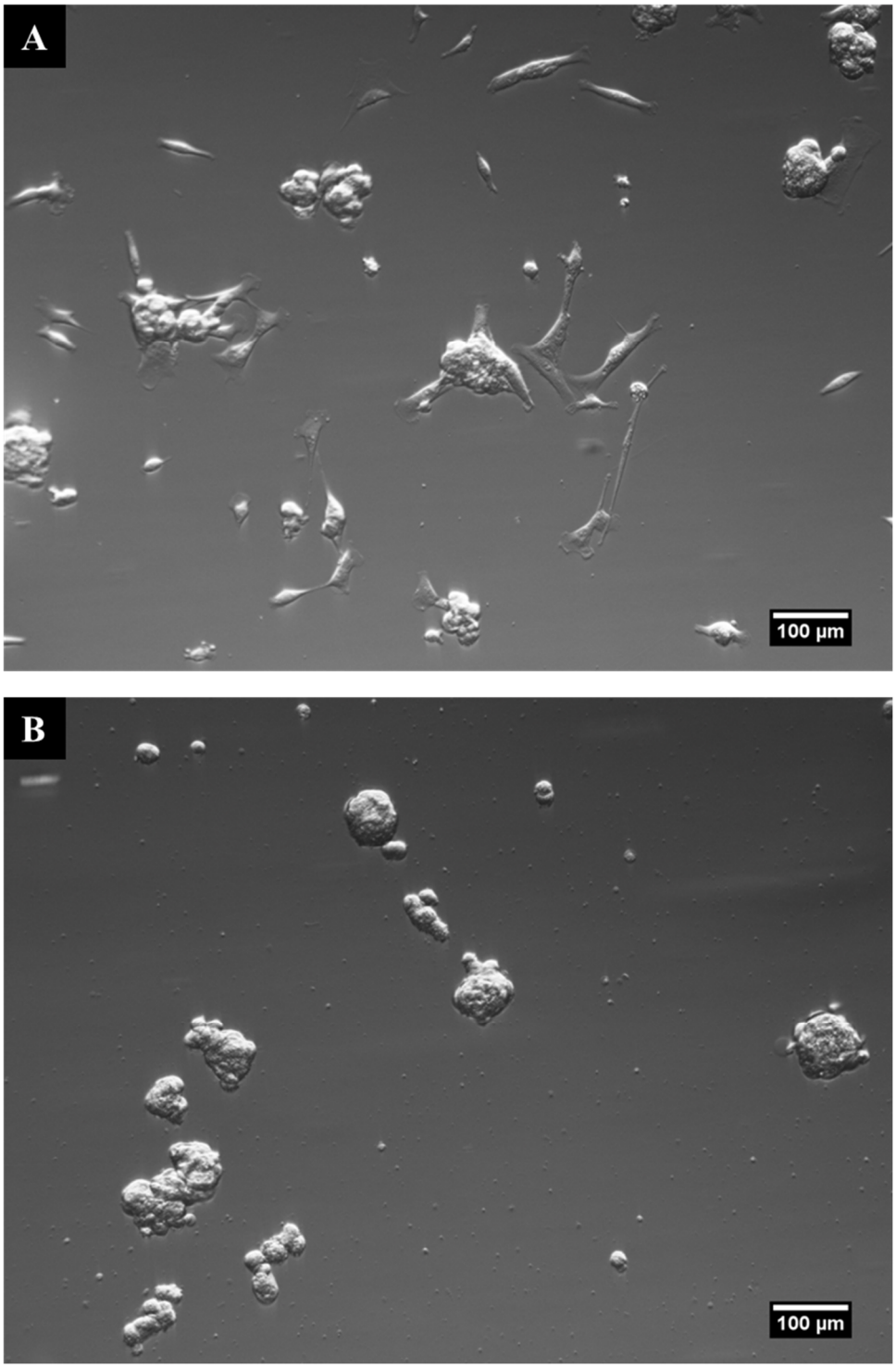


Figure AII-2: Optical light microscopic images of ihMSCs seeded on (A) nTC plate and (B) Pluronic 127 coated nTC plate. In the uncoated plate, some cells attached on the plate bottom but after coated, no cell was seen to attach onto the plate surface.

Appendix III. Counting of Viable Cells using Trypan Blue

Trypan blue is a coloured dye which cannot cross the intact membrane of a viable cell. It can, however, cross the compromised membrane of a dead cell, and can therefore be used to quantitatively assess cell viability. For cell counting and viability assessment, 100 μL of cell suspension was mixed with 100 μL of trypan blue. 10 μL of this mixture was then added to the counting chamber of an improved Neubauer haemocytometer and cell count performed for three major squares with each square covering sixteen minor squares. These counts were then averaged and converted to cell numbers per mL by multiplication of a factor 2×10^4.

Appendix IV. Calibration curves developed for ihMSCs Viability Assays

To produce a calibration curve for a series of number of cells (ihMSCs) versus RFU (relative fluorescent unit) values, a cell suspension with a concentration of 100 µL/mL was prepared following the procedure described in section 2.2.9 and then a series of diluted cell suspensions was prepared using serum free DMEM with the following concentrations: 0×10^3, 100×10^3, 200×10^3, 300×10^3, 400×10^3, 500×10^3, 600×10^3, 700×10^3, 800×10^3, 900×10^3 and1000×10^3. These cell suspensions were seeded on 12-well tissue-culture treated plates with three technical repeats and then incubated at 37ºC with 5 % v/v CO2 for 6 hours. Then the cultures were treated with the Presto Blue® cell viability assay kit and the RFU values against the number of cells were measured using a plate reader (Infinite™ M200, Tecan, USA) following the method described in section 2.2.11.ii. Figure AIV-1 shows a calibration curve developed for the above mentioned series of cell concentrations. The equation generated for this calibration curve was used to measure the viability of ihMSCs with Por-MPs prepared via conventional method, as described in Chapter 2.

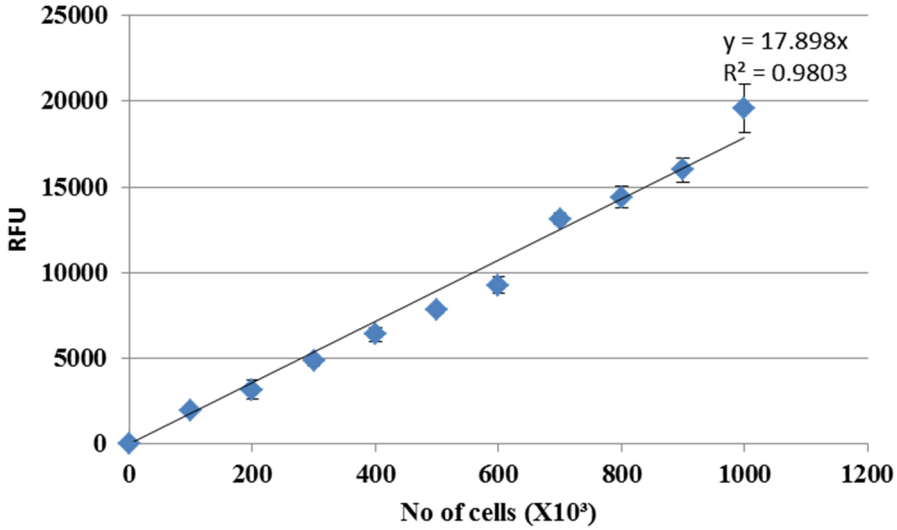


Figure AIV-1: Calibration curve for ihMSCs with concentrations of 0×10^3, 100×10^3, 200×10^3, 300×10^3, 400×10^3, 500×10^3, 600×10^3, 700×10^3, 800×10^3, 900×10^3 and1000×10^3 cells

Using the same procedure as described above, another calibration curve was developed for a different series of cell suspensions. The concentration of cells for this set was as follows: 0×10^3, 10×10^3, 20×10^3, 30×10^3, 40×10^3, 50×10^3, 60×10^3, 70×10^3, 80×10^3, $90 \times 10^3$and 100×10^3. The calibration curve developed for this series of cells is shown in Figure AIV-2. The equation generated from this calibration curve was used to measure the number of viable cells with Por-MPs prepared via membrane emulsification method, as described in Chapter 5.

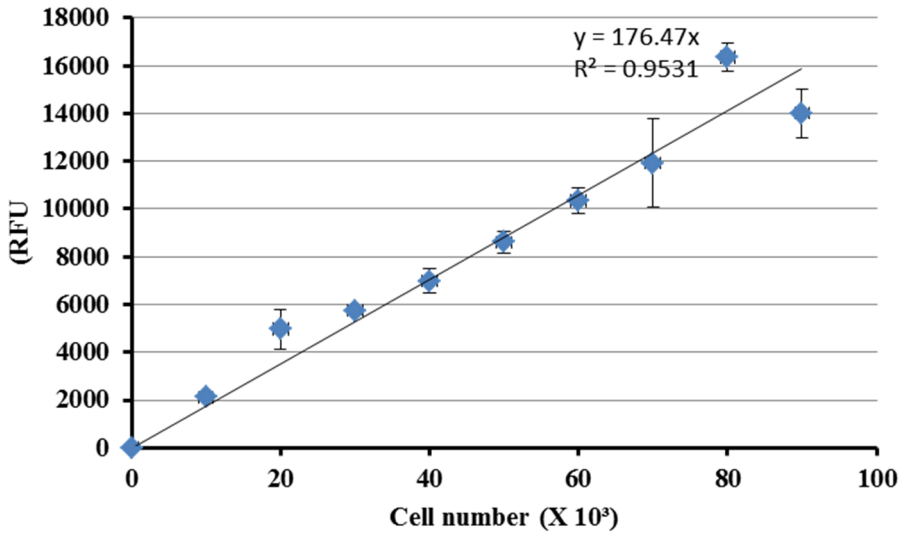


Figure AIV-2: Calibration curve for ihMSCs with concentrations from 0×10^3, 10×10^3, 20×10^3, 30×10^3, 40×10^3, 50×10^3, 60×10^3, 70×10^3, 80×10^3, $90 \times 10^3$and 100×10^3

Appendix V. Images of Supernatant Collected During Medium Removal for PrestoBlue® Cell Viability Assay

For PrestoBlue® cell viability assays, ihMSCs were seeded with porous PLGA MPs in Pluronic F127-coated nTC plates. Some of the cells did not attach with the MPs and remained floating in the culture. During removal of the medium for the assays, the floating cells were removed from the culture. The representative images from the supernatant for Por-CE MPs and Por-ME MPs are shown in Figure AV-1 and AV-2, respectively.

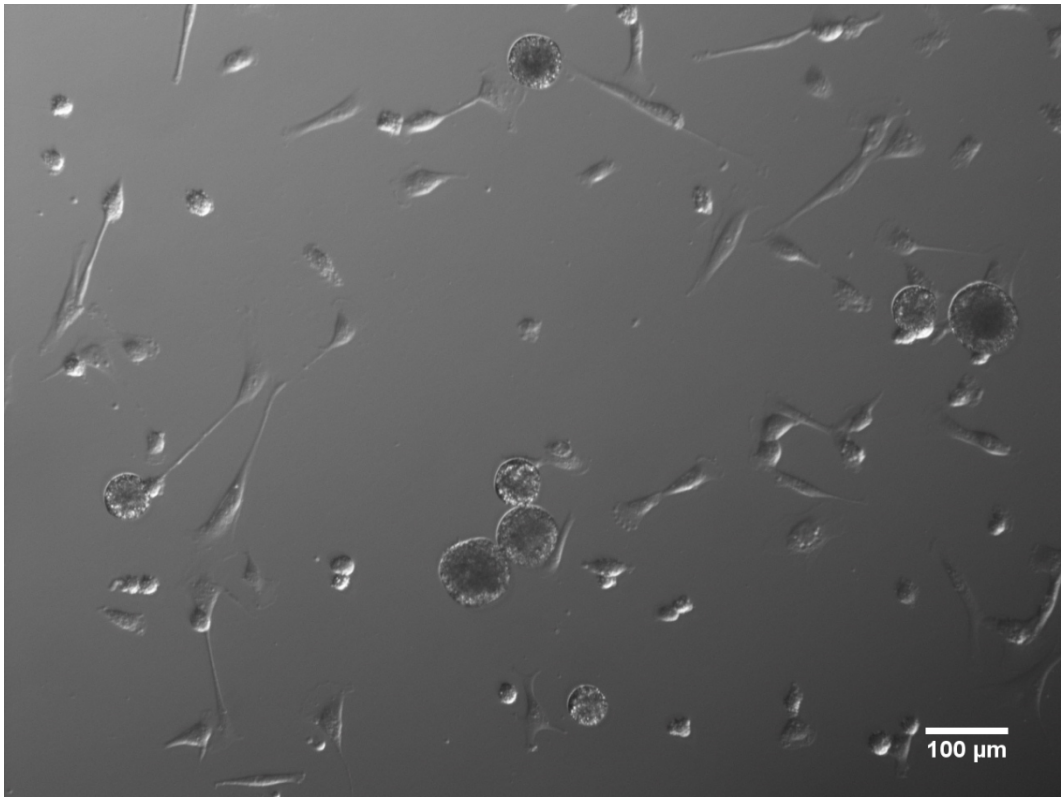


Figure AV-1: Representative images of the supernatant collected during PrestoBlue ® cell viability assay preparation on day 1 post-seeding of ihMSCs with Por-CE MPs. The images were captured after 24 hours of incubation of the sample at 37^{o}C in 5% w/v CO_2. Scale bar = 100 µm.

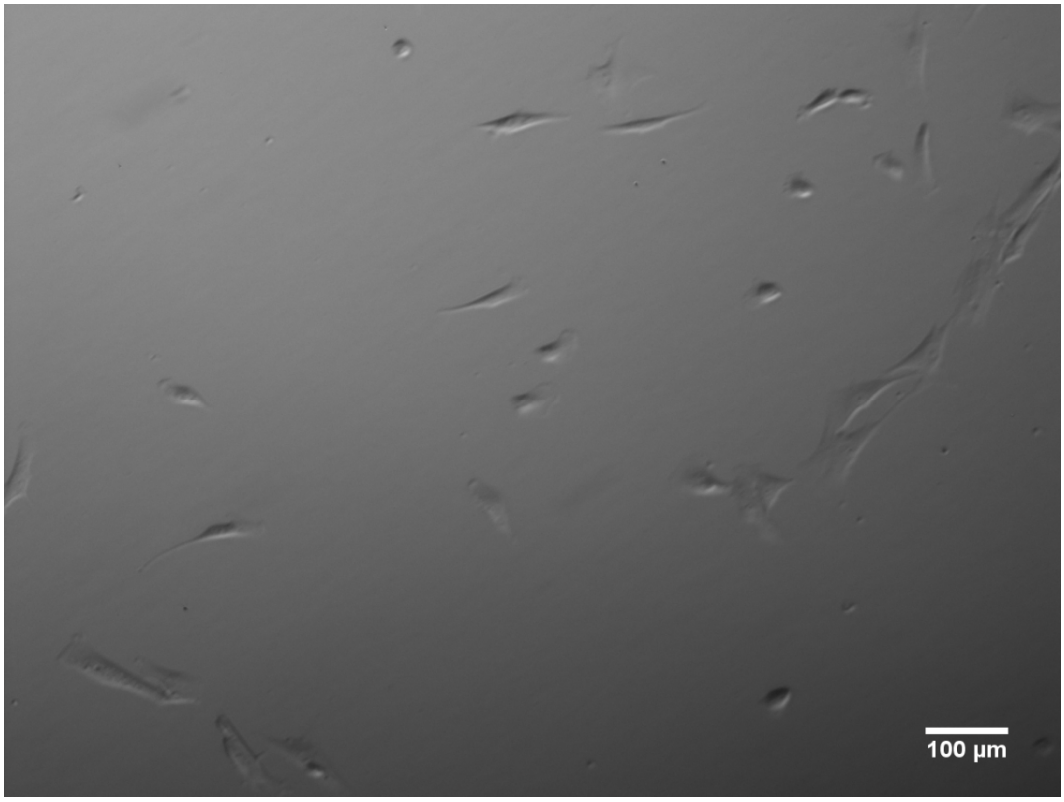


Figure AV-2: Representative images of the supernatant collected during PrestoBlue ® cell viability assay preparation on day 1 post-seeding of ihMSCs with Por-ME MPs. The images were captured after 24 hours of incubation of the sample at 37^{o}C in 5% w/v CO_2. Scale bar = 100 µm.

Appendix VI. Cleaning and Maintenance of SPG Membranes

After preparation of each batch of single (PCL in DCM) or double (PBS-in-PLGA-in-Water) emulsions, the membrane were thoroughly cleaned according to the following procedure: Approximately 200 ml of pure DCM was added in the pressure vessel of the emulsification kit (the vessel which contains DP) and then the membrane is flushed thoroughly with a nitrogen gas pressure of 80kPa. After that the membrane was placed in a glass cylinder (50 mL) and approximately 40 mL of DCM is added in the cylinder. The cylinder was then kept under sonication for 5 minutes. After that the membrane was removed from the cylinder to a glass beaker, place under a hood for 30 minutes and then left in an oven overnight for allowing the membrane to dry completely. On next day, the membrane was removed from the oven, allowed it to dry, placed in a sealable bag, sealed under vacuum using a vacuum packer (Orvid VM03, Scientific Laboratory Supplies Ltd.).

In order to prevent the membrane from wetting with DP (oil), it needs to wet with aqueous phase. The following procedure was used to wet the membrane before using for emulsification. The membrane is placed is dipped in dH_2O in a glass cylinder and left overnight. On the next day it was sonicated in water for 3 × 30 minutes. Is the membrane had not wetted properly (can be visualised by some whitish areas on the membrane, the appearance of which is different than other major portion of the membrane. In that case, another cycle of sonication for 3 × 30 minutes was repeated. The membrane thus became ready for the emulsification.

Appendix VII. GPC Sample Injection Report for PCL and PLGA polymers

Appendix VII-1: GPC Data for PLGA

Configuration

Concentration Source: RI
Flow Rate: 1.000 mL/min

RI Instrument: RI
Band Broadening Correction: n/a
Wavelength: 690.0 nm

Column: Polystyrene Calibration 19 Jan 16 1mlmin
Flow Marker: 21.808 mL
Mark-Houwink-Sakurada a: 0.000
Mark-Houwink-Sakurada K: 0.000 mL/g
Conventional Calibration Function Fit Standard Error: 0.0275772
Universal Calibration Function Fit Standard Error: 0
Calibration Technique: Conventional
Conventional Calibration Function: log(Molar Mass) = 14.6214 - 1.42897 v + 0.0711141 v^2 - 0.00160455 v^3

Solvent: chloroform
Refractive Index: 1.439

Fluid Connections

Source Instrument	Destination Instrument	Delay Volume (mL)
Generic Pump	Injector	0.000
Injector	DAWN EOS	0.000
DAWN EOS	Generic RI Instrument	0.280

Aux Connections

Source Instrument	Destination Instrument	Aux Channel	Calibration Constant
Generic RI Instrument	DAWN EOS	1	1.000

Processing

Collection Time: Thursday March 31, 2016 09:14:07 AM GMT Daylight Time
Processing Time: Friday April 01, 2016 05:16:53 PM GMT Daylight Time

Peak settings:

Peak Name	Peak 1
dn/dc (mL/g)	0.1850
Viscometry Model	Huggins
Huggins Equation Parameter	0
Kraemers Equation Parameter	0

Results Fitting Procedure:

Data	Fit Model	Degree	R^2	Extrapolation

Results

Peak Results

	Peak 1
Masses	
Calculated Mass (µg)	737203.80
Molar mass moments (g/mol)	
Mn	2.678×10^4 (±6.556%)
Mw	5.267×10^4 (±6.556%)
Mz	8.845×10^4 (±14.659%)
M(avg)	4.919×10^3 (±0.566%)
Polydispersity	
Mw/Mn	1.966 (±9.271%)
Mz/Mn	3.302 (±16.058%)

Appendix VII-2: GPC Data for Higher Molecular Weight PCL (PCL_{80kDa})

Configuration

Concentration Source: RI
Flow Rate: 1.000 mL/min

RI Instrument: RI
Band Broadening Correction: n/a
Wavelength: 690.0 nm

Column: Polystyrene Calibration 19 Jan 16 1mlmin
Flow Marker: 21.808 mL
Mark-Houwink-Sakurada a: 0.000
Mark-Houwink-Sakurada K: 0.000 mL/g
Conventional Calibration Function Fit Standard Error: 0.0275772
Universal Calibration Function Fit Standard Error: 0
Calibration Technique: Conventional
Conventional Calibration Function: log(Molar Mass) = 14.6214 - 1.42897 v + 0.0711141 v^2 - 0.00160455 v^3

Solvent: chloroform
Refractive Index: 1.439

Fluid Connections

Source Instrument	Destination Instrument	Delay Volume (mL)
Generic Pump	Injector	0.000
Injector	DAWN EOS	0.000
DAWN EOS	Generic RI Instrument	0.280

Aux Connections

Source Instrument	Destination Instrument	Aux Channel	Calibration Constant
Generic RI Instrument	DAWN EOS	1	1.000

Processing

Collection Time: Thursday March 31, 2016 08:42:03 AM GMT Daylight Time
Processing Time: Friday April 01, 2016 05:14:34 PM GMT Daylight Time

Peak settings:

Peak Name	Peak 1
dn/dc (mL/g)	0.1850
Viscometry Model	Huggins
Huggins Equation Parameter	0
Kraemers Equation Parameter	0

Results Fitting Procedure:

Data	Fit Model	Degree	R^2	Extrapolation

Results

Peak Results

	Peak 1
Masses	
Calculated Mass (µg)	1661416.68
Molar mass moments (g/mol)	
Mn	1.207×10^5 (±6.556%)
Mw	1.922×10^5 (±6.556%)
Mz	2.672×10^5 (±14.659%)
M(avg)	2.525×10^4 (±0.584%)
Polydispersity	
Mw/Mn	1.592 (±9.271%)
Mz/Mn	2.213 (±16.058%)

Appendix VII-3: GPC Data for Lower Molecular Weight PCL (PCL_{45kDa})

Configuration

Concentration Source: RI
Flow Rate: 1.000 mL/min

RI Instrument: RI
Band Broadening Correction: n/a
Wavelength: 690.0 nm

Column: Polystyrene Calibration 19 Jan 16 1mlmin
Flow Marker: 21.808 mL
Mark-Houwink-Sakurada a: 0.000
Mark-Houwink-Sakurada K: 0.000 mL/g
Conventional Calibration Function Fit Standard Error: 0.0275772
Universal Calibration Function Fit Standard Error: 0
Calibration Technique: Conventional
Conventional Calibration Function: $\log(\text{Molar Mass}) = 14.6214 - 1.42897\ v + 0.0711141\ v^2 - 0.00160455\ v^3$

Solvent: chloroform
Refractive Index: 1.439

Fluid Connections

Source Instrument	Destination Instrument	Delay Volume (mL)
Generic Pump	Injector	0.000
Injector	DAWN EOS	0.000
DAWN EOS	Generic RI Instrument	0.280

Aux Connections

Source Instrument	Destination Instrument	Aux Channel	Calibration Constant
Generic RI Instrument	DAWN EOS	1	1.000

Processing

Collection Time: Monday April 11, 2016 03:13:27 PM GMT Daylight Time
Processing Time: Monday April 11, 2016 06:02:57 PM GMT Daylight Time

Peak settings:

Peak Name	Peak 1
dn/dc (mL/g)	0.1850
Viscometry Model	Huggins
Huggins Equation Parameter	0
Kraemers Equation Parameter	0

Results Fitting Procedure:

Data	Fit Model	Degree	R^2	Extrapolation

Results

Peak Results

	Peak 1
Masses	
Calculated Mass (µg)	1545881.22
Molar mass moments (g/mol)	
Mn	4.982×10^4 (±6.556%)
Mw	7.626×10^4 (±6.556%)
Mz	1.100×10^5 (±14.659%)
M(avg)	1.695×10^4 (±0.582%)
Polydispersity	
Mw/Mn	1.531 (±9.271%)
Mz/Mn	2.208 (±16.058%)

Appendix VIII. Optimisation of Calcein AM and EthD-1 Concentration for Live/Dead Imaging

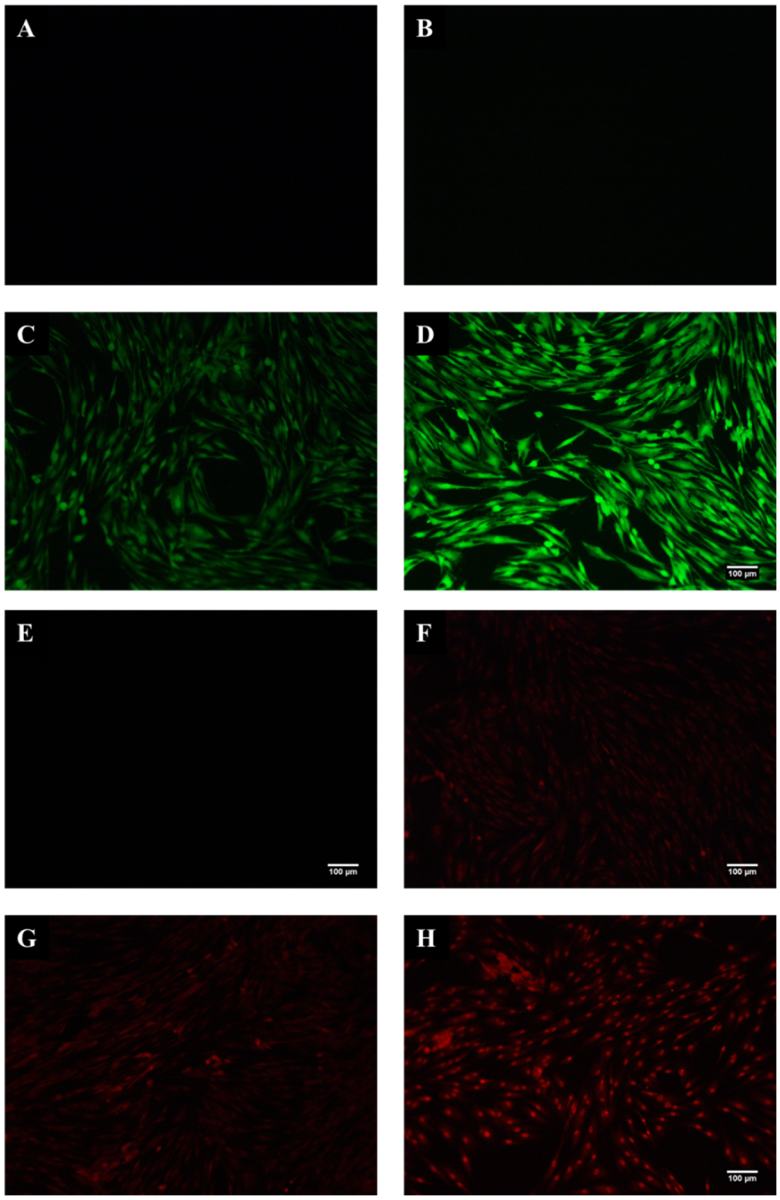


Figure AVII-1 Optimization of Calcein AM and EthD-1 concentration optimization for live/dead imaging. Images of live cells at (A) 0.1µM, (B) 1.0 µM, (C) 2.5 µM and (D) 5.0 µM Calcein AM; Images of dead cells at (E) 0.1µM, (F) 1.0 µM, (G) 2.5 µM and (H) 5.0 µM EthD-1. 2.5 µM Calcein AM and 5 µM EthD-1 was found the optimum concentration to stain the cytoplasm of live cells and the nulei of dead cells respectively.

Appendix IX. Preparation of 4 % w/v Paraformaldehyde (need to paraphrase)

In order to use in the paraformaldehyde (PFA) solution of 4% w/v solution, a 0.2 M phosphate buffer of pH 7.4 was made by dissolving Na_2HPO_4 (21.8 g) and NaH_2PO_4 (6.4 g) in distilled water (1 L). Using this stock, a solution of 0.1 M was prepared. PFA (40 g) was added to 0.1 M phosphate buffer (1 L) and then heated to 60-65°C with stirring to make a solution of PFA. The solution was made clear by dropwise adding 1 M sodium hydroxide. The solution was then cooled, tested for pH 7.4 with pH paper and passed through 0.22 μm filters. The solution was aliquoted and stored at -20°C, until use.